

University of Windsor

## Scholarship at UWindor

---

Electronic Theses and Dissertations

Theses, Dissertations, and Major Papers

---

2011

### Minimum Quantity Lubrication Machining of Aluminum and Magnesium Alloys

Sukanta Bhowmick  
*University of Windsor*

Follow this and additional works at: <https://scholar.uwindsor.ca/etd>

---

#### Recommended Citation

Bhowmick, Sukanta, "Minimum Quantity Lubrication Machining of Aluminum and Magnesium Alloys" (2011). *Electronic Theses and Dissertations*. 455.  
<https://scholar.uwindsor.ca/etd/455>

This online database contains the full-text of PhD dissertations and Masters' theses of University of Windsor students from 1954 forward. These documents are made available for personal study and research purposes only, in accordance with the Canadian Copyright Act and the Creative Commons license—CC BY-NC-ND (Attribution, Non-Commercial, No Derivative Works). Under this license, works must always be attributed to the copyright holder (original author), cannot be used for any commercial purposes, and may not be altered. Any other use would require the permission of the copyright holder. Students may inquire about withdrawing their dissertation and/or thesis from this database. For additional inquiries, please contact the repository administrator via email ([scholarship@uwindsor.ca](mailto:scholarship@uwindsor.ca)) or by telephone at 519-253-3000ext. 3208.

**MINIMUM QUANTITY LUBRICATION  
MACHINING OF ALUMINUM AND  
MAGNESIUM ALLOYS**

**By**

**SUKANTA BHOWMICK**

**A Dissertation  
Submitted to the Faculty of Graduate Studies  
through Engineering Materials  
in Partial Fulfillment of the Requirements for  
the Degree of Doctor of Philosophy at the  
University of Windsor**

**Windsor, Ontario, Canada**

**2011**

**© 2011 Sukanta Bhowmick**

**Minimum Quantity Lubrication Machining of  
Aluminum and Magnesium Alloys**

**By**

**Sukanta Bhowmick**

**APPROVED BY**

---

**P. Koshy (External Examiner)**

**Department of Mechanical Engineering, McMaster University**

---

**R. Carriveau (Outside Program Reader)**

**Civil and Environmental Engineering**

---

**D.O. Northwood (Program Reader)**

**Mechanical, Automotive and Materials Engineering**

---

**A. Edrisy (Program Reader)**

**Mechanical, Automotive and Materials Engineering**

---

**A.T. Alpas (Advisor)**

**Mechanical, Automotive and Materials Engineering**

---

**J. Urbanic (Chair of Defense)**

**Industrial and Manufacturing Systems Engineering**

# DECLARATION OF CO-AUTHORSHIP/PREVIOUS PUBLICATION

## I. Co-Authorship Declaration

I hereby declare that this thesis does not incorporate material that is result of joint research. In all cases, the key ideas, primary contributions, experimental designs, data analysis and interpretation, were performed collectively by the author and Dr. A.T. Alpas as advisor. Dr. M. J. Lukitsch of General Motors Global Research and Development Centre helped with the provision of samples, brought an industrial perspective and helped with the analyses of results in Chapters 4 and 5.

I certify that, with the above qualification, this thesis, and the research to which it refers, is the product of my own work.

## II. Declaration of Previous Publication

This thesis includes 5 original papers that have been previously published/ submitted for publication in peer reviewed journals/conference proceedings, as follows:

<b>Thesis chapter</b>	<b>Publication title/full citation</b>	<b>Publication status</b>
Chapter 3	Minimum quantity lubrication drilling of aluminum-silicon alloys in water using diamond-like carbon coated drills, International Journal of Machine Tools and Manufacture 48 (2008) 1429-1443.	Published
Chapter 4	Tapping of Al-Si alloys with diamond-like carbon coated tools and minimum quantity of lubrication, Journal of Materials Processing Technology 210 (2010) 2142-2153.	Published
Chapter 5	Dry and minimum quantity lubrication drilling of cast magnesium alloy (AM60), International Journal of Machine Tools and Manufacture 50	Published

	(2010) 444-457.	
Chapter 6	The role of diamond-like carbon coated drills on minimum quantity lubrication drilling of magnesium alloys, Surface and Coatings Technology	Submitted
Chapter 7	Minimum quantity lubrication drilling of lightweight aluminum and magnesium alloys used in automotive components, Proceedings of CIRP PMI 2010, June 10-11, 2010 Vancouver, Canada	Published

I certify that I have obtained a written permission from the copyright owner(s) to include the above published material(s) in my thesis. I certify that the above material describes work completed during my registration as graduate student at the University of Windsor.

I declare that, to the best of my knowledge, my thesis does not infringe upon anyone's copyright nor violate any proprietary rights and that any ideas, techniques, quotations, or any other material from the work of other people included in my thesis, published or otherwise, are fully acknowledged in accordance with the standard referencing practices. Furthermore, to the extent that I have included copyrighted material that surpasses the bounds of fair dealing within the meaning of the Canada Copyright Act, I certify that I have obtained a written permission from the copyright owner(s) to include such material(s) in my thesis.

I declare that this is a true copy of my thesis, including any final revisions, as approved by my thesis committee and the Graduate Studies office, and that this thesis has not been submitted for a higher degree to any other University or Institution.

## ABSTRACT

The use of minimum quantity lubrication (MQL) machining, i.e. drilling and tapping of aluminum and magnesium alloys using very low quantities of cutting fluids was studied and the MQL machining performance was compared to dry and conventional flooded conditions. An experimental drilling station with an MQL system was built to measure torque and thrust force responses. Uncoated and diamond-like carbon (DLC) coated HSS drills were tested against 319 Al and AZ91 alloys using 10-50 ml/h of distilled water (H<sub>2</sub>O-MQL) and a fatty acid based MQL agent (FA-MQL).

The results indicated that H<sub>2</sub>O-MQL used in conjunction with non-hydrogenated DLC (NH-DLC) coatings reduced the average torque and thrust-force compared to dry cutting and achieved a performance comparable with conventional flooded drilling. At least 10<sup>3</sup> holes could be drilled using NH-DLC in H<sub>2</sub>O-MQL and uncoated HSS in FA-MQL in drilling of both 319 Al and AZ91. MQL drilling and tapping provided a stable machining performance, which was evident from the uniform torque and force patterns and also resulted in desirable hole surface, thread quality and chip segments. The maximum temperature generated in the workpiece during MQL machining was lower than that observed in dry drilling and tapping, and comparable to flooded conditions. The mechanical properties of the material adjacent to drilled holes, as evaluated through plastic strain and hardness measurements, revealed a notable softening in case of dry drilling, with magnesium alloys exhibiting a recrystallized grain zone, but not for MQL drilling. Softened aluminum and magnesium promoted adhesion to the tools resulted built-up edge formation and consequently high torques and thrust-forces were generated. NH-DLC coatings' low COF in H<sub>2</sub>O-MQL against 319 Al (0.10) and AZ91 (0.12) compared to uncoated HSS (0.63 and 0.65) limited the temperature increase during NH-DLC in H<sub>2</sub>O-MQL drilling and hence both torques and thrust forces were effectively reduced.

## **DEDICATION**

I would like to dedicate this dissertation to my parents for their unconditional love, support and encouragement.

## ACKNOWLEDGEMENTS

I would like to express my sincere gratitude to my advisor Dr. A. T. Alpas for his constant supervision, encouragement, support and patience during my graduate studies at the University of Windsor. Working under his expert guidance has been a great learning experience.

I would like to thank to Dr. M. Elmadagli a former graduate of NSERC/GM IRC for his valuable contributions to the initial stages to my research. I would like to profusely acknowledge the assistance of Drs. M.J. Lukitsch, Y. -T. Cheng, J.M. Dasch and T. Perry of the GM Global Research and Development for their valuable suggestions.

I would like to thank my dissertation committee members for their valuable suggestions to improve the research work. Special thanks go to Mr. Andy, Mr. P. Seguin, Mr. Robinson and the members of technical support center for their precious technical assistance.

I am grateful to all past and current researchers of the NSERC/General Motors of Canada Industrial Research Chair in Tribology of Lightweight Materials for their help and friendship. Useful discussions with Drs. E. Konca, S.S. Akarca and M. Shafiei all former graduates of GM IRC are greatly appreciated.

Financial support from NSERC and GM of Canada through an Industrial Research Chair Program at the University of Windsor is also gratefully acknowledged.



# TABLE OF CONTENTS

<b>DECLARATION OF CO-AUTHORSHIP/PREVIOUS PUBLICATION</b> .....	iii
<b>ABSTRACT</b> .....	v
<b>DEDICATION</b> .....	vi
<b>ACKNOWLEDGEMENTS</b> .....	vii
<b>LIST OF TABLES</b> .....	xiii
<b>LIST OF FIGURES</b> .....	xiv
<b>NOMENCLATURE</b> .....	xxii
<b>CHAPTER 1</b> .....	1
Introduction.....	1
1.1. Driving Force for Dry and Near-Dry Machining.....	1
1.2. Dry Machining of Aluminum and Magnesium and Associated Problems .....	2
1.3. Alternative Approaches to Feasible the Aluminum and Magnesium Machining.....	3
1.4. The Scope for the Current Study .....	4
1.5. Objectives .....	5
1.5.1. Minimum quantity lubrication drilling of Al-Si alloys (319 Al) in water using DLC coated drills .....	6
1.5.2. Tapping of Al-Si alloys (319 Al) with DLC coated taps and minimum quantity lubrication .....	6
1.5.3. Dry and minimum quantity lubrication drilling of cast magnesium alloy (AM60) .....	6
1.5.4. Minimum quantity lubrication drilling of a magnesium alloy (AZ91) using DLC coated drills .....	7
1.6. Organisation of the Dissertation .....	7
References.....	9
<b>CHAPTER 2</b> .....	10
Literature Review.....	10
2.1. Dry Machining (orthogonal) of Aluminum .....	10
2.2. Dry Drilling of Aluminum.....	16
2.3. Dry Drilling of Magnesium .....	21

2.4. Performance of Carbon Based Coatings against Aluminum Diamond-like Carbon .....	22
2.4.1. Tribological Behaviour of Diamond-Like Carbon Coatings .....	23
2.4.1.1. Effect of Hydrogen Content of the DLC Films .....	28
2.4.1.2. Tribological Behaviour of Diamond-Like Carbon Coatings at Elevated Temperatures.....	30
2.4.1.3. Tribological Behaviour of Diamond-Like-Carbon (DLC) Coatings in Lubricating System .....	36
2.5. Tapping of Ferrous Alloys .....	50
2.5.1. Tapping of Aluminum Alloys.....	52
2.6. Near-Dry Machining.....	53
2.6.1. Near-Dry Machining of Ferrous Alloys.....	53
2.6.2. Near- Dry Machining of Aluminum Alloys.....	57
2.6.3. Near- Dry Machining of Magnesium Alloys .....	63
2.7. Summary of Literature Review.....	63
<b>CHAPTER 3</b> .....	74
Minimum Quantity Lubrication Drilling of Aluminum-Silicon Alloys in Water using Diamond-Like Carbon Coated Drills.....	74
3.1. Introduction.....	75
3.1.1. Tribological Behaviour of DLC Coatings in Water and High Relative Humidity (RH)    76	
3.1.2. Effect of MQL on the Machining of Aluminum Alloys by Uncoated HSS and Carbide Tools.....	77
3.2. Experimental Approach .....	80
3.2.1. Workpiece Material: 319 Al Alloy .....	80
3.2.2. Properties of HSS and DLC Coated Drills.....	80
3.2.3. Drilling Tests and MQL Supply .....	82
3.2.4 Drilling Tests under Dry and Flooded Conditions.....	85
3.2.5.Measurement of Cutting Torque and Thrust Force.....	86
3.2.6.Characterization of Drill Surfaces .....	88
3.3. Results and Discussion .....	91
3.3.1 Flooded versus Dry Drilling of 319Al.....	91

3.3.2. Analysis of Torque Curves: Comparison between Dry and H <sub>2</sub> O-MQL Drilling	92
3.3.2.1. Uncoated HSS Drills .....	92
3.3.2.2. H-DLC coated HSS Drills.....	96
3.3.2.3. NH-DLC Coated HSS Drills.....	97
3.3.3. Analysis of Thrust Force: Comparison between Dry and H <sub>2</sub> O-MQL Drilling	100
3.3.3.1. Uncoated HSS Drills.....	100
3.3.3.2. H-DLC Coated Drills .....	101
3.3.3.3. NH-DLC Coated HSS Drills.....	102
3.4. Observation of Cutting Edge by Optical Microscope.....	105
3.5. SEM Observation of Drill Flutes .....	107
3.6. Conclusions.....	111
List of References .....	112
<b>CHAPTER 4</b> .....	116
Tapping of Al-Si Alloys with Diamond-like Carbon Coated Tools and Minimum Quantity Lubrication.....	116
4.1. Introduction.....	117
4.2. Experimental details.....	121
4.2.1. Description of Workpiece Material and Cutting Tools for Drilling and Tapping .....	121
4.2.2. Description of Drilling and Tapping Tests .....	123
4.2.3. Tapping Torque Measurements: Average Forward and Backward Torques ....	125
4.2.4. Selection of Tapping Speed and MQL Flow Rate .....	126
4.2.5. Temperature Measurements, Metallographical Inspections and DSC.....	129
4.2.6 Pin-on-Disk Tests.....	130
4.3. Discussion .....	142
4.4.1. The Role of COF.....	144
4.4.2. The Role of Subsurface Hardening.....	146
4.4.3 MQL Fluid Effects.....	146
4.4. Conclusions.....	149
List of References .....	150

<b>CHAPTER 5</b> .....	153
Dry and Minimum Quantity Lubrication Drilling of Cast Magnesium Alloy (AM60)..	153
5.1. Introduction.....	153
5.2. Experimental procedures and analyses .....	157
5.2.1. Workpiece Material and Cutting Tool .....	157
5.2.2. Drilling Tests .....	158
5.2.3. Average Cutting Torque and Thrust Force .....	162
5.2.4. Selection of MQL Flow Rate.....	163
5.2.5. Temperature Measurements.....	164
5.2.6. Metallography of Hole Microstructure, Surface Roughness and Tool Tips.....	165
5.3. RESULTS AND ANALYSES.....	166
5.3.1. Torque and Thrust Force Curves .....	166
5.3.1.1. Dry Drilling.....	166
5.3.1.2. MQL Drilling.....	170
5.3.1.3. Flooded Drilling.....	173
5.3.2. Temperature Increases During Drilling .....	176
5.3.3. Surface Roughness.....	177
5.3.4. Chip Morphology.....	180
5.4. Discussion .....	181
5.5. Conclusions.....	189
List of references.....	190
<b>CHAPTER 6</b> .....	194
The role of diamond-like carbon coated drills on minimum quantity lubrication drilling of magnesium alloys .....	194
6.1. Introduction.....	194
6.2. Experimental Details.....	198
6.3. Experimental Results .....	203
6.4. Discussion .....	210
6.5. Conclusions.....	218
List of References: .....	219
<b>CHAPTER 7</b> .....	222

Minimum quantity lubrication drilling of lightweight aluminum and magnesium alloys used in automotive components.....	222
7.1 Introduction .....	222
7.2. Experimental approach .....	228
7.2.1. Workpiece Materials: 319 Al and AM60 Mg.....	228
7.2.2. Cutting Tools .....	228
7.2.3. Drilling Test .....	228
7.2.4. MQL Supply .....	229
7.2.5. Measurements of Torque, Thrust Force and Temperatures .....	229
7.3. Results.....	230
7.3.1. Analysis of Torque Responses.....	230
7.3.1.1 Drilling of 319 Al.....	230
7.3.1.2 Drilling of AM60 Mg.....	233
7.3.2. Analysis of Thrust Force Responses.....	234
7.3.2.1. Drilling of 319 Al.....	234
7.3.2.2. Drilling of AM60 Mg.....	236
7.3.3. Temperature Increase.....	236
7.3.4. SEM Observation of Drill Flutes .....	237
7.3.5. Analysis of BUE Formation.....	241
7.4. Discussion .....	241
7.5. Conclusion .....	244
List of References .....	245
<b>CHAPTER 8</b> .....	246
General Discussions.....	246
8.1. Adhesion of Al to the tools and role of COF .....	247
8.2. The role of Subsurface Softening on Adhesion of Workpiece Materials to the Tools 250	
8.3. Role of MQL Fluid in Reducing Al and Mg Adhesion to the Tools .....	255
8.4 Comparison of Dry Drilling Behaviour of Aluminum and Magnesium using DLC Coated Drills .....	258
8.5. Consideration of parameters to optimize the MQL machining .....	262
<b>CHAPTER 9</b> .....	265

<b>SUGGESTIONS FOR FUTURE WORK</b> .....	267
<b>APPENDIX</b> .....	268
<b>VITA AUCTORIS</b> .....	271

## LIST OF TABLES

### **Chapter 3**

<b>Table 3.1:</b> Comparison of torque and thrust force during dry, H <sub>2</sub> O-MQL and flooded drilling.....	105
--	-----

### **Chapter 4**

<b>Table 4.1:</b> Torque, temperature, chip length and chip width during HSS-dry, DLC-dry, MO-MQL, FA-MQL and flooded tapping of 319 Al.....	152
--	-----

### **Chapter 5**

<b>Table 5.1:</b> Torque, thrust force, temperature, surface roughness, chip length, chip width and percentage of area covered by adhered magnesium during dry, FA-MQL, H <sub>2</sub> O-MQL and flooded drilling of AM60 magnesium alloy .....	193
---	-----

### **Chapter 6**

<b>Table 6.1:</b> Maximum torque, range of average torque and maximum temperature during drilling of AZ91 alloy using uncoated and NH-DLC coated HSS drill in different conditions. Average coefficient of friction and average wear rate during sliding of AZ91 against uncoated M2 steel in dry, H <sub>2</sub> O-MQL, and flooded conditions and NH-DLC coated M2 steel in dry and H <sub>2</sub> O-MQL conditions.....	221
--	-----

## LIST OF FIGURES

**Figure 2. 1** (a) Schematic illustration of the main steps of microstructural evolution in 1100 Al subjected to orthogonal cutting. (b) The sequence of grain refinement events shown on the cross-section of the material ahead of the tool tip [2.4]. ..... 11

**Figure 2. 2** TEM micrographs of primary deformation zone showing elongated subgrains and smaller equiaxed grains (indicated by arrows) formed during orthogonal machining of Al; and the corresponding selected area diffraction pattern 1100 [2.4]. ..... 13

**Figure 2. 3** (a) TEM micrographs of machined chips showing elongated subgrains and small equiaxed grains formed during machining of Al 1100; (b) Higher magnification TEM micrograph showing nano-scale equiaxed grains [2.4]. ..... 14

**Figure 2. 4** (a) Comparison of drilling power required to drill holes in unamended B319 alloy vs. B319 alloy with Bi additions. Each peak corresponds to one hole being drilled. (b) Power plot during drilling of three different alloys. Each peak corresponds to a single hole being drilled [2.11]. ..... 17

**Figure 2. 5** Effect of hard-lubricant coatings on spindle torque: (a) uncoated tool and (b) TiAlN+WC/C coated HSS tool. TiAlN+WC/C reduces the increase of torque at the end of the hole presumably due to its low friction property [2.14]. ..... 18

**Figure 2. 6** Friction coefficients of hydrogenated DLC films under various water vapor pressures [2.37]. ..... 24

**Figure 2. 7** (a) The wear rates, and (b) the steady state COF values of the non-hydrogenated DLC coating against 319 Al and WC under various test environments. Presence of water vapour significantly reduced the COF and wear rates of the NH-DLC coatings against both counterfaces. The applied load and sliding speed were 4.9 N and 0.12 m/s [2.30]. ..... 27

**Figure 2. 8** Wear rates of DLC as a function of temperature with inserts of 3D surface profile images of the wear tracks at 25 °C, 200 °C and 400 °C [2.45]. ..... 30

**Figure 2. 9** (a) The variation of the wear rate of NH-DLC coating with temperature when tested against 319 Al, WC and sapphire at 25, 120 and 300 °C. Tests were run for 1500 m of sliding distance ( $2.5 \times 10^4$  revolutions) at 25 °C and for 60 m of sliding distance ( $10^3$  revolutions) at 120 and 300 °C using 5 N applied load. (b) The COF curves between 80-V DLC coated disc and 319 Al pin at 25, 120 and 300 °C. Tests were run for 60 m of sliding distance ( $10^3$  revolutions) using 5 N applied load, at 0.12 m/s sliding speed [2.50]. ..... 34

**Figure 2. 10** Comparison of the hydrogenated and non-hydrogenated DLC at 25°C (relative humidity 40%): (a) friction coefficient of DLC against 319 aluminum alloy and (b) wear coefficient [2.51]. ..... 35

**Figure 2. 11** Comparison of the hydrogenated and non-hydrogenated DLC at 240°C: (a) friction coefficient of DLC against 319 Al (b) wear coefficient [2.51]. ..... 36

**Figure 2. 12** SEM back-scattered electron images showing the built-up edge and aluminum transfer after dry cutting AlSi9Cu1 alloy. (a) uncoated HSS, after 2.7 min cutting time; (b) TiAlCrYN coated tool, after 4.3 min cutting time; (c) DLC coated tool, after 2.6 min cutting time; (d) TiAlN/VN coated tool, after 5.3 min cutting time [2.62]. 42

**Figure 2. 13** Optical, bright-field images of the flank faces of the drills after 100 holes or (\*) failure, depending on which occurred first. Lower build-up of materials was found for non-hydrogenated DLC (Graphit-iC™) coated drill [2.64]..... 45

**Figure 2. 14** Power plots during drilling of the first 25 holes in 319 Al with different drill coatings. Each peak corresponds to one (1) hole being drilled. The non-hydrogenated DLC1 and DLC 2 possibly worse than uncoated HSS in that power rose to 8 H.P.[2.65]. ..... 46

**Figure 2. 15** Torque plots: (a, b) representing the holes 1–25 and 25–49 with uncoated HSS where the drill failed at hole no. 49; (c, d) representing the torque responses of holes 1–25 and 125–150 for H-DLC-coated drill; (e, f) representing the torque responses of holes 1–25 and 125–150 for NH-DLC-coated drill [2.66]. ..... 47

**Figure 2. 16** Optical image of drill cutting edge consisting of (a) uncoated HSS after 49 holes; (b) SEM of insert in plate (a); (c) optical image of the cutting edge of H-DLC-coated drill after 150 holes; (d) SEM image of insert in plate (c); (e) optical image of the cutting edge of NH-DLC-coated drill after 150 holes and (f) SEM images of insert of plate (e). Figures show the buildup edge (BUE) on the tip of the cutting edge and the metal transfer on the flank face [2.66]..... 48

**Figure 2. 17** SEM secondary electron images showing the aluminum adhesion to drill flutes: (a) schematic representation of drill flute showing the area investigated; (b) uncoated HSS tool; (c) H-DLC-coated tool and (d) NHDLC-coated tool. The flute surface of uncoated HSS drill was almost entirely covered by adhered aluminum. The direction of chip flow is shown by the arrow [2.66]..... 49

**Figure 2. 18** Torque recorded for a TiAlN-coated Co-HSS twist drill (type D) during (a) the 51<sup>st</sup> and (b) the 351<sup>st</sup> drilling cycle: comparison between drilling with minimum quantity of lubrication (18 ml/h) and dry drilling [2.84]. ..... 55

**Figure 2. 19** Adhesion of work material (Al 356) to the surface of the cutter in dry machining: a) Section through the rake face, (b) section through flank face, and c) section through clearance face, d) Al adhesion to the rake and flank face [2.89]..... 58

**Figure 2. 20** Adhesion of work material to the surfaces of the cutting tool in “wet” machining: a) Flood lubricant application, and b) MQL application [2.89]..... 59

**Figure 2. 21** Cutting force as a function of cutting distance, for different lubrication application strategies [89]. ..... 60

**Figure 2. 22** The relationship between flank wear and the cutting distance in machining with dry, MQL and flood coolant [2.89]..... 61

**Figure 2. 23** Effect of cooling system on flank wear for uncoated carbide inserts at the cutting speed of 500 m/min, feed rate of 0.2 mm/tooth and 2 mm depth of cut [2.91].... 62



**Figure 3. 1** Geometry of twist drill of 6.35 mm in diameter. The drill consists of two flutes with high helix angle of  $37^\circ$  and point angle of  $118^\circ$ . The flute length is 70 mm and the shank length is 30 mm. .... 81

**Figure 3. 2** (a) Experimental set-up with MQL reservoir. (b) Close up view showing the non-contact torque and thrust force sensor (rotor and stator), H<sub>2</sub>O-MQL nozzle and drilled 319 Al block. .... 83

**Figure 3. 3** Three types of torque–thrust curves generated during drilling: (a) a uniform torque and thrust force curve, (b) a steady-state increasing torque and thrust force curve, and (c) a typical torque curve with a spike. To calculate the average torque and thrust forces, data was taken from the onset of chip clogging to the retraction of the drill..... 84

**Figure 3. 4** (a) Locations of SEM images taken on the drill flute. (b) BSE image of a section of the drill flute of the NH-DLC coated drill tested under dry conditions ..... 85

**Figure 3. 5** Comparison of average torque responses of uncoated HSS drills (under dry and flooded conditions) with the NH-DLC coated drills in dry condition. The figure shows reduced data for clarity. The error bars indicate the standard deviation of torque data for each hole. .... 87

**Figure 3. 6** The average torque variations for (a) uncoated HSS drills using flooded coolant system, (b) H-DLC coated drills using flooded coolant system, and (c) NH-DLC coated drills using flooded coolant system. .... 89

**Figure 3. 7** Torque plots (a, b) representing the last 24 holes with uncoated HSS drills in dry and H<sub>2</sub>O-MQL conditions, where the drill failed at hole 49 in dry conditions (shown by asterisk [\*]); (c, d, e, f) showing the torque responses of the last 25 (126–150) holes drilled with H-DLC and NH-DLC coated drills in dry and H<sub>2</sub>O-MQL conditions. .... 90

**Figure 3. 8** The cumulative mass of adhered aluminum on uncoated HSS, H-DLC and NH-DLC coated drills in dry and H<sub>2</sub>O-MQL conditions..... 93

**Figure 3. 9** Percentage of total holes that exhibited torque spikes during drilling with uncoated and DLC coated HSS drills. .... 94

**Figure 3. 10** The average torque variations for the first 49 holes for uncoated HSS during (a) drilling in dry ([\*] failure) and (b) H<sub>2</sub>O-MQL conditions. The error bar indicates the standard deviation of data for each hole; (c, d, e, f) represent the average torque variations of 150 holes for H-DLC and NH-DLC coated HSS drills in dry and H<sub>2</sub>O-MQL conditions. .... 95

**Figure 3. 11** Thrust force plots (a and b) showing the last 24 holes with uncoated HSS drills during drilling in dry conditions (a) ([\*] represents tool failure by adhesion) and H<sub>2</sub>O-MQL (b) conditions; (c, d, e, f) representing the thrust force responses of the last 25 (126–150) holes during drilling with H-DLC and NH-DLC coated drills in dry and H<sub>2</sub>O-MQL conditions. .... 99

**Figure 3. 12** Percentage of total holes that exhibited thrust force spikes during drilling with uncoated and DLC coated HSS drills. .... 101

**Figure 3. 13** (a) Average thrust force variations for (1–49) holes for uncoated HSS in dry conditions ([\*] failure condition); (b) average thrust force variations of (1–150) holes for

uncoated HSS in H<sub>2</sub>O-MQL conditions; (c and d) average thrust force variations of (1–150) holes for H-DLC in dry and H<sub>2</sub>O-MQL conditions; (e and f) average thrust force variations of (1–150) holes for NH-DLC in dry and H<sub>2</sub>O-MQL conditions. .... 103

**Figure 3. 14** Optical images of drill cutting edge consisting of (a) uncoated HSS after 49 holes in dry conditions; (b) uncoated HSS after 150 holes in H<sub>2</sub>O-MQL conditions; (c) HDLC coated drill after 150 holes in dry conditions; (d) H-DLC coated drill after 150 holes in H<sub>2</sub>O-MQL conditions; (e) NH-DLC coated drill after 150 holes in dry conditions; (f) NH-DLC coated drill after 150 holes in H<sub>2</sub>O-MQL conditions. Figures show the built-up edge (BUE) at the tip of the drill’s cutting edge..... 104

**Figure 3. 15** The reduction of average torque and thrust forces with the reduction of average BUE height from dry to H<sub>2</sub>O-MQL condition for (a) uncoated HSS; (b) HDLC coated HSS and (c) NH-DLC coated HSS..... 106

**Figure 3. 16** SEM secondary electron images showing aluminum adhesion to drill flutes: (a, b) uncoated HSS in dry and H<sub>2</sub>O-MQL conditions; (c, d) H-DLC coated drill in dry and H<sub>2</sub>O-MQL conditions; (e, f) NH-DLC coated drill in dry and H<sub>2</sub>O-MQL conditions. The flute surface of the uncoated HSS drill was almost entirely covered by adhered aluminum. .... 109

**Figure 3. 17** Effect of H<sub>2</sub>O-MQL on the percentage of the drill flute surface area covered by adhered aluminum. H<sub>2</sub>O-MQL reduced the percentage of area covered by adhered aluminum significantly for both uncoated and coated drills..... 110

**Figure 4. 1** A schematic of tap ..... 122

**Figure 4. 2** Close-up view of the experimental set-up. .... 124

**Figure 4. 3** A typical tapping torque curve showing the zones of average forward and backward torque calculations..... 126

**Figure 4. 4** Preliminary experiments performed to determine the optimum tapping speed. .... 127

**Figure 4. 5** Preliminary experiments performed to determine the optimum FA-MQL flow rate..... 128

**Figure 4. 6** Average forward torques for dry tapping (uncoated HSS, DLC-coated HSS), MQL tapping using uncoated HSS (MO-, FA-MQL) and flooded drilling (MO tap oil) using uncoated HSS. .... 132

**Figure 4. 7** Variations of torques during the tapping of each hole with the time. (a) HSS-dry tapping; (b) DLC-coated HSS-dry tapping; (c) MO-MQL tapping with HSS; (d) FA-MQL tapping with HSS; (e) flooded tapping with HSS. .... 134

**Figure 4. 8** Typical chips generated during (a and b) HSS-dry tapping; (c and d) DLC-dry tapping; (e and f) FA-MQL tapping with HSS; (g and h) flooded tapping with HSS. .... 136

**Figure 4. 9** Variation of workpiece temperatures during the tapping of each hole with the time. (a) HSS-dry tapping; (b) DLC-coated HSS-dry tapping; (c) MO-MQL tapping with

HSS; (d) FA-MQL tapping with HSS; (e) flooded tapping with HSS. (f) Maximum temperature variations with number of holes..... 139

**Figure 4. 10** (a) A close-up view of the tap showing the area investigated. SEM secondary electron images showing adhesion of aluminum to the threads in (b) HSS-dry tapping, (c) DLC-dry tapping, (d) FA-MQL, and (e) flooded tapping with HSS..... 140

**Figure 4. 11** Optical micrograph showing the thread morphology for (a) HSS-dry tapping, (b) DLC-dry tapping, (c) FA-MQL and (d) flooded tapping with HSS. .... 142

**Figure 4. 12** (a) COF vs. number of revolutions during pin-on-disc sliding tests. (b) COF plotted against the maximum and average tapping temperatures. .... 143

**Figure 4. 13** (a) Schematic diagram of a tapped hole showing the plane where microhardness indentations were made and (b) an optical micrograph showing the Vickers indentation impressions. (c) Subsurface hardness variation with the depth from the hole surface. .... 148

**Figure 5. 1** (a) Schematic diagram showing the experimental set-up, (b) close-up view showing the non-contact torque and thrust force sensor (rotor and stator), MQL nozzle, infrared thermometer and AM60 magnesium alloy workpiece. .... 160

**Figure 5. 2** The three types of torque (black) and thrust force (grey) curves generated during drilling: (a) ‘Type A’: a uniform (steady-state) torque and thrust force curve observed in both H<sub>2</sub>O-MQL and FA-MQL drilling; (b) ‘Type B’: characterized by a continuous increase in torque and (c) ‘Type C’: a torque curve that showed an abrupt increase in torque, indicating chip clogging at the end of the drilling cycle—typically encountered during dry drilling. .... 161

**Figure 5. 3** Calibration experiments performed to determine the optimum MQL rate. Average torque variation is plotted against the number of holes for different rates of FA-MQL supply. No significant difference was observed between flow rates of 30, 20 and 10 ml/h, while using a flow rate of 5 ml/h resulted in higher torques. The error bar indicates the standard deviation of torque data for each hole. .... 164

**Figure 5. 4** Variations in the torque profiles generated during the drilling of each hole with the time. (a) Torque data representing the first 25 (1st–25th) and last 25 (54th–78th) holes under dry drilling conditions. The last hole drilled before drill failure is identified by an asterisk. (b) Torque responses for the first 25 and last 25 (126th–150th) holes drilled using FA-MQL.(c) Torque responses for the first 25 and last 25 (126th–150th) holes drilled using H<sub>2</sub>O-MQL. (d) Torque responses for the first 25 and last 25 (126th–150th) holes drilled using flooded conditions..... 169

**Figure 5. 5** Percentage of holes that exhibited different types of torque responses (Types A–C) using dry, FA-MQL, H<sub>2</sub>O-MQL and flooded drilling conditions..... 171

**Figure 5. 6** A comparison of average torques under dry, FA-MQL, H<sub>2</sub>O-MQL and flooded drilling conditions. The figure shows reduced data for clarity. The error bars indicate the standard deviation of torque data for each hole. .... 172

**Figure 5. 7** A comparison of the average thrust forces under dry, FA-MQL, H<sub>2</sub>O-MQL and flooded drilling conditions. The error bars indicate the standard deviation of thrust force data for each hole. .... 173

**Figure 5. 8** Workpiece temperature increase with the drilling time for: (a) dry drilling, (b) FA-MQL drilling, and (c) maximum temperature variations for the first 25 holes drilled using dry, FA-MQL, H<sub>2</sub>O-MQL and flooded conditions. .... 176

**Figure 5. 9** Three-dimensional optical surface profilometry images of typical surfaces for (a) dry drilling, (b) FA-MQL drilling, (c) H<sub>2</sub>O-MQL drilling, (d) flooded drilling and (e) schematic diagram of a longitudinal cross-section of a drilled hole, identifying the locations of five areas on hole surface from which the average surface roughness,  $R_a$ , was calculated. The topographical images shown in (a)–(d) are taken from the same location—closest to the drill tip. (f) Comparison of average surface roughness variations under dry, FA-MQL, H<sub>2</sub>O-MQL and flooded drilling conditions. .... 179

**Figure 5. 10** Low magnification optical images showing typical chip shape for (a) dry, (b) FA-MQL, (c) H<sub>2</sub>O-MQL and (d) flooded conditions. .... 180

**Figure 5. 11** (a) Schematic diagram of a quarter section of a drilled hole showing the plane (mid-section of the hole parallel to the workpiece surface) where microhardness indentations were made, and an optical micrograph of this section with the Vickers indentation impressions. Indentations were made in a direction normal to the hole surface, and to a depth of approximately 300  $\mu\text{m}$  below the surface, where the hardness of the bulk material (unaffected by the heat) could be attained. Measurements were taken three times at each depth. (b) Average hole sub-surface hardness variations with increasing the depth from the hole surface for dry, FA-MQL and flooded conditions. . 184

**Figure 5. 12** Cross-sectional optical micrographs showing (a) the initial position of a grain boundary between two adjacent grains. Grain boundaries were assumed to be perpendicular to the hole surface. (b) The displacement of the grain boundary after drilling and a schematic diagram showing the determination of deformation angle  $\theta$  from the slope of the deformed grain boundary. (c) Variation of the shear strain with depth for dry, FA-MQL, H<sub>2</sub>O-MQL and flooded drilling conditions. .... 185

**Figure 5. 13** SEM secondary electron images showing the adhesion of magnesium to the drill flutes: (a) dry, (b) FA-MQL, (c) H<sub>2</sub>O-MQL and (d) flooded conditions. (e) Percentage of the drill flute surface area covered by adhered magnesium for all drilling conditions. The locations of the SEM images taken on the drill flute and a back-scattered electron image of a section of the drill flute tested under dry conditions are also shown. The reported values are the averages of values obtained from five images of each drill. .... 186

**Figure 5. 14** (a) Schematic representation of drill flute showing the area on which EDS compositional analyses were performed. (b) SEM image of the drill flute in FA-MQL conditions. (c) EDS spectra of insert in plate (b). (d) SEM image of the drill flute in H<sub>2</sub>O-MQL conditions. (e) EDS spectra of insert in plate (d). (f) SEM image of the drill flute in flooded conditions. (g) EDS spectra of insert in plate (f). .... 188

<b>Figure 6. 1</b> Tool life comparisons of uncoated HSS drills in dry, H <sub>2</sub> O-MQL and flooded conditions and NH-DLC-coated HSS drills in dry and H <sub>2</sub> O-MQL conditions. The drills did not fail in HSS/flooded and NH-DLC/H <sub>2</sub> O-MQL conditions. ....	202
<b>Figure 6. 2</b> Torque variations for (a) HSS/dry of last 25 holes; (b) HSS/flooded of last 25 holes; (c) entire drilling cycle for NH-DLC/dry and (d) NH-DLC/H <sub>2</sub> O-MQL of last 25 holes. Typical torque curves for NH-DLC/dry and NH-DLC/H <sub>2</sub> O-MQL are shown in the insets of Fig. 2 (c) and Fig. 2 (d).....	205
<b>Figure 6. 3</b> The average torque comparisons for uncoated HSS in dry and flooded conditions and NH-DLC-coated drills in dry and H <sub>2</sub> O-MQL conditions.....	206
<b>Figure 6. 4</b> Temperature profiles of the first 25 holes for (a) HSS/dry; (b) HSS/flooded; (c) NH-DLC/dry and (d) NH-DLC/H <sub>2</sub> O-MQL.....	209
<b>Figure 6. 5</b> Maximum temperature variations for the first 25 holes during drilling in dry, H <sub>2</sub> O-MQL and flooded conditions using uncoated, dry, H <sub>2</sub> O-MQL conditions with NH-DLC-coated HSS drills. ....	210
<b>Figure 6. 6</b> (a) Schematic diagram of half a drilled hole showing the plane where microstructures were observed. Subsurface microstructures of the last hole for (b) HSS/dry; (c) HSS/flooded; (d) NH-DLC/dry and (e) NH-DLC/H <sub>2</sub> O-MQL. R <sub>x</sub> indicates recrystallized Mg grains.....	211
<b>Figure 6. 7</b> (a) Locations of SEM images taken on the drill flute. SEM images showing magnesium adhesion to drill flutes: (b) HSS/dry; (c) HSS/flooded; (d) NH-DLC/dry and (e) NH-DLC/H <sub>2</sub> O-MQL.....	212
<b>Figure 6. 8</b> (a) Locations of SEM images taken on the drill cutting edge. SEM images of the cutting edge for (b) HSS/dry; (c) HSS/flooded; (f) NH-DLC/dry and (g) NH-DLC/H <sub>2</sub> O-MQL. ....	213
<b>Figure 6. 9</b> COF curves with number of revolutions during the sliding of AZ91 pin against NH-DLC-coated disks in dry and H <sub>2</sub> O-MQL conditions and uncoated HSS in flooded conditions.....	216
<b>Figure 7. 1</b> (a) A uniform torque curve generated during drilling in FA-MQL. Typical torque curve with a spike (b) 319 Al; (c) AM60 Mg. To calculate the average torque and thrust forces, data was taken from the onset of chip clogging to the retraction of the drill. ....	226
<b>Figure 7. 2</b> The average torque variations of the first 49 holes for dry and first 150 holes for H <sub>2</sub> O-MQL, FA-MQL and flooded conditions for (a) 319 Al; (b) AM60 Mg.....	227
<b>Figure 7. 3</b> The cumulative mass of adhered aluminum and magnesium in dry and H <sub>2</sub> O-MQL,.....	231
<b>Figure 7. 4</b> The average thrust force responses of the first 49 holes for dry and first 150 holes for H <sub>2</sub> O-MQL, FA-MQL and flooded conditions for (a) 319 Al; (b) AM60 Mg. ....	232
<b>Figure 7. 5</b> Maximum temperature variations for the first 25 holes during drilling in dry, FA-MQL, H <sub>2</sub> O-MQL and flooded conditions (a) 319 Al; (b) AM60 Mg. ....	235

<b>Figure 7. 6</b> SEM secondary electron images showing aluminum and magnesium adhesion to drill flutes: (a, b, c, d) HSS drill in dry, H <sub>2</sub> O-MQL, FA-MQL and flooded conditions for 319 Al; (e, f, g, h) HSS drill in dry, H <sub>2</sub> O-MQL, FA-MQL and flooded conditions for AM60 Mg. ....	238
<b>Figure 7. 7</b> Optical micrographs of cutting edge after drilling of 319 Al in (a) dry; (b) H <sub>2</sub> O-MQL; (c) FA-MQL; (d) flooded conditions. Optical micrographs of cutting edge after drilling of AM60 Mg in (e) dry; (f) H <sub>2</sub> O-MQL; (g) FA-MQL; (h) flooded conditions. ....	239
<b>Figure 7. 8</b> The EDS spectra of inset in plate Figure 7.7 (a) and 7.7 (b) showing (a) the BUE was composed of Al and other alloying elements during drilling of 319 Al; (b) the BUE was composed of Mg, O and Al in drilling of AM60. ....	240
<b>Figure 8. 1</b> (a) COF vs. number of revolutions during pin-on-disk tests, where a 319 Al pin was sliding against DLC coated disk. (b) COF plotted against the maximum and average torque; (c) COF plotted against the maximum and average temperatures. The tests were done at the speed of 0.12 m/sec and at the load of 5 N. ....	250
<b>Figure 8. 2</b> (a) Schematic diagram of the hole with the inserted thermocouple. Temperature responses in dry, H <sub>2</sub> O-MQL and flooded conditions for (b) 319 Al and (c) AM60 Mg. ....	253
<b>Figure 8. 3</b> (a) Schematic diagram of a quarter section of a drilled hole showing the plane (mid-section of the hole parallel to the workpiece surface) where microhardness indentations were made. Average hole sub-surface hardness variations with increasing the depth from the hole surface for dry, FA-MQL and flooded conditions (b) 319 Al and (c) AM60 Mg. ....	254
<b>Figure 8. 4</b> NMR analysis of MQL showing (a) the presence of S-based additives and (b) the presence of P-based additives. A proton NMR ( <sup>1</sup> H) in CHCl <sub>3</sub> environment was chosen to identify the additives in MQL agent. ....	256
<b>Figure 8. 5</b> DSC spectra for (a) conventional flooded tap oil and (b) MQL. Thermal analysis was performed using a DSC-TGA Q600 manufactured by TA Instrument at a heating rate of 10 °C/min. Argon gas was used to prevent oxidation of the samples. After heating, nitrogen-cooling was used for all runs. Exothermic peak reveals the thermal degradation of lubricants. ....	257
<b>Figure 8. 6</b> COF curves with number of revolutions during the sliding of AZ91 and 319 Al pin against NH-DLC-coated disks in dry and H <sub>2</sub> O-MQL conditions and uncoated HSS in flooded conditions. The applied load and sliding speed were 5 N and 0.12 m/sec. ....	261
<b>Figure 8. 7</b> The flow chart for the MQL machining processes of aluminum and magnesium. ....	262

## NOMENCLATURE

### Abbreviations

COF	Coefficient of friction
CVD	Chemical vapour deposition
DM	Dry machining
DLC	Diamond- like carbon
H-DLC	Hydrogenated diamond- like carbon
HSS	High speed steel
MQL	Minimum quantity of lubrication
NDM	Near- dry machining
NH-DLC	Non- hydrogenated diamond like carbon
PECVD	Plasma enhanced CVD
Ra	Average surface roughness
RH	Relative humidity
RPM	Revolution per minute
SEM	Scanning electron microscope
TM	Trade mark

# CHAPTER 1

## Introduction

### 1.1. Driving Force for Dry and Near-Dry Machining

Concerns about environmental issues have emphasized the importance of reduction or total elimination of the use of metal removal fluids (MRF's) in the manufacturing industry. Government regulations for example in North America, the National Institute for Occupational Safety and Health (NIOSH) recommends that occupational exposures to cutting fluid aerosols be limited to  $0.5 \text{ mg/m}^3$  from its current standard value of  $5 \text{ mg/m}^3$ . Detrimental effects of cutting fluid aerosols on machine shop workers and the environment are well documented [1.1, 1.2]. Thus, elimination of the use of metalworking fluids will have a substantial impact on the improvement of the quality of the working environment.

The elimination of use of cutting fluid has the potential of providing economic benefits. The process of recycling dry chips does not consist of a cleaning operation before their reuse in another form. According to [1.3, 1.4], the cost of fluid filtration, disposal and maintenance of the cutting fluid system is estimated to be about 17% of the overall manufacturing cost. It makes intuitive sense that a cut on the manufacturing cost will result in economic benefits for both the manufacture and consumer. However, at present the complete elimination of cutting fluids is not possible as they have their advantages and functions. A viable alternative to conventional flood machining is the application of cutting fluids in very small quantities to the small area where actual machining takes place. This technique, as explained in Chapter 2, is also known as the



minimum quantity of lubrication (MQL) method. The cutting fluid in flood cooling has an important function of removing heat from cutting zone. With the depleted amount of cutting fluid in case of MQL the heat removal function will be affected, but the cutting fluid in MQL can provide sufficient lubrication to prevent the generation of heat in the first place [1.5].

## **1.2. Dry Machining of Aluminum and Magnesium and Associated Problems**

North American automotive manufactures have been constantly seeking new ways of increasing fuel efficiency of their vehicles by reducing the mass of the vehicles. Substitute steel or cast iron with aluminum and magnesium alloys brings approximately 66% and 78% reduction in weight due to the lower density of the latter (2.7, 1.7 vs. 7.8 g/cm<sup>3</sup>). For this reason, automotive companies have been interested in replacing steel or cast iron components with those made of Al and Mg wherever possible. Nowadays, most of the engine components such as block engine, upper valve components and some chassis parts are made out of different aluminum and magnesium alloys.

The dry machining (i.e. machining without the use of MRF's) of steel and other ferrous materials is a relatively established technology, but the dry machining especially dry drilling of aluminum and magnesium has proven difficult due to aluminum and magnesium's adhesion to the drill [1.6, 1.7]. The chips that adhere to the drill, particularly to the high speed steel (HSS) drills create obstacles to chip evacuation through the drill flutes. Such chip clogging often results in rapid drill failure. The clogged

drills do not last long in service; the average number of holes that an uncoated high speed steel drill can achieve in dry drilling of 319 Al and AM60 Mg alloy block is less than 70, far from meeting the goal of  $1 \times 10^4$  holes set by the industry [1.6, 1.7].

### **1.3. Alternative Approaches to Feasible the Aluminum and Magnesium Machining**

As abundant metal removal fluid is harmful for human health and environment, it is a promising concern to develop alternate process to facilitate the dry machining of aluminum and magnesium. To accomplish this, the steel or carbide tool can be coated with a material which is chemically inert to and magnesium and aluminum or recently, a new environment-friendly technique has been developed when small quantities of lubricant are fed to the cutting edges of the tool, called minimum quantity of lubrication (MQL) or near- dry machining (NDM).

The term MQL is generally used to refer to the supply of the lubricant in the form of an aerosol. When oils are used as the MQL medium, the emphasis is on their good lubrication properties. Their function is to reduce friction and adhesion between the workpiece, the chip and the tool [1.6]. Thus, the amount of friction heat generated is also reduced. Consequently, the tool and the workpiece are exposed to less heat than they would be if the machining operation was performed completely dry [1.7].

In MQL operations, the MQL agent used is generally straight oil, but some applications have also utilized an emulsion or water. These fluid media are fed to the tool and/or machining point in the rate of ml/hr. This is done with the help of an air stream. In

this case, the medium is atomized in a nozzle to form extremely fine droplets, which are then fed to the machining point in form of a spray [1.7- 1.8].

MQL eliminates the following cost associated with conventional MRF:

1. The use of MQL as ml/hr instead of l/min helps to reduce the volume of conventional MRF significantly. Thus reducing both the cost of purchasing and disposing of conventional cutting fluid.
2. The installation of MQL equipments is rather simpler. In MQL process the machine tool components like lubricant filters are not necessary. Shed plates and sloped floors that allow continuous, direct draining to the metal removal fluid system that prevents stagnation or chip accumulation is not required.
3. The entire process is environmentally friendly i.e. there is no fluid to treat, recycle or dispose of. The fluid itself is 100% biodegradable, and is consumed in the process.

#### **1.4. The Scope for the Current Study**

Some tool coatings cannot tackle the excessive aluminum adhesion. Traditional hard coatings like TiN, TiAlN, TiCN, etc exhibit poor performance in machining of aluminum alloys due to strong adhesion and chemical reactions. An alternative is carbon based coatings which have been shown an improved performance due to their low friction property and minimum aluminum and magnesium adhesion under ambient condition. An attempt can be made to evaluate the cutting performance of such carbon

based coatings i.e. diamond-like carbon (DLC) coatings over the uncoated HSS during dry machining of aluminum and magnesium alloys.

Another aspect is now demanding, which understands the feasibility of minimum quantity of lubrication (MQL) technique when discharging very small amounts of cutting fluids with compressed air. One of the primary driving forces behind the implementation of MQL is waste reduction. In the North America, approximately 3% of its annual gross domestic product (GDP) is spent on Machining, out of which the cost of coolants and cutting tools is approximately 7.5%. Based on these statistics, it seems incomprehensible why all innovations and activities for cost improvement in machining during the past few decades have neglected the minimization of cutting fluids. For example, in manufacturing camshaft for engines, the increasing costs associated with the use and disposal of cutting fluids is up to 17% per part manufactured [1.5]. To enhance the cutting performance of both coated and uncoated tools during dry drilling in aluminum and magnesium alloys, this recent environmentally friendly and cost effective technique should be assessed. The effects of the water MQL process were considered in this study (Chapter 3 and Chapter 6) not only because water provides an environmentally sustainable MQL fluid, but also because DLC coatings revealed favourable tribological properties under high humidity.

## **1.5. Objectives**

The objective of this work was to assess whether minimum quantity lubrication (MQL) drilling and tapping of aluminum and magnesium alloys is advantageous over the dry and to consider whether the use of MQL can demonstrate a comparable performance

to conventional flooded drilling and tapping conditions. The objectives of this work are elucidated in the following four groups:

#### **1.5.1. Minimum quantity lubrication drilling of Al-Si alloys (319 Al) in water using DLC coated drills**

1. To assess the cutting performance of conventional uncoated HSS and diamond-like carbon (DLC) coated drills by measuring the torque and thrust forces generated during dry and water MQL (H<sub>2</sub>O-MQL) drilling.
2. Identify the types and stages of the torque and thrust force curve.
3. To study the transfer and adhesion of aluminum to both cutting edges and drill flute surfaces.

#### **1.5.2. Tapping of Al-Si alloys (319 Al) with DLC coated taps and minimum quantity lubrication**

1. To study the feasibility of deep hole drilling and tapping using hydrogenated diamond-like carbon in conjunction with H<sub>2</sub>O-MQL.
2. To study the mechanism of aluminum transfer to the threads and the formation of built- up edge and thread quality.

#### **1.5.3. Dry and minimum quantity lubrication drilling of cast magnesium alloy (AM60)**

1. To investigate the effect of fatty acid based MQL (FA-MQL) agent on the cutting torque and thrust forces of uncoated HSS tool.
2. To study the effect of FA-MQL on the adhesion of magnesium to the drill and hole surface quality.

#### **1.5.4. Minimum quantity lubrication drilling of a magnesium alloy (AZ91) using DLC coated drills**

1. To assess the drilling performance of uncoated HSS and diamond-like carbon (DLC) coated drills by measuring the torque, thrust forces and temperature generated during dry, H<sub>2</sub>O-MQL and flooded drilling.
2. To investigate the mechanism of materials transfer to the tools in dry, H<sub>2</sub>O-MQL and flooded drilling conditions.

### **1.6. Organisation of the Dissertation**

**Chapter 1** gives a general introduction on dry and MQL machining, the scope of current study and the general objective of this dissertation.

**Chapter 2** gives a literature survey on types of machining process, dry machining of aluminum and magnesium alloys, tribological behaviour of diamond like carbon (DLC) coatings, performances of DLC coatings in aluminum machining and the near-dry machining of aluminum alloys and magnesium alloys.

**Chapter 3** includes the results and discussion of the cutting performance of conventional uncoated HSS and DLC coated HSS by measuring the torque and thrust forces generated during dry and H<sub>2</sub>O-MQL drilling in 319 Al (Al-6.5% Si). The results also compared with the conventional flooded drilling condition.

**Chapter 4** explains the details of the investigations of the tapping performance of uncoated and DLC coated taps during deep hole tapping of 319 Al in dry, H<sub>2</sub>O-MQL and

flooded conditions. The cutting performances were assessed by measuring torque, thrust force and temperature generated during drilling, which are well discussed in this chapter.

**Chapter 5** clarifies the effect of MQL agents (water and fatty acid) during drilling in a cast magnesium alloys (AM60) with uncoated HSS. The comparison between cutting performance in dry and MQL condition in terms of torque, thrust force, hole quality, chip morphology and characterization of transferred materials to the tools are also discussed.

**Chapter 6** describes the minimum quantity water lubrication and dry drilling behaviour of a cast magnesium alloy (AZ91) using non-hydrogenated DLC coated HSS drills. A correlation between coefficient of friction (COF) and drilling temperature was established and hence both drill wear and magnesium adhesion are effectively discussed.

**Chapter 7** describes the minimum quantity lubrication drilling of automotive power components using H<sub>2</sub>O-MQL and a fatty acid based MQL agents (FA-MQL). The performance of H<sub>2</sub>O-MQL and FA-MQL using uncoated HSS in drilling of 319 Al and AM60 are discussed.

**Chapter 8** includes the general discussion of the present work and establishes a relation between the laboratory tests to the industrial MQL machining processes.

**Chapter 9** includes the overall summary of the dissertation.

## References

- [1.1] H.K. Tonshoff, W. Spintig, W. König, A. Neises, Machining of holes, developments in drilling technology, *Annals of the CIRP* 43/2 (1994) 551-561.
- [1.2] A. Rivero, G. Aramendi, S. Herranz, L.N. Lopez de Lacalle, An experimental investigation of the effect of coatings and cutting parameters on the dry drilling performance of aluminum alloys, *International Journal of Advanced Manufacturing Technology* 28 (2006) 1–11.
- [1.3] International Standard, ISO 14001, Environmental management systems-specification with guidance for use, First Edition, 1996-09-01.
- [1.4] US National Institute for Occupational Safety and Health Publication No 98-102, Occupational exposure to metalworking fluids: a criteria for a recommended standard, January (1998) 1, 2, 44, 143.
- [1.5] A.D. Kardekar, Modeling and optimization of machining performance measures in face milling of automotive aluminum alloy A380 under different lubrication/cooling conditions for sustainable manufacturing, MASC Thesis, University of Kentucky (2005) 1-5.
- [1.6] S. Bhowmick, M.J. Lukitsch, A.T. Alpas, Dry and minimum quantity lubrication drilling of cast magnesium alloy (AM60), *International Journal of Machine Tools and Manufacture* 50 (2010) 444- 457.
- [1.7] S. Bhowmick, A.T. Alpas, Minimum quantity lubrication drilling of aluminum-silicon alloys in water using diamond-like carbon coated drills, *International Journal of Machine Tools and Manufacture* 48 (2008) 1429-1443.



## CHAPTER 2

### Literature Review

Machining is a process of the removal of excess material from a component in order to impart to it the required dimension and finish. The importance of the machining process can be appreciated by the fact that nearly every device produced today has one or more machined surface or holes. Research into this field is mainly driven by the need to improve cutting techniques, which may further ramify into improvements in the productivity, greater precision of finished product, and longevity of the same, as well as advancement in the rate and efficiency of production. This chapter reviews the open literature on the drilling process involved in the dry machining and near-dry machining of aluminum alloys. It begins by providing a brief literary description of the existing literature on the dry (orthogonal) machining of aluminum alloys (**Section 2.1**), whereas **Section 2.2** focuses on the dry drilling of aluminum alloys. **Section 2.3** concentrates on the tribological behaviour of diamond-like carbon (DLC) coatings--including data from testing done at elevated temperatures and in lubricating systems, as well as the performance of carbon based coatings in aluminum machining. **Sections 2.4** and **2.5** discuss the existing literature regarding the near-dry machining of ferrous and non-ferrous materials, with an emphasis on aluminum and magnesium alloys.

#### 2.1. Dry Machining (orthogonal) of Aluminum

Chips are removed from the workpiece material during machining by a process of intense plastic deformation at a high strain rate within the primary and secondary shear zones that subjects the cutting face to high temperature and pressure. Tool wear becomes severe during dry machining due to high friction and heat accumulation. Aluminum

alloys are extensively used for manufacturing components for automotive and aerospace industry. High strength-to-weight ratio and good surface finish provided by these alloys are the primary reason for their popularity. Depending on the alloying elements present and the heat treatment given to these alloys, they exhibit a vast range of mechanical properties [2.1-2.2]. During dry machining of an aluminum alloy, the tool wear is mainly caused by the formation of an adhesive aluminum layer and built-up edge [2.3], both of which greatly affect the quality of the machined surface.

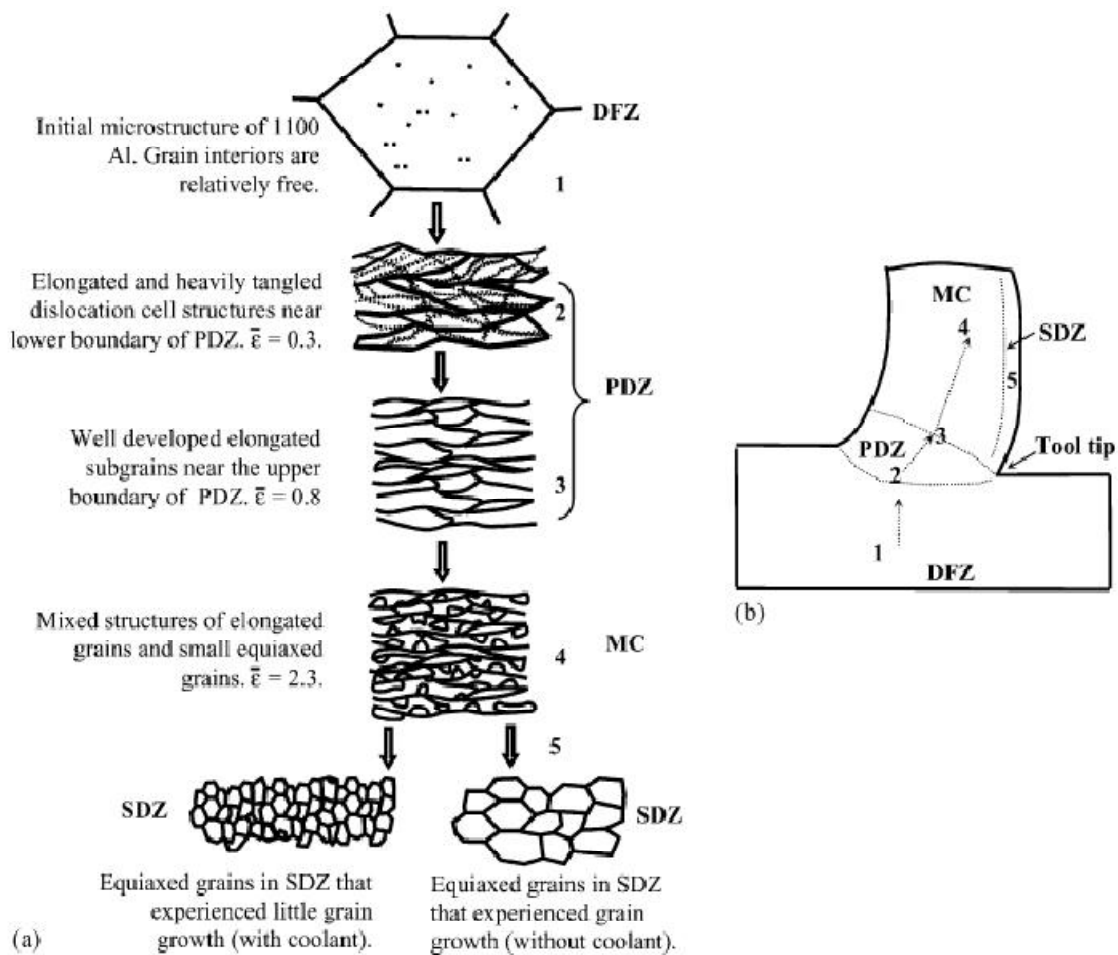


**Figure 2. 1** (a) Schematic illustration of the main steps of microstructural evolution in 1100 Al subjected to orthogonal cutting. (b) The sequence of grain refinement events shown on the cross-section of the material ahead of the tool tip [2.4].

List et al. [2.3] used a WC-Co tool for the orthogonal cutting of the aluminum alloys 2024-T351 (3.8-4.9 Cu, 0.1% Cr, 0.5% Fe, 1.2-1.8 Mg) under dry conditions at the cutting speed of 6 and 60 m/min. The results suggested that adhesion of workpiece materials to the tools surface and the formation of built-up edge (BUE) was the main reason for tool failure for both speeds.

Ni et al. [2.4] studied the microstructure generated during orthogonal cutting of Al 1100. Samples were examined under TEM and a mechanism was proposed for evolution of microstructure during the process, as is shown in **Fig. 2.1**. The small elongated subgrains resulted from the initial grain structure fragmenting into smaller grains at relatively lower strains as are present at the lower boundary of the primary deformation zone, with the boundaries between these units accommodating the lattice misorientation that accompany the process. Elongated subgrains with almost dislocation free interiors and smaller equiaxed grains are formed as strains increased further. Sections from the primary deformation zone showed the presence of grains elongated along the direction of the induced strain, forming lamellar structure when examined under TEM (**Fig. 2.2**). The microstructure present in the zone was found to be considerably smaller than the bulk microstructure with newly formed grains showing almost identical orientation in the primary deformation zone. Evidence for recrystallization in the zone was also found in the form of the presence of very small grains (**Fig. 2.3**). The chip microstructure was also investigated and revealed elongated grains and high volume fraction of small equiaxed grains with aspect ratio the same as those formed in the primary deformation zone, which showed that there was no further refinement in grain size after passing through the primary deformation zone, even as the plastic strains increased in magnitude from around

0.8 in the primary deformation zone to 2.3 in the chip. Based on the microstructural evidence, it was concluded that dynamic recrystallization started as strains rose to about 1.0 and was completed in the secondary deformation zone where evidence of extensive grain growth was found.

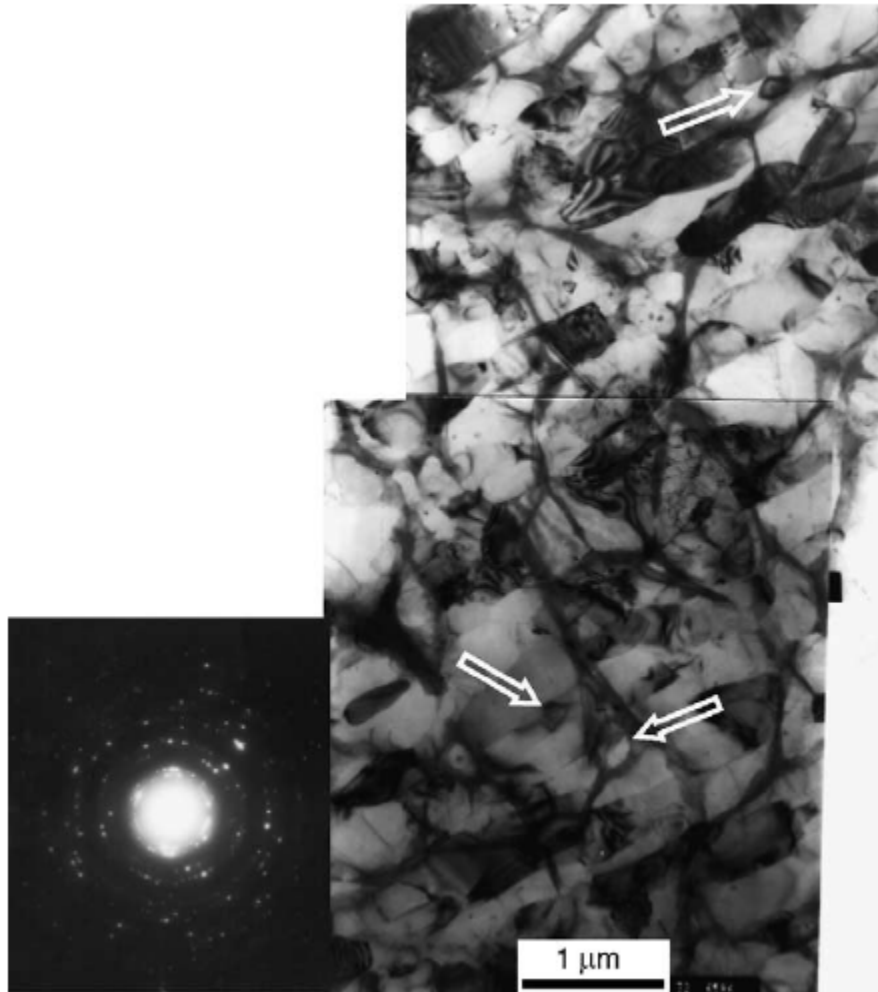


**Figure 2. 2** TEM micrographs of primary deformation zone showing elongated subgrains and smaller equiaxed grains (indicated by arrows) formed during orthogonal machining of Al; and the corresponding selected area diffraction pattern 1100 [2.4].

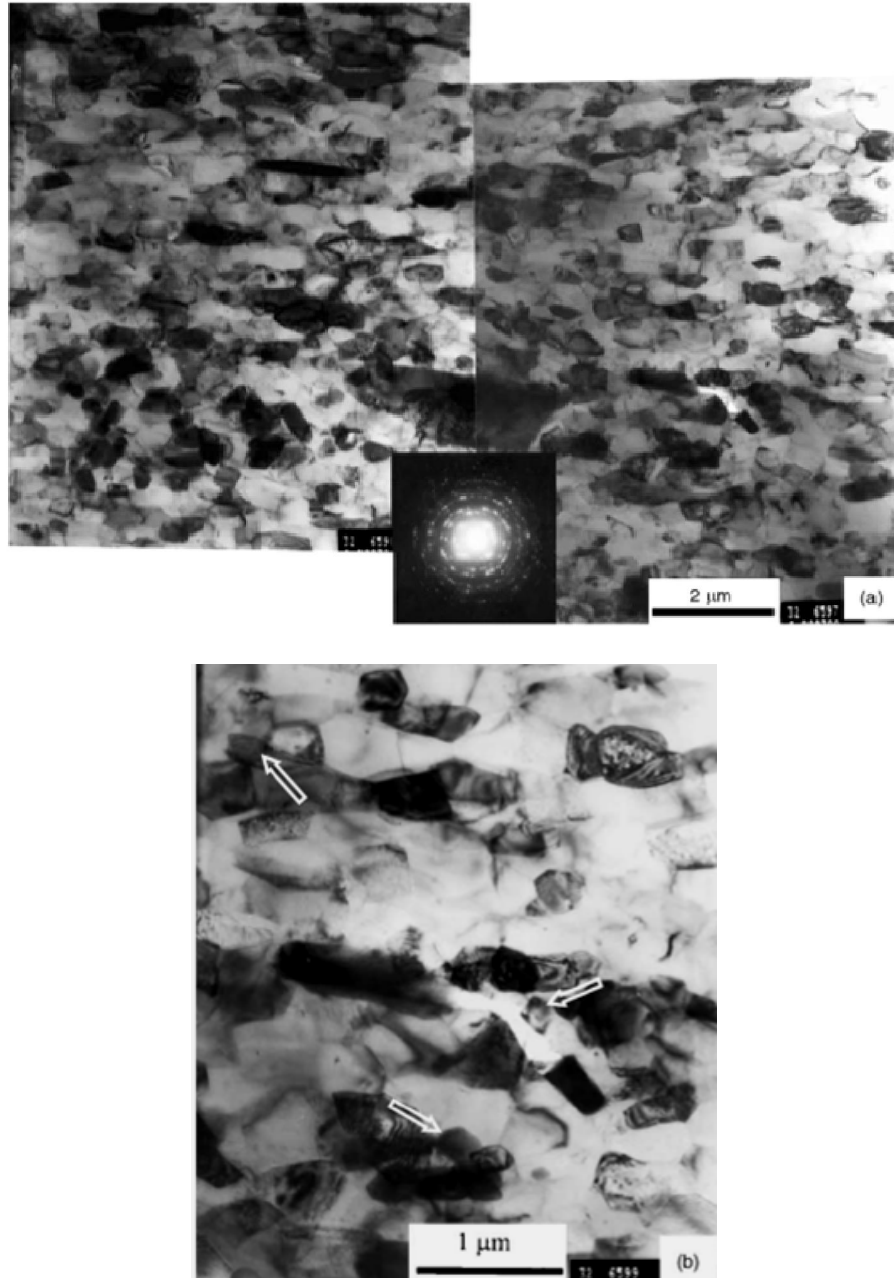


**Figure 2. 3** (a) TEM micrographs of machined chips showing elongated subgrains and small equiaxed grains formed during machining of Al 1100; (b) Higher magnification TEM micrograph showing nano-scale equiaxed grains [2.4].

Most researchers who study dry machining focus their attention on determining plastic deformation during chip formation and establishing a stress-strain relationship using a quick-stop device. Jasper et al. [2.5] studied the material behaviour in the

orthogonal cutting of steel AISI 1045 and aluminum AA 6082-T6 and established a model to measure the stress-strain in the deformation zone. They discovered large deformation imposed on the workpiece material at high speeds in very small areas. They also proposed that the shear strain in the primary shear zone is very large and that the workpiece is sheared considerably to equivalent strains in the order of 1 and 1.5 in the case of aluminum alloys.

Song et al. [2.6] observed the deformation microstructures of the material ahead of the tool tip during the orthogonal cutting of 1100 Al under feed rates of 0.25 and 0.80 mm/rev. They developed a stress-strain relationship using a Voce type exponential equation. A saturation flow stress of 302 MPa was found for 1100 Al. They also observed that the energy consumption increased as the depth of the cut increased, at the same feed rate. The increment was approximately 165% when the depth of the cut increased from 0.25 mm to 0.80 mm.

Zhang and Alpas [2.7] studied the deformation microstructures that developed in the material ahead of the tool tip in the 6061 Al alloy during an orthogonal cutting process and found that the plastically deformed zone in the material at the tool tip penetrated to a distance of 400  $\mu\text{m}$  below the cutting line. They calculated the equivalent strain along the distance from the cutting line with the largest strains occurring in the material at the rake face, 300  $\mu\text{m}$  above the tool tip.

Basavakumar et al. [2.8] studied the influence of grain refiner and turning inserts (uncoated and diamond coated) on the cutting force and surface integrity when turning Al-12Si and Al-12Si-3Cu cast alloys in dry environments using a lathe machine. They found that the combined addition of grain refiner and modifier (Al-1Ti-3B-Sr) to Al-

12Si–3Cu cast alloy showed lower cutting forces and improved surface finish compared to untreated alloys. They also found that the performance of the diamond coated insert resulted in lower cutting forces and the workpiece surface roughness compared to uncoated inserts. Also, the tendency for material build-up at the cutting edge was reduced when a diamond coated insert was used.

## **2.2. Dry Drilling of Aluminum**

The dry machining, especially dry drilling of aluminum, is exceedingly difficult due to the tendency of aluminum to adhere to the drill. The hot chips that are formed during drilling tend to adhere to the steel or carbide drill, creating an obstacle for the ejection of chips through the drill flutes, and ultimately resulting in drill failure. A process must be developed to facilitate the dry drilling of aluminum, and tool coatings are one of the most significant variables used to mitigate excessive aluminum adhesion. The ability to select an appropriate tool coating would provide better performance during the dry drilling of aluminum [2.9]. But traditional hard coatings such as TiN, TiC, CrN, and AlN have displayed unfavourable tribological performance compared to the uncoated HSS in the machining of aluminum alloys due to their strong adhesive and chemical reactions with aluminum [2.10]. Previous studies of the dry drilling of aluminum alloys are discussed below:

Dasch et al. [2.11] studied the effect of Bi (0.5%) and Sn (0.5%) on the dry drilling of 319 Al. The authors measured the power generation in drilling and found that the addition of Sn to 319 Al reduced the power by 60% and 85% compared to the 0.5%

Bi and base 319 Al (**Fig. 2.4**). The authors suggested that low melting point of Sn (232 °C) provided a lubricious effect in drilling.

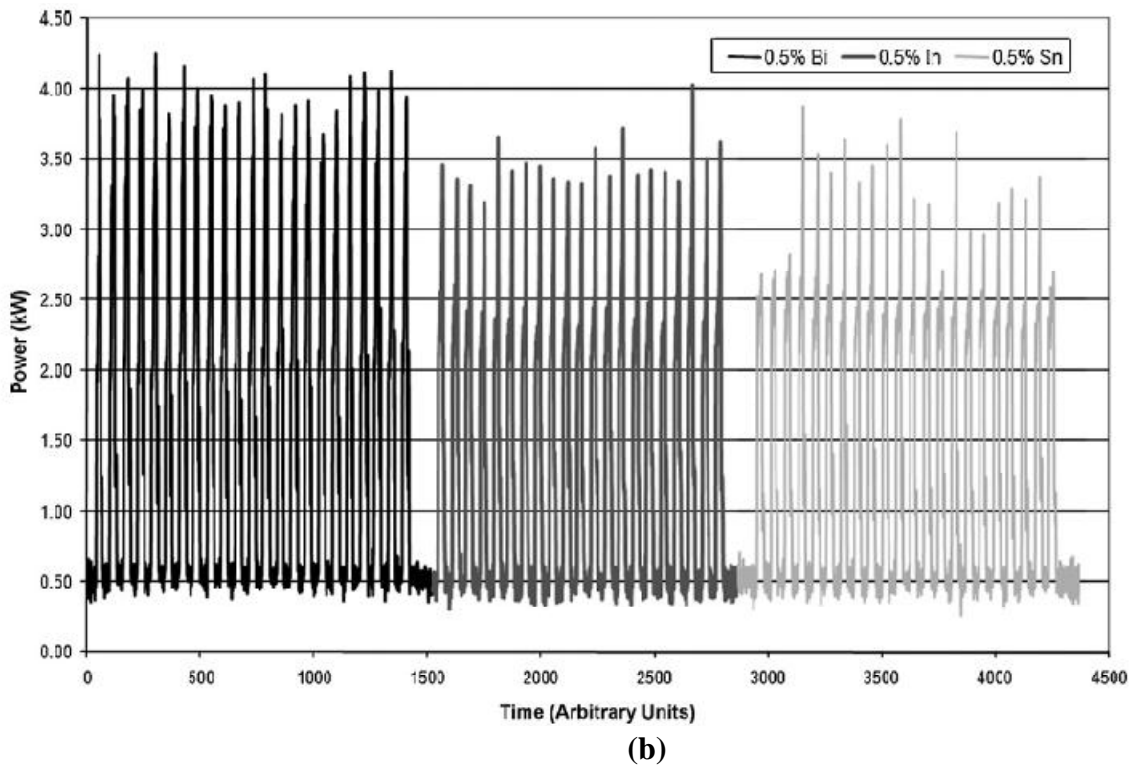
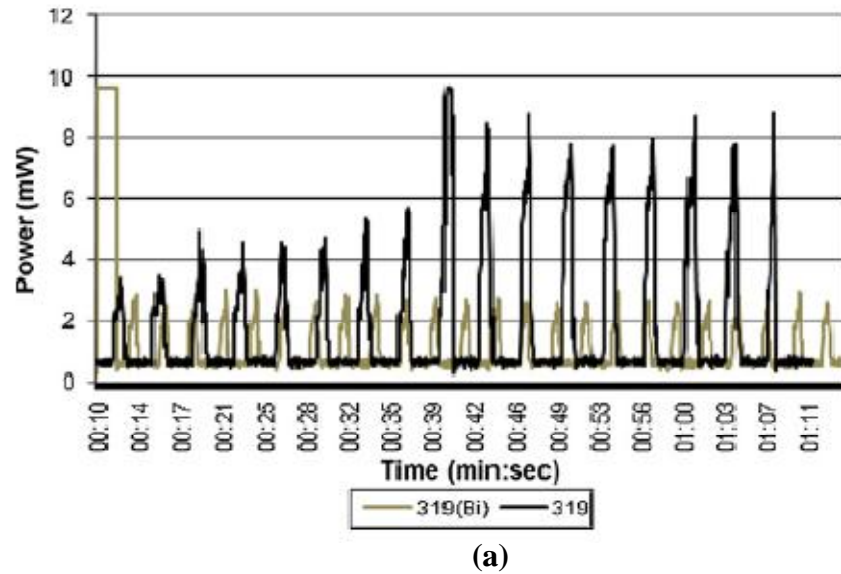


**Figure 2. 4** (a) Comparison of drilling power required to drill holes in unamended B319 alloy vs. B319 alloy with Bi additions. Each peak corresponds to one hole being drilled. (b) Power plot during drilling of three different alloys. Each peak corresponds to a single hole being drilled [2.11].



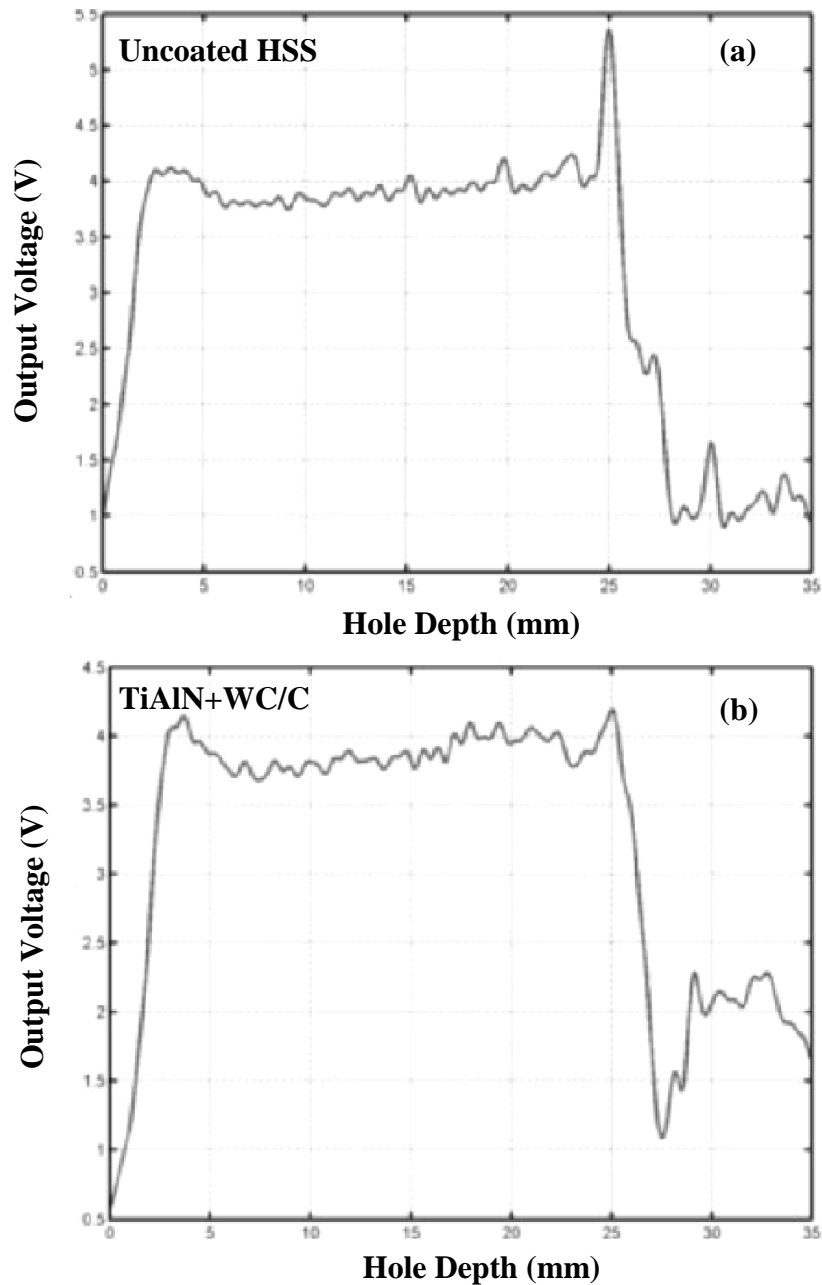


**Figure 2. 5** Effect of hard-lubricant coatings on spindle torque: (a) uncoated tool and (b) TiAlN+WC/C coated HSS tool. TiAlN+WC/C reduces the increase of torque at the end of the hole presumably due to its low friction property [2.14].

Chen and Alpas [2.12] studied the effect of Bi (0.5-1.0)% in dry orthogonal cutting of Al-16 wt.% Si and found that the cutting force reduced from 490 N to 425 N when the amount of Bi increased from 0% Bi to 1% Bi. The authors suggested that the addition of Bi helped to produce discontinuous chips compared to base alloys.

Kalidas et al. [2.13] performed the dry and conventional flooded drilling of 356 Al with TiAlN/TiN (multilayer, 0.0-5.0  $\mu\text{m}$  thickness) and TiAlN (1.5-5.0  $\mu\text{m}$  thickness) coated HSS drills. The authors measured the torque and thrust force in two speed (1600, 2200 rev/min) and feed rate (0.083, 0.162 mm/rev) combinations. The hole depth was 10 mm. The authors found that conventional flooded drilling produced high torque (4.0 N-m) and thrust force (550 N), whereas in dry conditions the torque and thrust force were 2.0 N-m and 450 N, respectively. The authors observed extensive chip clogging in flooded drilling compared to dry drilling. The authors also reported similar average surface roughness ( $R_a$ ) readings for the drilled holes that ranged from 0.78 to 4.91  $\mu\text{m}$  when machining in conventional flooded condition, whereas readings of 5.56 -9.68  $\mu\text{m}$  were attained when drilling in dry conditions.

Rivero et al. [2.14] observed an increased trend of torque and power with feed rates (0.2-0.6 mm/rev) in the speed range of 150-250 m/min during the dry drilling of 7075-T6 aluminum alloy using a TiAlN+WC/C coated drill. A uniform torque pattern (4.0 N-m) was also found using a TiAlN+WC/C coated drill, with respect to uncoated tools (5.5 N-m). **Fig. 2.5** displays torque spikes at the end of the hole when an uncoated tool is used--indicating that the chips need to be pushed out along the flute of the drill, thus requiring a higher force. On the other hand, the presence of a lubricant layer allows the chips to glide along the flute more easily when a TiAlN+WC/C coated drill is used.

Tash et al. [2.15] studied the effect of metallurgical parameters such as cooling rate and hardness on the drilling performance of Sr-modified and heat treated 356 (8 h, 540  $^{\circ}\text{C}$ ) and 319 (8 h, 495  $^{\circ}\text{C}$ ) aluminum alloys at 11000 rpm (speed) and 0.10 mm/rev (feed rate). They concluded that the cutting force and torque are slightly influenced by

cooling rates. As the heat treatments increase the hardness of the materials (110 HB), both cutting force (400 N) and torque (30 N-m) increased with the hardness compared to base alloys (88 HB).

Based on torque and thrust force, Sakurai et al. [2.16] investigated the effect of feed rate (0.15, 0.5, 1.0 mm/rev) in drilling of aluminum alloys (A1050, A2017 and A6061) at a constant rotational speed of 1500 rpm. The torque and thrust force increased with the increase in feed rates. The authors found that the drilling of A1050 (max. torque 11 N-m and thrust force 2500 N) was significantly more difficult than drilling the A2017 (max. torque 5.5 N-m and thrust force 1900 N) and the A6061 (max. torque 4 N-m and thrust force 1500 N) due to long chips and extensive adhesion to the tools.

Naito et al. [2.17] found an undesirable roundness error in the drilled hole when drilling hypereutectic Al-Si alloys (Al-20%Si). They observed an alteration in torque and its fluctuations in both dry and flooded conditions where dry conditions produced a higher torque (approx. 4.5 N-m) than that found in flooded conditions (2.0 N-m). They concluded that a higher torque was required under dry conditions with an increased number of holes and that the excess size of the holes was always significant for holes that had been drilled in dry conditions.

Bono et al. [2.18] studied that roundness errors tend to range from 0 to 26  $\mu\text{m}$  during the drilling of cast aluminum alloy A319. While hole diameters varied depending on the depth of the part, the roundness variations within individual holes ranged from 17 to 26  $\mu\text{m}$ . They also analyzed many competing effects to determine the final shape of a hole, including the wandering of the drill or built-up edge formation, the wandering of the drill point during initial entry into the workpiece, the running out of the machine spindle,

the vibration of the drill and the machine and cutting at the drill margins, and the dynamic deflection of the drill due to unbalanced forces. The hole drilled in the 319 Al had a bell shape and was smaller at the top than at the bottom.

### **2.3. Dry Drilling of Magnesium**

The low density of magnesium, i.e.  $1.74 \text{ g/cm}^3$ , which is approximately two-thirds that of aluminum ( $2.70 \text{ g/cm}^3$ ) and one-fifth of iron ( $7.87 \text{ g/cm}^3$ ), makes it attractive for applications where weight reduction is critical, for example, in the automotive, aerospace, and other industries. Magnesium alloys offer good strength-to-weight ratio, machinability, and corrosion resistance [2.19]. The machinability of magnesium alloys has been reported to be good and characterized by low cutting force and well broken chips [2.20]. Nevertheless, dry machining, especially dry drilling of magnesium alloys, is exceedingly difficult because the reaction between magnesium and atmospheric air causes ignition of fine particles [2.21]. This section reviews the existing literature of the drilling of magnesium alloys.

Gariboldi [2.22] investigated the cutting performances of uncoated HSS and TiN, CrN and ZrN coated HSS drill during the drilling in magnesium alloy (AM60). All drilling tests were performed at a constant speed of 63 m/min with different feed rates of 0.27, 0.37, and 0.50 mm/rev. It was found that the TiN coated HSS drill showed better cutting performance in terms of tool life (6.3 m) than the uncoated HSS (4.2 m), CrN (3.9 m), and ZrN (1.4 m) coated HSS drill at the low feed rate (0.27 mm/rev). However, at high feed rate (0.50 mm/rev), CrN (22.1 m) showed better performance than the uncoated HSS (10.3 m), TiN (14.3 m), and ZrN (16.8 m) coated HSS drill. All tools failed due to extensive adhesion of magnesium to the cutting edge and drill flutes.

Fang et al. [2.23] measured the temperature generated during high speed dry milling of magnesium alloy (AZ91) using a contact thermocouple. The tools used were micro grained tungsten carbide tools. They found that the temperature increased with the increase of cutting speeds (408-1088 m/min). The maximum temperature was as high as 302 °C at the cutting speed of 1088 m/min.

Tonshoff and Winkler [2.24] investigated the performance of polycrystalline diamond coatings during the dry turning of magnesium alloy (AZ91). The cutting speed and feed rate were 900 m/min and 0.4 mm/rev. Polycrystalline diamond showed uniform force responses when compared to uncoated carbide tools. Flank build-up was observed during the cutting with uncoated and TiN coated carbide tools. No significant amount of BUE was observed during machining with polycrystalline diamond coated tools.

## **2.4. Performance of Carbon Based Coatings against Aluminum Diamond-like Carbon**

Diamond is considered to be one of the best engineering materials because it is the hardest and stiffest material, and it has the highest thermal conductivity at room temperature. Also, it is transparent over a wide range of wavelengths, and it is chemically inert. These greater properties attracted researchers to use diamond based materials in applications which require high hardness and stiffness and in applications which require chemical stability and thermal conductivity [2.25]. Generally, materials with high hardness and stiffness have high wear resistance although there is not a direct relationship. Diamond-like coatings were used in a wide area of applications including

optical windows, magnetic data storage, car parts, biomedical applications, micro-electromechanical systems (MEMS), and machine tools. Because traditional hard coatings have displayed weak performance when machining aluminum alloys [2.26], researchers have attempted carbon based tool coatings such as diamond or diamond-like carbon (DLC) that have achieved improved performance during the machining of aluminum alloys due to their low friction properties and chemical inertness when in contact with aluminum [2.27, 2.28-2.30].

### **2.4.1. Tribological Behaviour of Diamond-Like Carbon Coatings**

This section will review the tribological behaviour of DLC coatings. To date, DLC coatings have accomplished superior tribological performance and are attracting scientific and industrial attention because of their low coefficient of friction and wear rates. Aluminum does not stick to DLC coatings under ambient conditions, a common property of DLC coatings regardless of their structure and hydrogen content [2.26].

DLCs can be applied using different deposition techniques such as plasma assisted chemical vapour deposition (PACVD) [2.31], cathodic arc deposition [2.32], ion beam deposition [2.33], and magnetron sputtering PVD [2.34]. Graphite and hydrocarbon gas ( $\text{CH}_4$ ) are the most common source materials in DLC deposition. Various types of DLC coatings are usually deposited by the above techniques. These are:

- [I] Amorphous carbon (a-C) with mainly  $\text{sp}^2$  bonds, and tetrahedral amorphous (ta-C) with mainly  $\text{sp}^3$  bonds.
- [II] When hydrogen is added in the structure of the DLC film, DLC can be denoted as a-C:H and ta-C:H.

[III] The doping of metals in DLCs extends their high temperature stability and these are designated as Me:C and Me:C:H (Metallic DLC) .

A detailed explanation of the deposition and characterization of DLC coatings can be found in [2.6].

The tribological behaviour of DLC coatings is influenced by testing conditions, including temperature, applied load, speed, water vapour, and other gaseous species in the test environment.

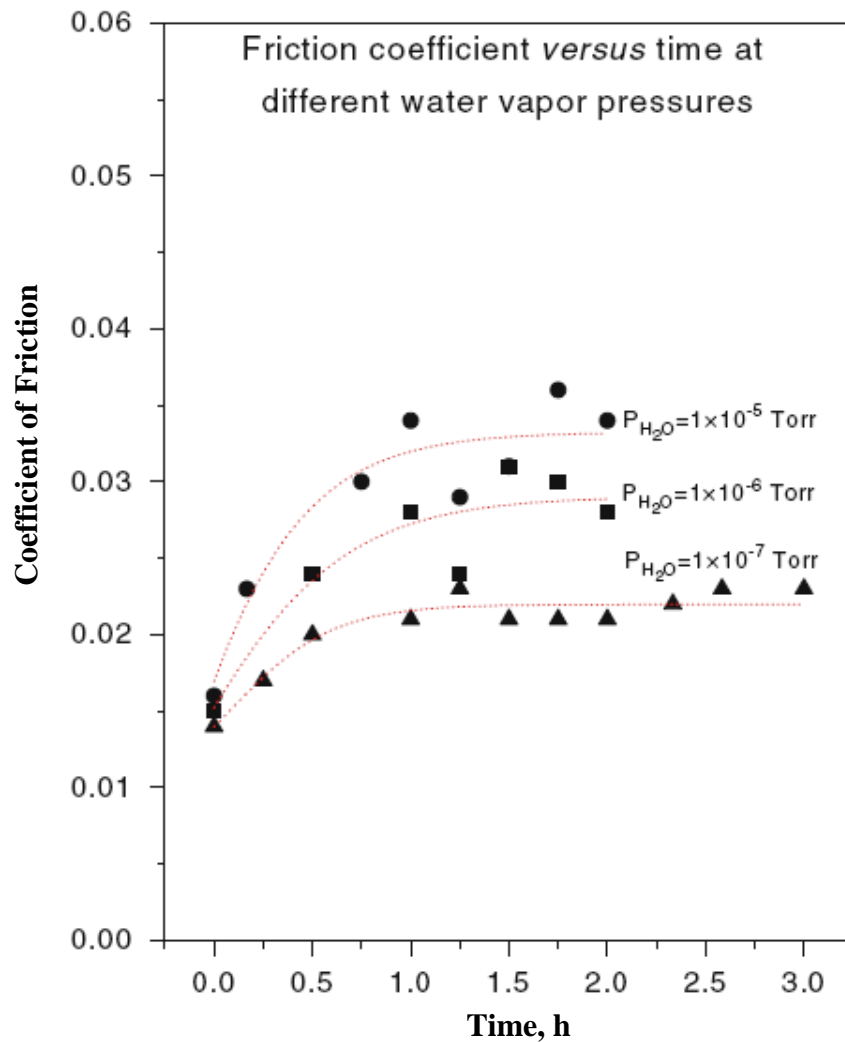


**Figure 2. 6** Friction coefficients of hydrogenated DLC films under various water vapor pressures [2.37].

Heimberg et al. [2.35] investigated the friction behaviour of DLC coatings under controlled environments including dry nitrogen, dry, and ambient air. They performed friction tests with a reciprocating ball-on-flat tribometer in a nominally dry nitrogen environment at speeds 0.01 to 5 mm/s. They observed very low COF 0.003-0.008 at speeds above 1 mm/s, but the COF increased to 0.01-0.1 at lower speeds (<0.5 mm/s) in dry and ambient air. It was pointed out that gas-surface interactions play a strong role in friction behaviour. Andersson et al. [2.36] conducted sliding tests between hydrogenated DLC coated steel surfaces by a pin-on-disc machine under 1 N load and varying sliding speeds in the range 0.025-0.075 m/s under vacuum environment. They have reported that hydrogenated films exhibit COFs of 0.01 under vacuum, but if water vapour is added to the environment, COF increased to 0.07 linearly with vapour pressure. On the other hand, in non-hydrogenated films, the COF was measured to be 0.6 under vacuum and decreased to 0.07 with the introduction of water vapour into the chamber. A similar result was also reported by Gao et al. [2.37] who carried out ball-on-disk friction tests on hydrogenated DLC films coated on steel surfaces under vacuum environment. They reported an increase in COF with the increase in water vapour pressure as shown in **Fig. 2.6**. In addition, they observed that introduction of oxygen, nitrogen, and hydrogen did not affect the friction significantly. On the other hand, Kim et al. [2.38] reported an increase of COF with the addition of oxygen, as well as addition of water vapour. They explained the change in the COF due to oxygen and water vapour addition by Auger electron spectroscopy analysis, and it was claimed that the increase of friction COF is due to the weakly adsorbed gas molecules that influence the friction property by physically separating the hydrogenated DLC interface. Konca et al. [2.30] studied the effects of test



atmosphere (vacuum, nitrogen, dry air) on the tribological behaviour of the NH-DLC against 319 aluminum alloy. The authors found high coefficients of friction (COF [0.46, 0.47, and 0.44]) and high wear rates ( $2.48 \times 10^{-4}$ ,  $3.60 \times 10^{-4}$ , and  $6.64 \times 10^{-5}$  mm<sup>3</sup>/m) for the NH-DLC coatings in vacuum, nitrogen, and dry air (0% RH). In air with a relative humidity of 20% RH, however, a lower COF (0.16) and low wear rate ( $2.31 \times 10^{-6}$  mm<sup>3</sup>/m) were observed (**Fig. 2.7**). Tay et al. [2.38] observed the frictional behaviour of tetrahedral amorphous carbon (ta-C) films under different test conditions (applied load, static sliding partners-steel, sapphire, and silicon nitride balls) and a variety of testing environments (nitrogen, oxygen, and low/high humidity). The authors recorded low COFs when the amorphous carbon films slide against a sapphire ball in all environments, which process is thought to be the formation of the interfacial film (due to tribochemical reactions) and strongly depends on the reactive species such as oxygen or hydrogen. Donnet [2.39] studied the tribological behaviour of DLC films doped with Si, F, N, and various metals. Doping with Si reduced the internal stress, surface energy, and COF of the DLC films. The tribological performance of the metal doped DLC films was almost independent in humidity compared to the undoped DLC films.

Liu et al. [2.40] investigated the correlation between graphitization and the frictional behaviour of H-DLC films (2 μm thicknesses deposited on SiC substrate). The tests were done in a pin-on-disk arrangement at sliding velocities between 0.06 and 1.6 m/s under 1 and 10 N loading levels using ZrO balls as the pin material. The authors concluded that sliding velocity and contact load have an immense influence on the graphitization process, and suggested that higher sliding velocities would increase the contact frequency and temperature, thereby assisting the release of hydrogen atoms from

the  $sp^3$  bond structure. Higher loading increases the shear deformation that helps to transform the weakened hydrogen-depleted DLC structure into graphite.

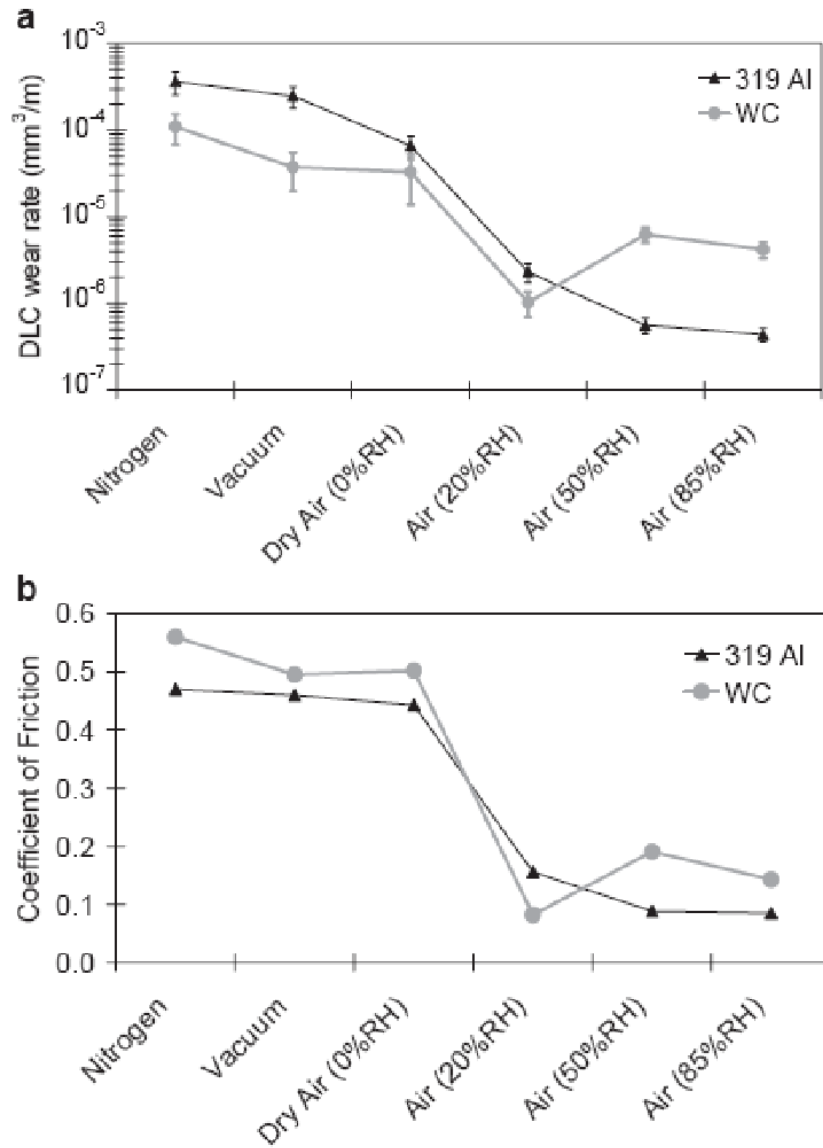


**Figure 2. 7** (a) The wear rates, and (b) the steady state COF values of the non-hydrogenated DLC coating against 319 Al and WC under various test environments. Presence of water vapour significantly reduced the COF and wear rates of the NH-DLC coatings against both counterfaces. The applied load and sliding speed were 4.9 N and 0.12 m/s [2.30].

### 2.4.1.1. Effect of Hydrogen Content of the DLC Films

The presence of hydrogen in the DLC film is the most important factor when determining its tribological behaviour in different environments [2.39-2.44]. As mentioned earlier, hydrogen has a strong effect on the properties of DLC films, and most DLC films contain significant amounts of hydrogen. For NH-DLC films, hydrogen content is in the order of 1-2%, and in H-DLC films there is 10-50% of hydrogen. Incorporation of hydrogen was generally carried out by using a reactive gas containing hydrocarbons in deposition process. Hydrogen causes the formation of more  $sp^3$  bonded carbon and properties close to diamond. The films which contain different amounts of hydrogen contents have different physical properties such as refractive index, hardness, internal stress, and tribological behaviours in controlled conditions [2.39].

Erdemir [2.41] has carried out a comprehensive analysis on the effect of H-DLC films in tribological properties. H-DLC films coated on steel surfaces were produced using a PECVD under various reactive gases, and friction properties of films were measured by sliding DLC surfaces on each other under various environments by a ball-on-disc machine. It was reported that NH-DLC exhibit high friction (COF = 0.25) under dry  $N_2$ , however H-DLC showed very low friction (COF < 0.005) in these environments due to elimination of strong carbon-carbon interaction by hydrogen. It was observed that H-DLC shows low friction only under inert gas and vacuum conditions, but in ambient air their COF significantly increased. On the other hand, NH-DLC exhibit low friction in the presence of moisture or other species in the environment. It was believed that the reason for super low friction of H-DLC films under vacuum and inert gas environment is due to the elimination of strong covalent and  $\pi$ - $\pi^*$  interactions at sliding DLC interfaces,

plus better shielding of carbon atoms by di-hydration. Ronkainen et al. [2.42] studied the tribological performance of H-DLC (~30% H) and NH-DLC films where the H-DLC was deposited using a radio frequency (rf) (13.56 MHz) plasma and the NH-DLC was deposited by using the pulsed vacuum arc discharge technique. The counterparts were polished balls (10 mm dia) made of AISI 52100 steel (100 Cr 6) and alumina ( $\text{Al}_2\text{O}_3$ ). They found that the lowest friction coefficient values for NH-DLC were 0.1, while the COF of the H-DLC was 0.02 in a normal atmosphere. The authors also found that the COF of the NH-DLC film in dry air (0% relative humidity) was 0.71, but when the coating was doped with hydrogen, the friction coefficient decreased. They concluded that the tribological performance was usually dominated by the presence of hydrogen.

Donnet et al. [2.43] studied the effect of hydrogen on DLC films during tribological testing with a pin-on-flat configuration, using a reciprocating motion over 2 mm at a sliding speed of 1 mm/s and a maximum Hertzian contact pressure of 0.5 GPa. Two kinds of H-DLC films (34 and 40% H) were deposited on silicon substrates by dc PECVD from acetylene at two different substrate biases (-800 and -500 V). The authors found that the films with a higher hydrogen content (40%) exhibited a super low COF of 0.005 when compared to DLC films (COF 0.01) with a hydrogen content of 34%.

Donnet and Grill [2.44] observed the tribological behavior of DLC films in ultra high vacuum (UHV). The H-DLC films were deposited by d.c. PACVD process where the substrate was polished 440 C steel ( $R_a < 0.1 \mu\text{m}$ ). They tested six H-DLC films to cover a wide range of hydrogen content: 20, 24, 28, 30, 34 and 42% H. The authors did not note any significant difference in COF based on the hydrogen content in ambient

conditions. However, in UHV the H-DLC films with a high hydrogen content (42%) showed a low COF of 0.02 when compared to H-DLC with 34% H (COF = 0.5).

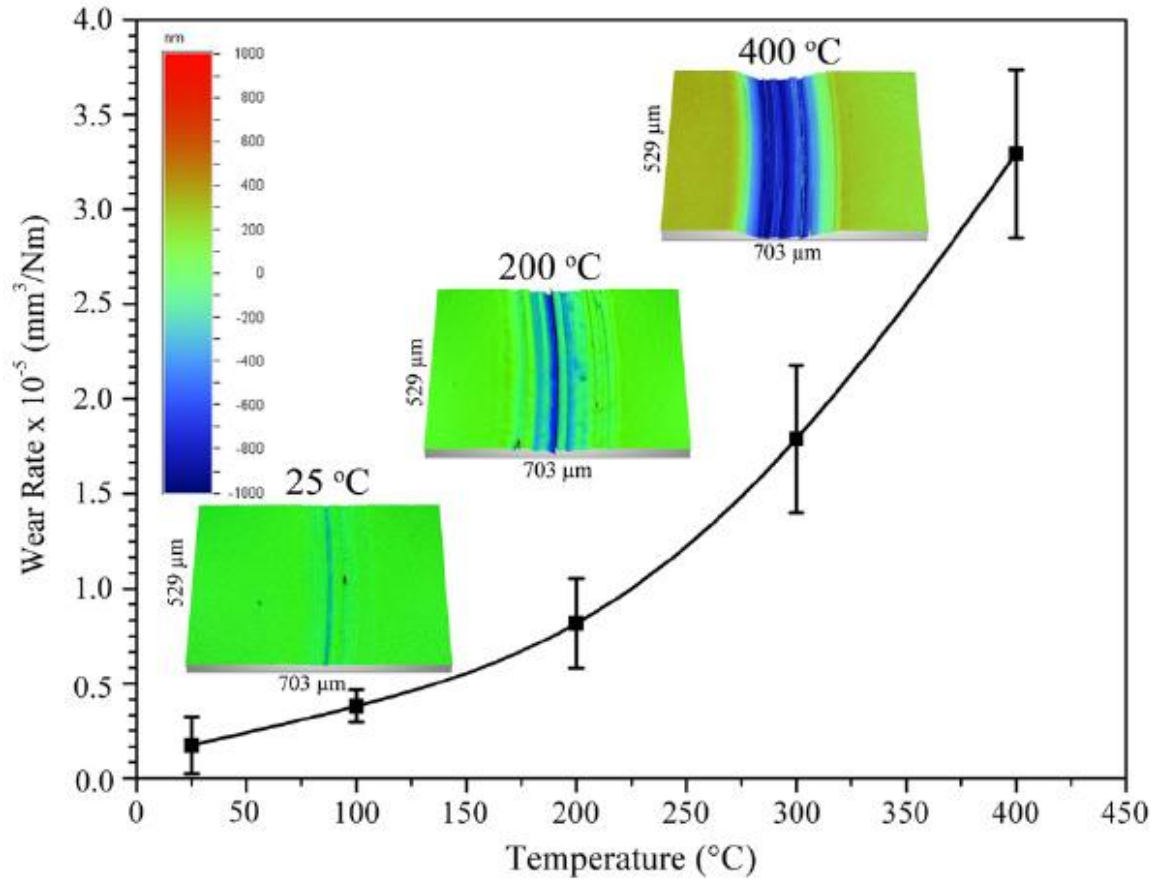


**Figure 2. 8** Wear rates of DLC as a function of temperature with inserts of 3D surface profile images of the wear tracks at 25 °C, 200 °C and 400 °C [2.45].

#### 2.4.1.2. Tribological Behaviour of Diamond-Like Carbon Coatings at Elevated Temperatures

In machining, heat is released during chip formation due to extensive plastic deformation, making it important to understand the tribological performance of the DLC coatings at elevated temperatures. It has been shown that increasing the test temperature

increases the wear rate of the DLC coatings against aluminum, and there is a temperature limit above which the DLC coatings graphitize and oxidize quickly [2.26].

Gharam et al. [2.45] studied the high temperature tribological behaviour of DLC coatings in sliding contact with 319 Al. The tests were done at 25, 100, 200, 300 and 400 °C at the 0.1 m/s linear speed and under constant normal load of 5.0 N. Results revealed that the COF decreased from room temperature (0.20) to 200 °C (0.06) but increased at 300 °C (0.3) to 400 °C (0.65). At high temperatures, a significant amount of adhered aluminum was observed in wear track. The wear rate of DLC increased from  $0.2 \times 10^{-5}$  mm<sup>3</sup>/Nm to  $3.5 \times 10^{-5}$  mm<sup>3</sup>/Nm when the temperature increased from 25 to 400 °C (**Fig. 2.8**).

Vanhusel et al. [2.46] studied the wear behaviour of diamond-like coatings (H-DLC containing 35% H) against corundum balls from ambient conditions to 300 °C using a low-amplitude oscillatory test machine. They found a lower COF of 0.07 at 300 °C compared to that recorded in ambient conditions (0.13). The wear scars became larger as the temperature increased, and the authors found structural changes ( $sp^3$ - $sp^2$  change and dehydrogenation) on the top of the surface layer when the coatings were simultaneously exposed to load and heat.

Krumpiegl et al. [2.47] studied the tribological behaviour of three different DLC coatings, such as NH-DLC, H-DLC and Ti-doped H-DLC against steel at high temperatures (up to 450 °C) and in high vacuum (up to  $3 \times 10^{-3}$  Pa). At 450 °C, the NH-DLC coating failed rapidly (10 m sliding distance), displaying an increased coefficient of friction from 0.35 to 0.6. H-DLC and Ti-doped H-DLC achieved a longer sliding distance (100 m) and only showed a slow increase of the COF from 0.30 to 0.55. The authors

revealed a drastic drop in the hardness of each coating after heating them to 450 °C, a detail that was thought to be related to the heavy oxidation of the coatings.

Bremont et al. [2.48] observed the tribological behaviour of H-DLC (10% hydrogen) coated 100C6-steel samples in pin-on-disc configuration at 25 °C, 200 °C and 400 °C. From room temperature to 200 °C, the COF did not exceed 0.3, but reached 0.6-0.7 at 400 °C. They concluded that the degradation of the DLC coating was due to structural modification and the softening of the substrate.

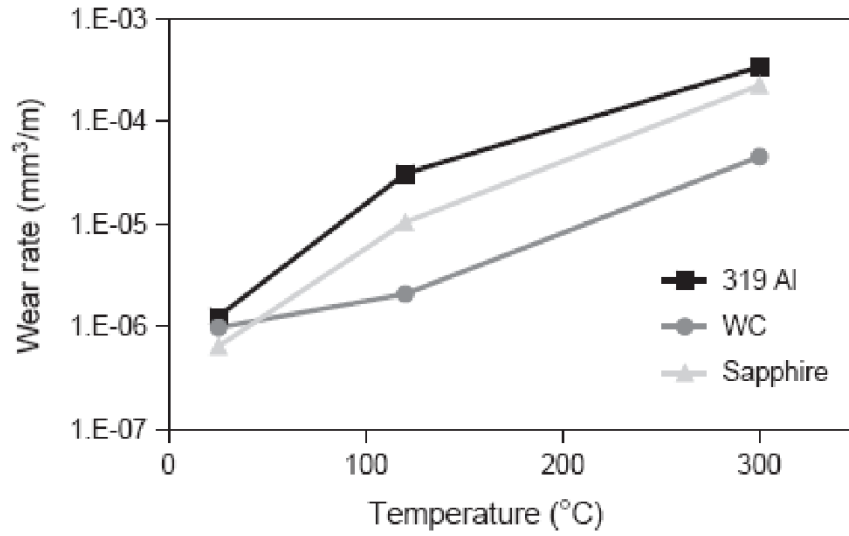
Liu et al. [2.49] studied the tribological behaviour of DLC films, which were deposited on silicon wafers using CH<sub>4</sub> gas in an rf-PACVD system against alumina balls. The tests were performed at room temperature, 200°C, and 300 °C. The resulting COF was approximately 0.2 below at 100 °C and 0.1 above at 200 °C. Film life became abruptly shortened at temperatures above 300°C while at room temperature, 100°C, and 200°C the wear rate of DLC films and the alumina balls were  $1 \times 10^{-9} \text{ Nm}^{-1}$  and rose slightly with the temperature. Once the temperature climbed above 200 °C, however, the wear rates of both the DLC films and the alumina balls increased drastically by a factor of  $10^3$ - $10^4$ .

Konca et al. [2.50] studied the tribological behaviour of NH-DLC coatings at elevated temperatures against 319 aluminum alloy at a constant load of 4.9 N and constant sliding speed of 0.12 m/s. Tests were done at 25 °C, 120 °C, 300 °C and 400 °C in air. At 25 °C, the steady-state coefficient of friction between the 319 Al pin and the DLC was 0.17, and the wear rate of the DLC was  $1.25 \times 10^{-6} \text{ mm}^3/\text{m}$  with no material transfer from the 319 Al pin to the coating surface. At 120 °C, the steady-state COF was 0.30, which is two times higher than the ambient conditions. The wear rate was  $3.08 \times$

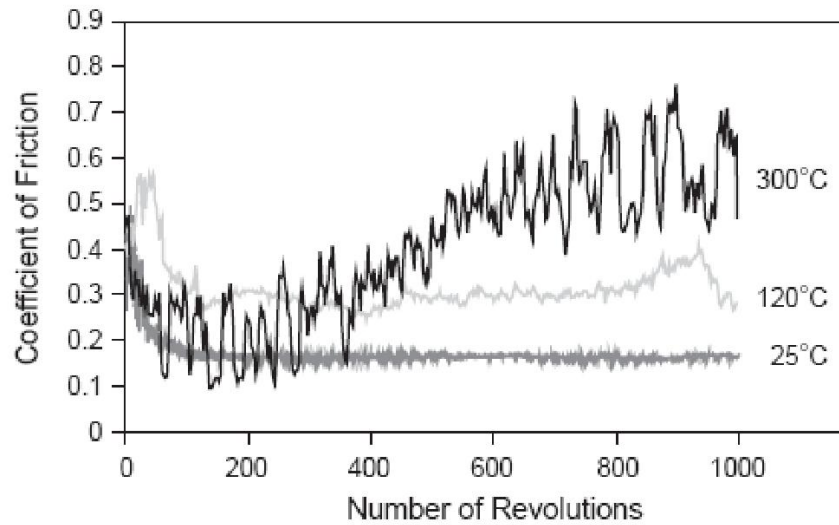
$10^{-5}$  mm<sup>3</sup>/m--an order of magnitude higher than the wear rate at 25 °C. The authors observed the highest wear rate at 300 °C ( $3.36 \times 10^{-4}$  mm<sup>3</sup>/m) (**Fig. 2.9a**). At 300 °C, the coefficient of friction was initially 0.2, then rose to 0.55 after 700 revolutions (**Fig. 2.9b**). The authors suggested that the presence of adsorbed water was essential for producing low friction and wear properties in the NH-DLC coatings.

Ni et al. [2.51] observed the tribological behaviour (pin-on-disk) of H- and NH-DLC coatings against aluminum alloys (319 Al) at elevated temperatures (25 °C, 120 °C, 240 °C and 300 °C). Aluminum did not stick to either the H-DLC or the NH-DLC coatings in ambient air (25 °C), and both displayed a low COF of 0.11 (**Fig. 2.10**). At 240 °C, however, aluminum did adhere to the NH-DLC, whereas the H-DLC was able to preserve its repellent nature (**Fig. 2.11**). The authors suggested that the low COF displayed by NH-DLC coatings in ambient air was caused by adsorbed gaseous species (such as water and oxygen), which passivates carbon dangling bonds, but at elevated temperatures the gaseous species desorbed and the carbon dangling bonds were exposed--leading to a strong interaction between the NH-DLC and the aluminum counterpart. Due to the transfer of aluminum to the DLC, an aluminum-aluminum contact was established in subsequent sliding at the interface, causing a high friction coefficient.





(a)



(b)

**Figure 2. 9 (a)** The variation of the wear rate of NH-DLC coating with temperature when tested against 319 Al, WC and sapphire at 25, 120 and 300 °C. Tests were run for 1500 m of sliding distance ( $2.5 \times 10^4$  revolutions) at 25 °C and for 60 m of sliding distance ( $10^3$  revolutions) at 120 and 300 °C using 5 N applied load. **(b)** The COF curves between 80-V DLC coated disc and 319 Al pin at 25, 120 and 300 °C. Tests were run for 60 m of sliding distance ( $10^3$  revolutions) using 5 N applied load, at 0.12 m/s sliding speed [2.50].

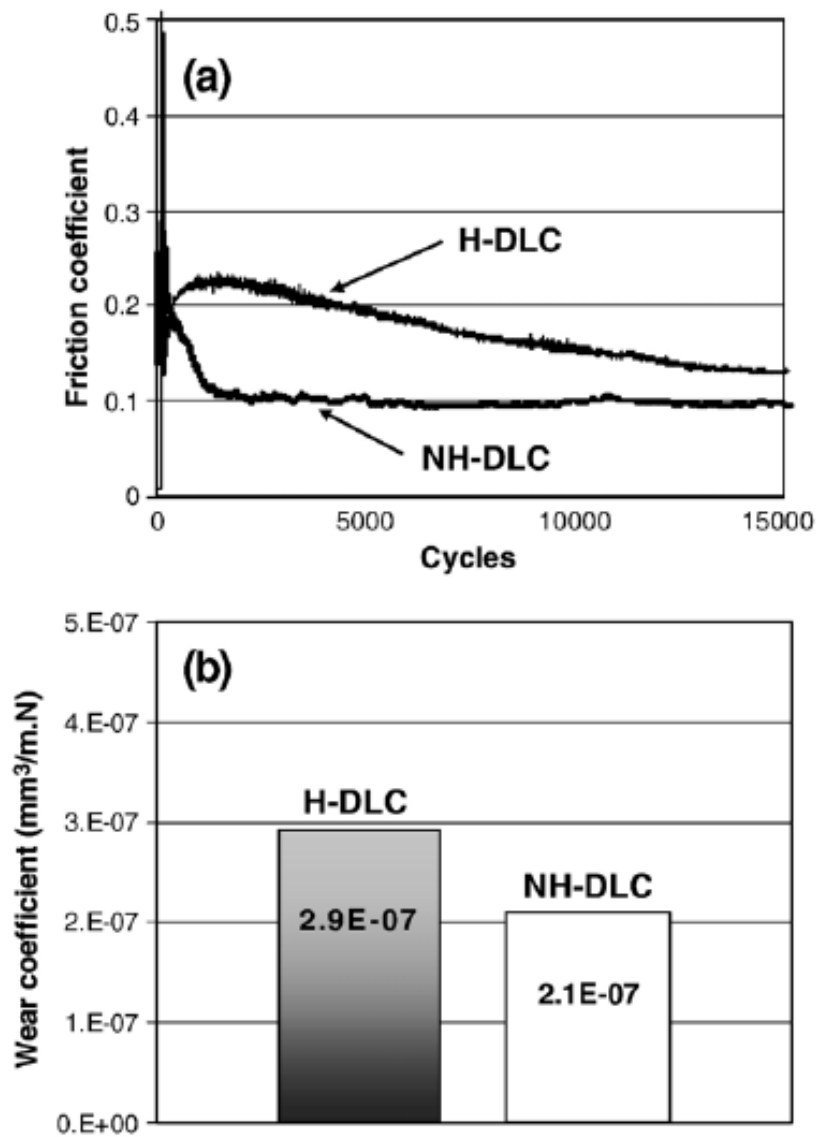


**Figure 2. 10** Comparison of the hydrogenated and non-hydrogenated DLC at 25°C (relative humidity 40%): (a) friction coefficient of DLC against 319 aluminum alloy and (b) wear coefficient [2.51].

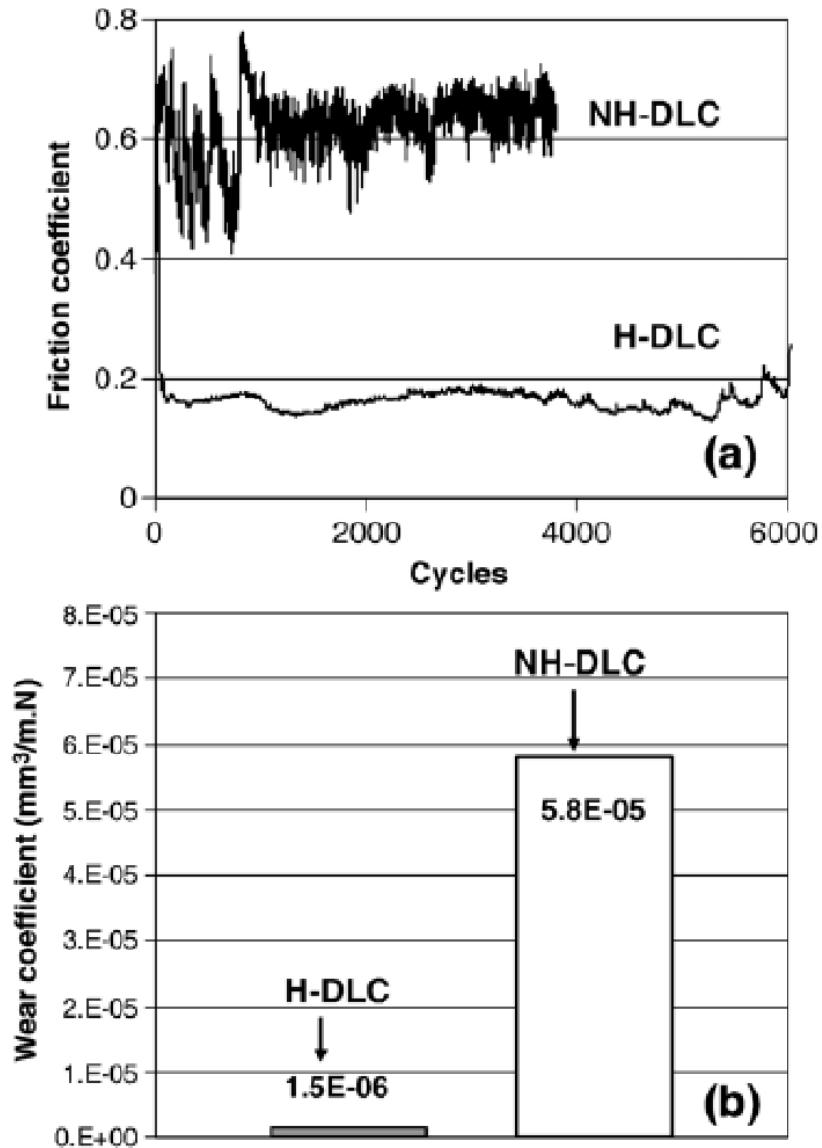


**Figure 2. 11** Comparison of the hydrogenated and non-hydrogenated DLC at 240°C: (a) friction coefficient of DLC against 319 Al (b) wear coefficient [2.51].

### 2.4.1.3. Tribological Behaviour of Diamond-Like-Carbon (DLC)

#### Coatings in Lubricating System

Sometimes diamond-like carbon coatings are exposed to humid environments. In machining operations, the DLC coated part can also be exposed to the cutting fluid,

which makes it necessary to investigate the performance of DLC coatings in lubricating systems.

Ronkainen et al. [2.52] observed the tribological performance of both H-DLC and NH-DLC in water lubricated conditions. The tribological tests consisted of reciprocating sliding tests with a sliding velocity of 0.004 m/s. Alumina balls were considered as the counterparts, the normal load was 5N, and a variety of coating deposition methods (Plasma-assisted chemical vapour deposition, Magnetron sputtering, Ion beam, Pulsed vacuum arc discharged, and Vacuum arc discharged) were analyzed. The authors noted that the H-DLC coating performed poorly in water lubricated conditions due to rapid wear out, whereas the doped (Si-doped a-Si<sub>1-x</sub>-C<sub>x</sub>:H layers) H-DLC showed a significant improvement in wear resistance. The study revealed that the COF (0.7) of the H-DLC film was higher than that of the other DLC coatings--which had COF values in the range of 0.04–0.1. The NH-DLC deposited by vacuum arc discharge displayed the lowest COF--initially a high 0.6 at the beginning of the test that decreased until it reached 0.05.

Stallard et al. [2.31] studied the tribological behaviour of the NH-DLC and H-DLC by testing them in air, water, and oil. Each coating type was tested at three normal applied forces (10, 40, and 80 N). NH-DLC with chromium interlayer coating was deposited by closed field unbalanced magnetron sputter ion plating from carbon and chromium targets, while H-DLC was deposited by plasma enhanced chemical vapour deposition (PECVD). The NH-DLC coating exhibited low wear rates under all three environmental conditions, but the H-DLC coatings failed rapidly when tested in water. In air and oil environments, the H-DLC coating exhibited lower wear rates than the NH-DLC coating. The authors suggested that passivation of carbon dangling bonds by H and

–OH was the main mechanism for better tribological behaviour of NH-DLC compared to H-DLC.

Persson et al. [2.53] observed the tribological behaviour of tungsten carbide-doped DLC coatings (WC/C) using a water-based emulsion. They used three types of tribological test equipment--pin-on-disc, four ball method extreme pressure, and Reichert. Both the pin and the disc were made of ball bearing steel, with a hardness of 62–65 HRC. In the pin-on-disc arrangement, the COF of the well lubricated contacts did not change significantly with the coating. They observed a low COF for the DLC even in poor lubricants (10% polypropylene glycol and water) during the pin-on-disc test. Water based lubricants worked well for the four ball weld load arrangement instead of pure oil and water, and a decreased wear rate was observed in Reichert measurements--especially in the running-in behaviour of the DLC coating for water-based lubricants.

Podgornik et al. [2.54] studied the tribological reactions between oil additives and DLC coatings. They used pure poly-alpha-olefin (PAO) oil (viscosity of 46.6 mm<sup>2</sup>/s), as well as PAO mixed with a sulfur-based EP or phosphorus-based AW additive (concentrations from 0.01% to 10%) as lubricants. The authors observed lower friction and wear with the steel/W-DLC combination as the EP additive concentration increased. In the case of pure PAO oil with low additive concentrations, the authors concluded that the tribological behaviour of the DLC coatings was governed by the transfer of coating material to the steel counter-surface (C and WC) and the resulting formation of a low-friction transfer layer.

Kalin et al. [2.55] observed the effect of doping elements (Ti–DLC, W–DLC and Si–DLC) and oil additives (high-purity paraffinic base oil with anti-wear/extreme-

pressure additive, i.e., dialkyl dithiophosphate) on the tribological behaviour of DLC/DLC contact and found improved wear resistance when the additives were added to the mineral base oil, regardless of the coating type. The additives also helped to protect the doped DLC surface from the occurrence of coating spallation.

In summary, the NH-DLC coating exhibited low wear rates and COF under lubricated conditions, but the H-DLC coatings did not achieve a reasonable performance when tested in a lubricated environment. Doped DLC coatings exhibited better performance in an oil with additives environment.

#### **2.4.2. Performance of Carbon Based Coatings in Aluminum Machining**

The combination of low coefficient of friction and high wear resistance attributed to carbon based coatings makes them particularly useful in industrial machining applications.

Kanda et al. [2.56] observed the cutting performance of diamond coated cutting tools during the drilling of aluminum alloys (A390) using a water soluble emulsion. The speed, feed rate, and hole depth were 4250 rpm, 0.10 mm/rev, and 10 mm, respectively. They found the tool life of uncoated carbide (160 holes) was greatly improved by a diamond coating (8075 holes) when drilling A390 (Al- 18% Si), but scarcities still remain an issue in the machining of Al-Si alloys because of the abrasion characteristics of silicon particles, which cause the debonding of the diamond coating from the cutting edge.

To reduce the debonding tendency and to improve the adhesion of diamond coatings on cutting edges, Hanyu et al. [2.57] optimized the construction of coated drills by changing the shape of the cutting edges. They found, when comparing the torque of drills with  $20^{\circ}$  and  $38^{\circ}$  rake angles, that the torque of the  $20^{\circ}$  rake angle was 15% larger than that of the  $38^{\circ}$  rake angle drill, while the torque of the drill with the  $12^{\circ}$  rake angle was 20% larger than that of the  $20^{\circ}$  rake angle. They concluded that the drill with the  $20^{\circ}$  rake angle achieved the best performance during the drilling of high aluminum-silicon (Al-23%Si) alloys. These authors also compared the cutting performance of rough and smooth surface diamond coated drills during dry drilling of 12% silicon aluminum alloys. They confirmed that the finely crystallized smooth diamond coatings carried a 10% smaller thrust force than the rough surface diamond coatings when drilling aluminum alloys, due to the lower friction on the surface of the diamond coatings.

Fukui et al. [2.58] evaluated the cutting performance of NH-DLC coated tools in the dry milling of aluminum alloys. According to their findings, the cutting force, the feed force, and the back force were all less for the NH-DLC coated insert than they were for the uncoated insert when cutting an AlMg2.5 alloy. The cutting force was also reduced approximately in half (from 600 N to 325 N) by using a NH-DLC coating under dry conditions, and from 538 N to 253 N under flooded conditions. They also observed a superior surface finish using DLC coated tools during the machining of Al-12% Si with 4.5% Cu alloys--to where the surface roughness of a 9 m cutting uncoated insert was equal to a 72 m cutting NH-DLC coated insert.

Cutting performance of H-DLC, NH-DLC, and diamond coated inserts were examined by Vandeveldt et al. [2.59] when tested in the dry turning of Al-SiC metal

matrix composites (AlSi10Mg+20%SiC) and the dry milling of aluminum alloys (AlZnMnCu0.5). During the dry turning of the Al–SiC composites, H-DLC and NH-DLC did not achieve superior performances because their coatings were worn away after approximately the same turning time (1.33 min). CVD diamond coated inserts of 6 and 20  $\mu\text{m}$  thickness displayed better performance thanks to a prolonged turning time (12 and 30 min) and reduced built-up edge. In the case of the dry milling of aluminum alloys, the hard carbon coating did not significantly improve the original tool lifetime (1.33 min). The DLC layers endured a cutting length of 50 m and the diamond coated end-mills (cutting length 25 m) performed even more poorly than the uncoated WC-Co (50 m) due to the adhesion failure of the diamond coating.

Dai et al. [2.60] found that diamond coated inserts worked much better than DLC coated inserts in the dry cutting of Al-22% wt. Si alloys. The cutting conditions were as follows: cutting speed 180 m/min, cutting depth 0.2 mm, feed rate 0.1 mm/rev., and dry cutting. They concluded that the flank wear life of the diamond coated insert was 55 times longer than the uncoated inserts, whereas the wear of the DLC coated inserts was almost the same as uncoated inserts.

Lahres et al. [2.61] studied the applicability of different hard coatings in the dry milling of wrought and cast aluminum alloys (AlZnMgCu1.5, AlSi10Mg). They found that the traditional hard coatings, including CrN, MoS<sub>2</sub>, TiN and TiAlN, did not show any acceptable performance during milling of the wrought aluminum alloy (AlZnMgCu1.5) due to the formation of excessive BUE. They also identified a chemical reaction and diffusion between the elements in the coatings (Cr, Mo, Ti) and elements in the workpiece material (Al, Zn, Mg, Cu). In contrast, H-DLC and diamond coatings showed



lesser BUE formation. They attributed this to the low chemical affinity between carbon and aluminum. In the milling of aluminum cast alloys (AlSi10Mg), they determined that the softer coatings (WC/C, CrC/C) showed minor built-up edges during dry milling, but exceeded the flank wear values for the uncoated tool under flooded milling conditions. On the other hand, combining a hard coating (e.g., TiN) with a top covered “softer” coating (e.g., MoS<sub>2</sub>) provided a better performance during dry milling than an uncoated tool under flooded milling conditions. The diamond coatings (CVD) resulted in an increased tool life of about 30% for dry milling, compared to the uncoated tool under flooded conditions.

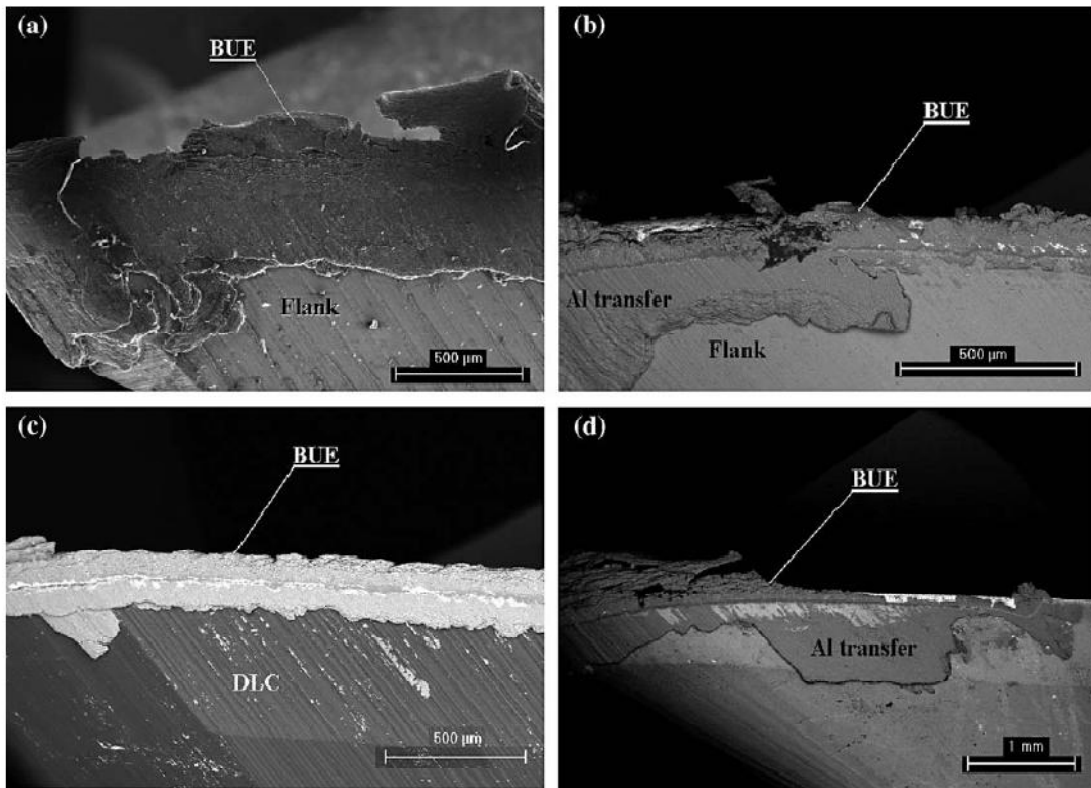


**Figure 2. 12** SEM back-scattered electron images showing the built-up edge and aluminum transfer after dry cutting AlSi9Cu1 alloy. (a) uncoated HSS, after 2.7 min cutting time; (b) TiAlCrYN coated tool, after 4.3 min cutting time; (c) DLC coated tool, after 2.6 min cutting time; (d) TiAlN/VN coated tool, after 5.3 min cutting time [2.62].

Hovsepian et al. [2.62] evaluated the performance of superlattice structured TiAlN/VN, H-DLC, TiAlCrYN coated and uncoated tools during the dry, high-speed milling of aluminum alloys 7010 Al-T7651 and AlSi9Cu. During the milling of the 7010 Al-T7651 alloy, TiAlN/VN and H-DLC coated tools showed comparable performances, both outperforming TiAlCrYN coated and uncoated tools by a factor of 2.3 and 3.5, respectively. In the case of milling AlSi9Cu, the H-DLC coatings did not achieve a better performance--failing to construct any lifetime improvement. The authors also noted a prolonged tool life for TiAlCrYN (65%) and TiAlN/VN (100%) compared to that of the uncoated tools in the milling of AlSi9Cu. They also observed that TiAlN/VN reduces the cutting forces and the surface finish as well. SEM observation of the cutting edge after testing showed that the TiAlN/VN coating significantly reduced aluminum transfer and built-up edge formation compared to TiAlN (**Fig. 2.12**).

Coldwell et al. [2.63] assessed cutting performance in terms of tool life/wear, cutting force/torque, chip morphology, hole diameter, cylindricity (dispersion of hole diameter), and out of roundness during the drilling of ASTM 2014 aluminum alloys with a composition of 3.9-5 wt.% Cu, 0.5-0.9 wt.% Si. They investigated the cutting performance of different types of coatings, including NH-DLC, H-DLC and Ti containing MoS<sub>2</sub> (MoST) with and without a hard coating under layer (CrTiAlN, ZrN, MoZrN, CrC) whereas CrC under layer was used for the NH-DLC and H-DLC coatings. They found that coating combination had little or no effect on hole quality. Thrust force and torque values ranged from 1000 to 1600 N and 2–8 N-m, respectively. The authors suggested that high torque was correlated with high cylindricity values, indicating problems with chip evacuation. The buildup of aluminum was found after drilling 30

holes with the MoST coating. For the H-DLC coated drill, aluminum buildup was observed after drilling 60 holes. The NH-DLC coated drill showed the lowest buildup of aluminum on the drill surface after 100 holes had been drilled with each coating, which indicated its resistance to aluminum adhesion.

Wain et al. [2.64] also tested NH-DLC, H-DLC, MoS<sub>2</sub> containing Ti and TiB<sub>2</sub> coated drills during the dry drilling of as-cast A319 (6% Si, 3.5% Cu) in dry, direct air (high-pressure air of 60 psi directed at the tool), and indirect air (low pressure air of 20 psi directed at the workpiece) conditions. They found a prolonged tool life in all cases for NH-DLC coatings due to their intact durability even at failure condition. All the coatings were ranked by the authors in terms of tool life (best > worst): NH-DLC > H-DLC > TiB<sub>2</sub> > MoST. They also observed adherent workpiece material on the flank face of the drill in all coatings. However, the NH-DLC coating showed the smallest amount of adherent material for a given condition (after 100 holes), which is shown in **Fig. 2.13**.

Dasch et al. [2.65] tested different carbon based coatings such as metal-containing carbon (Me-a-C:H), H-DLC, NH-DLC, and diamond (t-C) during the dry drilling and pin-on-disc testing of 319 Al. Based on power consumptions, the authors observed that the blend coated (NH-DLC/H-DLC) drill was superior, in that power never rose far above 4 HP. The H-DLC coating was worse than the uncoated in that the power rose to 8 HP, which was thought to be related to the high aluminum adhesion and flute clogging. When comparing with hydrogen-free DLC coatings, they observed lower power consumption (< 6HP) for the H-DLC coated drill (**Fig. 2.14.**), whereas H-DLC coatings out-performed the rest in pin-on-disc tests--yielding better results even at 400°C.

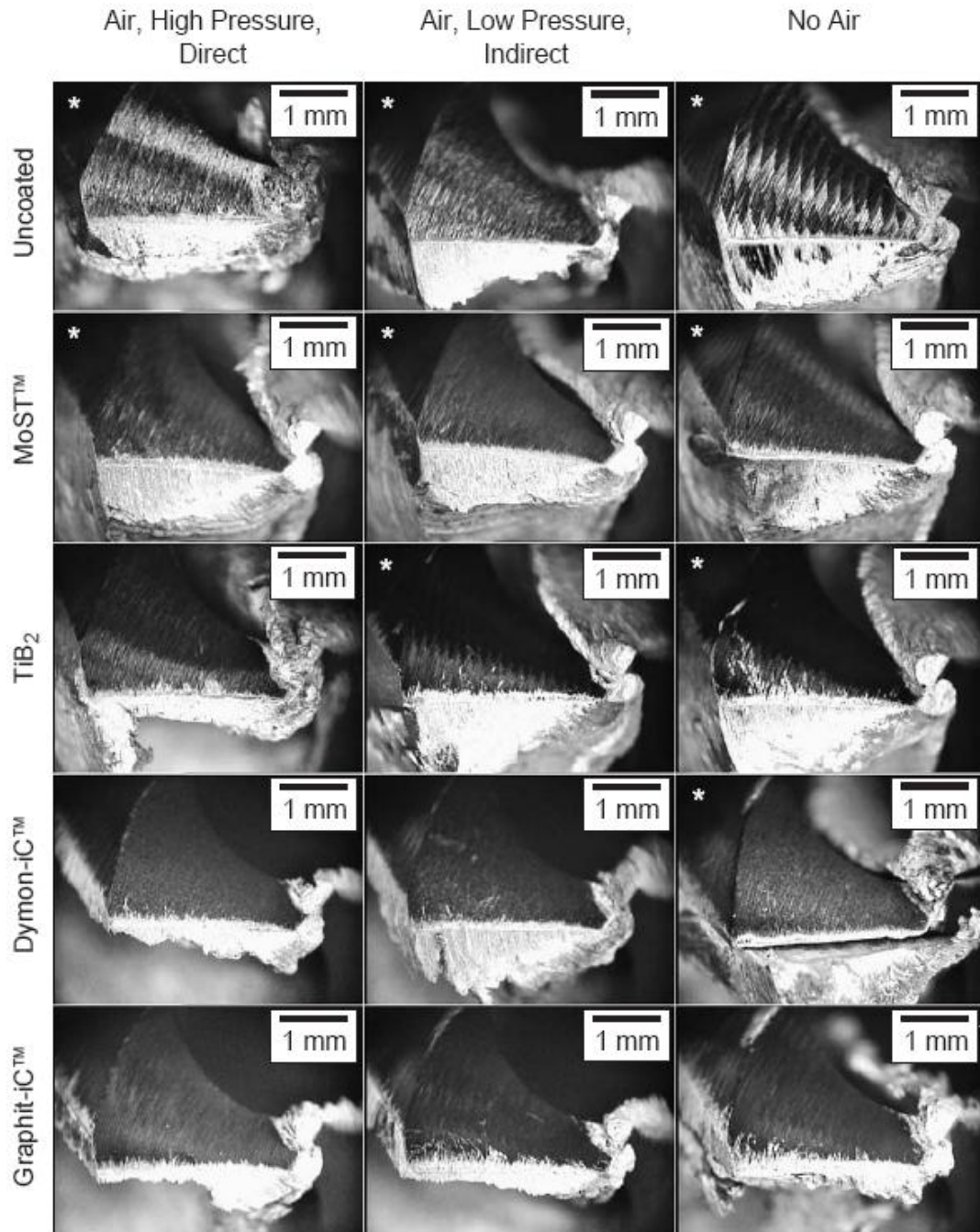


**Figure 2. 13** Optical, bright-field images of the flank faces of the drills after 100 holes or (\*) failure, depending on which occurred first. Lower build-up of materials was found for non-hydrogenated DLC (Graphit-iC<sup>TM</sup>) coated drill [2.64].

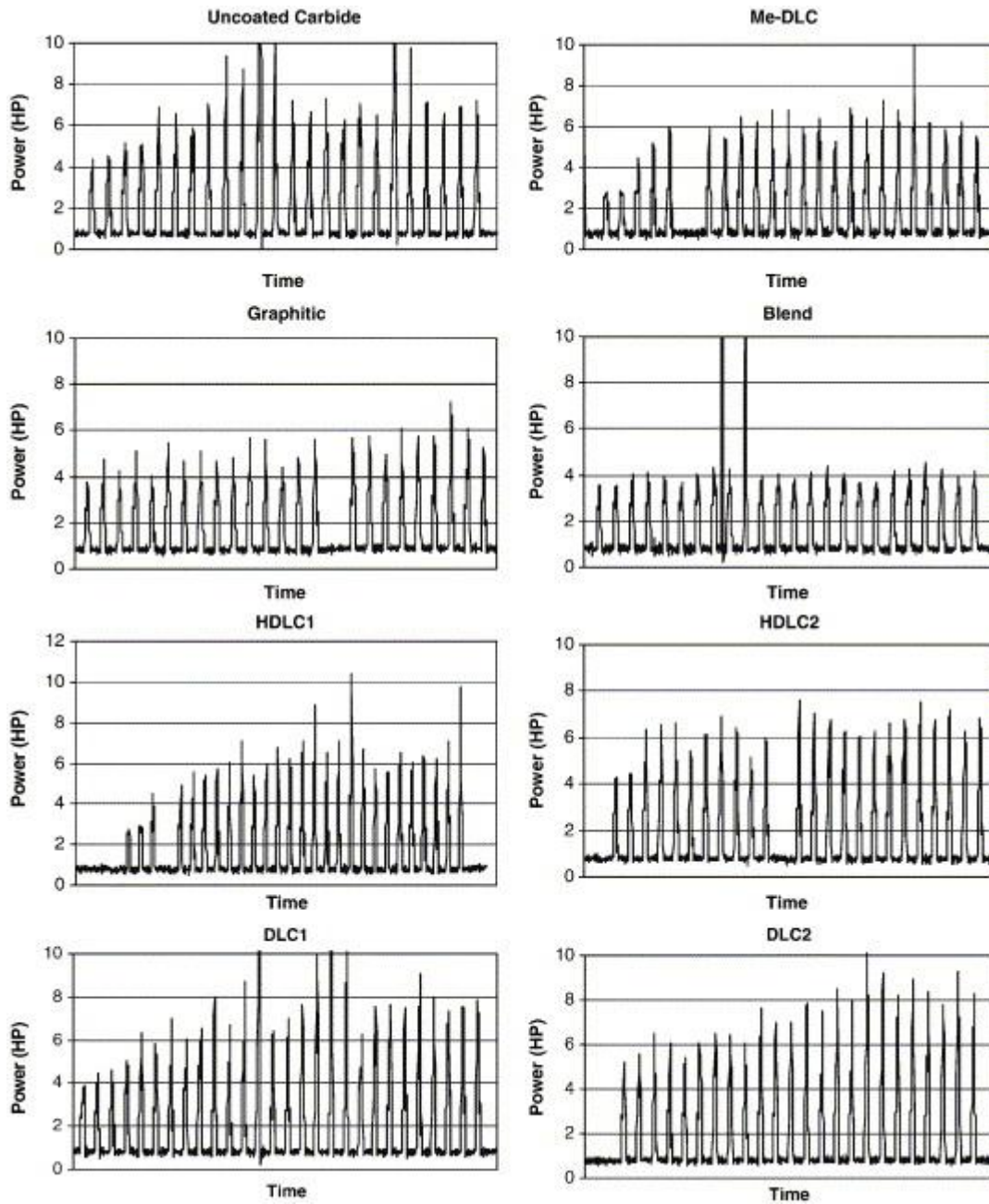


**Figure 2. 14** Power plots during drilling of the first 25 holes in 319 Al with different drill coatings. Each peak corresponds to one (1) hole being drilled. The non-hydrogenated DLC1 and DLC 2 possibly worse than uncoated HSS in that power rose to 8 H.P.[2.65].

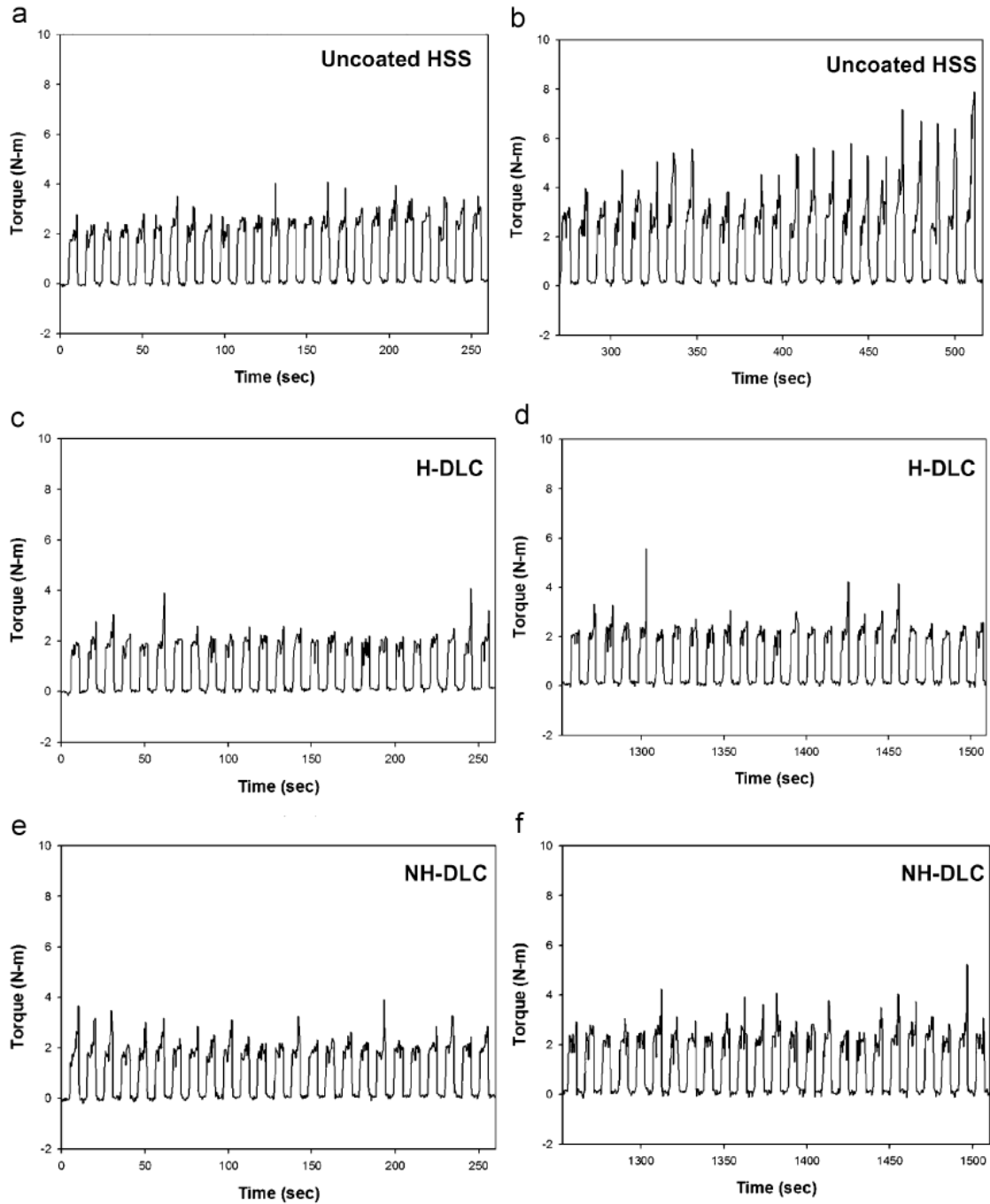


**Figure 2.15** Torque plots: (a, b) representing the holes 1–25 and 25–49 with uncoated HSS where the drill failed at hole no. 49; (c, d) representing the torque responses of holes 1–25 and 125–150 for H-DLC-coated drill; (e, f) representing the torque responses of holes 1–25 and 125–150 for NH-DLC-coated drill [2.66].

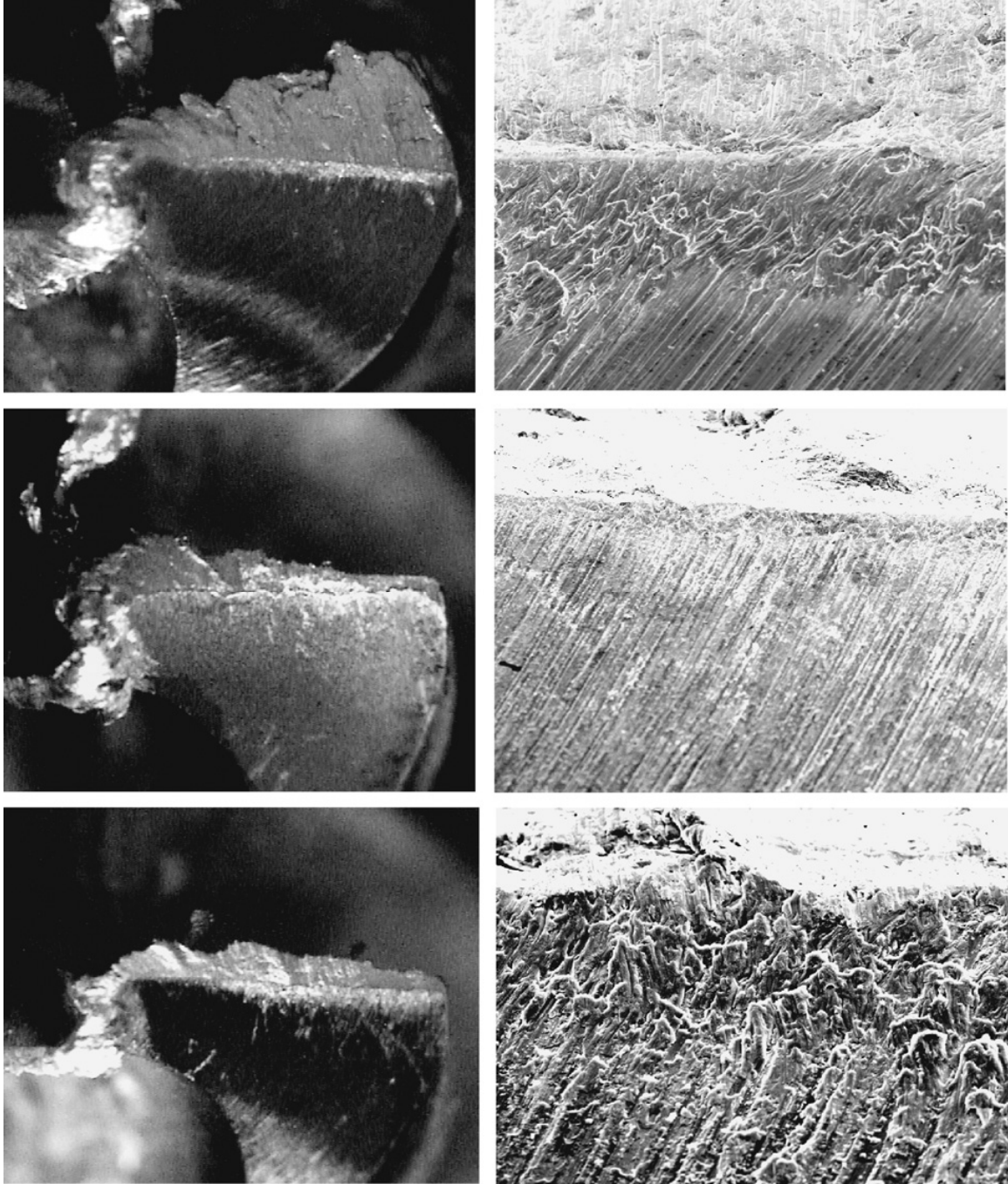


**Figure 2. 16** Optical image of drill cutting edge consisting of (a) uncoated HSS after 49 holes; (b) SEM of insert in plate (a); (c) optical image of the cutting edge of H-DLC-coated drill after 150 holes; (d) SEM image of insert in plate (c); (e) optical image of the cutting edge of NH-DLC-coated drill after 150 holes and (f) SEM images of insert of plate (e). Figures show the buildup edge (BUE) on the tip of the cutting edge and the metal transfer on the flank face [2.66].

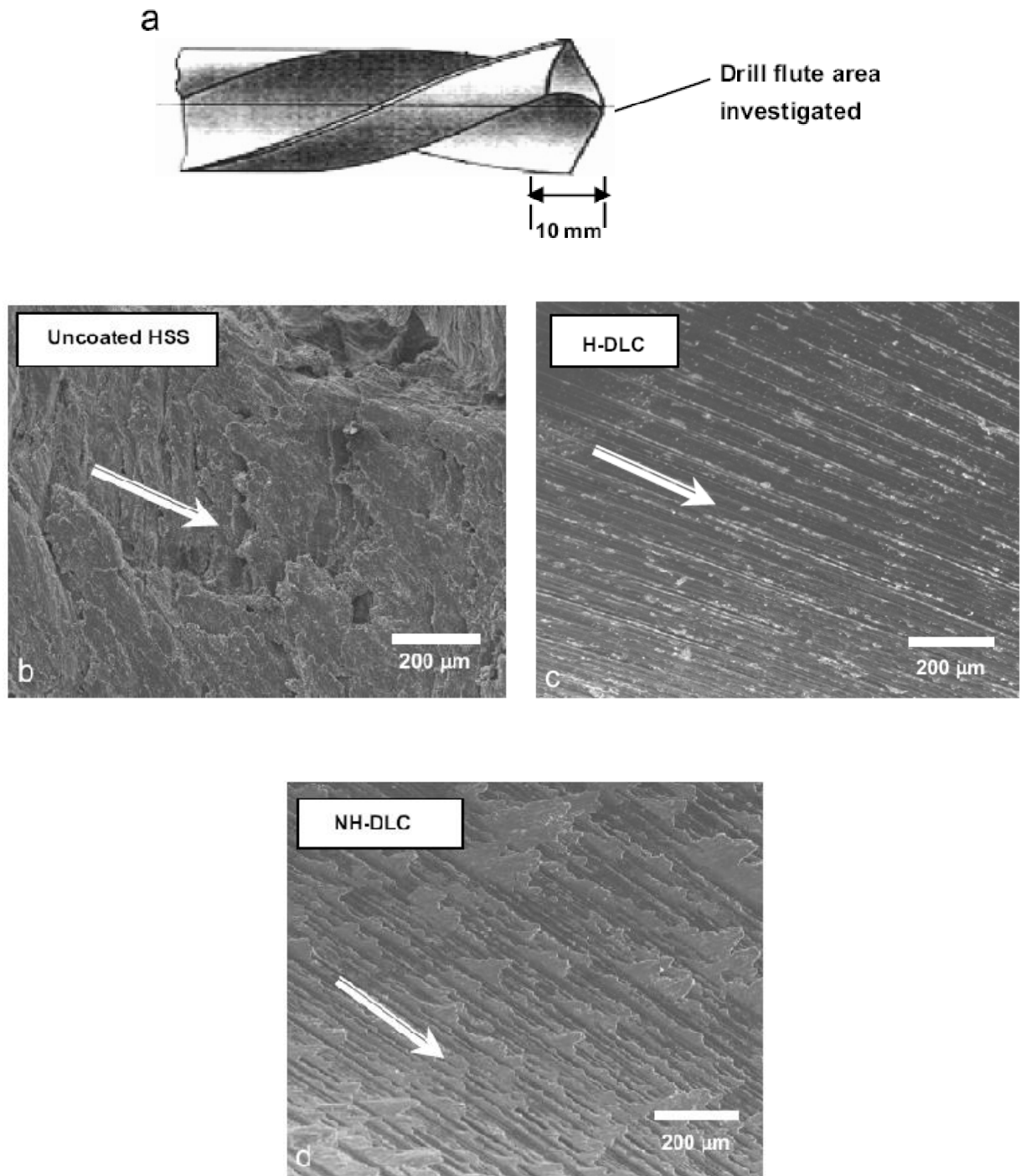


**Figure 2. 17** SEM secondary electron images showing the aluminum adhesion to drill flutes: (a) schematic representation of drill flute showing the area investigated; (b) uncoated HSS tool; (c) H-DLC-coated tool and (d) NHDLC-coated tool. The flute surface of uncoated HSS drill was almost entirely covered by adhered aluminum. The direction of chip flow is shown by the arrow [2.66].



Bhowmick and Alpas [2.66] studied the performance of H- and NH-DLC during dry drilling of 319 Al. The results indicated that superior cutting performance was achieved, in both torque and thrust force responses, using DLC coated drills rather than uncoated high-speed steel (HSS) drills. The uncoated HSS drills failed after drilling only 49 holes as a result of excessive aluminum adhesion. At least 150 holes could be drilled using the DLC coated drills, and both the torque and thrust forces generated during drilling were lower than those with uncoated HSS drills. In addition, a smaller proportion of holes exhibited abrupt increases in torque (at the end of the drilling cycle) during drilling with the DLC coated drills (**Fig. 2.15**). Scanning electron microscopy (SEM) investigations showed that the H-DLC drill flutes displayed minimal aluminum clogging, which resulted in lower torque (**Fig. 2.16**). H-DLC coating also diminished metal transfer and buildup edge formation on the drill's flank face and cutting edge (**Fig. 2.17**). Thus, torque and thrust force measurements, supported by metallographic data, indicated that H-DLC coated drills provided better dry drilling performance than NH-DLC.

## **2.5. Tapping of Ferrous Alloys**

Tapping is one of the most intensively used machining operations to obtain internal threads; it is a geometrically complex cutting process due to the action of multi-edges and long contact lengths between the cutting edges and the workpiece [2.67-2.69]. Tapping is one of the last operations to be performed, which makes its reliability extremely important. When a tapping tool fails, the workpiece already has significant added value and, in most cases, the cost of scrapping it or re-working it are very high.

Breakage of a thread-cutting tool significantly impacts the productivity of the process. This section reviews the existing literature on the tapping of ferrous alloys.

Chen et al. [2.70] studied the role of cutting edge geometry by comparing the performances of straight fluted tap of helix angle  $0^\circ$  and spiral pointed tap of helix angle  $34^\circ$  during tapping in an austenitic stainless steel in conventional flooded (oil-water emulsion) tapping conditions at the speed of  $\sim 60$  rpm and at the feed rate of 1.00 mm/rev. A slight decrease in average torque to 4.5 N-m was observed during tapping with spiral flute compared to the conventional straight flute taps (5.0 N-m).

Veldhuis et al. [2.71] studied the influence of perfluoropolyether (PFPE) film on torque responses during the tapping of mild steel in flooded (oil-water emulsion) tapping conditions at the speed of 260 rpm and at the feed rate of 1.58 mm/rev. PFPE was deposited by dipping the part into the solution, which resulted in a molecular monolayer that provided an even coating to a rough tool surface. The PFPE on HSS tool surface reduced the torque to  $\sim 21$  N-m compared to  $\sim 25$  N-m when an uncoated tap was used.

Reiter et al. [2.72] evaluated the performance of conventional hard coatings, including CrN, CrC, TiCN, TiAlN, in comparison with the carbon based coatings consisting of WC/C and diamond-like carbon coatings (DLC) during dry tapping of austenitic stainless steel. DLC coatings showed the lowest average torque of 5.25 N-m when compared to TiAlN (7.43 N-m), CrN (7.19 N-m), TiCN (6.85 N-m), and CrC (6.55 N-m) coated HSS tools. However, flank built-up edges (BUE) were observed during the tapping with DLC coated tools, while no significant BUE occurred with conventional TiCN or TiAlN coatings.

### 2.5.1. Tapping of Aluminum Alloys

Only a few studies have been conducted on the tapping of aluminum alloys. Srivastava et al. [2.73] investigated the performance of uncoated HSS, uncoated carbide, and TiN coated HSS tap during the form tapping of 319 Al alloys in flooded (semi-synthetic oil) tapping conditions at the speed and feed rate of 1100 rpm and 1.25 mm/rev. In form tapping, thread is not created by chip removal but by the displacement of the workpiece. TiN coated HSS taps produced lower torque responses ( $\sim 0.07$  N-m) when compared to uncoated HSS ( $\sim 0.61$  N-m) and uncoated carbide ( $\sim 0.14$  N-m) tools.

Zedan et al. [2.74] investigated the effects of iron content during the conventional tapping of Al-Si alloys using TiN-coated HSS taps at speed and feed rates of 400 rpm and 1.25 mm/rev, respectively, in flooded tapping conditions (synthetic fluid). An increase in the average tapping force of 470N was observed for Al-12% Si-0.46% Fe due to a significant amount of iron-rich intermetallics compared to Al-7% Si-0.30% Fe (250 N).

Bhowmick et al. [2.75] studied the deep hole drilling and tapping of automotive powertrain components made of 319 Al alloys using DLC coated taps and 80 ml/h of MQL. HSS-dry tapping caused immediate tool failure within less than 20 holes due to aluminum adhesion, resulting in high forward and backward torques. DLC-dry tapping improved tool life considerably and exhibited small torques. The second set of tapping experiments used MQL and only uncoated HSS taps. The use of MQL at the rate of 80 ml/h produced similar average torques to flooded tapping, and a high thread quality was observed. The details of this study can be found in **Chapter 4**.

## **2.6. Near-Dry Machining**

A large body of previous work exists regarding the application of near dry machining applying a minimum quantity of lubricant (MQL) to the tool tip or drill flute region. In all studies, the MQL agents were supplied externally. This section surveys the machining of ferrous alloys (**Section 2.4.1.**), while **Section 2.4.2.** and **Section 2.4.3.** focus on the near-dry machining of aluminum and magnesium alloys.

### **2.6.1. Near-Dry Machining of Ferrous Alloys**

Khan et al. [2.76] studied the effects of minimum quantity lubrication on turning AISI 9310 alloy steel using vegetable oil-based cutting fluid. The MQL flow rate was 100 ml/h. The authors measured the tool-chip interface temperature and surface roughness and found that MQL produced lowest temperature (1100 °C) and surface roughness compared to dry (1200 °C) and flooded conditions (1150 °C). The authors suggested that vegetable oil was very effective to reduce the cutting temperature compared to flooded coolant.

Liao et al. [2.77] investigated the effect of the minimum quantity lubrication in high-speed end milling of hardened steel by coated carbide tool. The MQL oil mist was supplied at the rate of 10 ml/h. The authors found that the surface roughness increased with the feed rate in dry, MQL, and flooded conditions. MQL showed average surface roughness of 0.32  $\mu\text{m}$ , which is equivalent to the flooded conditions (0.31  $\mu\text{m}$ ) and 47% better than dry conditions (0.47  $\mu\text{m}$ ).

Tasdelen et al. [2.78] presented the effect of MQL, emulsion, and air cooling on tool wear, surface finish, and cutting forces when drilling hardened steel. The highest force was recorded for air cooling, and the lowest for emulsion. MQL outperformed air cooling and emulsion in terms of tool wear. In addition, MQL recorded similar surface roughness value as that of flooded conditions.

Dhar et al. [2.79] studied the influence MQL had on cutting temperature and chip and product quality while turning in AISI-1040 steel. The use of MQL reduced the temperature--improving the chip--tool interaction, and maintained the sharpness of the cutting edges. For an example, a lower cutting temperature (~650 °C) was observed at a feed rate of 0.10 mm/rev even at a higher cutting speed (130 m/min) when using MQL of 60 ml/hr. On the other hand, higher temperatures (~700 °C and ~690 °C) were noted during both dry and flooded conditions. The steel chips morphology was favourable while machining with MQL due to effective lubrication. An improved dimensional accuracy was observed when using MQL and attributed to low tool wear and damage.

Zeilmann and Weingaertner [2.80] studied the temperature increase during the MQL drilling of Ti6Al4V--employing carbide drills with and without hard coatings (TiAlN, CrCN or TiCN). They used both external (12 l/min) and internal nozzles (50 ml/hr) in the MQL system and found that the measured temperatures with the application of internal MQL were 50% smaller than those obtained when MQL was applied with an external nozzle. The authors analyzed the temperature formation for the different coatings, but could not discover the detrimental differences between the various coatings. The CrCN coating did display a slight inclination towards smaller recorded values. For the other coatings, TiAlN and TiCN, the temperatures differed by only a few degrees.

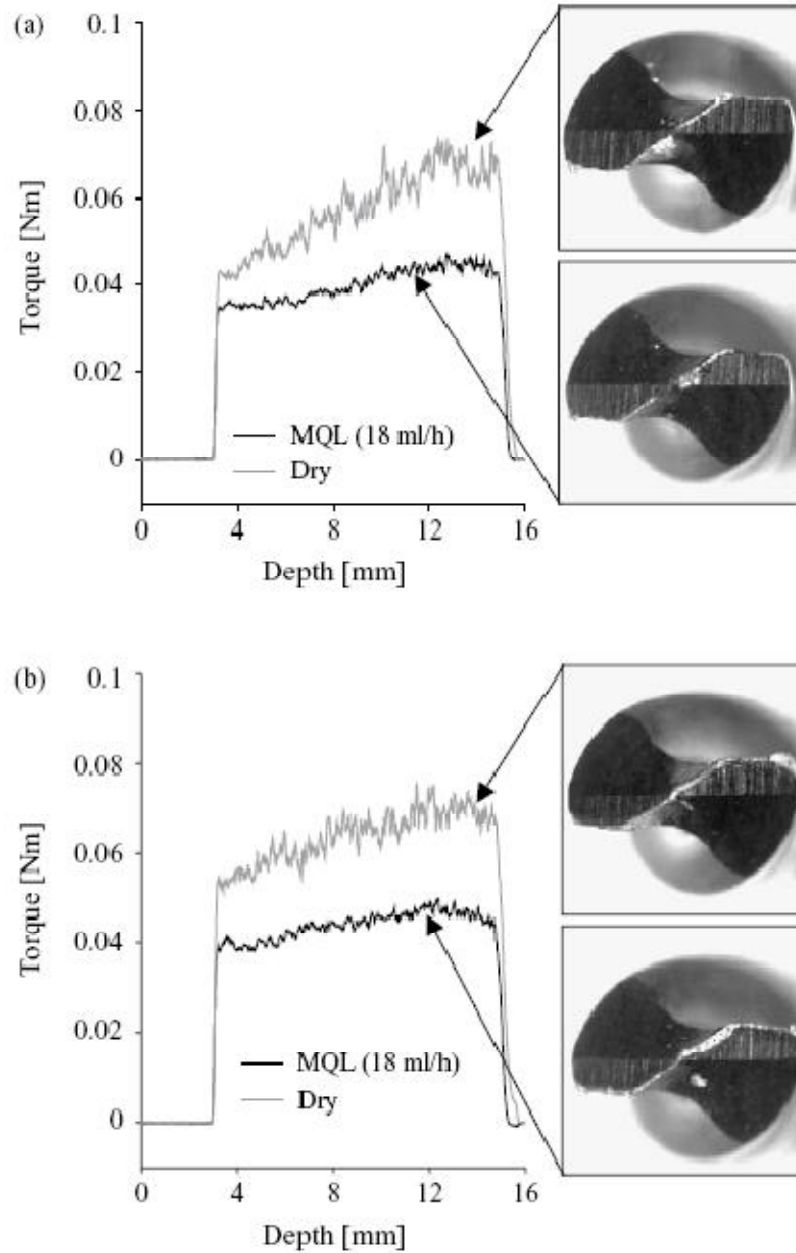


**Figure 2. 18** Torque recorded for a TiAlN-coated Co-HSS twist drill (type D) during (a) the 51<sup>st</sup> and (b) the 351<sup>st</sup> drilling cycle: comparison between drilling with minimum quantity of lubrication (18 ml/h) and dry drilling [2.84].

Attanasio et al. [2.81] observed the influence of MQL on tool wear during the turning of normalized 100Cr6 steel (200–220 HB). They used ester oil with an EP additive as an MQL agent. The flow rate was 20 ml/hr, and they used MQL in the flank

and the rake face of the tool distinctively. They found that lubricating the flank surface reduced tool wear and increased tool life rather than dry cutting and applying MQL on the rake face.

Rahman et al. [2.82] studied the effect of MQL (8.5 ml/ h) in the end milling of 718HH steel (0.33% C, 0.30% Si, 0.80% Mn). The authors did not note any significant difference in cutting force between flooded conditions and MQL. The surface roughness generated by the MQL (0.8  $\mu\text{m}$ ) was also similar to that obtained by flood cooling (1.2  $\mu\text{m}$ ).

Machado and Wallbank [2.83] applied MQL (200-300 ml/h) during the turning of a normalized forged steel bar (AISI 1040). Feed forces are reduced when using a MQL agent at low cutting speeds (30 m/min) and high feed rates (0.45 mm/rev). Under the aforementioned machining conditions, air with water provided the lowest feed force (1856 N  $\pm$  46.6), then dry (2041 N  $\pm$  37.7 ), air stream (1847 N  $\pm$  57.2), and flooded condition (1870 N  $\pm$  73.4). Air with coolant (soluble oil) produced the highest force (1917 N  $\pm$  52.9), while a superior surface finish and chip thickness were found with the mixture of air and water.

Heinemann et al. [2.84] studied the effect of MQL (18 ml/hr) on the tool life of small twist drills in 15 mm hole drilling. The workpiece material was plain carbon steel (0.45% C). The lubricant used was a fatty acid ester with 20% alcohol. They found a continuous MQL supply was beneficial in terms of tool life (558 holes) for small diameter twist drills in deep hole drilling, whereas discontinuous MQL supply provided a substantial drop in tool life (13 holes). They also observed that in the dry drilling of plain carbon steel (0.45%C), TiAlN was required to achieve a satisfactory tool life due to

reduced cutting temperature. The TiN-coated drill proved inefficient for dry drilling because of the insufficient hot hardness of the coating, but an MQL with high water content (40%) and low viscosity was efficient in deep hole drilling because of the improved penetration capability of the less viscous fluids. They also found less torque fluctuations during drilling with MQL as compared to dry drilling (**Fig. 2.18**).

Varadarajan et al. [2.85] observed the effect of minimal cutting fluid in the turning of hardenable steel (AISI 4340) using mineral oil as an MQL agent. Cutting fluid was applied at a rate of 0.3 ml/hr. They found that the overall cutting performance (i.e., cutting force, tool life, surface finish, cutting ratio, cutting temperature, and tool--chip contact length) of the MQL application was superior when compared to dry and almost similar to the use of flood conditions. Authors suggested that the minimal cutting fluid technique is a viable alternative to conventional flooded turning.

### **2.6.2. Near- Dry Machining of Aluminum Alloys**

Extensive examinations of the application of MQL during the machining of aluminum alloys have been reported. This section summarizes previous studies on the near-dry machining of aluminum alloys.

Klocke et al. [2.86] studied the effect of MQL on the drilling of cast aluminum alloys (AlSi9Cu3). They used synthetic ester as an MQL agent with a flow rate of 10 ml/h. They used TiCN, TiAlCN, MoS<sub>2</sub>, and Me-C:H coated drills while drilling in MQL. In terms of feed force, torque and hole diameter, there were no significant differences between MQL and flooded drilling. The smallest variations were found in the cases of TiAlCN + Me-C:H and TiAlCN + MoS<sub>2</sub> coatings, and the holes displayed better surface



roughness with MQL (average surface roughness of 15-35  $\mu\text{m}$ ) when compared to dry cutting (average surface roughness of 25-65  $\mu\text{m}$ ).

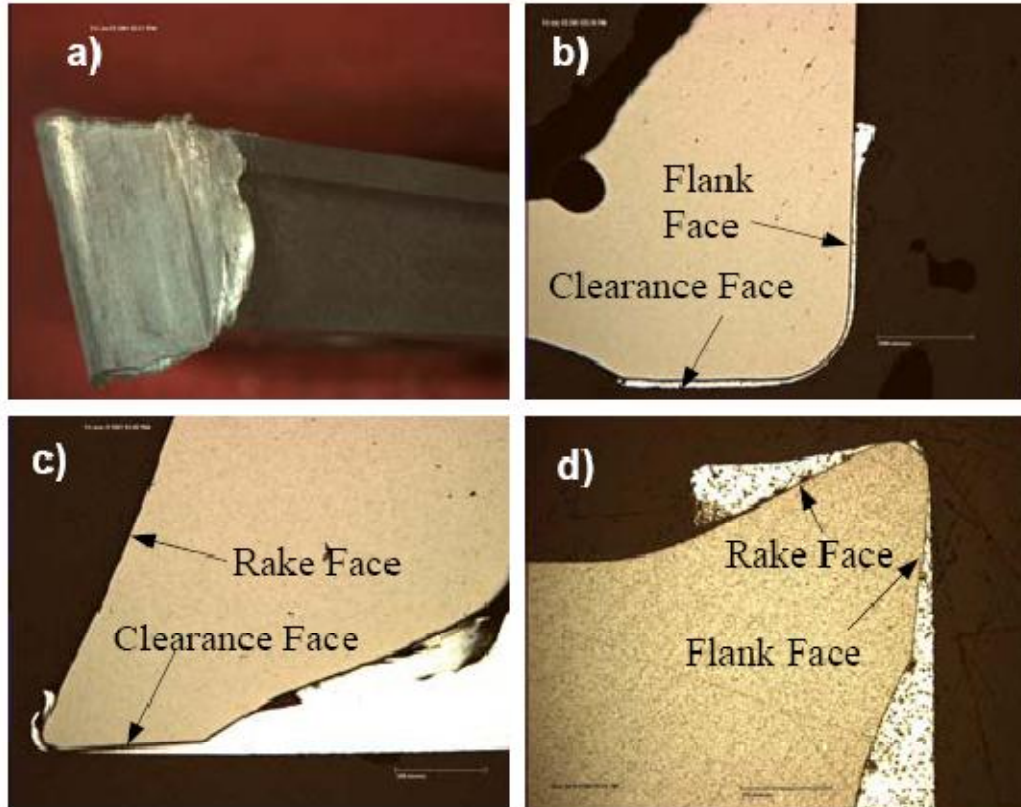


**Figure 2. 19** Adhesion of work material (Al 356) to the surface of the cutter in dry machining: a) Section through the rake face, (b) section through flank face, and c) section through clearance face, d) Al adhesion to the rake and flank face [2.89].

On the theme of chip formation in drilling of cast aluminum, Liu et al. [2.87] observed that the fan-shaped chips were formed in the initial stage of the drilling process, while the curling of the chips was caused by the restriction of the flute and resulting impact with the flute. Chip fracture was caused by the bending moment at the chip-flute impact or chip-hole wall impact. Air and MQL (oil mist) were forced through the drill hole to understand the chip shaping process. Compared with dry drilling, smaller curl

chips were found during drilling with air blowing, while the smallest size of chips was observed with MQL.

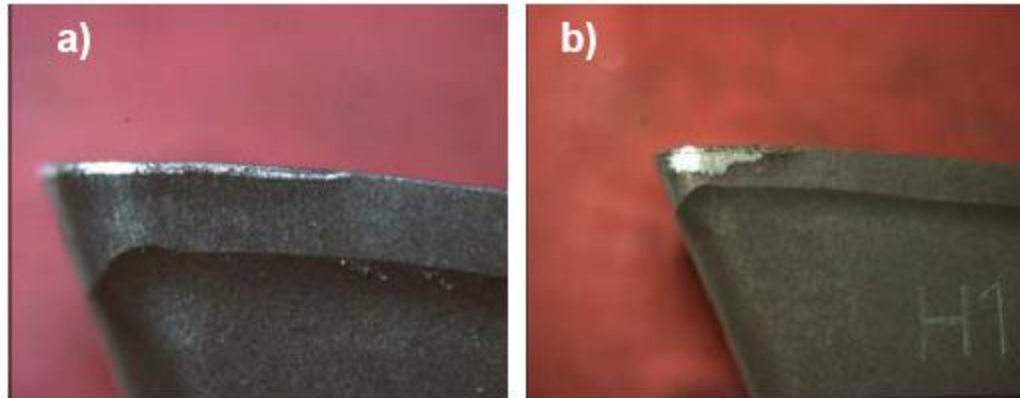


**Figure 2. 20** Adhesion of work material to the surfaces of the cutting tool in “wet” machining: a) Flood lubricant application, and b) MQL application [2.89].

Davim et al. [2.88] studied the formation of cutting power and forces during the drilling of aluminum (AA1050) in dry, MQL (250 ml/h), and flood-lubricated (120 000 ml/h) conditions. The authors found that the cutting power increased with the feed and cutting speed. Higher cutting power and specific cutting force were found for dry drilling in all speed and feed rate combinations, whereas they did not show much variation during MQL and conventional flooded conditions. Similar surface roughness was found for both MQL and flooded conditions in all feed and speed combinations. The authors suggested that the MQL can replace conventional flooded conditions because of similar power generation and surface roughness.

Bardetsky et al. [2.89] evaluated the tool wear suppression in the applications of MQL during the high speed milling of aluminum-silicon alloys (319 Al). The cutting speed, axial depth of cut, and feed rate were 4290 m/min, 2.0 mm and 0.08 mm/tooth,

respectively. They concluded that dry machining produced the highest degree of aluminum adhesion with a significant amount of the workpiece material adhering to the flank, clearance, and rake faces (**Fig. 2.19**). On the other hand, in the case of MQL application, moderate adhesion (discontinuous areas) was found on the flank, rake, and clearance surfaces (**Fig. 2.20**). The smallest amount of adhesion to the rake and flank faces was found in the flood coolant application. A lower resultant cutting force was observed in the case of the flood cooling system due to the formation of a thick boundary layer that reduced the direct contact between the tool and workpiece material. The highest resultant cutting force was found during dry machining due to significant aluminum adhesion. Resultant cutting force as a function of cutting distance for dry, MQL, and flood coolant systems are shown in **Fig. 2.21**.

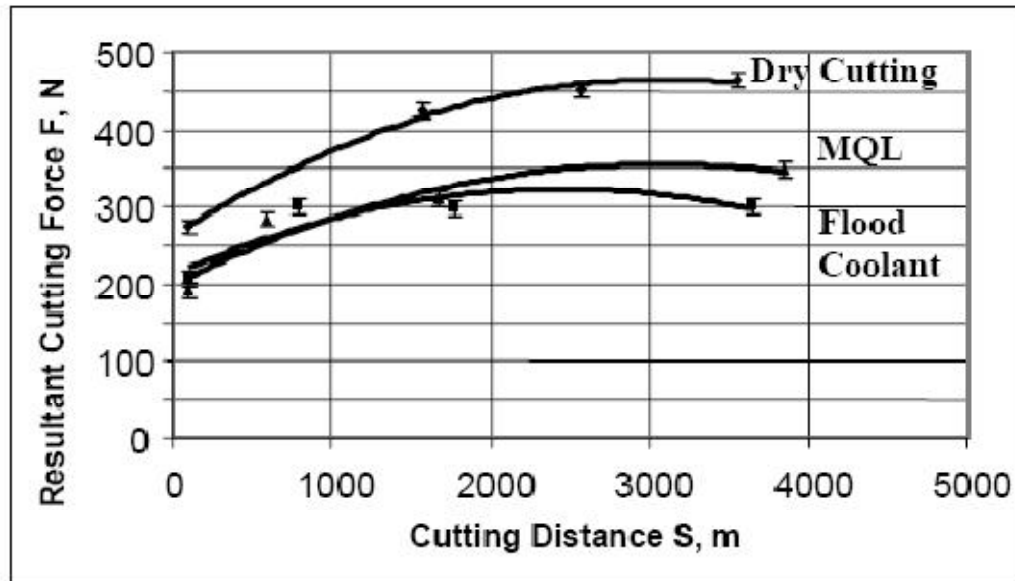


**Figure 2. 21** Cutting force as a function of cutting distance, for different lubrication application strategies [89].

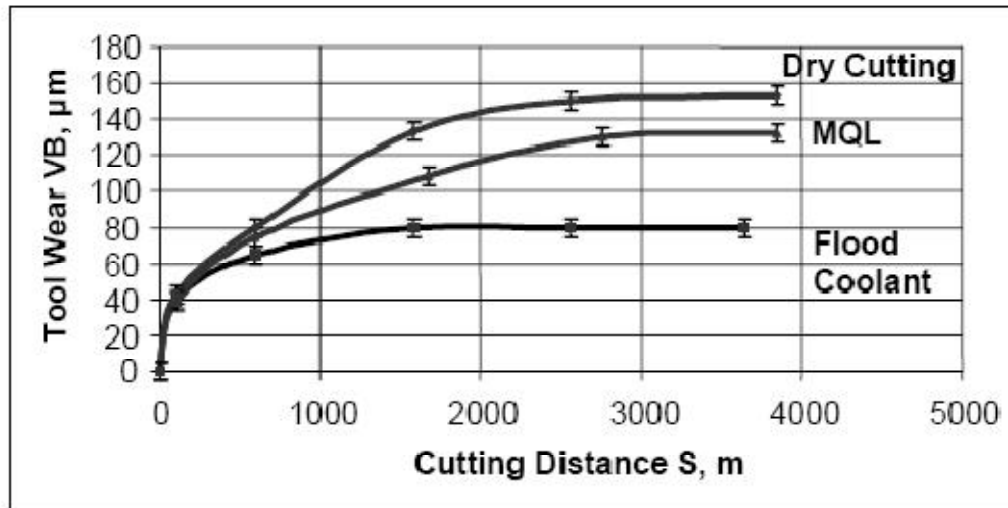


**Figure 2. 22** The relationship between flank wear and the cutting distance in machining with dry, MQL and flood coolant [2.89].

Kishawy et al. [2.90] investigated the effects of coolant strategy (flooded lubrication, minimum quantity of lubrication) on tool wear, chip morphology, surface quality, and cutting forces during the milling of A356 (6.69% Si, 0.44% Mg, 0.02% Cu) aluminum alloys. For the MQL, a synthetic phosphate ester with extreme pressure additives was used. The flow rate was 30 ml/h. The authors found that the MQL technology could be a viable alternative to the flooded drilling. The lowest resultant cutting force belonged to the flood coolant application method, due to the ability of the coolant to reduce material adhesion and friction forces. The MQL displays reduced friction forces, but authors suggested that the MQL with additives will have to be customized for the A356 alloy to reduce cutting forces.

Kelly and Cotterell [2.91] studied the effect of minimal lubrication during the drilling of a 5080 aluminum alloy. The authors compared feed force, torque and surface roughness for flood (mineral soluble oil, flow rate of 5.2 l/min), and MQL (vegetable oil,

20 ml/h) as well as dry conditions. They found that a reduction in torque and thrust force is obtained for both MQL and flooded application with an increase in cutting speed (25 – 105 m/min) and feed rate (0.15 – 0.30 mm/rev). The MQL application was superior to other cooling conditions at higher speeds and feed rates (**Fig 2.23**). MQL displayed similar hole surface roughness compared to the flooded drilling conditions.

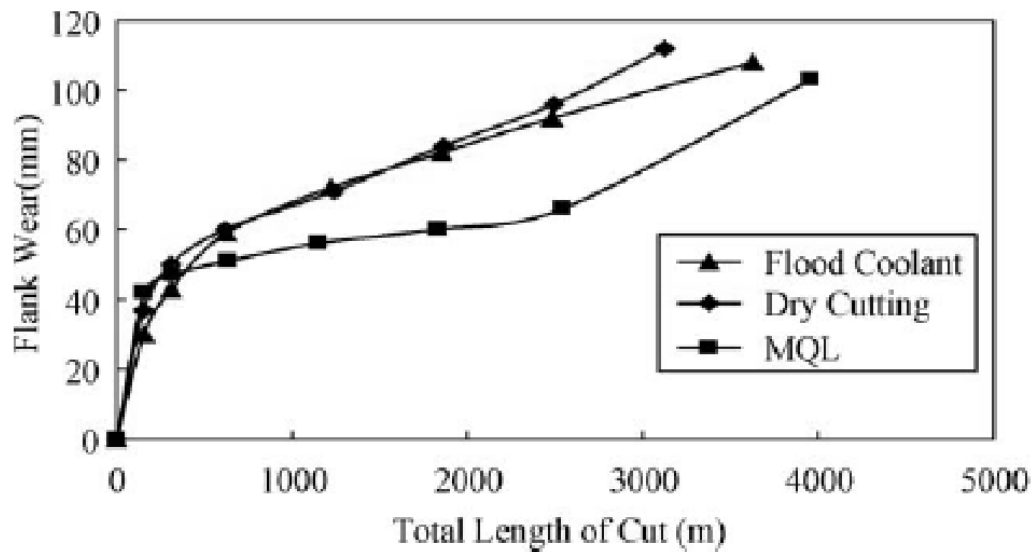


**Figure 2. 23** Effect of cooling system on flank wear for uncoated carbide inserts at the cutting speed of 500 m/min, feed rate of 0.2 mm/tooth and 2 mm depth of cut [2.91].

Braga et al. [2.92] studied the drilling performance of the uncoated and diamond coated carbide drills under both MQL (10 ml/h of mineral oil pulverized in an air flow of 72 m<sup>3</sup>/h and 4.5 bar of pressure) and flood of soluble oil (1 part of oil for 25 parts of water with a flow rate of 2.4 m<sup>3</sup>/h) lubrication conditions in the drilling of aluminum-silicon alloys (A356). Their evaluations showed that the performance of the drilling (in terms of forces, tool wear, and hole quality) when using MQL was very analogous to that found using a high amount of soluble oil, with both diamond coated and uncoated drills.

The power consumed when using flooded conditions (0.80 kW) was higher than when using MQL (0.70 kW) for both uncoated and diamond coated drills.

### **2.6.3. Near- Dry Machining of Magnesium Alloys**

To the author's knowledge, there is only one piece of literature available on the application of MQL in drilling of magnesium alloys. Bhowmick et al. [2.93] studied the effect of water (H<sub>2</sub>O-MQL) and fatty acid based MQL (FA-MQL) in drilling of cast AM60 Mg using uncoated HSS drills. The highest torque values observed during H<sub>2</sub>O-MQL (2.43 N-m) drilling were consistently lower than those obtained during dry drilling (9.32 N-m). A lower resultant torque (2.55 N-m) and better surface quality was observed when using FA-MQL compared dry (9.32 N-m) drilling. The details of this work can be seen in **Chapter 5**.

## **2.7. Summary of Literature Review**

The conclusions and helpful suggestions emerging from the dry drilling and MQL literature survey are as follows:

1. The dry drilling of aluminum and magnesium is exceedingly difficult due to the adhesion of aluminum and magnesium to the drills. The chips that are formed during drilling and tapping tend to adhere to the steel or carbide drill and provide an obstacle to the dislocation of chips through the drill flutes. This type of clogging often causes drill failure.

2. Diamond- like carbon (DLC) coatings provide a promising option for reducing the aluminum adhesion in dry machining. Based on tribological tests conducted in ambient conditions, the DLC coatings have no tendency towards aluminum and magnesium adhesion.
3. The performance of DLC coatings strongly depends on the test conditions, including temperature, applied load, speed, and the presence of water vapour and other gaseous species in the test environment.
4. Improved tool life was achieved using DLC coated cutting tools during the dry drilling of aluminum alloys.
5. The use of MQL to replace flooded conditions in machining operations has been demonstrated by several researchers. The process offers an economic advantage over completely dry and flooded machining. MQL machining also offers good physical and thermal tools and workpiece properties, more so than dry machining.
6. Surface finish, torque, and thrust force variations and chip thickness ratio are all affected beneficially using MQL when compared to conventional flooded and dry machining.

## References

- [2.1] G.E. Totten, D.S. Mackenzie, Handbook of aluminum: physical metallurgy and processes, CRC Press (2003),1063-1103.
- [2.2] D.A. Stephenson, J.S. Agapiou, Metal cutting theory and practice, Second Edition ed., CRC Press, Florida, (2006),17-20,371-416,459-478,551-697.
- [2.3] G. List, M. Nouari, D. G'éhin, S. Gomez, J.P. Manaud, Y. Le Petitcorps, F. Girot, Wear behaviour of cemented carbide tools in dry machining of aluminium alloy, Wear 259 (2005) 1177–1189.
- [2.4] H. Ni, M. Elmadagli, A.T. Alpas, Mechanical properties and microstructures of 1100 aluminum subjected to dry machining, Materials Science and Engineering A 385 (2004) 267-278.
- [2.5] S.P.F.C. Jaspers, J.H. Dautzenberg, Material behaviour in metal cutting: strains, strain rates, and temperatures in chip formation, Journal of Materials Processing Technology 121 (2002) 123- 135.
- [2.6] X. Song, MSc Thesis, Experimental studied and numerical simulations of continuous and discontinuous chip formation during orthogonal cutting, University of Windsor, 2005.
- [2.7] H. Zhang, A.T. Alpas, Quantitative evaluation of plastic strain gradients generated during orthogonal cutting of an aluminum alloy, Materials Science and Engineering A 332 (2002) 249–254.
- [2.8] K.G. Basavakumar, P.G. Mukunda, M. Chakraborty, Influence of grain refinement and modification on dry sliding wear behaviour of Al–7Si and Al–7Si–2.5Cu cast alloys, Journal of Materials Processing Technology 186 (2007) 236–245.
- [2.9] J. McCabe, Dry Holes, Cutting Tool Engineering 54 (2002) 44- 50.
- [2.10] K. Kanda, S. Takehana, S. Yoshida, R. Watanaba, S. Takano, Application of Diamond-Coated Cutting Tools, Surface and Coatings Technology 73 (1995) 115-120.
- [2.11] J.M. Dasch, C.C. Ang, C.A.Wong, R.A.Waldo, D. Chester, Y.T. Cheng, B.R. Powell, A.M. Weiner, E. Konca, The effect of free-machining elements on dry



- machining of B319 aluminum alloy, *Journal of Materials Processing Technology* 209 (2009) 4638–4644.
- [2.12] P. Chen, H. Hu, A.T. Alpas, Effect of bismuth on the tensile properties and dry machining performance of Al-12.7 wt.% Si alloy, *Ceramic Transactions* 207 (2009) 215-223.
- [2.13] S. Kalidas, R.E. DeVor, S. G. Kapoor, Experimental investigation of the effect of drill coatings on hole quality under dry and wet drilling conditions, *Surface and Coatings Technology* 148 (2001) 117–128.
- [2.14] A. Rivero, G. Aramendi, S. Herranz, L.N. Lopez de Lacalle, An experimental investigation of the effect of coatings and cutting parameters on the dry drilling performance of aluminum alloys, *International Journal of Advance Manufacturing Technology* 28 (2006) 1–11.
- [2.15] M. Tash, F.H. Samuel, F. Mucciardi, H.W. Doty, S. Valtierra, Effect of metallurgical parameters on the machinability of heat-treated 356 and 319 aluminum alloys, *Materials Science and Engineering A* 434 (2006) 207–217.
- [2.16] K. Sakurai, K. Adachi, G. Kawai, T. Sawai, K. Ogawa, High feed rate drilling of aluminum alloy, *Materials Science Forum* 331-337 (2000) 625- 630.
- [2.17] K. Naito, T. Suzuki, M. Nakamura, A. Gun, A. Ken, Undesirable phenomena in drilling hypereutectic Al- Si alloys, *Aluminum* 60 (1984) 513- 516.
- [2.18] M. Bono, J. Ni, The effects of thermal distortions on the diameter and cylindricity of dry drilled holes, *International Journal of Machine Tools and Manufacturer* 41 (2001) 2261- 2270.
- [2.19] H. Chen, A.T. Alpas, Sliding wear map for the magnesium alloy Mg-9Al-0.9Zn (AZ91), *Wear* 246 (2000) 106–116.
- [2.20] H.J. Morales, Magnesium, machinability and safety, SAE Technical paper No.800418, SAE, Detroit, Michigan, 1980.
- [2.21] K.Z. Chong, T.S. Shih, Optimizing drilling conditions for AZ61A magnesium alloy, *Materials Transactions* 43 (2002) 2148-2156.
- [2.22] E. Gariboldi, Drilling a magnesium alloy using PVD coated twist drills, *Journal of Materials Processing Technology* 134 (2003) 287-295.

- [2.23] F.Z. Fang, L.C. Lee, X.D. Liu, Mean flank temperature measurement in high speed dry cutting of magnesium alloy, *Journal of Materials Processing Technology* 167 (2005) 119–123.
- [2.24] H.K. Tonshoff, J. Winkler, The influence of tool coatings in machining of magnesium, *Surface and Coatings Technology* 94-95 (1997) 610-616.
- [2.25] P. May, The new diamond age, *Science* 319 (2008) 1490.
- [2.26] E. Konca, PhD Dissertation, Adhesion and material transfer between aluminum and surfaces coated with diamond- like carbon and other coatings, University of Windsor, 2005.
- [2.27] A. Abougharam, MSc Thesis, Tribological behaviour of hydrogenated and non-hydrogenated diamond like carbon coatings in dry and lubricated sliding, University of Windsor, 2008.
- [2.28] Y. Zhang, MSc Thesis, Tribological properties of diamond-like carbon and boron carbide coatings against aluminum: adhesion and friction at different temperatures and environments, University of Windsor, 2007.
- [2.29] Konca, Y.-T. Cheng, A.M. Weiner, J.M. Dasch, A. Erdemir, A.T. Alpas, Transfer of 319 Al alloy to titanium diboride and titanium nitride based (TiAlN, TiCN, TiN) coatings: effects of sliding speed, temperature and environment, *Surface & Coatings Technology* 200 (2005) 2260– 2270
- [2.30] E. Konca, Y.-T. Cheng, A.M. Weiner, J.M. Dasch, A.T. Alpas, Effect of test atmosphere on the tribological behaviour of the non-hydrogenated diamond-like carbon coatings against 319 Aluminum alloy and tungsten carbide, *Surface and Coatings Technology* 200 (2005) 1783 – 1791.
- [2.31] J. Stallard, D. Mercks, M. Jarratt, D.G. Teer, P.H. Shipway, A study of the tribological behaviour of three carbon-based coatings, tested in air, water and oil environments at high loads, *Surface and Coatings Technology* 177 –178 (2004) 545–551.
- [2.32] A. Kimura, Y. Azuma, T. Suzuki, T. Saito, Y. Ikuhara, Microstructure of diamond-like carbon films prepared by cathodic arc deposition, *Diamond and Related Materials* 11 (2002) 1436–1440.

- [2.33] B. Rother, Calculations on ion-assisted deposition techniques examined in relation to the deposition of diamond-like carbon coatings, *Surface and Coatings Technology* 46 (1991) 361-369.
- [2.34] S.K. Field, M. Jarratt, D.G. Teer, Tribological properties of graphite-like and diamond-like carbon coatings, *Tribology International* 37 (2004) 949-956.
- [2.35] J. Heimberg, K. Wahl, I. Singer, A. Erdemir, Superlow friction behavior of diamond-like carbon coatings: Time and speed effects, *Applied Physics Letters* 78 (17) (2001) 2449.
- [2.36] J. Andersson, R.A. Erck, A. Erdemir, frictional behavior of diamond-like carbon films in vacuum and under varying water vapor pressure, *Surface and Coatings Technology* 163–164 (2003) 535.
- [2.37] F. Gao, A. Erdemir, W. Tysoe, The tribological properties of low- friction hydrogenated diamond-like carbon measured in ultrahigh vacuum, *Tribology Letters* 20 (3-4) (2005) 221.
- [2.38] B.K. Tay, D. Sheeja, Y.S. Choong, S.P. Lau, X. Shi, Pin-on-disk characterization of amorphous carbon films prepared by filtered cathodic vacuum arc technique, *Diamond and Related Materials* 9 (2000) 819–824.
- [2.39] C. Donnet, Recent progress on the tribology of doped diamond-like and carbon alloy coatings, A review, *Surface and Coatings Technology* 100-101 (1998) 180-186.
- [2.40] Y. Liu, A. Erdemir, E.I. Meletis, An investigation of the relationship between graphitization and frictional behavior of DLC coatings, *Surface and Coatings Technology* 86-87 (1996) 564-568.
- [2.41] A. Erdemir, The role of hydrogen in tribological properties of diamond-like carbon films, *Surface and Coatings Technology* 146 –147 (2001) 292–297.
- [2.42] H. Ronkainen, S. Varjus, J. Koskinen, K. Holmberg, Differentiating the tribological performance of hydrogenated and hydrogen-free DLC coatings, *Wear* 249 (2001) 260–266.
- [2.43] C. Donnet, J. Fontaine, A. Grill and T. Le Mogne, The role of hydrogen on the friction mechanism of diamond-like carbon films, *Tribology Letters* 9 (2000).

- [2.44] C. Donnet, A. Grill, Friction control of diamond-like carbon coatings, *Surface and Coatings Technology* 94-95 (1997) 156-462.
- [2.45] A. Abou Gharam, M.J. Lukitsch, M.P. Balogh, A.T. Alpas, High temperature tribological behaviour of carbon based ( $B_4C$  and DLC) coatings in sliding contact with aluminum, *Thin Solid Films* 519 (2010) 1611–1617.
- [2.46] Vannhulsel, B. Blanpain, J.P. Celis, J. Roos, E. Dekempeneer, J. Smeets, Study of the wear behaviour of diamond-like coatings at elevated temperatures, *Surface and Coatings Technology* 98 (1998) 1047.
- [2.47] T. Krumpiegl, H. Meerkamm, W. Fruth, C. Schaufler, G. Erkens, H. Bohner, Amorphous carbon coatings and their tribological behaviour at high temperatures and in high vacuum, *Surface and Coatings Technology* 120– 121 (1999) 555.
- [2.48] F. Bremond, P. Fournier, F. Platon, Test temperature effect on the tribological behavior of DLC-coated 100C6-steel couples in dry friction, *Wear* 7 – 8 (254) (2003) 774.
- [2.49] Y. Liu, A. Erdemir, E.I. Meletis, An investigation of the relationship between graphitization and frictional behavior of DLC coatings, *Surface and Coatings Technology* 86-87 (1996) 564-568.
- [2.50] E. Konca, Y.-T. Cheng, A.M. Weiner, J.M. Dasch, A.T. Alpas, Elevated temperature tribological behavior of non-hydrogenated diamond-like carbon coatings against 319 aluminum alloy, *Surface and Coatings Technology* 200 (2006) 3996 – 4005.
- [2.51] W. Ni, Y.-T. Cheng, A. M. Weiner, T. A. Perry, Tribological behavior of diamond-like-carbon (DLC) coatings against aluminum alloys at elevated temperatures, *Surface and Coatings Technology* 201 (2006) 3229–3234.
- [2.52] H. Ronkainen, S. Varjus, K. Holmberg, Tribological performance of different DLC coatings in water-lubricated conditions, *Wear* 249 (2001) 267-271.
- [2.53] K. Persson, R. Gahlin, Tribological performance of a DLC coating in combination with water-based lubricants, *Tribology International* 36 (2003) 851–855.
- [2.54] B. Podgornik, D. Hren, J. Vizintin, S. Jacobson, N. Stavlid, S. Hogmark, Combination of DLC coatings and EP additives for improved tribological behaviour of boundary lubricated surfaces, *Wear* 261 (2006) 32–40.

- [2.55] M. Kalin, J. Vizintin, J. Barriga, K. Vercammen, K. van Acker, A. Arnsek, The effect of doping elements and oil additives on the tribological performance of boundary-lubricated DLC/DLC contacts, *Tribology Letters* 17 (2004) 679- 688.
- [2.56] K. Kanda, S. Takehana, S. Yoshida, R. Watanaba, S. Takano, Application of diamond-coated cutting tools, *Surface and Coatings Technology* 73 (1995) 115-120.
- [2.57] H. Hanyu, S. Kamiya, H. Odagi, Y. Murakami, M. Saka, Development of high performance diamond-coated drills for cutting high silicon aluminum alloy, *Thin Solid Films* 413 (2002) 139.
- [2.58] H. Fukui, J. Okida, N. Omori, H. Moriguchi, K. Tsuda, Cutting performance of DLC coated tools in dry machining aluminum alloys, *Surface and Coatings Technology* 187 (2004) 70.
- [2.59] T.C.S. Vandeveld, K. Vandierendonck, M. Van Stappen, W. Du Mong, P. Perremans, cutting application of DLC, hard carbon and diamond films, *Surface and Coatings Technology* 113 (1999) 80-85.
- [2.60] M. Dai, K. Zhou, Z. Yuan, Q. Ding, Z. Fu, The cutting performance of diamond and DLC-coated cutting tools, *Diamond and Related Materials* 9 (2000) 1753-1757.
- [2.61] M. Lahres, G. Jorgensen, Properties and Dry Cutting Performance of Diamond-Coated Tools, *Surface and Coatings Technology* 96 (1997) 198-204.
- [2.62] P.Eh. Hovsepian, Q. Luo, G. Robinson, M. Pittman, M. Howarth, D. Doerwald, R. Tietema, W.M. Sim, A. Deeming, T. Zeus, TiAlN/VN superlattice structured PVD coatings: a new alternative in machining of aluminum alloys for aerospace and automotive components, *Surface and Coatings Technology* 201 (2006) 265–272.
- [2.63] H.L. Coldwell, R.C. Dewes, D.K. Aspinwall, N.M. Renevier, D.G. Teer, The use of soft/lubricating coatings when dry drilling BS L168 aluminum alloy, *Surface and Coatings Technology* 177 –178 (2004) 716–726.
- [2.64] N. Wain, N.R. Thomas, S. Hickman, J. Wallbank, D.G. Teer, Performance of low-friction coatings in the dry drilling of automotive Al–Si alloys, *Surface and Coatings Technology* 200 (2005) 1885.

- [2.65] J. M. Dasch, C. C. Ang, C. A. Wonga, Y. T. Cheng, A. M. Weiner, L. C. Lev, E. Konca, A comparison of five categories of carbon-based tool coatings for dry drilling of aluminum, *Surface and Coatings Technology* 200 (2006) 2970-2977.
- [2.66] S. Bhowmick, A.T. Alpas, The performance of hydrogenated and non-hydrogenated diamond like carbon tool coatings during the dry drilling of 319 Al, *International Journal of Machine Tools and Manufacture* 48 (2008) 802-814.
- [2.67] R. T. Coelho, R. Arai, H. M. Watanuki, E. Borges, An experimental investigation on wear aspects of tapping operation on hardened steels, *Machining Science and Technology* 10 (2006) 235-250.
- [2.68] C. Warrington, S. Kapoor, R. DeVor, Experimental investigation of thread formation in form tapping, *Journal of Manufacturing Science and Engineering* 127 (2005) 829-836.
- [2.69] G. Boothroyd, W.A. Knight, *Fundamentals of machining and machine tools*, CRC Press, Taylor and Francis, 2006, p. 190.
- [2.70] M. Chen, G. Liu, X. Zhang, Optimization studies on hole-making tools for high-performance cutting austenitic stainless steel, *Machining Science and Technology* 11 (2007) 183-200.
- [2.71] S.C. Veldhuis, G.K. Dosbaeva, G. Benga, Application of ultra-thin fluorine-content lubricating films to reduce tool/workpiece adhesive interaction during thread cutting operations, *International Journal of Machine Tools and Manufacture* 47 (2007) 521-528.
- [2.72] A.E. Reiter, B. Brunner, M. Ante, J. Rechberger, Investigation of several PVD coatings for blind hole tapping in austenitic stainless steel, *Surface and Coatings Technology* 200 (2006) 5532-5541.
- [2.73] A.K. Srivastava, M.E. Finn, M.A. Kinney, Tool/work material/cutting fluid interaction while tapping into AA-319 and AA-A356 T6 lost foam aluminum castings, *Transaction of NAMRI/SME* 32 (2004) 263-270.
- [2.74] Y. Zedan, F.H. Samuel, A.M. Samuel, H.W. Doty, Effects of Fe intermetallics on the machinability of heat-treated Al- (7-11)% Si alloys, *Journal of Materials Processing Technology* 210 (2010) 245-257.

- [2.75] S. Bhowmick, M.J. Lukitsch, A.T. Alpas, Tapping of Al-Si alloys with diamond-like carbon coated tools and minimum quantity of lubrication, *Journal of Materials Processing Technology* 210 (2010) 2142-2153.
- [2.76] M.M.A. Khan, M.A.H. Mithu, N.R. Dhar, Effects of minimum quantity lubrication on turning AISI 9310 alloy steel using vegetable oil-based cutting fluid, *Journal of Materials Processing Technology* 209 (2009) 5573–5583.
- [2.77] Y.S. Liao, H.M. Lina, Y.C. Chen, Feasibility study of the minimum quantity lubrication in high-speed end milling of NAK80 hardened steel by coated carbide tool, *International Journal of Machine Tools & Manufacture* 47 (2007) 1667–1676.
- [2.78] B. Tasdelen, H. Thordenberg, D. Olofsson, An experimental investigation on contact length during minimum quantity lubrication (MQL) machining, *Journal of Materials Processing Technology* 203 (2008) 221–231.
- [2.79] N.R. Dhar, M.W. Islam, S. Islam, M.A.H. Mithu, The influence of minimum quantity of lubrication (MQL) on cutting temperature, chip and dimensional accuracy in turning AISI-1040 steel, *Journal of Materials Processing Technology*, 171 (2006) 93–99.
- [2.80] R. P. Zeilmann, W. L. Weingaertner, Analysis of temperature during drilling of Ti6Al4V with minimal quantity of lubricant, *Journal of Materials Processing Technology*, 179 (2006) 124–127.
- [2.81] Attanasio, M. Gelfi, C. Giardini, C. Remino, Minimal quantity lubrication in turning: effect on tool wear, *Wear* 260 (2006) 333–338.
- [2.82] M. Rahman, A. S. Kumar, M.U. Salam, Evaluation of minimal quantities of lubricant in end milling, *International Journal of Advanced Manufacturing Technology*, 18 (2001) 235–241.
- [2.83] A.R. Machado, J. Wallbank, Effect of extremely low lubricant volumes in machining, *Wear*, 210 (1997) 76- 82.
- [2.84] R. Heinemann, S. Hinduja, G. Barrow, G. Petuelli, Effect of MQL on the tool life of small twist drills in deep-hole drilling, *International Journal of Machine Tools & Manufacture*, 46 (2006) 1–6.

- [2.85] A.S. Varadarajan, P.K. Philip, B. Ramamoorthy, Investigations on hard turning with minimal cutting fluid application (HTMF) and its comparison with dry and wet turning, *International Journal of Machine Tools & Manufacture*, 42 (2002) 193–200.
- [2.86] F. Klocke, T. Beck, G. Eisenblatter, R. Fritsch, D. Lung, M. Pohls, Application of Minimal Quantity of Lubrication (MQL) in Cutting and Grinding, *The British Library- The World's Knowledge*, 967 – 980.
- [2.87] M. Liu, J. Takagi, K. Yanagida, A Study of the Chip Formation and Chip Removal in Dry Drilling of Aluminum Cast Alloy, *Key Engineering Materials*, 257-258 (2004) 575-580.
- [2.88] J P Davim, P S Sreejith, R Gomes, and C Peixoto, Experimental Studies on Drilling of Aluminium (AA1050) under Dry, Minimum Quantity of Lubricant, and Flood-Lubricated Conditions, *Proc. IMechE Vol. 220 Part B: J. Engineering Manufacture* 220 (2006)1605- 1611.
- [2.89] Bardetsky, H. Attia, M. Elbestawi, Evaluating of Tool Wear Suppressive Ability of Lubricants Used in Minimum Quantity of Lubrication Application in High Speed Machining of Cast Aluminum Alloys, *Proceedings of ASME International Mechanical Engineering Congress and Exposition, IMECE 2005-80597*, 1-7.
- [2.90] H.A. Kishawy, M. Dumitrescu, E.-G. Ng, M.A. Elbestawi, Effect of coolant strategy on tool performance, chip morphology and surface quality during high-speed machining of A356 aluminum alloy, *International Journal of Machine Tools & Manufacture*, 45 (2005) 219–227.
- [2.91] J.F. Kelly, M.G. Cotterell, Minimal lubrication machining of aluminium alloys, *Journal of Materials Processing Technology*, 120 (2002) 327–334.
- [2.92] D.U. Braga, A.E. Diniz, G.W.A. Miranda, N.L. Coppini, Using a minimum quantity of lubricant (MQL) and a diamond coated tool in the drilling of aluminum–silicon alloys, *Journal of Materials Processing Technology*, 122 (2002) 127–138.
- [2.93] S. Bhowmick, M.J. Lukitsch, A.T. Alpas, Dry and minimum quantity lubrication drilling of cast magnesium alloy (AM60), *International Journal of Machine Tools and Manufacture* 50 (2010) 444-457.



## CHAPTER 3

### **Minimum Quantity Lubrication Drilling of Aluminum-Silicon Alloys in Water using Diamond-Like Carbon Coated Drills**

The dry drilling of aluminum-silicon (Al-Si) alloys is an exceedingly difficult machining process, due to aluminum's tendency to adhere to the drills. In this chapter, the feasibility of the use of a minimum quantity lubrication (MQL) process as an appropriate alternative to the dry and traditional flooded drilling of a 319 grade Al-Si alloy has been discussed. Diamond-like carbon (DLC) coatings improve the dry drilling performance due to their adhesion mitigating properties, which is discussed in Section 3.1. The experimental approach consisted of the evaluation of the cutting performance of diamond-like carbon (DLC) coated HSS drills in a distilled water spray (30 ml/h) used as the MQL agent, which is discussed in Section 3.2. The H<sub>2</sub>O-MQL cutting of 319 Al using DLC coated drills reduced both the drilling torque and the thrust force when compared to dry drilling, which is also comparable to the traditional flooded condition. An added advantage of the H<sub>2</sub>O-MQL drilling was that the process became more stable; a smaller percentage of drilled holes exhibited "torque spikes" i.e. an abrupt increase in torque, indicative of adhesion. H<sub>2</sub>O-MQL cutting using non-hydrogenated DLC is preferred to hydrogenated DLC because it resulted in smaller built-up edge (BUE) formation and also less amount of drill flute aluminum adhesion resulting in less torque and thrust force being required during drilling. The results in conjunction with discussion are approached in Section 3.3. The conclusions of the experimental results are written in Section 3.4.

### 3.1. Introduction

Metal removal fluids decrease friction between the cutting tool and the workpiece material, preventing tool wear and, in the case of aluminum, reducing adhesion to the tool. Current environmental and health concerns, however, require manufacturers to reduce the volume of their waste streams [3.1]. The dry machining process (i.e. machining without the use of metal removal fluids) satisfies the aforementioned circumstances in steel and other ferrous materials [3.2, 3.3], but the dry machining of aluminum and especially the dry drilling of cast Al- Si alloys has proven difficult due to aluminum's adhesion to the drill. The chips that adhere to the drill, particularly to the high speed steel (HSS) drills create obstacles to chip evacuation through the drill flutes. Such chip clogging often results in rapid drill failure. The challenge is to minimize the adhesion of aluminum to the drill, which can be achieved to a certain degree with the use of certain types of carbon based coatings, primarily diamond-like carbon (DLC) coatings [3.2, 3.4-3.9]. Meanwhile, an environmentally friendly technique that feeds minute quantities of lubricant i.e. 5-50 ml/h [3.10] to the cutting edge of the tool---a method known as Minimum Quantity Lubrication (MQL) is promising and could be used in conjunction with the DLC coated drills. This work investigates the application of aluminum adhesion mitigating DLC coatings in the MQL drilling of Al-Si alloys. The effects of the water MQL process were considered not only because water provides an environmentally sustainable MQL fluid, but also because DLC coatings revealed favourable tribological properties under high humidity. It is therefore useful to review the existing literature on the friction and wear of DLC coatings in water environments.

### **3.1.1. Tribological Behaviour of DLC Coatings in Water and High Relative Humidity (RH)**

Traditional hard coatings based on nitrides, including TiN, TiCN and CrN, demonstrate poor adhesion-mitigating performance against aluminum alloys, generating high coefficient of friction (COF) and an unacceptably high amount of aluminum transfer during pin-on-disc tests [3.2, 3.3]. Carbon based tool coatings, on the other hand, particularly DLC coatings, display improved performance during dry tribological tests, with a low COF and minimum aluminum adhesion under ambient testing conditions compared to other hard coatings [3.3, 3.5-3.7]. In practice, when diamond-like carbon coatings are exposed to humid environments their performance becomes sensitive to the hydrogen content of the coatings [3.8-3.10]. Ronkainen et al. [3.11] compared the tribological performance of hydrogenated DLC (H-DLC with 40% H) and non-hydrogenated DLC (NH-DLC with <1% H) in water. The tribological tests consisted of reciprocating sliding tests against alumina balls under a normal load of 5N. The H-DLC coating performed poorly under water lubricated conditions, resulting in rapid wear. The COF of the H-DLC film was higher than that of the NH-DLC film, which was as high as 0.6 at the beginning of the test but then decreased until it reached a low value of 0.05. Stallard et al. [3.12] studied the tribological behaviour of two commercial carbon-based coatings (NH-DLC-designated as Graphit-iC and H-DLC-designated as Dymon-iC) by testing them in air, water and oil. Each coating type was tested using a pin-on-disc arrangement at three applied forces of 10, 40 and 80 N against a WC-6%Co ball. The NH-DLC coating showed an initial COF of 0.08 in ambient air, which was higher than that of the H-DLC with a COF of 0.04 at high load of 80 N. The NH-DLC coating exhibited a slightly lower COF of 0.07 when tested in water, and wear rates were low

( $2.3 \times 10^{-17} \text{ m}^3\text{N}^{-1}\text{m}^{-1}$ ), but the H-DLC coatings failed rapidly when tested in water. Suzuki et al. [3.13] studied the tribological properties of H-DLC films using a ball-on-plate reciprocating friction tester in a water environment against a martensitic stainless steel (AISI 440C) ball. They found that the COF and the specific wear rate of H-DLC films were 0.07 and  $10^{-8} \text{ mm}^3/\text{N}\cdot\text{m}$ , respectively. On the other hand, the COF and wear rate in ambient air were 0.03 and  $10^{-7} \text{ mm}^3/\text{N}\cdot\text{m}$ . In water testing environment the ball surface was covered with more transferred materials than it was in air. Konca et al. [3.4] studied the effects of testing atmosphere on the tribological behaviour of the NH-DLC against the same 319 aluminum-silicon alloy that is used in this work and measured high COFs (0.46, 0.47, and 0.44) and high wear rates ( $2.48 \times 10^{-4}$ ,  $3.60 \times 10^{-4}$  and  $6.64 \times 10^{-5} \text{ mm}^3/\text{m}$ ) for the NH-DLC coatings in vacuum, nitrogen and dry air (0% RH) at 1N load. The lowest COF (0.08) and wear rate ( $4.38 \times 10^{-7} \text{ mm}^3/\text{m}$ ), however, were observed in air with an 85% RH. It was generally thought that the presence of hydrogen in water promotes the formation of C-H bonds, which helps to passivate the carbon bonds on DLC film surfaces [3.5-3.10].

### **3.1.2. Effect of MQL on the Machining of Aluminum Alloys by Uncoated HSS and Carbide Tools**

A relatively small number of studies have been reported on the application of MQL when machining aluminum alloys, and most of them use uncoated steel or carbide drills. Kishawy et al. [3.14] compared the effects of flooded lubrication and MQL on tool wear, chip morphology, surface quality and cutting forces during the milling of an A356 aluminum-silicon alloy (6.69% Si, 0.44% Mg, 0.02% Cu) using an uncoated carbide tool. For the MQL, a synthetic phosphate ester (30 ml/h) with “extreme pressure additives”

was used. The MQL displayed reduced friction forces (142 N) when compared to flooded lubrication (146 N) at a speed of 5000 m/min and a feed rate of 0.2 mm/tooth. Kelly and Cotterell [3.15] studied the effects of MQL used during the drilling of an aluminum-magnesium alloy (4.50% Mg, 0.70% Mn) with uncoated HSS. The authors compared feed force, torque and surface roughness for flooded (mineral soluble oil, flow rate of 5.2 l/min), MQL mist (vegetable oil, 20 ml/h) and dry conditions. Reductions in torque and feed force were obtained for all methods of coolant application with an increase in cutting speed (25 - 105 m/min) and feed rate (240 - 500 mm/min). In torque responses, the mist applications (2.2 N-m) performed better than the flooded (2.4 N-m) and dry conditions (3.8 N-m). The mist application was also superior in feed force responses (400 N) at higher speeds and feed rates than the other cooling conditions (flood - 450 N, dry - 675 N). Braga et al. [3.16] studied the drilling performance of the uncoated and diamond coated carbide drills under both MQL (10 ml/h of mineral oil) and a flood of soluble oil (1 part of oil for 25 parts of water) in the drilling of A356 aluminum-silicon alloys. Their evaluations revealed that the performance of the drilling in terms of feed forces when using MQL (max. feed force 1.26 kN) was very analogous to that found using a high amount of flooded soluble oil (max. feed force 1.25 kN). The power consumed when using flooded soluble oil (max. consumed power 0.86 kW) was slightly higher than that when using MQL (max. consumed power 0.80 kW) for uncoated carbide drills.

Consequently, according to the studies reviewed above, the MQL performed better than both dry and flooded coolants when cutting aluminum alloys. In contrast, Bardetsky et al. [3.17] observed that flooded coolant (40 l/min) outperformed MQL (10 ml/h) during the high speed milling of 319 Al alloys. They used cemented carbide inserts

(Coromant grade H13A) and a synthetic phosphate ester liquid (BM2000) as the MQL lubricant. The cutting speed, axial depth of cut and feed rate were 4,290 m/min, 2.0 mm and 0.08 mm/tooth, respectively. A lower resultant cutting force (300 N) was observed in the case of the flooded cooling system compared to MQL (350 N). The highest resultant cutting force (450 N) was observed during dry machining, due to significant aluminum adhesion. The authors stated that in flooded conditions, the formation of a thick boundary layer of lubricant reduced the direct contact between the tool and workpiece material.

In summary, published reports agree (except [3.17]) that MQL performs better than flooded lubrication during aluminum machining. The development of an effective MQL drilling process ultimately depends on the i) type of MQL agent; ii) composition of the aluminum alloy being machined and; iii) tribological properties of the drill surfaces. The survey also indicates that DLC's may be beneficial as tool coatings. In this respect, reliable measurement methods that can distinguish between the drilling performances of DLC coated drills with different compositions in MQL machining must be developed. This approach will help to select the optimum MQL-DLC coating conditions for aluminum drilling.

This study evaluates systematically the cutting performance of uncoated and DLC coated HSS drills during the MQL drilling of 319 Al using distilled water. We have examined the dry drilling performance of DLC coatings in a recent publication [3.18]. We use the same methodology here to analyze the MQL response of the DLC coatings against 319 Al. 319 Al was chosen due to its extended application in automotive components like engine blocks and heads, where drilling is one of the most vital machining process. The drilling performance was assessed by measuring the torque and

thrust force generated during drilling. This approach allows us to compare dry drilling with MQL drilling as well as comparing H-DLC and NH-DLC tool coatings with the uncoated high-speed steel (HSS) drills. The resulting torque and thrust force measurements were complemented by quantitative metallographic analyses of the tested drill surfaces to establish correlations between measured parameters and aluminum adhesion to the tool surface.

## **3.2. Experimental Approach**

### **3.2.1. Workpiece Material: 319 Al Alloy**

The workpiece material was a sand cast 319 Al alloy tested in rectangular blocks of  $30 \times 15 \times 2.54\text{-cm}^3$  in as-cast condition, supplied by General Motors Co. (Michigan, USA). 319 Al is a hypoeutectic aluminum alloy containing (in wt. %) 6.0% Si, 3.5% Cu, 0.26% Fe, 0.1% Mg, 0.01% Mn, 0.01% Ni, 0.08% Ti and the balance Al. The bulk hardness of the 319 Al was 72.40 HR-15T, measured as Rockwell Superficial Hardness using a 1/16 in. (1.59 mm) diameter ball and a 15 kg load. The matrix microhardness of the 319 Al was measured as  $HV_{10} 65.00 \pm 7.50$ . The microstructure of the 319 Al consisted of an  $\alpha$ -Al matrix and mainly eutectic silicon particles. There were intermetallic phases as well that consisted of  $Al_5Cu_2Mg_8Si_6$ ,  $Al_{15}(Fe,Mn)_3Si_2$  and  $CuAl_2$ .

### **3.2.2. Properties of HSS and DLC Coated Drills**

The cutting tools used for the drilling were  $6.35 \pm 0.01$  mm-diameter high-speed steel (HSS) twist drills manufactured by Precision Twist Drill Co. (Illinois, USA). The chemical composition of the HSS (in wt. %) was 0.95% C, 6.00% W, 5.00% Mo, 4.20% Cr, 2.00% V, and the balance Fe. The average Rockwell hardness of the HSS twist drills was 64 HRC. A schematic representation of the uncoated HSS twist drill and the terms used in describing its geometry are shown in Fig. 3.1.

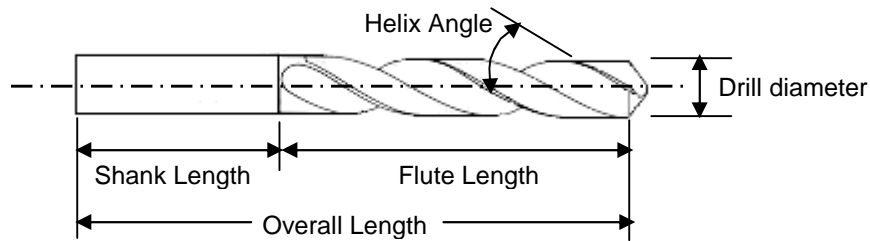


**Figure 3. 1** Geometry of twist drill of 6.35 mm in diameter. The drill consists of two flutes with high helix angle of  $37^\circ$  and point angle of  $118^\circ$ . The flute length is 70 mm and the shank length is 30 mm.

Two types of DLC-based drill coatings were deposited on the twist drills. Among these, NH-DLC (Graphit-iC) was deposited on the HSS twist drills by closed field unbalanced magnetron sputter ion plating. The H-DLC (Dymon-iC) was deposited using a hybrid of unbalanced magnetron sputtering and plasma enhanced chemical vapour deposition process (PECVD). Both types of DLC coated drills were supplied by Teer Coatings Ltd. (Worcestershire, UK) and coating deposition, parameters and details of coating characteristics can be found elsewhere [3.12, 3.19]. The NH-DLC coatings incorporated less than 2% hydrogen in their structure, and were sputtered from two graphite and two chromium targets. A Cr interlayer of 0.1-  $\mu\text{m}$  thickness was deposited on the HSS drill surface to improve bonding between the DLC and the steel. The



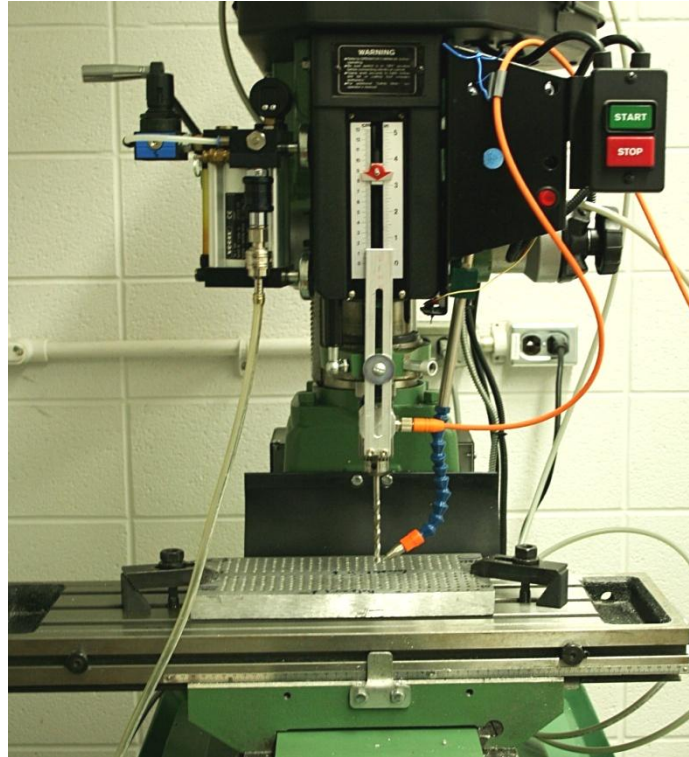
hardness of the NH-DLC coating was 14.5 GPa. The H-DLC (40 at. % H) coatings were deposited using 12.56-MHz RF generator and by applying pulsed d.c. bias on the substrate [3.19]. A Cr interlayer followed by a CrC layer was deposited with the addition of butane. The hardness of the H-DLC coatings was 17.9 GPa.

### 3.2.3. Drilling Tests and MQL Supply

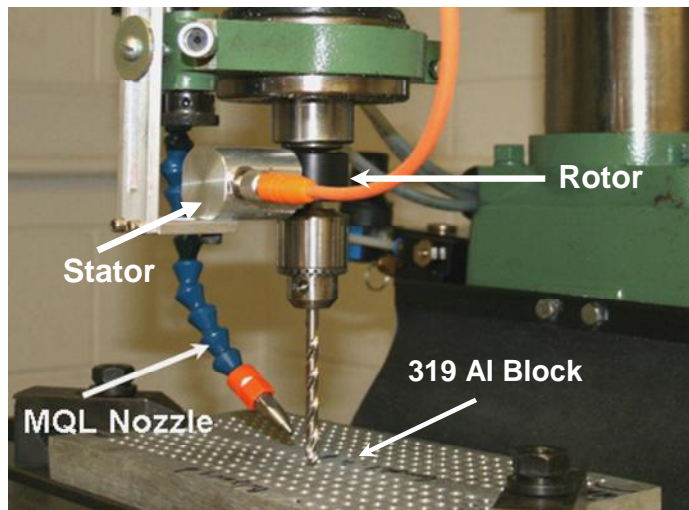
Drilling tests were performed using a computer numerically controlled (CNC) drill press with a maximum power of 2.237 kW and a maximum rotational speed of  $5 \times 10^3$  rpm (100 m/min). The drilling station was equipped with an external MQL system (LubriLean Smart, Vogel, Germany) (Fig. 3.2a). A non-contact magneto-static torque sensor was mounted on the chuck located between the drill tip and the drill motor to measure the torque and thrust force generated during drilling. Details of the torque and thrust force measurements are given in [3.18]. The drilling tests were performed at cutting speeds of 2500 rpm (50 m/min) using a feed rate of 0.25 mm/rev. During each drilling cycle a 19 mm deep hole was made.

Distilled water was supplied using the external MQL system. The MQL nozzle is shown in Fig. 3.2 (b). Compressed air was fed to the system through the air hose to pressurize water in the reservoir, prompting the transportation of the water from the reservoir through a system of ducts and lines to the spray nozzle, where an aerosol of water on air droplet is produced at the nozzle outlet. Water and atomized air were fed through coaxial lines from the MQL system to the spray nozzle. The MQL agents were

directed to the tip of the drill using a flow rate of 30 ml/h. Here, this process is referred to as H<sub>2</sub>O-MQL.



(a)



(b)

**Figure 3. 2** (a) Experimental set-up with MQL reservoir. (b) Close up view showing the non-contact torque and thrust force sensor (rotor and stator), H<sub>2</sub>O-MQL nozzle and drilled 319 Al block.

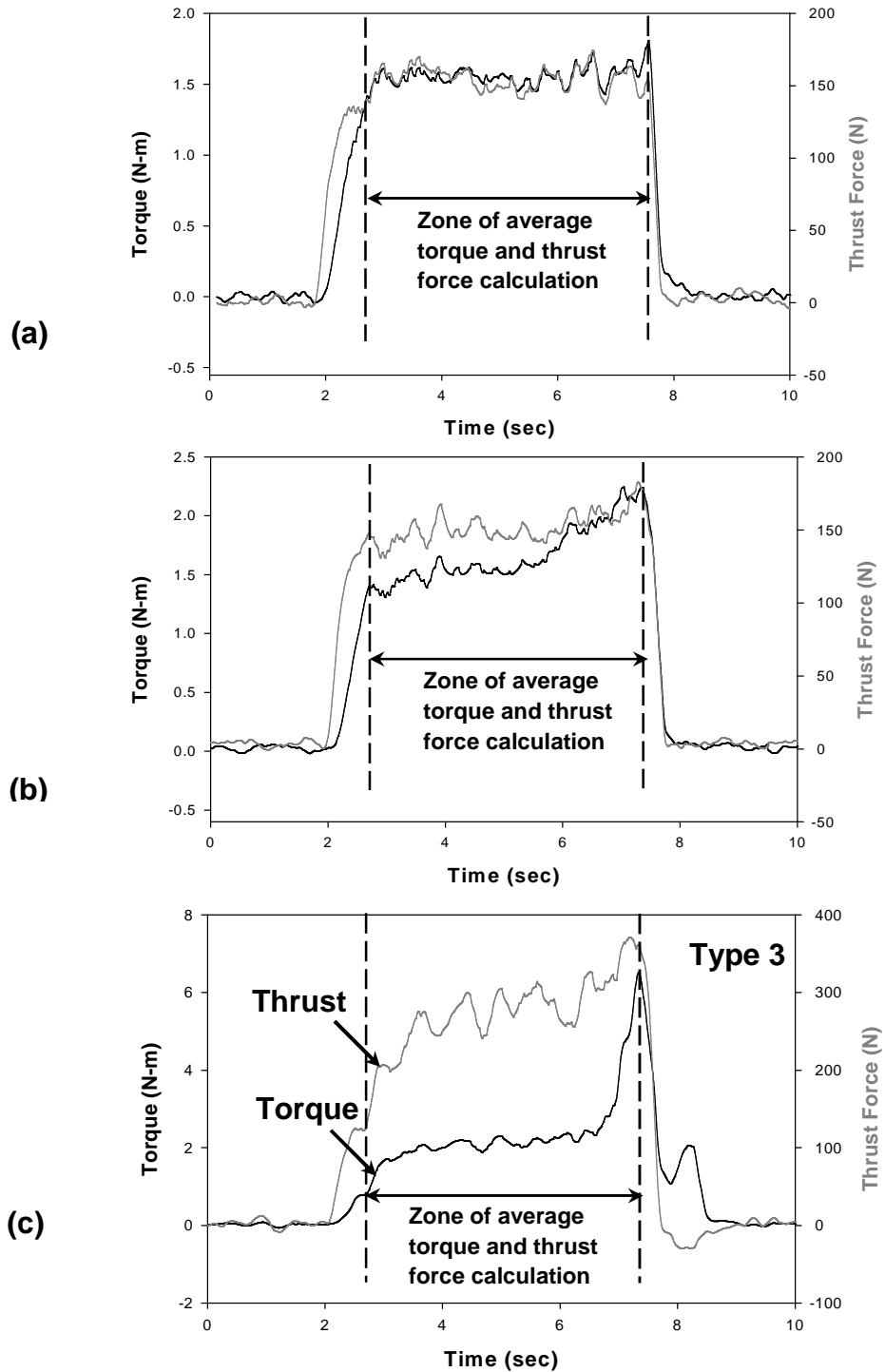


**Figure 3. 3** Three types of torque–thrust curves generated during drilling: (a) a uniform torque and thrust force curve, (b) a steady-state increasing torque and thrust force curve, and (c) a typical torque curve with a spike. To calculate the average torque and thrust forces, data was taken from the onset of chip clogging to the retraction of the drill.

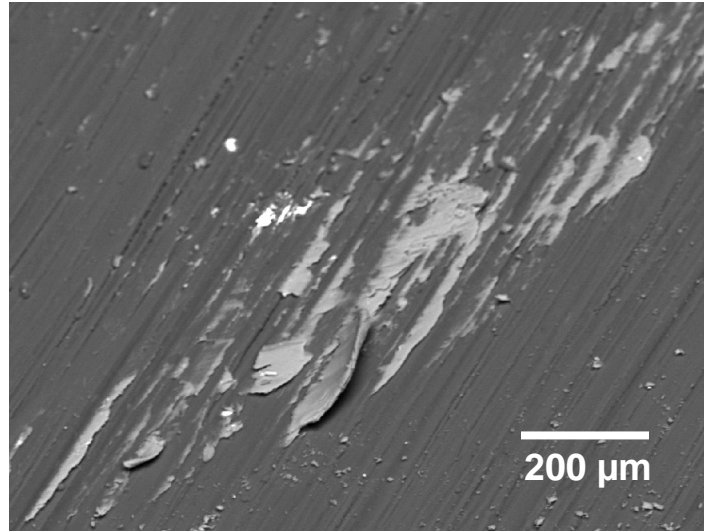
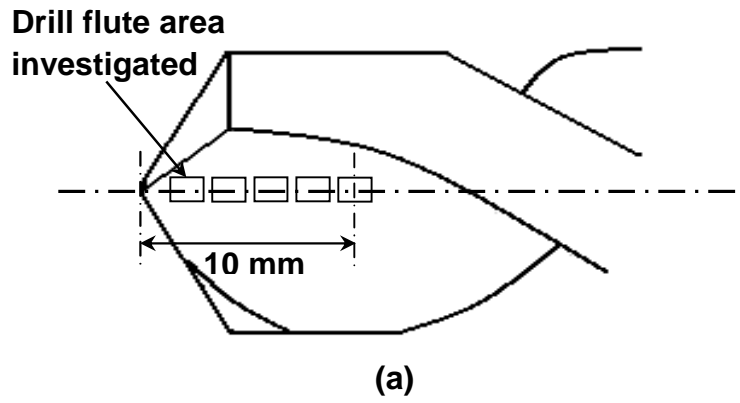


**Figure 3. 4** (a) Locations of SEM images taken on the drill flute. (b) BSE image of a section of the drill flute of the NH-DLC coated drill tested under dry conditions

### 3.2.4 Drilling Tests under Dry and Flooded Conditions

During the first step of this work, the drilling performance of uncoated HSS in H<sub>2</sub>O-MQL was compared with the uncoated HSS in abundant flooded coolant system. A commercial water soluble coolant (Hangsterfers 500S, USA) in a flow rate of 30000 ml/h was used as the flooded coolant. Some tests were done without the use of any metal removal fluid (i.e. under the dry drilling condition) in ambient air with a relative humidity

(RH) of 25%. A total of 150 holes were drilled in the 319 Al workpiece in rows with a horizontal, center-to-center spacing of 10 mm between the adjacent holes.

### 3.2.5. Measurement of Cutting Torque and Thrust Force

The torque required to drill each hole was measured. Each drilling cycle had a duration of approximately 5 seconds between the initial contact and the complete retraction of the drill bit. The plateau formed during a given drilling cycle was used to measure the average torque required to drill one hole. More specifically, the average torque (in N-m) was calculated from the difference in torque between the onset of chip clogging and the drill's retraction, as depicted in Fig. 3.3. Fig. 3.7 displays the torque responses of the last 25 holes drilled using uncoated HSS and DLC coated drills. A close inspection of Fig. 3.7 reveals that the torque response of each hole is different, but generally the torque curves can be categorised into three types, these are shown in Fig. 3.3. Fig. 3.3 (a) illustrates a typical uniform torque curve where there is no significant difference in torque between entrance and exit. The holes starting at 260 s. in Fig. 3.7 (a) and those starting at 1260 s. in Fig. 3.7 (b) provide examples of this type (indicated as type 1) of torque response. The majority of the holes drilled under H<sub>2</sub>O-MQL conditions exhibited torque curves in the form of Type 1. Fig. 3.3 (b) shows an almost steadily increasing torque curve (Type 2) where chip clogging occurred continuously. An example is the hole starting at 370 s. in Fig. 3.7 (a). In certain holes, at the hole's innermost position (19 mm) the chips did not evacuate through the drill flute, causing the formation of a "torque spike" at the end of the drilled hole as depicted in Fig. 3.3 (c). The

holes starting at 430 and 460 s. in Fig. 3.7 (a) exhibit a typical torque spike. These are labeled as Type 3 in Fig. 3.7 (a).

Thrust forces were measured together with torque for the first 150 holes drilled using uncoated HSS and DLC coated drills (e.g. see Fig. 3.11). Similar to torque curves, each plateau in Fig. 3.11 corresponds to one hole being drilled. The average thrust force was calculated from the onset of chip clogging to drill retraction---indicated in Fig. 3.3.

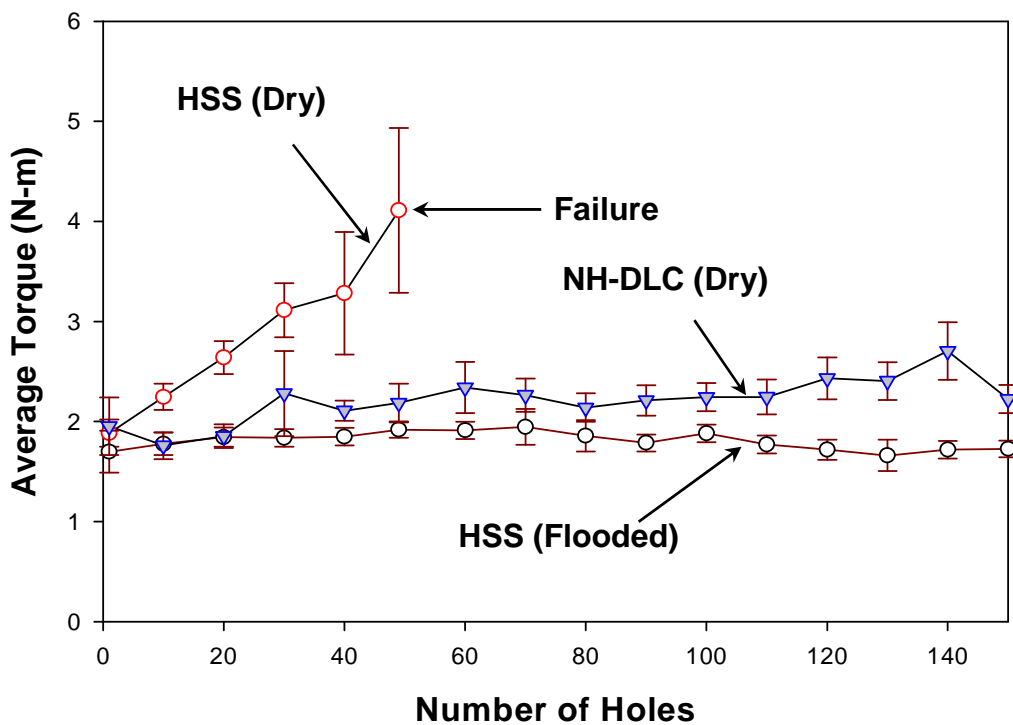


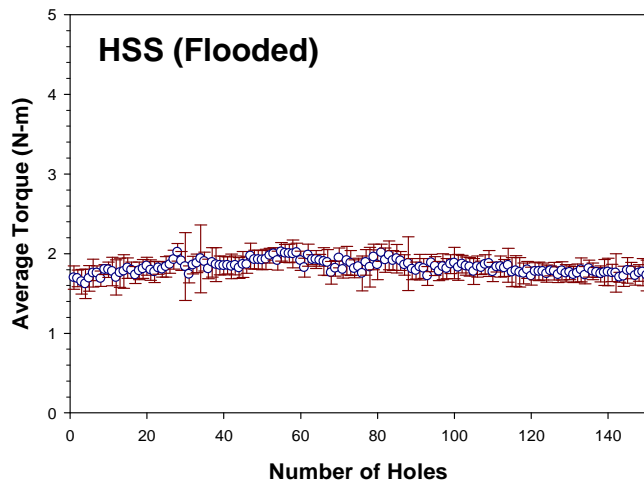
**Figure 3. 5** Comparison of average torque responses of uncoated HSS drills (under dry and flooded conditions) with the NH-DLC coated drills in dry condition. The figure shows reduced data for clarity. The error bars indicate the standard deviation of torque data for each hole.

### 3.2.6. Characterization of Drill Surfaces

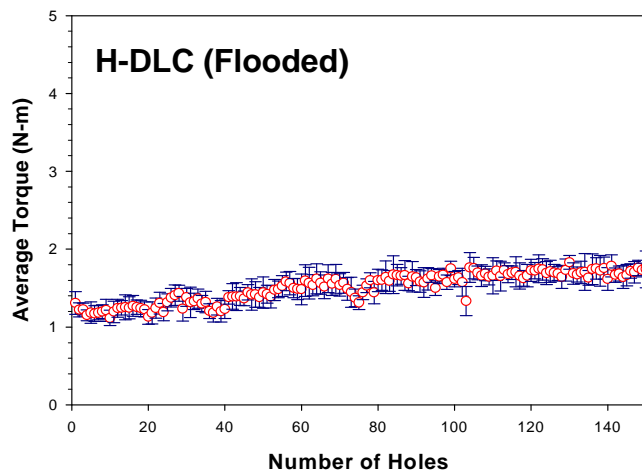
The drills that were tested were analysed using a scanning electron microscope (JEOL JSM- 5800LV SEM) to investigate the formation of build-up edge (BUE) at the drill's cutting edge. The SEM was also used to investigate aluminum chips that had adhered to the flute faces.

An image analysis program was used to determine the percentage of the area covered by the adhered aluminum for each image. The reported values are the averages of values obtained from five images from each drill surface. The SEM images were taken from each location of drill flutes shown in [Fig. 3.4 \(a\)](#). Elements with larger atomic masses appear brighter than the lighter ones in the back scattered electron imaging (BSE) mode of the SEM. Thus, (BSE) images provide a convenient way to differentiate the substrate material from the adhered aluminum. The BSE image in [Fig. 3.4 \(b\)](#) shows that the contrast between the adhered aluminum and NH-DLC coating surface is clearly defined.

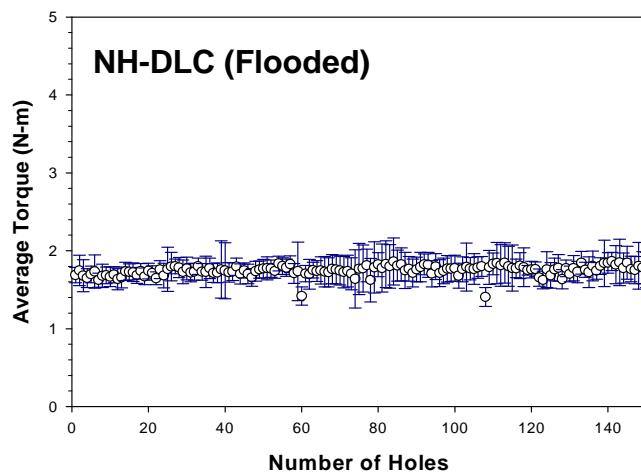
The mass of the adhered aluminum was calculated by measuring the difference between the mass of the drill before and after the drilling experiments, using a balance with sensitivity of  $\pm 10^{-4}$  g.



(a)



(b)



(c)

**Figure 3. 6** The average torque variations for (a) uncoated HSS drills using flooded coolant system, (b) H-DLC coated drills using flooded coolant system, and (c) NH-DLC coated drills using flooded coolant system.



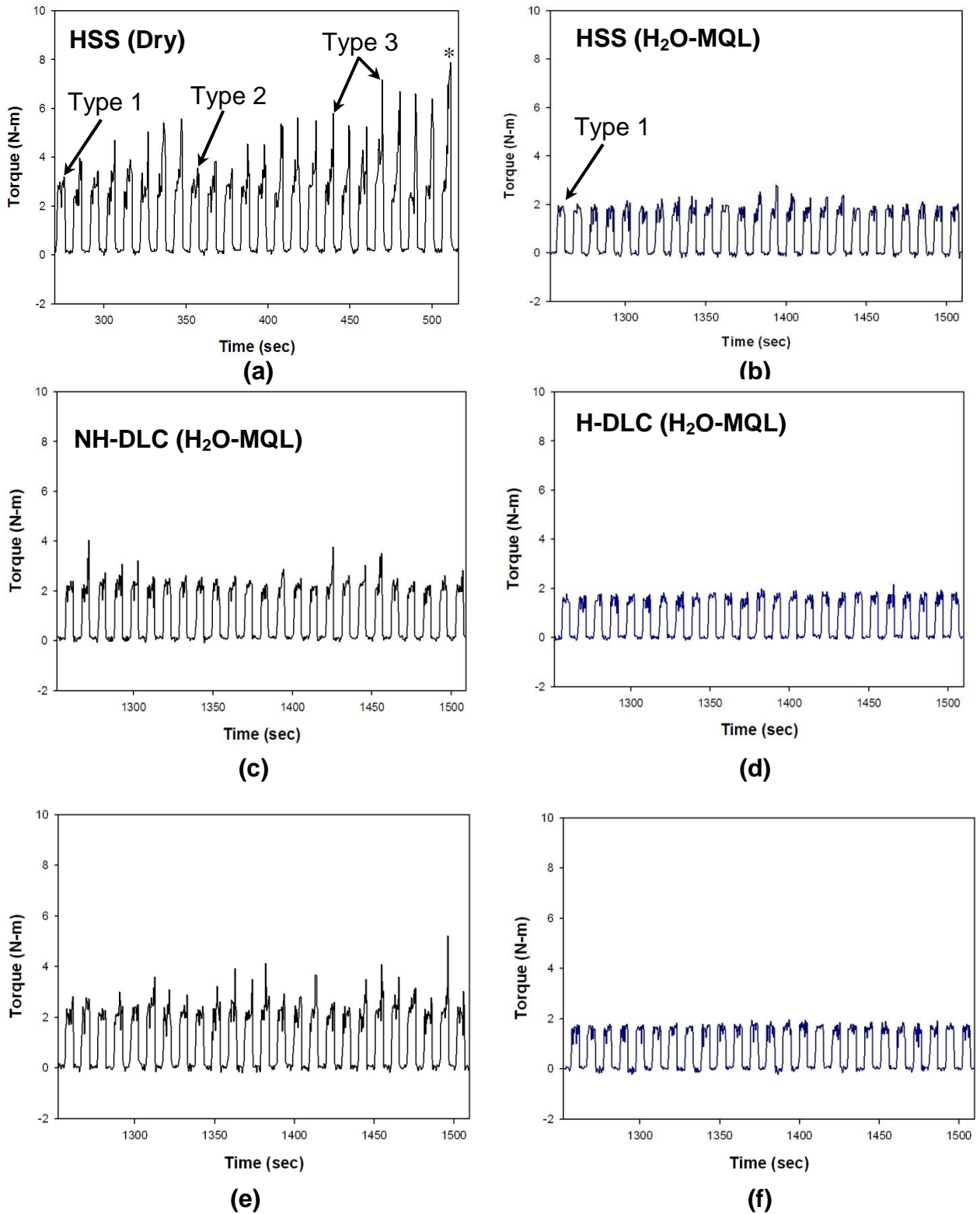


**Figure 3. 7** Torque plots (a, b) representing the last 24 holes with uncoated HSS drills in dry and H<sub>2</sub>O-MQL conditions, where the drill failed at hole 49 in dry conditions (shown by asterisk [\*]); (c, d, e, f) showing the torque responses of the last 25 (126–150) holes drilled with H-DLC and NH-DLC coated drills in dry and H<sub>2</sub>O-MQL conditions.

### 3.3. Results and Discussion

#### 3.3.1 Flooded versus Dry Drilling of 319Al

The first step of the experimental methodology consisted of comparing the drilling response of 319 Al under flooded and dry drilling conditions. This comparison helps to clarify why it is significant to study MQL drilling of this alloy using DLC coated drills and compare the results with dry drilling condition, rather than the fully flooded drilling. Fig. 3.5 serves to illustrate a summary of the variation of the average torques generated during drilling of 319 Al under different conditions. Under the conventional flooded drilling conditions little resistance is offered by the 319 Al samples to drilling with HSS drill as evident by the small torque values that maintained an average of 1.75 N-m throughout the drilling experiments. More specifically, as the complete set of data for each hole for the first 150 drilling cycles show the average torque increased hardly from 1.69 N-m (1<sup>st</sup> hole) to 1.73 N-m (150<sup>th</sup> hole) by 2% in flooded coolant system (Fig. 3.5a). The problem arises when the HSS drills were used to drill the same 319 Al block under the dry conditions where a drastic increase in average torque to 4.11 N-m (Fig. 3.5a) led to drill failure only of the 49 tries (see Section 3.2 for details). This shows that the use of uncoated HSS drills is out of question for dry drilling of 319 Al due to excessive adhesion to drill surfaces [3.18]. A considerable improvement in drilling performance of 319 Al can be achieved when DLC coated HSS drills are used instead of uncoated drills. This is seen in Fig. 3.5 (a) in the case of a non-hydrogenated DLC (NH-DLC) coated drills for which drilling of 319 Al blocks needed application of torque no larger than 2.18 N-m. There is a slight increase in the average values of torque as the

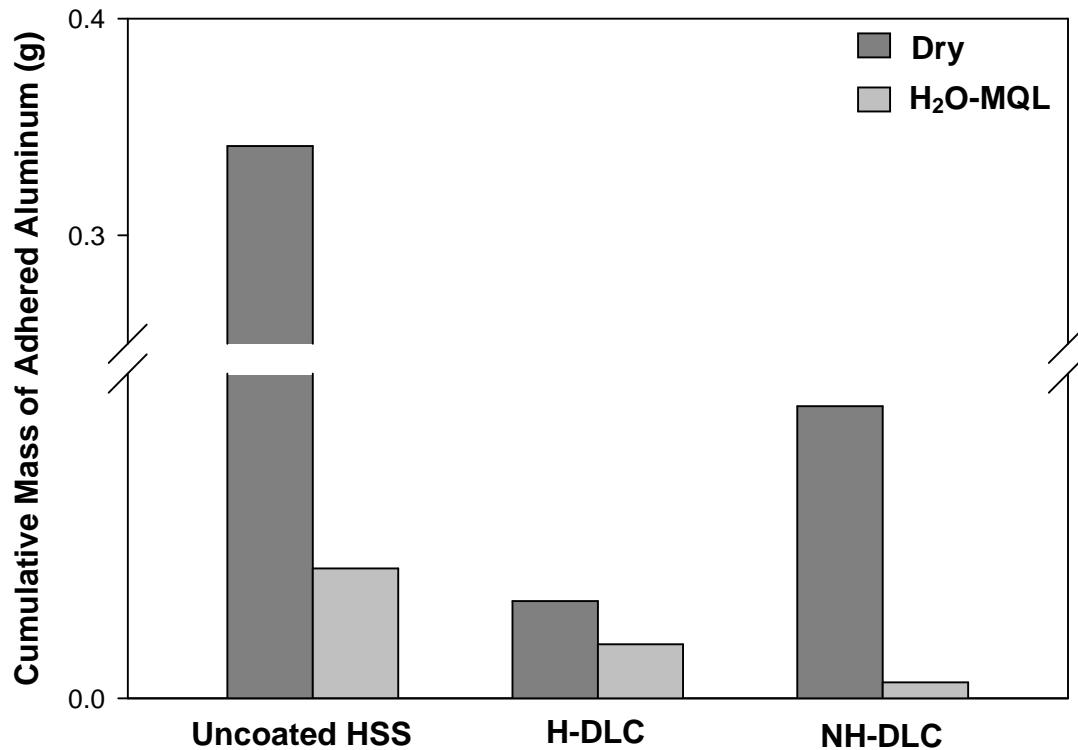
number of drilled holes increase but the targeted number of holes, 150, could be drilled without much difficulty. Some problems remain however, as will be discussed in detail in the rest of this paper, including generation of occasional torque spikes (type 3, see Fig. 3). Then the question becomes whether further improvements would be possible if the use of minimal quantity lubrication is used in drilling 319 Al with DLC coated HSS drills. The target is to improve the drilling performance to the level of flooded drilling with the use of DLC coated drills. For this reason the drilling performance of NH-DLC coated HSS against 319 Al blocks were determined and the results are reported in Fig. 3.5 (b). A 4% increase in average torque was found between the 1<sup>st</sup> (1.68 N-m) and 150<sup>th</sup> hole (1.75 N-m) in flooded coolant system. Thus the overall flooded drilling performance of coated drills can be considered equivalent to uncoated drills, which is the bench-mark (lower bond of torque values). The objective of detailed analyses provided in the rest of this section is to show that with DLC coated tools, the minimal quantity lubrication using water, for the reasons described in Section 3.2, provides an improved performance over dry drilling and also assess whether a particular type of DLC (hydrogenated or non-hydrogenated) would be more suitable for H<sub>2</sub>O-MQL.

### **3.3.2. Analysis of Torque Curves: Comparison between Dry and H<sub>2</sub>O-MQL Drilling**

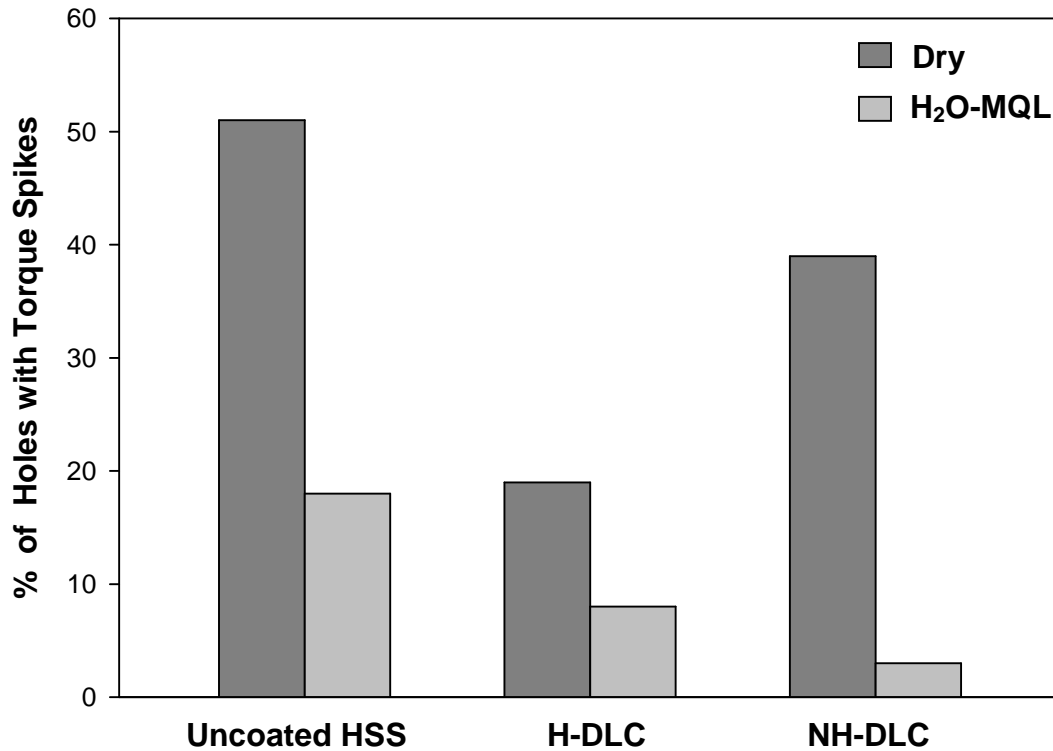
#### **3.3.2.1. Uncoated HSS Drills**

Fig. 3.7 (a) shows the torque responses of the 24 (25<sup>th</sup>-49<sup>th</sup>) holes formed by dry drilling. The drill became adhered to the 319 Al block while drilling the 49<sup>th</sup> hole and

could not be retrieved, hence this condition represented the drill failure by adhesion. The maximum torque reached 7.96 N-m at the onset of the failure as shown by the large torque spike marked by the [\*] in Fig. 3.7 (a). The mass of aluminum that had adhered to the drill surfaces (i.e. cutting edge and drill flutes) after the 49<sup>th</sup> hole was  $342 \times 10^{-3}$  g (Fig. 3.8). A total of 32 holes---namely 65% of 49 holes---drilled exhibited torque spikes (i.e. Type 3 curves) during drilling (Fig. 3.9).



**Figure 3. 8** The cumulative mass of adhered aluminum on uncoated HSS, H-DLC and NH-DLC coated drills in dry and H<sub>2</sub>O-MQL conditions.



**Figure 3. 9** Percentage of total holes that exhibited torque spikes during drilling with uncoated and DLC coated HSS drills.

Fig. 3.7 (b) displays the torque responses of the last 25 (125<sup>th</sup>-150<sup>th</sup>) holes during H<sub>2</sub>O-MQL drilling using the uncoated HSS drill. The drill did not fail at the 49<sup>th</sup> hole--- in fact, no excessive aluminum adhesion was noted when the test stopped after drilling the 150<sup>th</sup> hole. Meanwhile, the maximum torque measured during drilling with H<sub>2</sub>O-MQL did not exceed 3.20 N-m and at the end of the test, the mass of adhered aluminum was only  $4.8 \times 10^{-3}$  g (Fig. 3.8). During H<sub>2</sub>O-MQL drilling a smaller number of torque spikes was also observed. A total of 27 spikes were found--indicating that 18% of 150 holes exhibited spikes (Fig. 3.9).

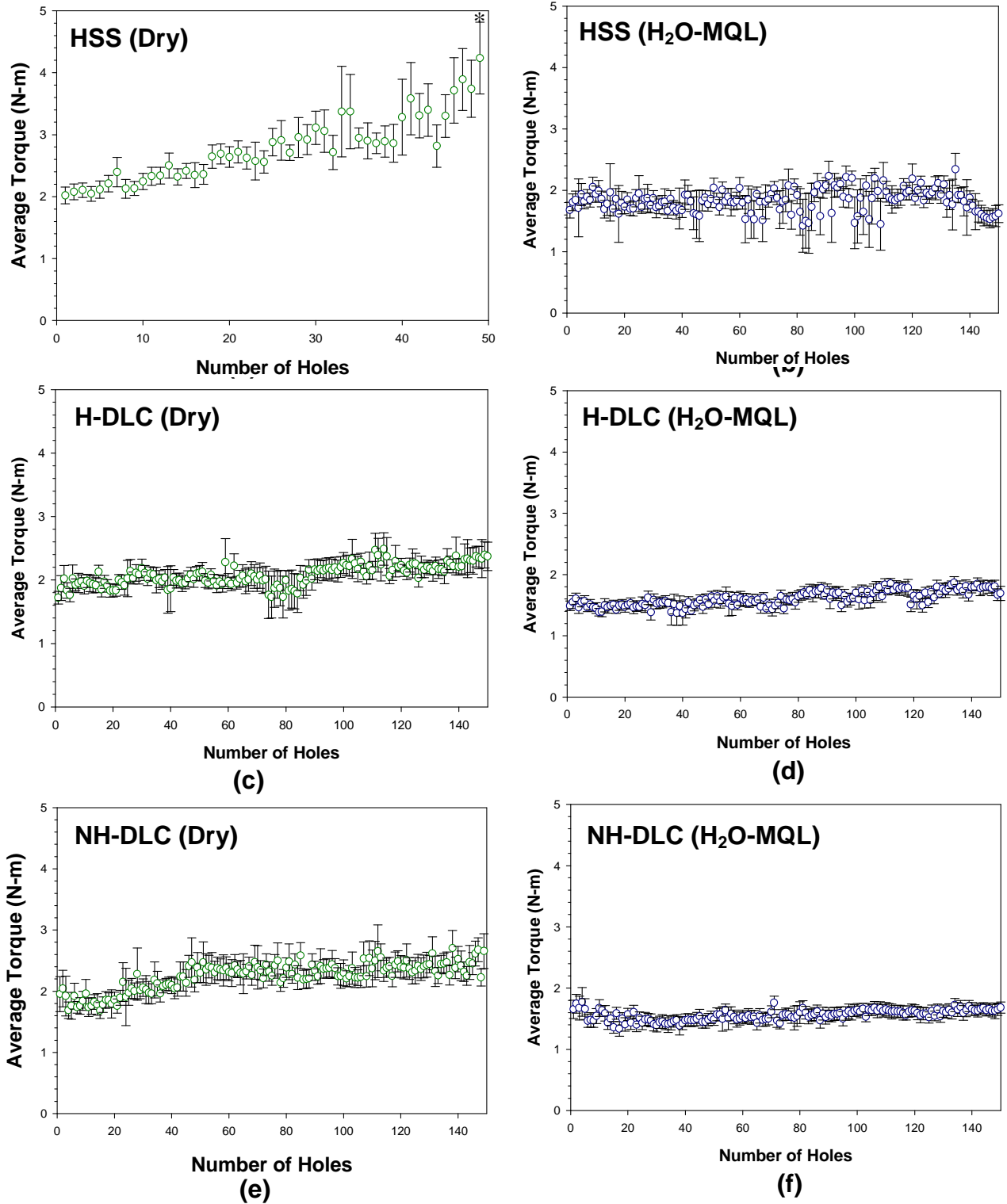


**Figure 3. 10** The average torque variations for the first 49 holes for uncoated HSS during (a) drilling in dry ([\*] failure) and (b) H<sub>2</sub>O-MQL conditions. The error bar indicates the standard deviation of data for each hole; (c, d, e, f) represent the average torque variations of 150 holes for H-DLC and NH-DLC coated HSS drills in dry and H<sub>2</sub>O-MQL conditions.

During dry drilling by uncoated HSS drill, the average torque calculated according to the method described in Section 2.4 increased considerably; an increase from 2.01 N-m in the 1<sup>st</sup> hole to 4.11 N-m in the 49<sup>th</sup> hole was noted---resulting in an increase of 105% (Fig. 3.10a). In contrast, only a gradual increase occurred in the average torque generated during H<sub>2</sub>O-MQL drilling up to the 130- 135<sup>th</sup> hole, where an increase of 15% was noted from the first hole 1.67 N-m to 1.92 N-m. The average torque then decreased to 1.62 N-m at the 150<sup>th</sup> hole (Fig. 3.10b). According to visual observations made during drilling tests, this decrease was attributed to the adhered aluminum peeling away from the tip of the drill's cutting edge.

In summary, the torque data obtained during H<sub>2</sub>O-MQL drilling using uncoated HSS drills suggested improvements over dry drilling with the same type of drill, characterized by a reduction in torque and an increase in stability over the range studied. The long term chemical stability of steel drills operating in a water environment should be carefully considered, however, because water spray would cause corrosion [3.20, 3.21]. The DLC coatings are unlikely to suffer from corrosion problems under H<sub>2</sub>O-MQL conditions. Their behaviour is addressed in the following sections.

### **3.3.2.2. H-DLC coated HSS Drills**

Fig. 3.7 (c) shows the torque responses for the last 25 (125<sup>th</sup> -150<sup>th</sup>) holes drilled by H-DLC coated drills in the dry condition. At the end of the test, the mass of adhered aluminum was  $3.6 \times 10^{-3}$  g (Fig. 3.8). Thus, in addition to the fact that tool life increased at least three times compared to the uncoated HSS in the dry condition, the amount of adhered aluminum decreased almost 100%. Only 28 holes with torque spikes were found

among the 150 holes drilled---with a mere 19% of the total number of holes exhibiting spikes (Fig. 3.9).

Fig. 3.7 (d) shows the torque responses of the last 25 (126<sup>th</sup>-150<sup>th</sup>) holes drilled by H-DLC coated drill under the H<sub>2</sub>O-MQL condition. Only 12 among the 150 holes made (8% of the total number) had torque spikes (Fig. 3.9). The rest of the curves were Type 1. After 150 holes, the mass of adhered aluminum was  $2.0 \times 10^{-3}$  g (Fig. 3.8) i.e., 44% less than the mass adhered to the H-DLC coated drill in dry drilling. In the H<sub>2</sub>O-MQL, the maximum torque did not exceed 2.10 N-m, while during the dry drilling, the torque exceeded this value several times and reached 5.97 N-m at the 129<sup>th</sup> hole. Clearly, a more stable trend was achieved using H-DLC compared to the dry drilling condition. When using the H-DLC coated drills in dry drilling, the average torque increased from 1.72 N-m at the 1<sup>st</sup> hole to 2.11 N-m at the 150<sup>th</sup> hole (Fig. 3.10c)---an increase of 23%, that compared favourably with 105% of the HSS drills with much higher average torque values at the onset of drill failure (Fig. 3.10a). The increase in the average torque for the H<sub>2</sub>O-MQL drilling was less---from 1.48 N-m at the 1<sup>st</sup> hole to 1.69 N-m at the 150<sup>th</sup> hole (Fig. 3.10d). This increase of 14% compares favourably with that the uncoated HSS in H<sub>2</sub>O-MQL (Fig. 3.10b).

### 3.3.2.3. NH-DLC Coated HSS Drills

Fig. 3.7 (e) shows the torque responses during dry drilling with the NH-DLC coated drills. The dry cutting performance of NH-DLC coated drills were analogous to H-DLC coated drills in that they did not fail for at least 150 holes but the numbers of Type 2 and 3 torque curves were higher in the former. The mass of adhered aluminum was 10.08



$\times 10^{-3}$  g after the drilling of 150 holes (Fig. 3.8). A total of 58 out of 150 holes---39% of the total number---produced torque spikes (Fig. 3.9). An increase of average torque responses was observed up to 46 holes (Fig. 3.10e), with the average torque increasing from 1.89 N-m in the 1<sup>st</sup> hole to 2.47 N-m in the 46<sup>th</sup> hole---a corresponding increase of 31%. The average torque increase between the 46<sup>th</sup> hole (2.47 N-m) and the 150<sup>th</sup> hole (2.63 N-m), however, was much less significant (6%) so that almost constant torque values were recorded between the 46<sup>th</sup> and 150<sup>th</sup> holes---suggesting that both types of DLC coated drills are effective in improving the drilling performance of 319 Al when compared to machining with uncoated HSS drills. Fig. 3.7 (f) shows the torque responses for the last 25 of the total 150 holes drilled by NH-DLC coated drills in H<sub>2</sub>O-MQL, where the maximum torque responses did not exceed 1.97 N-m. However, the dry drilling torque exceeded 6.17 N-m at the 116<sup>th</sup> hole. The H-DLC coating has an advantage over the NH-DLC in dry cutting thanks to lower torque and thrust forces, which are discussed in more detail in a recent publication [3.18]. In contrast, the H<sub>2</sub>O-MQL results suggested that there were beneficial effects of the use of NH-DLC under an MQL environment, compared to H-DLC---as described below. No more than 5 spikes were observed among the 150 holes---3% of the total number of holes (Fig. 3.9). This corresponded to less than those during drilling with H-DLC. The average torque decreased by 19% between the 1<sup>st</sup> hole (1.65 N-m) and the 17<sup>th</sup> hole (1.33 N-m) (Fig. 3.10f). A 9% increase in average torque was observed between the 17<sup>th</sup> and 150<sup>th</sup> holes, compared to 14% when using the H-DLC coated drill in H<sub>2</sub>O-MQL. After drilling 150 holes the mass of the drill was  $0.4 \times 10^{-3}$  g---80% less than the H-DLC coated drill in H<sub>2</sub>O-MQL (Fig. 3.8). Thus the use of the NH-DLC in H<sub>2</sub>O-MQL drilling provided less aluminum adhesion and a more stable torque response compared to H-DLC.

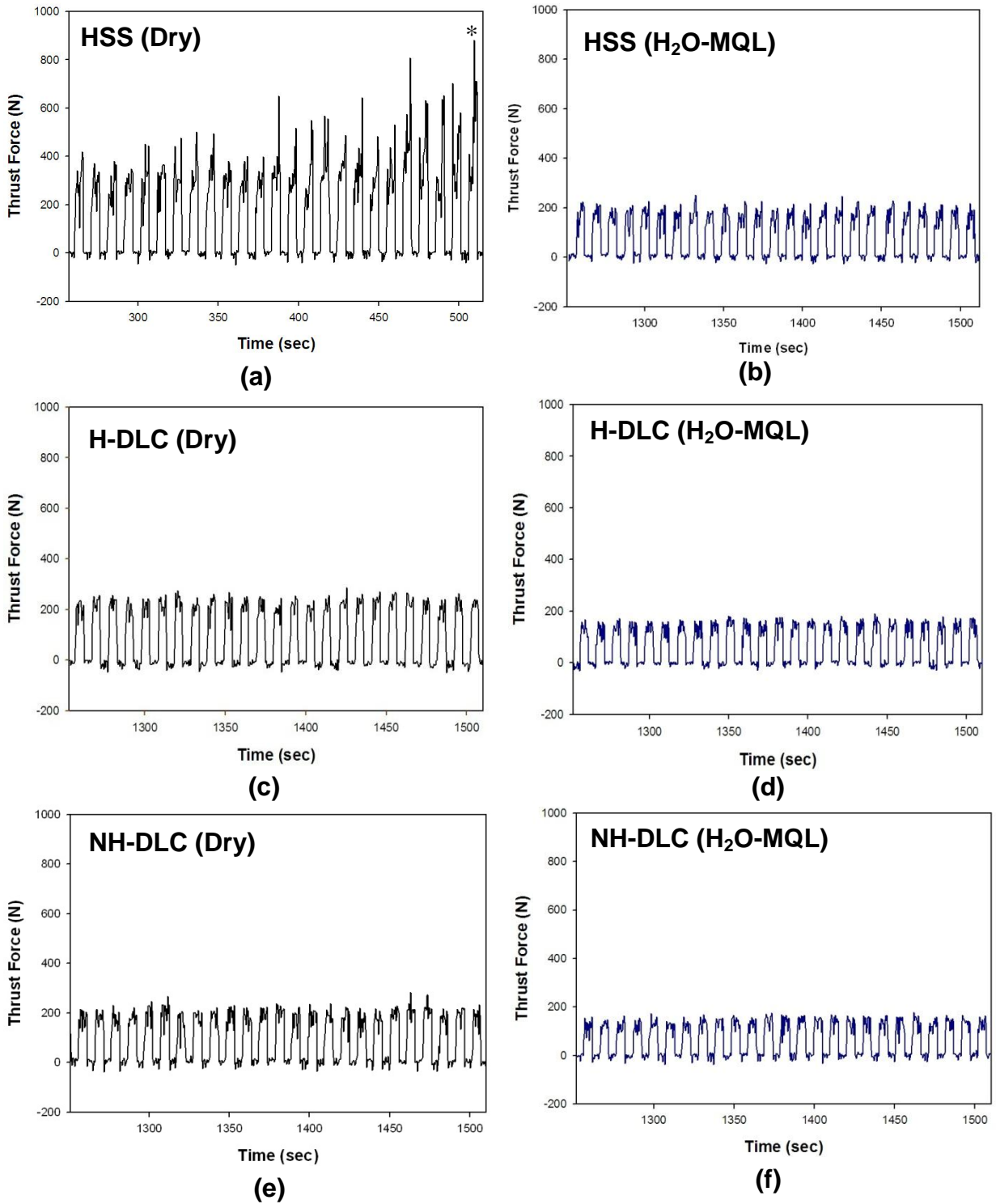


**Figure 3. 11** Thrust force plots (a and b) showing the last 24 holes with uncoated HSS drills during drilling in dry conditions (a) ([\*] represents tool failure by adhesion) and H<sub>2</sub>O-MQL (b) conditions; (c, d, e, f) representing the thrust force responses of the last 25 (126–150) holes during drilling with H-DLC and NH-DLC coated drills in dry and H<sub>2</sub>O-MQL conditions.

### 3.3.3. Analysis of Thrust Force: Comparison between Dry and H<sub>2</sub>O-MQL Drilling

#### 3.3.3.1. Uncoated HSS Drills

Fig. 3.11 (a) displays the thrust force responses of the last 24 (25<sup>th</sup>-49<sup>th</sup>) holes drilled by the HSS drills. In general, thrust forces followed the same trends as the drilling torque response. A total of 21 holes exhibited thrust force spikes during drilling with the uncoated HSS i.e., 43% of the 49 holes drilled (Fig. 3.12). The maximum thrust force reached 840 N at the 49<sup>th</sup> hole, indicating that the dry cutting of 319 Al with uncoated HSS would require the application of high thrust forces. According to Fig. 3.13 (a) an increase in the average thrust force from 300 N at the 1<sup>st</sup> hole to 619 N at the 49<sup>th</sup> hole was recorded, corresponding to an increase of 106%. This analysis agrees with the average torque response (Fig. 3.10a), which increased a similar 105%.

While drilling in H<sub>2</sub>O-MQL, the maximum thrust force recorded (at the hole no. 86) did not exceed 273 N. Only 12 holes exhibited thrust force spikes---8% of the 150 holes, which was a drastic decrease as plotted in Fig. 3.12. Fig. 3.11 (b) shows the thrust force variations of uncoated HSS for the last 25 (125-150) holes in H<sub>2</sub>O-MQL. The average thrust force increased by 75% between the 1<sup>st</sup> hole (148 N) and the 150<sup>th</sup> hole (259 N) (Fig. 3.13b) and the increase in thrust force was faster than the average torque. The difference may be attributed to the MQL performance, because the use of MQL might diminish the adhesion of aluminum to the drill flutes more effectively than it does to the aluminum adhesion to the cutting edges (discussed in detail in Sections 4 and 5). When drilling in H<sub>2</sub>O-MQL, both the torque and thrust force responses decreased after the 135<sup>th</sup> hole, possibly due to the peeling off of adhered aluminum from the drill's cutting edges and flutes. In summary, considering the first 150 drilling cycles, MQL was

effective while drilling with the uncoated HSS, with the water spray reducing torque and thrust force as well as the overall number of spikes.

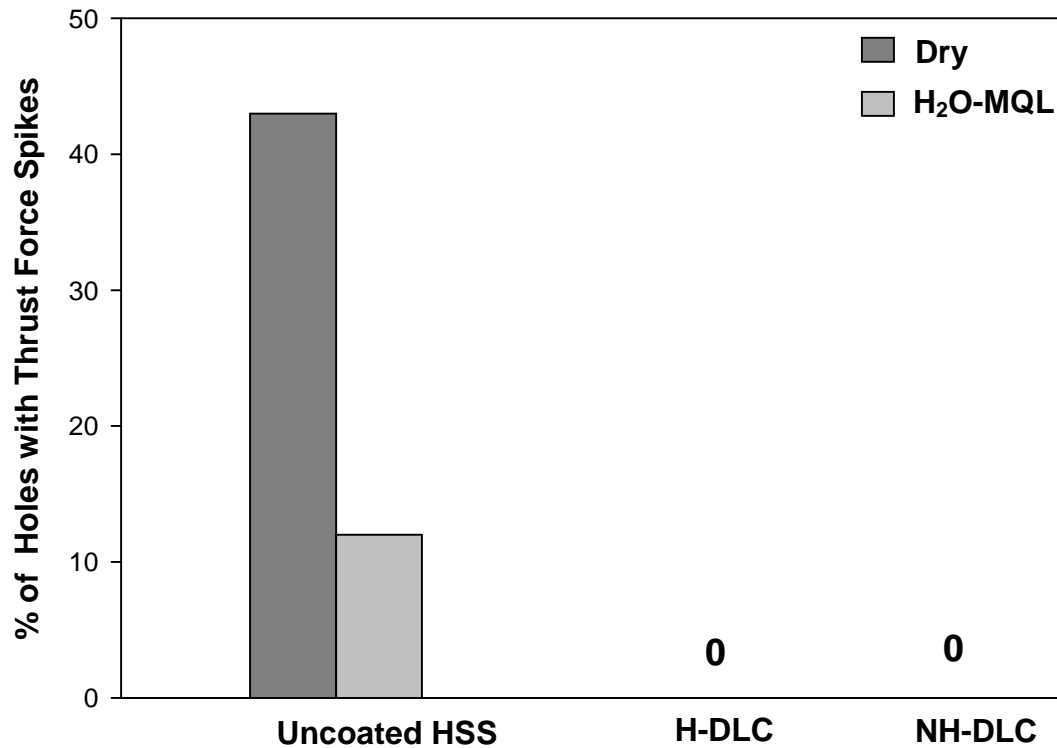


**Figure 3. 12** Percentage of total holes that exhibited thrust force spikes during drilling with uncoated and DLC coated HSS drills.

### 3.3.3.2. H-DLC Coated Drills

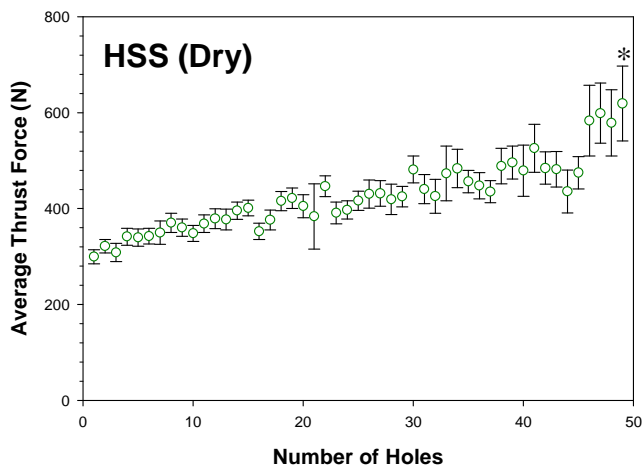
Fig. 3.11 (c) and (d) display the thrust force variation of an H-DLC coated drill used in dry and H<sub>2</sub>O-MQL conditions. The average thrust forces during dry drilling increased from 182 N at the 1<sup>st</sup> hole to 226 N at the 150<sup>th</sup> hole---an increase of only 24%. This suggests that the increase in average thrust force values is very gradual between the 1<sup>st</sup> and 150<sup>th</sup> holes (Fig. 3.13c) as opposed to the uncoated HSS (106 %). Similar to the torque responses in H<sub>2</sub>O-MQL, a near steady-state trend of average thrust forces was

found (Fig. 3.13d). The average thrust force increased by a mere 10% between 137 N (1<sup>st</sup> hole) and 150 N (150<sup>th</sup> hole)---illustrating that the H-DLC performed better in an MQL environment with better average thrust force responses than the uncoated HSS did in an H<sub>2</sub>O-MQL environment. The maximum thrust force in H<sub>2</sub>O-MQL did not exceed 221 N--a slight improvement over the maximum thrust force of 244 N in dry conditions.

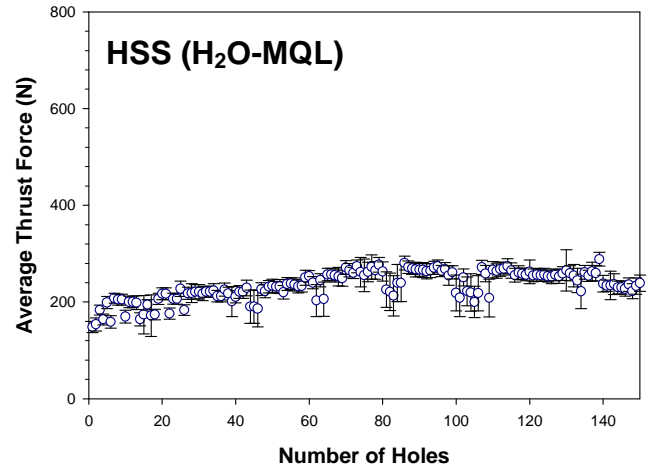
### 3.3.3.3. NH-DLC Coated HSS Drills

Fig. 3.11 (e) shows the thrust force variation in dry drilling condition when drilling with NH-DLC coated drills, which is similar to the results gained with H-DLC coated drills under dry condition. A near steady-state thrust force variation in H<sub>2</sub>O-MQL can be seen in Fig. 3.11 (f). In an H<sub>2</sub>O-MQL environment, the maximum thrust forces did not exceed 175 N, however, the thrust force was as high as 256 N in dry condition.

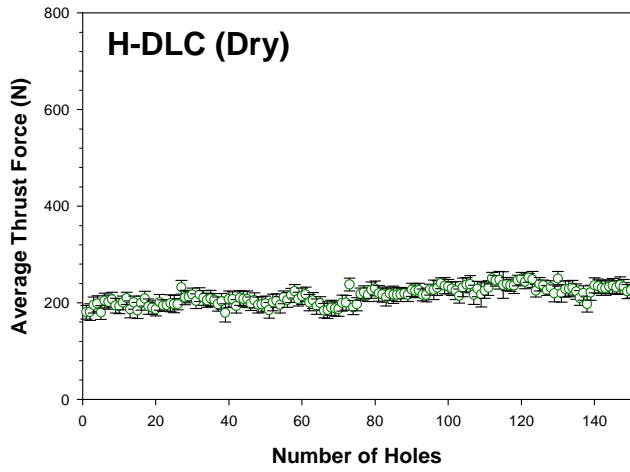
According to Fig. 3.13 (e), the average thrust force increased by 41% from the 1<sup>st</sup> hole (118 N) to the 46<sup>th</sup> hole (166 N), while an almost constant plateau was formed with a limited increase of less than 10% from the 46<sup>th</sup> hole (166 N) to the 150<sup>th</sup> hole (180 N). Considering the whole data set, the increase in average thrust forces (52%) was higher than that for the H-DLC coated drills in dry condition. However in H<sub>2</sub>O-MQL: the increase in average thrust forces was significantly lower than that seen for the H-DLC drills. The average thrust force responses (Fig. 3.13f) in H<sub>2</sub>O-MQL reveal that the thrust force increased by just 8% between the 1<sup>st</sup> hole (139 N) and the 150<sup>th</sup> hole (151 N). This result provides additional evidence that the use NH-DLC coated drills resulted in more stable drilling response in H<sub>2</sub>O-MQL compared to drilling using H-DLC coated drills.



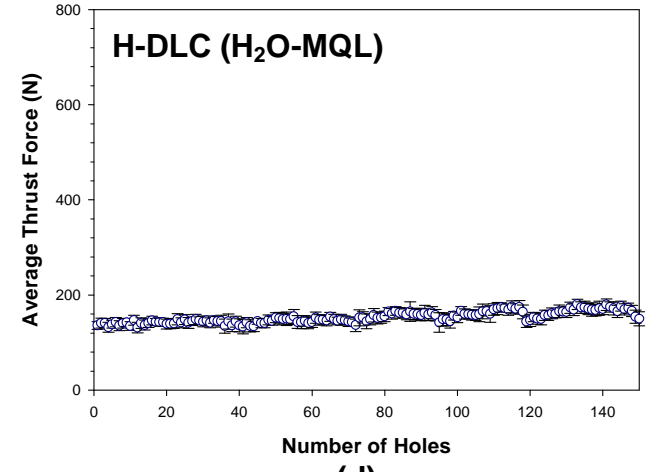
(a)



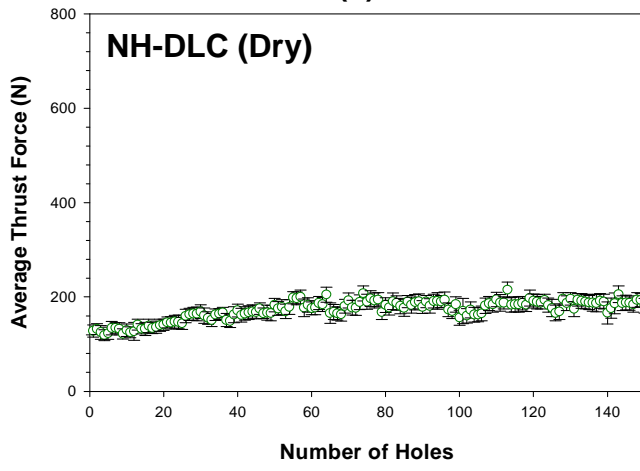
(b)



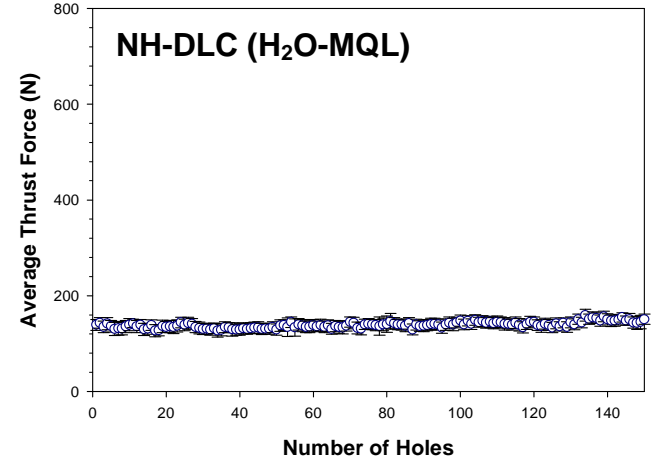
(c)



(d)



(e)



(f)

**Figure 3. 13** (a) Average thrust force variations for (1–49) holes for uncoated HSS in dry conditions ([\*] failure condition); (b) average thrust force variations of (1–150) holes for uncoated HSS in H<sub>2</sub>O-MQL conditions; (c and d) average thrust force variations of (1–150) holes for H-DLC in dry and H<sub>2</sub>O-MQL conditions; (e and f) average thrust force variations of (1–150) holes for NH-DLC in dry and H<sub>2</sub>O-MQL conditions.

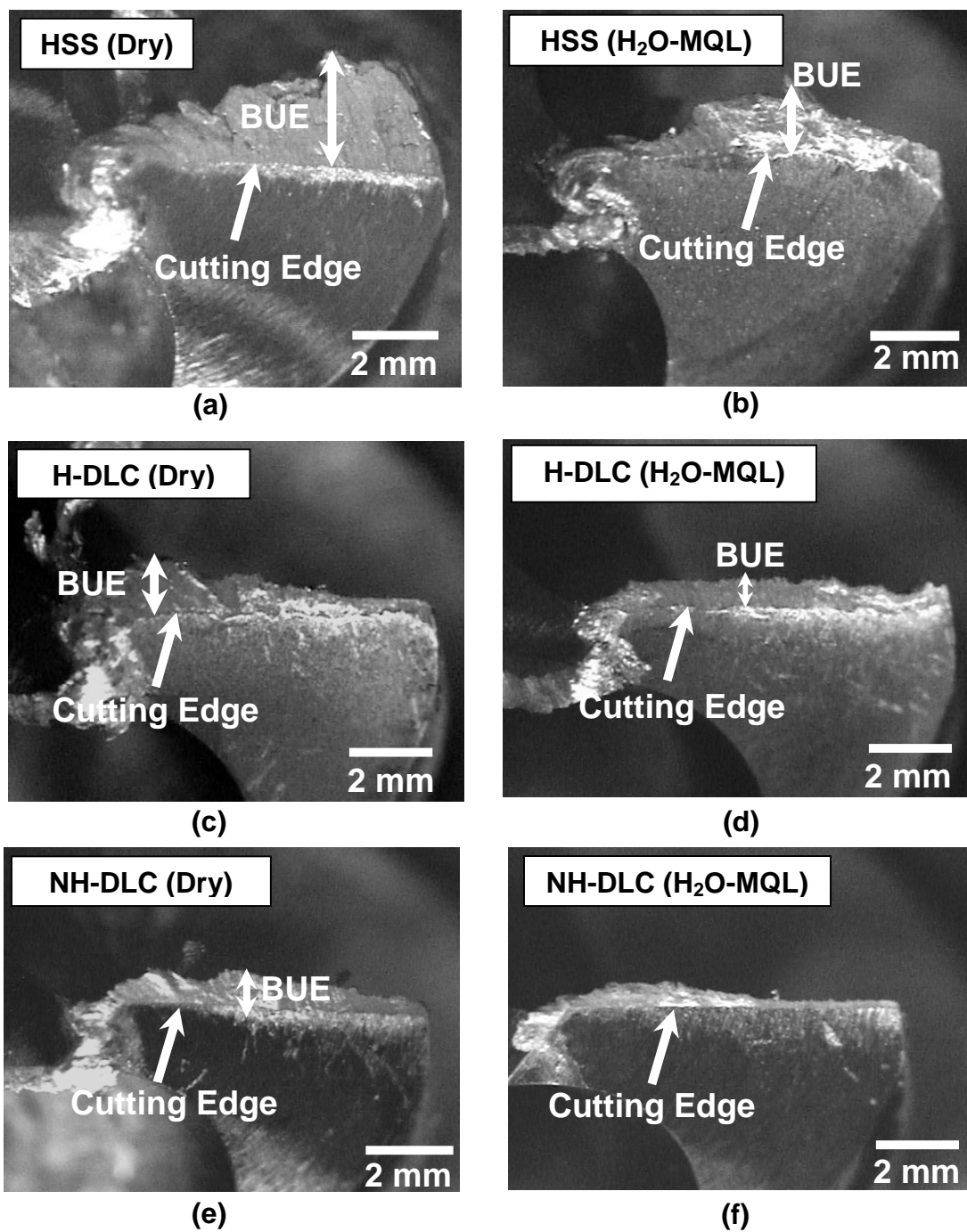


**Figure 3. 14** Optical images of drill cutting edge consisting of (a) uncoated HSS after 49 holes in dry conditions; (b) uncoated HSS after 150 holes in H<sub>2</sub>O-MQL conditions; (c) HDLC coated drill after 150 holes in dry conditions; (d) H-DLC coated drill after 150 holes in H<sub>2</sub>O-MQL conditions; (e) NH-DLC coated drill after 150 holes in dry conditions; (f) NH-DLC coated drill after 150 holes in H<sub>2</sub>O-MQL conditions. Figures show the built-up edge (BUE) at the tip of the drill's cutting edge.

### 3.4. Observation of Cutting Edge by Optical Microscope

Figs. 3.14 (a-f) show drill morphologies after the 49<sup>th</sup> and 150<sup>th</sup> holes for the uncoated tool in dry and MQL conditions. Figs. 3.14 (a and b) provide optical images of the uncoated HSS drill's cutting edge in dry drilling (after 49 holes) and H<sub>2</sub>O-MQL (after 150 holes) conditions, respectively. Adhered aluminum can be seen on the drill tips in both cases. An irregular built-up edge (BUE) is formed along the cutting edge of the uncoated tool in dry conditions (Fig. 3.14a), while the uncoated HSS in H<sub>2</sub>O-MQL also exhibited a BUE (Fig. 3.14b), but it was not as prominent as those found on the uncoated HSS in dry conditions.

Figs. 3.14 (c and d) give the BUE morphology on the cutting edge of the H-DLC coated drills in dry and MQL conditions after drilling 150 holes. Figs. 3.14 (e and f) provide optical images of the NH-DLC coated drill's cutting edge in dry and H<sub>2</sub>O-MQL conditions, respectively. Again, aluminum adhesion can be seen on the cutting edge of the drills, where a BUE formation of a lesser degree than that on the uncoated HSS drill was observed along the cutting edge. The conventional uncoated HSS drill generated the highest levels of torque and thrust force in dry conditions, due to the formation of a large BUE. The presence of a large BUE would alter the geometry of the drill by increasing its the drill diameter so that and the actual feed rate during cutting would increase due to the growth of the BUE, as indicated in [23, 24]. Accordingly, the torque and cutting forces are expected to increase during drilling with uncoated HSS, as confirmed by the torque and force measurements shown in Figs. 3.10 and 3.13.



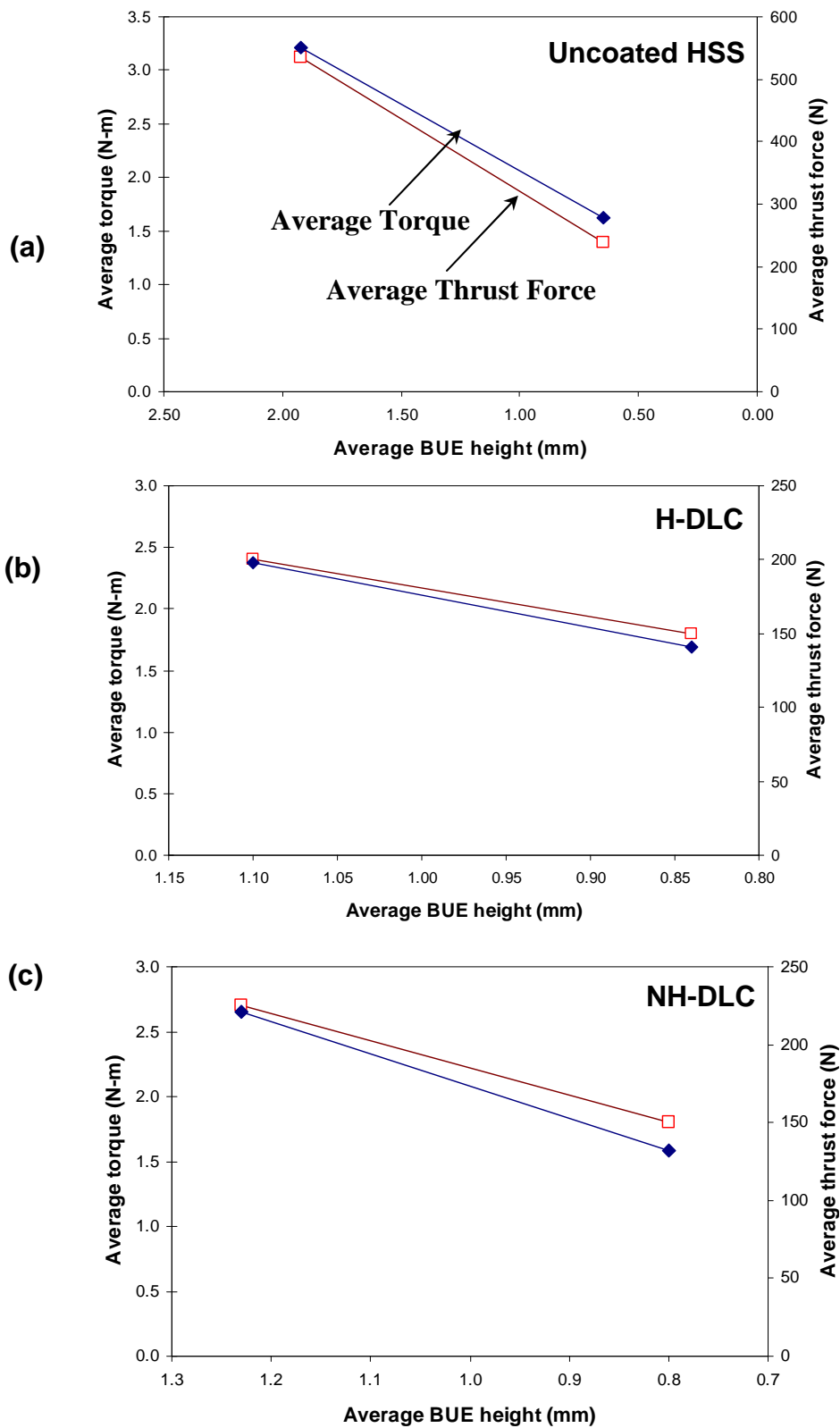


**Figure 3. 15** The reduction of average torque and thrust forces with the reduction of average BUE height from dry to H<sub>2</sub>O-MQL condition for (a) uncoated HSS; (b) HDLC coated HSS and (c) NH-DLC coated HSS.

A semi quantitative correlation can be established between the measured torque and thrust forces, and the BUE size. The BUE height was estimated by drawing a perpendicular line to the cutting edge of the drills. The average BUE decreased from 1.9 mm in the 49<sup>th</sup> hole (dry) to 0.85 mm in the 150<sup>th</sup> hole (H<sub>2</sub>O-MQL) during the drilling of uncoated HSS. Meanwhile, the average torque and thrust forces decreased by 50% and 55% when compared to the last hole in dry conditions and H<sub>2</sub>O-MQL conditions, which corresponds to a decrease of 36% in BUE size (Fig. 3.15a). The average BUE size for the H-DLC coated drill decreased from 1.10 mm (dry) to 0.84 mm (H<sub>2</sub>O-MQL) after the drilling of 150 holes. The average BUE size decreased from 1.23 mm (dry) to 0.69 mm (H<sub>2</sub>O-MQL) during drilling with the NH-DLC coated drill. The variations of torque and thrust forces with respect to BUE for H- DLC and NH-DLC coated drills are shown in Figs. 3.15 (b and c). It is concluded that the NH-DLC drill, that had the lowest torque and thrust force responses among the drills. It also had the smallest BUE formation.

### 3.5. SEM Observation of Drill Flutes

Fig. 3.16 provides SEM micrographs that show drill flute morphologies that display extensive transfer of aluminum onto the drill flutes---especially when using an uncoated HSS drill in dry conditions (Fig. 3.16a). The percentage of the drill flute area covered by aluminum (measured as described in section 2.7) was 100% (Fig. 3.17). The transferred aluminum is expected to provide an obstacle to the ejection of chips, resulting in higher torque generation. The transfer of aluminum was also observed during drilling in H<sub>2</sub>O-MQL conditions (Fig. 3.16b), but the amount of adhered aluminum did not exceed 37%---almost 3 folds lower than that found in dry conditions, revealing that the evacuation of chips through the drill flutes was more easily achieved in H<sub>2</sub>O-MQL than it

was in dry condition. Figs. 3.16 (c and d) show SEM micrographs of the drill flutes of an H-DLC coated drill in both dry and H<sub>2</sub>O-MQL conditions. More 319 Al transfer was observed in the drill flutes during drilling in dry condition (Fig. 3.16c) compared to drilling done in H<sub>2</sub>O-MQL condition (Fig. 3.16d). The percentage of area covered by aluminum was 35% and 18% in dry and H<sub>2</sub>O-MQL conditions, respectively (Fig. 3.16). Like the H-DLC coated drill, extensive metal transfer was observed in dry conditions when drilling with an NH-DLC coated drill (Figs. 3.16 (e and f)). Once more, less aluminum adhesion was evident in MQL conditions (Fig. 3.16f) compared to dry conditions. The area covered by transferred aluminum decreased sharply from 40% (dry) to 4% (H<sub>2</sub>O-MQL) (Fig. 3.17). An almost clear drill flute surface was observed in H<sub>2</sub>O-MQL (Fig. 3.16f). Fresh drill flutes means that there was no obstacle to the evacuation of the chips through the drill flutes, resulting in lower torque values.

In summary, the drilling of 319 Al with DLC coated drills required lower torque and thrust force than the uncoated HSS in both dry and MQL conditions (Table 1). Also, the average torque and thrust force values were lower and more stable. The mass of transferred aluminum on the drill was smaller, and there was a smaller BUE. These observations correlate with the resulting decrease in torque spikes (Figs. 3.8 and 3.9) for DLC coated drills. NH-DLC performed better than H-DLC in all of these aspects in H<sub>2</sub>O-MQL conditions. The amount of aluminum transferred to the NH-DLC coated drill flute is significantly diminished during drilling in H<sub>2</sub>O-MQL. These results are in agreement with the tribological test results on DLC against 319 Al reported in [3.4].

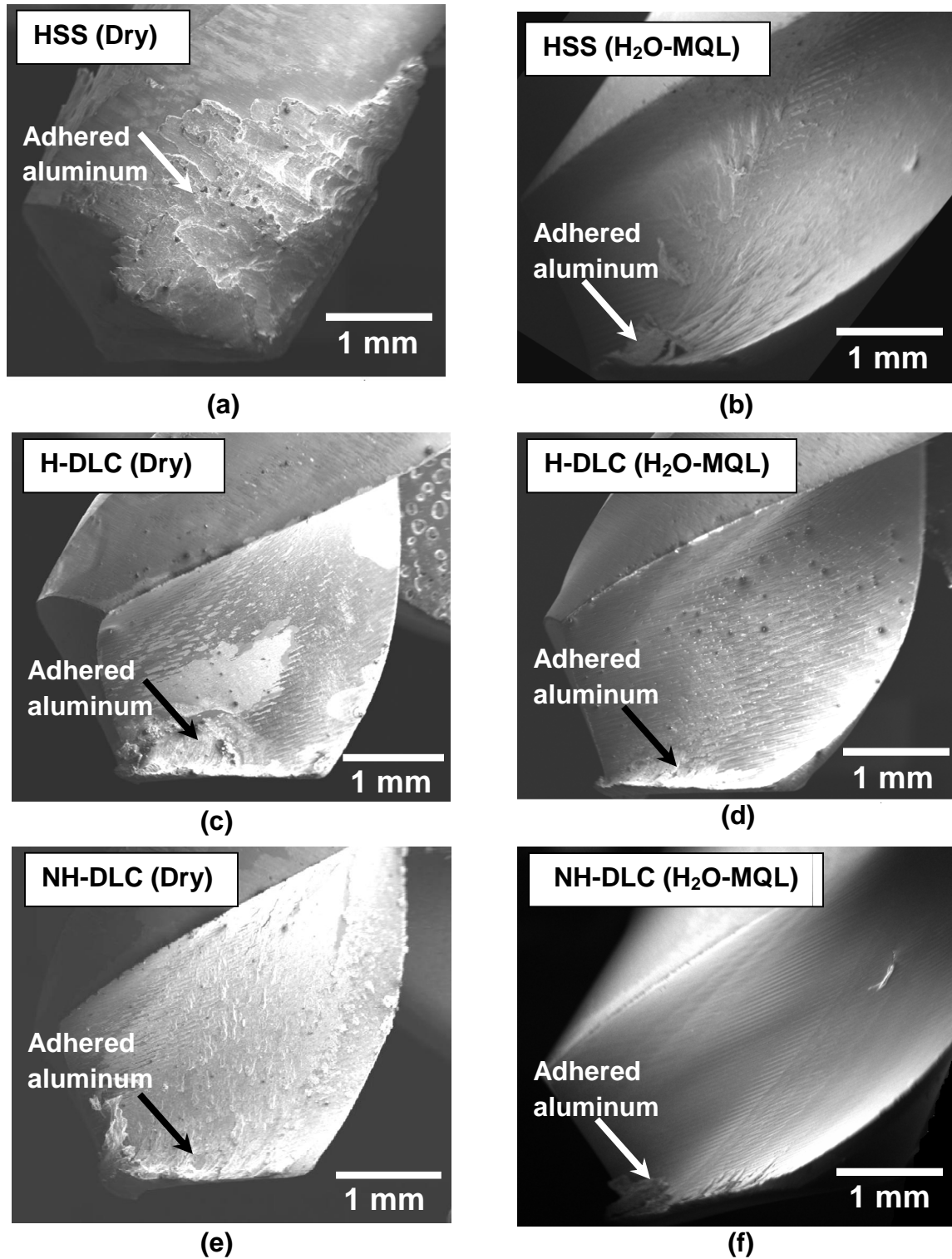


**Figure 3. 16** SEM secondary electron images showing aluminum adhesion to drill flutes: (a, b) uncoated HSS in dry and H<sub>2</sub>O-MQL conditions; (c, d) H-DLC coated drill in dry and H<sub>2</sub>O-MQL conditions; (e, f) NH-DLC coated drill in dry and H<sub>2</sub>O-MQL conditions. The flute surface of the uncoated HSS drill was almost entirely covered by adhered aluminum.

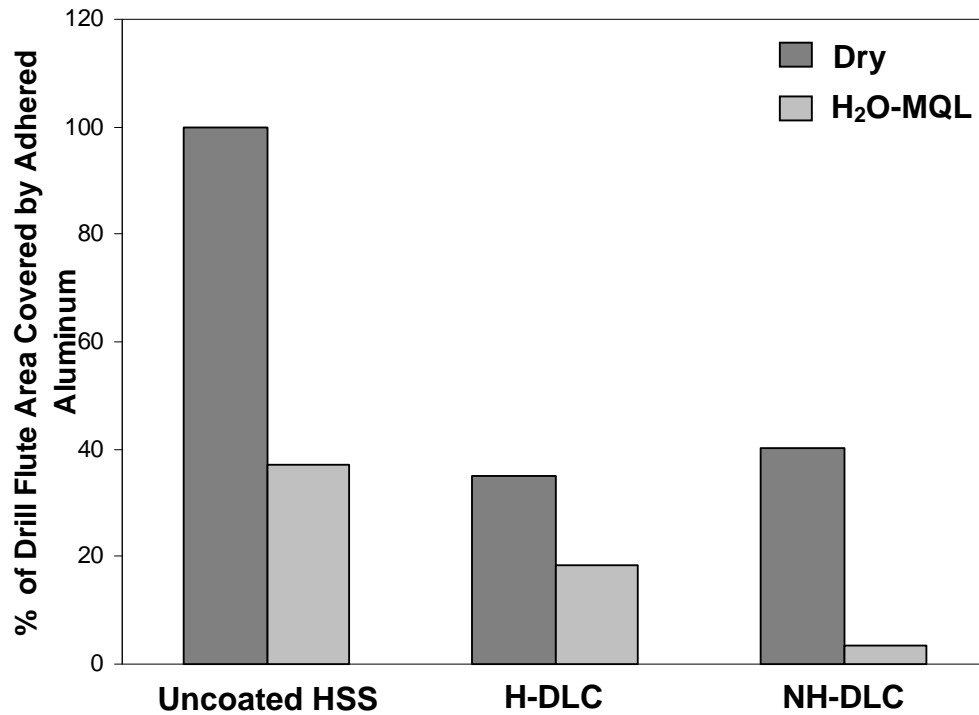


**Figure 3. 17** Effect of H<sub>2</sub>O-MQL on the percentage of the drill flute surface area covered by adhered aluminum. H<sub>2</sub>O-MQL reduced the percentage of area covered by adhered aluminum significantly for both uncoated and coated drills.

Studies show that under an ambient atmosphere, H-DLC shows a COF of 0.02 against steel [3.24] and 0.13 against aluminum [3.6], ---values that are typically lower than those of NH-DLC against the same materials. Water passivates the free (or dangling) carbon bonds on the NH-DLC's surface as more H and OH are provided to this free carbon atoms [3.25]. Qi et al. [3.25] used first principles calculations to show how H<sub>2</sub>O dissociates at the diamond surface into OH and H, where a chemical bonding between the diamond surface and OH is then established. The H atom serves as a bridge between the two carbon atoms. Aluminum that would transfer to a clean diamond surface will not transfer easily to H or OH passivated diamond surfaces, because these surfaces have a much smaller work of separation (e.g. 0.02 J/m<sup>2</sup> for the Al/H and 0.2 J/m<sup>2</sup> for the Al/OH terminated diamond) compared to a Al-non passivated diamond interface (4.5 J/m<sup>2</sup>).

Consequently, it is conceivable that the adhesion between the aluminum and a drill bit coated with NH-DLC will be lower at high levels of humidity.

### **3.6. Conclusions**

The key observations of the above work can be summarized as follows:

[1] Drilling a 319 grade Al-Si alloy workpiece using 30 ml/h water spray (H<sub>2</sub>O-MQL) required lower torque and thrust forces compared to dry drilling. Both the uncoated HSS and DLC coated drills showed lower torque and thrust force (both in terms of maximum and average values) during H<sub>2</sub>O-MQL drilling. The average torque responses obtained in H<sub>2</sub>O-MQL is comparable to that for conventional flooded cooling.

[2] During H<sub>2</sub>O-MQL drilling, the mass of aluminum that adhered to drill bits decreased considerably. In addition, a more stable cutting condition was reached as evidenced by the lower number of spikes (sudden jumps due to aluminum adhesion) in torque and thrust force curves, which drastically decreased compared to dry drilling.

[3] Under H<sub>2</sub>O-MQL conditions and among the DLC coatings, NH-DLC coatings (with a maximum torque of 1.97 N-m and a maximum thrust force of 175 N) showed lower peak torque and thrust forces compared H-DLC (with 2.10 N-m maximum torque and 221 N maximum thrust forces). Also, the average torque and thrust force values were lower in the case of NH-DLC.

[4] Optical and electron microscopy observations confirmed that the smallest BUE formation on the cutting edge of the drill, as well as aluminum adhesion to the drill flutes, occurred in H<sub>2</sub>O-MQL drilling with NH-DLC, revealing that this type of

DLC coating is the preferred coating for drilling Al-Si alloys using a minimum quantity of lubrication.

### **List of References**

[3.1] K. Weinert, I. Inasaki, J.W. Sutherland, T. Wakabayashi, Dry machining and minimum quantity lubrication, *CIRP Annals - Manufacturing Technology* 53 (2004) 511-537.

[3.2] E. Konca, Y.-T. Cheng, A.M. Weiner, J.M. Dasch, A. Erdemir, A.T. Alpas, Transfer of 319 Al alloy to titanium diboride and titanium nitride based (TiAlN, TiCN, TiN) coatings: effects of sliding speed, temperature and environment, *Surface & Coatings Technology* 200 (2005) 2260-2270.

[3.3] F. Klocke, G. Eisenblaetter, Dry cutting, *CIRP Annals- Manufacturing Technology* 46 (1997) 519-526.

[3.4] E. Konca, Y.-T. Cheng, A.M. Weiner, J.M. Dasch, A.T. Alpas, Effect of test atmosphere on the tribological behaviour of the non-hydrogenated diamond-like carbon coatings against 319 Aluminum alloy and tungsten carbide, *Surface and Coatings Technology* 200 (2005) 1783-1791.

[3.5] E. Konca, Y.-T. Cheng, A.M. Weiner, J.M. Dasch, A.T. Alpas, The role of hydrogen atmosphere on the tribological behaviour of non-hydrogenated DLC coatings against aluminum, *Tribology Transactions* 50 (2007) 178-186.

[3.6] W. Ni, Y.-T. Cheng, A.M. Weiner, T.A. Perry, Tribological behaviour of diamond-like-carbon (DLC) coatings against aluminum alloys at elevated temperatures, *Surface and Coatings Technology* 201 (2006) 3229–3234.

[3.7] J.M. Dasch, C.C. Ang, C.A. Wong, Y.-T. Cheng, A.M. Weiner, L.C. Lev, E. Konca, A comparison of five categories of carbon-based tool coatings for dry drilling of aluminum, *Surface and Coatings Technology* 200 (2006) 2970-2977.

- [3.8] E. Konca, Y.-T. Cheng, A.M. Weiner, J.M. Dasch, A.T. Alpas, Elevated temperature tribological behaviour of non-hydrogenated diamond-like carbon coatings against 319 aluminum alloy, *Surface and Coatings Technology* 200 (2006) 3996 – 4005.
- [3.9] N. Wain, N.R. Thomas, S. Hickman, J. Wallbank, D.G. Teer, Performance of low-friction coatings in the dry drilling of automotive Al–Si alloys, *Surface and Coatings Technology* 200 (2005) 1885.
- [3.10] G. Boothroyd, W.A. Knight, *Fundamentals of Machining and Machine Tools*, CRC Press, Taylor and Francis, 2006, p 190.
- [3.11] H. Ronkainen, S. Varjus, K. Holmberg, Tribological Performance of Different DLC Coatings in Water-Lubricated Conditions, *Wear* 249 (2001) 267-271.
- [3.12] J. Stallard, D. Mercs, M. Jarratt, D.G. Teer, P.H. Shipway, A Study of The Tribological Behaviour of Three Carbon-Based Coatings, Tested in Air, Water and Oil Environments at High Loads, *Surface and Coatings Technology* 177 –178 (2004) 545–551.
- [3.13] M. Suzuki, A. Tanaka, T. Ohana, W. Zhang, Frictional Behaviour of DLC films in a Water Environment, *Diamond and Related Materials* 13 (2004) 1464-1468.
- [3.14] H.A. Kishawy, M. Dumitrescu, E.-G. Ng, M.A. Elbestawi, Effect of coolant strategy on tool performance, chip morphology and surface quality during high-speed machining of A356 aluminum alloy, *International Journal of Machine Tools & Manufacture* 45 (2005) 219–227.
- [3.15] J.F. Kelly, M.G. Cotterell, Minimal lubrication machining of aluminium alloys, *Journal of Materials Processing Technology* 120 (2002) 327–334.
- [3.16] D.U. Braga, A.E. Diniz, G.W.A. Miranda, N.L. Coppini, Using a minimum quantity of lubricant (MQL) and a diamond coated tool in the drilling of aluminum–silicon alloys, *Journal of Materials Processing Technology* 122 (2002) 127–138.
- [3.17] A. Bardetsky, H. Attia, M. Elbestawi, Evaluating of tool wear suppressive ability of lubricants used in minimum quantity of lubrication application in high speed



machining of cast aluminum alloys, Proceedings of ASME International Mechanical Engineering Congress and Exposition IMECE 2005-80597, 1-7.

[3.18] S. Bhowmick, A.T. Alpas, The performance of hydrogenated and non-hydrogenated diamond-like carbon tool coatings during the dry drilling of 319 Al, International Journal of Machine Tools and Manufacture 48 (2008) 802-814.

[3.19] S.K. Field, M. Jarratt, D.G. Teer, Tribological properties of graphite-like and diamond-like carbon coatings, Tribology International 37 (2004) 949-956.

[3.20] A.R. Machado, J. Wallbank, The effect of extremely low lubricant volumes in machining, Wear 210 (1997) 76-82.

[3.21] M.C. Shaw, Metal Cutting Principles, Oxford University Press, Oxford, 1984.

[3.22] V.C. Venkatesh, W. Xue, A study of the built- up edge in drilling with indexable coated carbide inserts, Journal of Materials Processing Technology 58 (1996) 379-384.

[3.23] P. Matthew, P.L.B. Oxley, Predicting the cutting conditions at which built- up edge disappear when machining plain carbon steels, Annals of the CIRP 29 (1980) 11-16.

[3.24] H. Ronkainen, S. Varjus, J. Koskinen, K. Holmberg, Differentiating the tribological performance of hydrogenated and hydrogen-free DLC coatings, Wear 249 (2001) 260–266.

[3.25] Y. Qi, E. Konca, A.T. Alpas, Atmospheric effects on the adhesion and friction between non-hydrogenated diamond-like carbon (DLC) coating and aluminum – A first principles investigation, Surface Science 600 (2006) 2955–2965.

**Table 3.1** Comparison of torque and thrust force during dry, H<sub>2</sub>O-MQL and flooded drilling.

	Dry			H <sub>2</sub> O-MQL			Flooded		
	HSS	H-DLC	NH-DLC	HSS	H-DLC	NH-DLC	HSS	H-DLC	NH-DLC
Range of Average Torque (N-m)	2.01-4.11	1.72-2.11	1.89-2.63	1.67-1.92	1.48-1.69	1.33-1.65	1.69-1.73	1.31-1.74	1.68-1.75
Maximum Torque (N-m)	7.96	5.97	6.17	3.20	2.10	1.97	2.16	2.17	2.01
Range of Average Thrust Force (N)	300-619	182-226	118-180	148-259	137-150	139-151	157.97-148.80	136.44-171.23	143.31-130.09
Maximum Thrust Force (N)	840	244	256	273	221	175	231	251	176

## CHAPTER 4

### **Tapping of Al-Si Alloys with Diamond-like Carbon Coated Tools and Minimum Quantity Lubrication**

The deep hole drilling and tapping of automotive powertrain components made of hypoeutectic Al-Si alloys are of considerable importance. This chapter discusses the dry and minimum quantity lubricated (MQL) tapping of Al-6.5%Si (319 Al) alloys as alternatives to conventional flooded tapping. A comprehensive literature review is provided in Section 4.1, which envelops the historical perspectives and recent progresses in tapping operations for both ferrous and non-ferrous alloys. Two types of tests were done in comparison with flooded tapping. In the first set dry tapping experiments were performed using diamond-like carbon (DLC) coated and uncoated HSS taps. The second set of tapping experiments used MQL and only uncoated HSS taps. The details of experimental approach are well discussed in Section 4.2. Results revealed that DLC-dry tapping improved tool life considerably and exhibited small torques, which is discussed in Section 4.3.1 to 4.3.2. The use of MQL at the rate of 80 ml/h produced similar average torques to flooded tapping, and a high thread quality was observed, which is discussed in Section 4.3.3 to 4.3.4. The temperature increases in tapping in different conditions (dry, MQL and flooded) and the temperature effect on aluminum adhesion are discussed in Section 4.3.5 to 4.3.6. The low COF of DLC against aluminum was responsible for preventing built-up edge (BUE) formation and thus, instrumental in improving thread quality, which is discussed in Section 4.1. The mechanical properties of the material adjacent to tapped holes, evaluated using hardness measurements, revealed a notable softening in the case of HSS-dry tapping, but not for MQL tapping are discussed in Section 4.2. The role of MQL fluid on the

adhesion of aluminum to the tools is discussed in Section 4.3. The conclusions of the Chapter 4 are written in Section 5.

## **4.1. Introduction**

Tapping is one of the most intensively utilized machining operations for obtaining internal threads in Al- Si castings. Tapping is also typically one of the final machining operations to be performed as such if a tapping tool fails, the workpiece has already accrued significant added value and, in most cases, the costs of scraping or re-working it are very high. The breakage of a thread-cutting tool significantly impacts the productivity of the process. In the case of Al- Si castings--an important class of lightweight materials--a leading cause of tool breakage is the transfer of aluminum onto the tool surface. Warrington et al. (2005) reported that during dry tapping, the aluminum chips formed have a tendency to adhere to the thread surfaces, causing them to clog in a very short period of time. This adhesive interaction affects the tool surface, making it difficult for the chips to be cleared from the cutting zone. Consequently, chips fill the pitches of the tap, causing the torque to increase and with it, the probability of tool breakage increases substantially.

Dasch et al. (2006) reported the benefits of using carbon-based tool coatings, specifically diamond-like carbon coatings (DLC) to reduce the intensity of the tool/workpiece adhesive interaction during the dry drilling of Al-Si alloys. This report is in agreement with the tribological tests, which have clearly demonstrated the aluminum adhesion mitigating properties and low friction characteristics of DLC coatings as noted by Konca et al. (2006). Bhowmick and Alpas (2008a) observed that in addition to prolonged tool life, lower torques and thrust forces

were also maintained--particularly when 40 at% hydrogen-containing DLC coatings on HSS steel drills were used during dry drilling. Another strategy for reducing adhesion between the workpiece and the tool is to use a minimum quantity of lubrication (MQL)—fed to the machining point in fine droplets at the rate of 10- 100 ml/h (Boothroyd and Knight, 2006). The MQL agent is generally mineral oil, but some applications have also utilized an emulsion or water (Bhowmick et al., 2010). Previous studies of the tapping of ferrous alloys investigated the tapping operation with taps that had a variety of different cutting edge geometries or in conjunction with a suitable coating. A survey of the existing literature on tapping research as it relates to ferrous and nonferrous alloys, principally aluminum alloys, is given in the following paragraphs.

Chen et al. (2007) studied the role that cutting edge geometry played in the tapping of austenitic stainless steel by comparing the performances of straight fluted taps with a helix angle of 0° and spiral pointed taps with a helix angle of 34° --both in conventional flooded (oil-water emulsion) conditions at a speed of ~60 rpm and a feed rate of 1.00 mm/rev. A slight decrease in average torque to 4.5 N-m was observed during tapping with the spiral flute compared to the conventional straight flute taps (5.0 N-m). Veldhuis et al. (2007) studied the influence that the presence of a perfluoropolyether (PFPE) film on HSS steel tools had on torque responses during the tapping of mild steel in flooded (oil-water emulsion) tapping conditions at a speed of 260 rpm and a feed rate of 1.58 mm/rev. PFPE was deposited by dipping the tool into the solution, which provided an even coating to the rough tool surface. The presence of PFPE on the HSS tool surface reduced the torque slightly to ~21 N-m, compared to ~25 N-m when an uncoated tap was used. Reiter et al. (2006) evaluated the dry tapping performance of austenitic stainless steel using conventional hard metallurgical coatings, including CrN, CrC, TiCN and TiAlN--comparing

them to the new, diamond like carbon (DLC) coatings that incorporate WC. DLC coatings displayed the lowest average torque (5.25 N-m) followed by TiAlN (7.43 N-m), CrN (7.19 N-m), TiCN (6.85 N-m) and CrC (6.55 N-m)-coated HSS tools. Flank built-up edges (BUEs) were observed during the tapping with DLC coated tools however, while no significant BUE occurred with conventional TiCN or TiAlN coatings.

Only a few studies have been conducted on the tapping of aluminum alloys. Srivastava et al. (2004) investigated the form tapping of 319 Al alloys and focussed on the performance of uncoated HSS, uncoated carbide and TiN-coated HSS taps in flooded (semi-synthetic oil) conditions at a speed of 1100 rpm and a feed rate of 1.25 mm/rev. In form tapping, threads are not created by chip removal, but by the plastic deformation and displacement of the material. TiN-coated HSS taps produced lower torque (~0.07 N-m) when compared to uncoated HSS (~0.61 N-m) and uncoated carbide (~0.14 N-m) tools. Zedan et al. (2010) investigated the effects of iron content during the conventional tapping of Al-Si alloys using TiN-coated HSS taps at speed and feed rates of 400 rpm and 1.25 mm/rev, respectively, in flooded tapping conditions (synthetic fluid). An increase in the average tapping force of 470 N was observed for Al-12% Si-0.46% Fe, due to a significant amount of iron-rich intermetallics--compared to Al-7% Si-0.30% Fe (250 N).

Meanwhile, some research has been conducted on the application of MQL to the drilling of aluminum alloys, a machining process akin to tapping, but ultimately less complicated. Klocke and Eisenblaetter (1997) investigated the effect that MQL has on the drilling of aluminum- 9% silicon alloys using a carbide drill. It was reported that a synthetic ester-based MQL fluid supplied at a rate of 10 ml/h resulted in a decrease in cutting torque to ~3 N-m compared to the ~10 N-m generated during dry drilling. Kelly and Cotterell (2002) conducted a

comparative study of the dry, MQL and flooded drilling of a wrought aluminum-4.5% magnesium alloy (5080 Al). The maximum torque generated during MQL drilling using vegetable oil-based MQL supplied at 20 ml/h was 2.2 N-m, which compared favourably with dry drilling conditions using a carbide drill, which generated a maximum torque of 3.8 N-m. MQL appeared to perform slightly better than flooded drilling with mineral soluble oil, for which the highest torque was 2.4 N-m.

Braga et al. (2002) studied the MQL drilling of an aluminum 319 alloy using a carbide drill, and reported that MQL drilling using mineral oil supplied at a rate of 10 ml/h generated a maximum thrust force of 1,260 N--comparable to the 1,250 N measured during soluble oil flooded drilling. Results revealed that the average torque of 3.71 N-m measured for the flooded drilling of aluminum 319 alloy conditions was comparable to that measured for the vegetable oil MQL using DLC coated HSS drills (Dosbaeva et al., 2008). The cutting performance of DLC-coated HSS drills in a distilled water spray (30 ml/h) used as the MQL agent (H<sub>2</sub>O-MQL) was also examined by Bhowmick and Alpas (2008b). The H<sub>2</sub>O-MQL cutting of 319 Al using DLC-coated drills reduced the average drilling torque to 1.65 N-m, compared to dry drilling (4.11 N-m) at a level similar to the performance under the water soluble flooded conditions (1.75 N-m).

Despite the research efforts reviewed above, a significant knowledge gap exists regarding the effects that MQL tapping has on tool life, torque requirements and the thread quality of aluminum alloys. The objective of this work is to assess whether the MQL tapping of Al-6.5% Si (319 Al) can demonstrate a comparable performance to conventional flooded tapping. The role of DLC coated tools in reducing the torque and increasing the tool life during dry tapping of 319Al are also considered. This particular alloy was selected due to the widespread use of 319 Al castings in automotive engine blocks, cylinder heads, crank cases, transmission cases and

especially for upper valve components--where deep hole drilling and tapping are the essential machining operations. In the meantime, it should be noted that tapping at high speeds will contribute to the industry's efforts to reduce overall production times. Currently, tapping operations on aluminum are typically performed in medium speed ranges of 400 (10 m/min)-1000 rpm (25 m/min) (Srivastava et al., 2004; Zedan et al., 2010). With this in mind, the tapping experiments in this work were conducted at 2000 rpm (50 m/min). Tapping performance was evaluated through forward and backward torque measurements in the workpiece material. The heat generated during tapping using coated and uncoated tools under various conditions was determined and correlated with the results of tribological tests, which were used to determine coefficients of friction (COFs) between 319 Al and DLC coated and uncoated HSS steel under dry and lubricated sliding contact. The quantitative metallography of the tool surfaces and a differential scanning calorimetry (DSC) of the MQL fluid were also carried out and used to analyze the factors influencing aluminum adhesion to the tool surface as a way of rationalizing performance measures like tool life and thread quality.

## **4.2. Experimental details**

### **4.2.1. Description of Workpiece Material and Cutting Tools for Drilling and Tapping**

The workpiece material tested was a sand-cast hypoeutectic 319 grade aluminum-silicon alloy consisting of (in wt %) 6.5% Si, 3.5% Cu, 0.1% Mg, 0.5% Mn, 0.35% Ni, 1.0% Zn, 1.0% Fe, 0.25% Ti and the balance aluminum. The bulk hardness of the 319 Al was 72.40 HR-15T, measured as Rockwell Superficial Hardness using a 1.59 mm diameter ball and a 15 kg load. The workpiece was in the form of rectangular blocks of  $30 \times 15 \times 2.5\text{-cm}^3$  and tested in as-cast condition.



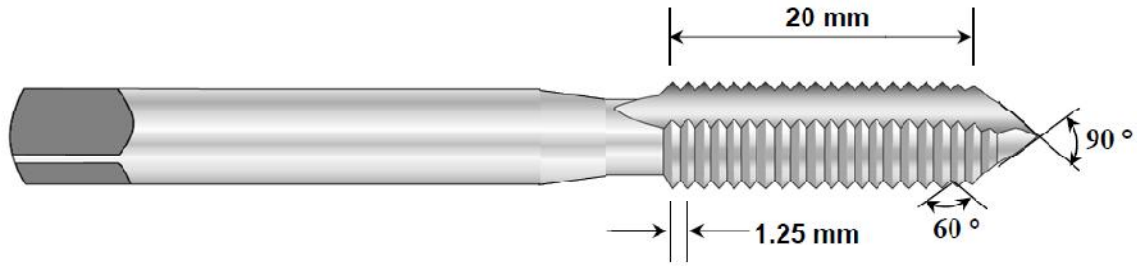


**Figure 4. 1** A schematic of tap

The cutting tools used for the tapping were  $8.00 \pm 0.01$  mm-diameter high-speed steel (HSS) spiral taps with the commercial designation of  $M8 \times 1.25$  with the following composition (in wt.%): 0.95% C, 6.00% W, 5.00% Mo, 4.20% Cr, 2.00% V, and the balance Fe. A schematic of the spiral taps used is shown in [Fig. 4.1](#). The tap consists of 3 spiral flutes with 1.25 mm pitch lengths and  $90^\circ$  flute angle. The angle between pitches is  $60^\circ$ . The diameter of the tap is 8 mm and the overall length is 95 mm. The cutting tools used for the drilling (prior to the tapping experiments) were  $6.35 \pm 0.01$  mm-diameter twist drills, also made of the same HSS material as the taps, The average hardness of the HSS steel was  $64 \pm 2.50$  HRC.

Dry tapping tests were performed using HSS and diamond like carbon (DLC)-coated HSS taps. The coatings were deposited on the taps using a plasma-enhanced chemical vapour deposition process (PECVD). The DLC coatings had an amorphous structure characterized primarily by  $sp^3$  type carbon bonding and incorporated 40 at % H. The deposition was done by Oerlikon Balzers Coatings Ltd. (South Carolina, USA). The microhardness of the DLC coatings was 26.8 GPa. The average thickness of the DLC coatings was  $2.10 \mu\text{m}$ . The details of the deposition parameters and properties of the coatings can be found in Reiter et al. (2006).

#### 4.2.2. Description of Drilling and Tapping Tests

All drilling and tapping experiments were carried out on a vertical milling machine (Haas Automation Inc., CA, USA) with a maximum power of 2.95 kW and a maximum rotational speed of  $4 \times 10^3$  rpm as shown in [Fig.4. 2](#). Prior to tapping, a total of 150 holes were drilled in rows with a horizontal, center-to-center spacing of 12 mm between the adjacent holes using an MQL agent, FA-MQL, (described later) supplied at a flow rate of 80 ml/h. Each drilled hole was 25 mm deep. A cutting speed of 2,500 rpm (50 m/min) and a feed rate of 0.25 mm/rev were used for drilling.

Tapping tests were performed on the MQL-drilled 319 Al workpiece at a constant feed rate of 1.25 mm/rev. A cutting speed of 2,000 rpm (50 m/min) was used for most of the tests after preliminary tests were conducted at various speeds (see Section 2.4 for the selection of tapping speed). Forward and backward torques generated during the tapping of each hole was measured simultaneously using a non-contact magneto-static torque sensor ([Fig. 4.2](#)).

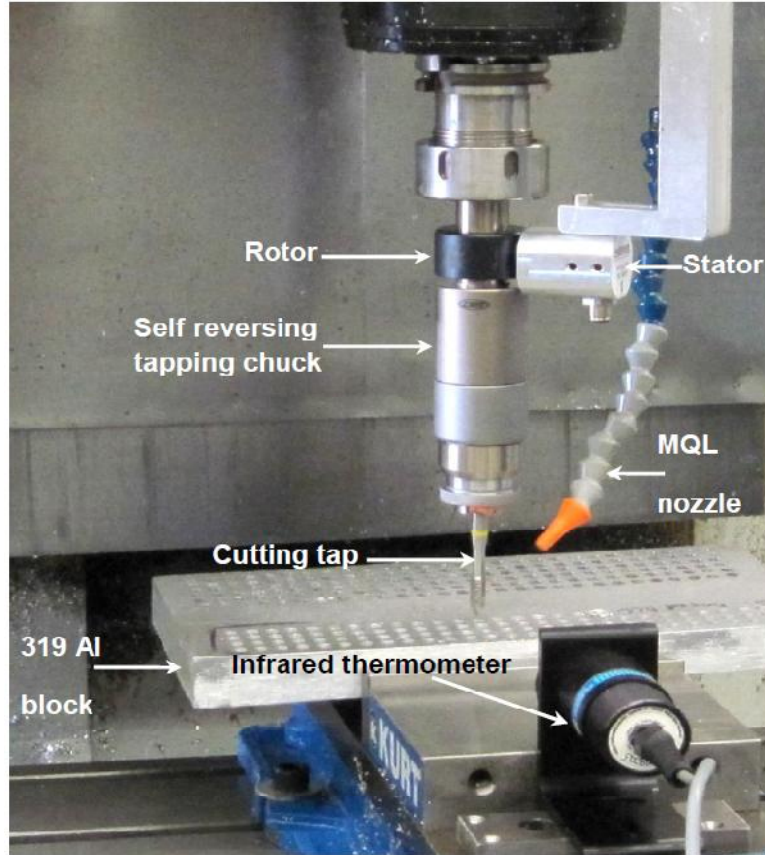


**Figure 4. 2** Close-up view of the experimental set-up.

One set of tapping tests were carried out without the use of any lubricant (i.e. under dry conditions). Dry tests were performed using both the uncoated HSS and DLC-coated HSS taps. The experimental set-up was equipped with an external MQL system (Fig. 4.2). A fatty acid-based MQL agent, FA-MQL, (LubriFluid F100, Vogel, Germany) as well as a commercially available tap oil (mineral oil based, MO-MQL) was supplied --both at a flow rate of 80 ml/h (See **Section 2.4** for the determination of MQL flow rate). The density of FA-MQL was  $0.84 \text{ mg/m}^3$ , measured at  $25 \text{ }^\circ\text{C}$  and a viscosity of  $75 \text{ mm}^2/\text{s}$ , also measured at  $25 \text{ }^\circ\text{C}$ . The FA-MQL fluid contained sulphur (S) and phosphorus (P) additives, as determined using a JEOL 300 MHz nuclear magnetic resonance (NMR) instrument. Although the FA-MQL showed the presence of

P and S, none of these elements were present in the MO type oil used as an MQL agent in flooded conditions.

Flooded tapping tests were conducted using the same commercial mineral-based tap oil (MO) supplied at the rate of 10000 ml/h. The density and viscosity of the commercial mineral-based tap oil were determined to be  $0.78 \text{ mg/m}^3$  and  $72 \text{ mm}^2/\text{s}$ , respectively, at  $25 \text{ }^\circ\text{C}$ .

#### **4.2.3. Tapping Torque Measurements: Average Forward and Backward Torques**

The average forward and backward tapping torques (in N-m) generated during the tapping of each individual hole were calculated over the range of time intervals indicated in [Fig. 4.3](#) that show a typical torque variation profile during one complete tapping cycle consisting of insertion (A, B) and retraction (B, C) of the tap inside a single hole. The average torque is the arithmetic mean of all recorded data points between the initial contact of the tap with the entrance of the hole at the 319 workpiece's top surface (Point A in [Fig. 4.3](#)) and contact at the deepest point inside the hole--after completion of the revolution of the 18th thread of the tap inside the previously drilled 25 mm depth hole (Point B in [Fig. 4.3](#)). The backward torque was calculated during retraction between Point B and the last contact with the hole surface upon the exit of the tap (Point C in [Fig. 4.3](#)).

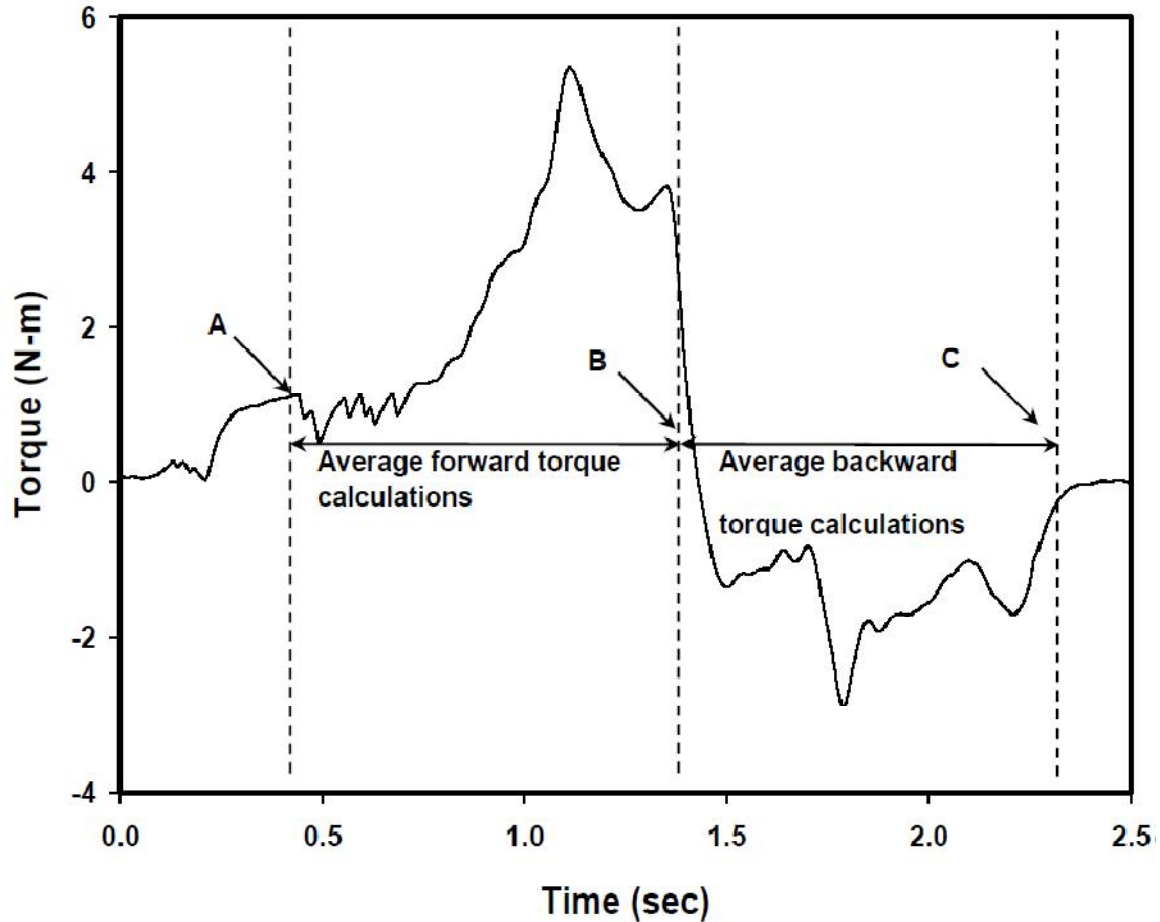


**Figure 4. 3** A typical tapping torque curve showing the zones of average forward and backward torque calculations.

#### 4.2.4. Selection of Tapping Speed and MQL Flow Rate

Experiments were designed in order to select the constant tapping speed used in the rest of the dry, MQL and flooded tapping conditions used in these studies. For this reason, a set of initial tapping tests were conducted in the MQL-drilled holes at speeds of 400 rpm (10 m/min), 800 rpm (20 m/min) and 2000 rpm (50 m/min) (Fig. 4.4) under dry conditions, against uncoated HSS taps. An increase in average forward torque was observed from the 1<sup>st</sup> hole to the 25<sup>th</sup> hole in all cases. A faster increase in average forward torque with the number of tapped holes was evident at higher speeds. Notably, the average torque increased by 80% after the 16<sup>th</sup> hole during

the tapping using a speed of 2,000 rpm. The tapping time,  $t$ , is inversely proportional to the feed rate and cutting speed by  $t = \frac{L}{fn}$  where  $L$  is the total hole depth,  $f$  is the feed rate and  $n$  is the spindle speed (Isakov, 2003).

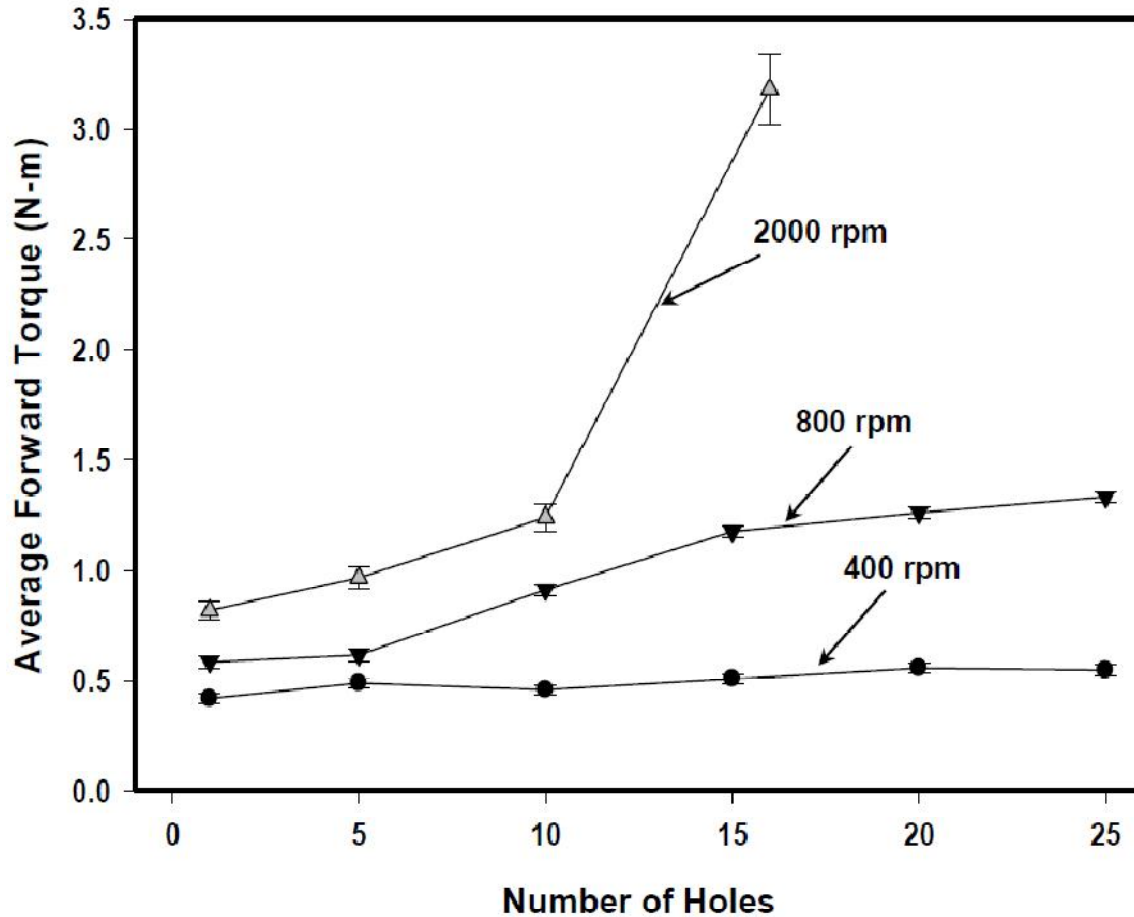


**Figure 4. 4** Preliminary experiments performed to determine the optimum tapping speed.

In the current tapping experiments,  $L$  (25 mm) and  $f$  (1.25 mm/rev) were both constant, making the tapping time an inverse function of the cutting speed, so that with an increase in cutting speed from 400 rpm to 2,000 rpm, the total tapping time decreases from 500 sec to 100 sec per 100 holes. As a result, the highest speed in Fig. 4.4 --2,000 rpm--was selected to perform the experiments aimed as assessing the behaviour of DLC-coated taps in dry conditions and their

tapping performance under MQL conditions. As previously indicated, this is considered a relatively high speed for the tapping process, and thus represents demanding machining conditions for the Al-Si alloys. Machining at high speeds increases industrial productivity. However, the surface quality and tool life should not be compromised. These two important aspects of tapping are among the parameters examined in this study.

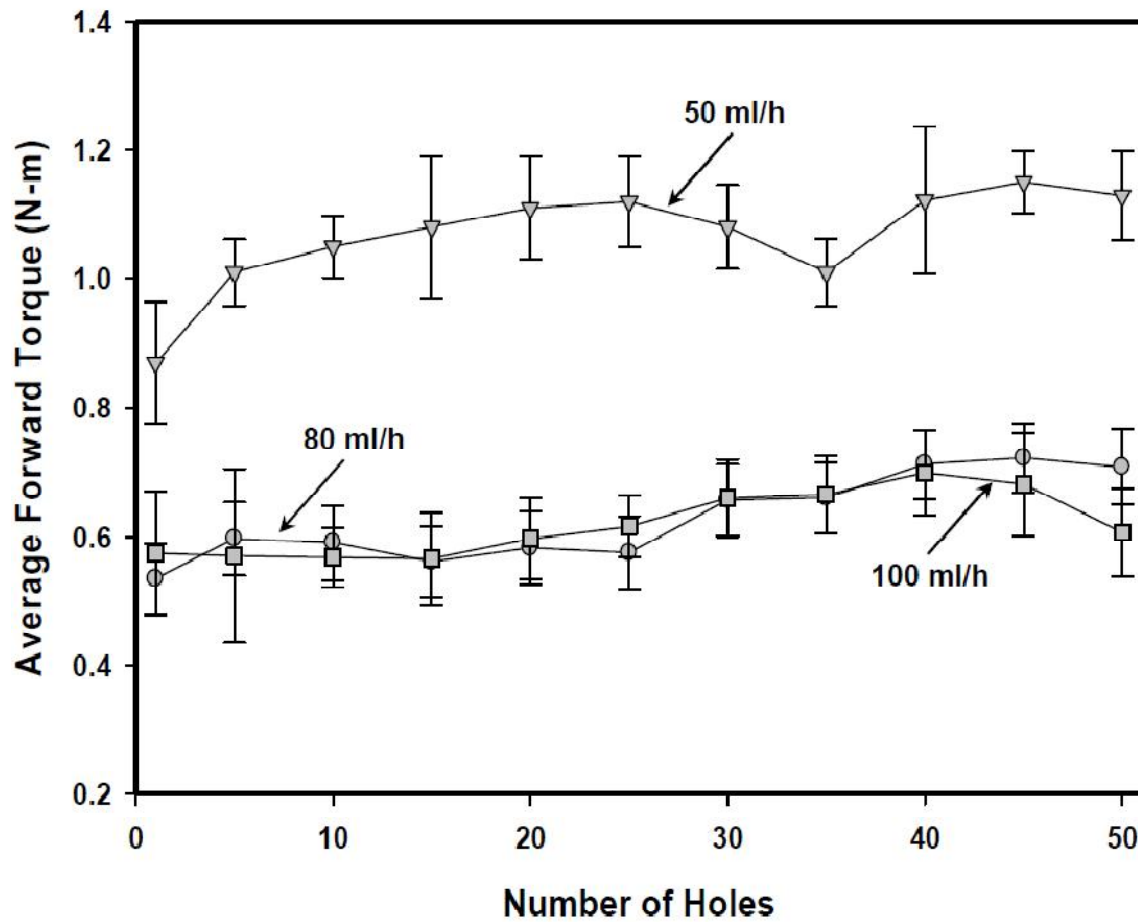


**Figure 4. 5** Preliminary experiments performed to determine the optimum FA-MQL flow rate.

In a separate set of preliminary experiments undertaken to determine an optimum MQL flow rate (Fig. 4.5), the average forward torque increased when an FA-MQL stream lower than 80 ml/h was used, as evident from the 30% increase in average torque when a flow of 50 ml/h

MQL was employed. There was no significant difference in average tapping torque responses when a flow rate of either 80 or 100 ml/h was used. Consequently, MQL agents were applied at the rate of 80 ml/h throughout the rest of the tapping experiments.

#### **4.2.5. Temperature Measurements, Metallographical Inspections and DSC**

The temperature increase in the 319 Al workpiece subjected to tapping for the first 50 holes was measured by a non-contact, infrared thermometer from one side of the workpiece--3 mm away from the first row of holes being tapped (Fig. 4.2). A non-contact, infrared thermometer was chosen because it is a practical and effective temperature measurement technique for moving, or inaccessible objects (Sullivan and Cotterell, 2001). A detailed explanation of the measurement technique using an infrared thermometer can be found in Bhowmick et al. (2010).

The last holes tapped before tool failure in the case of dry tapping, or upon completion of the predetermined numbers of test cycles (for MQL and conventional tap oil conditions) were subjected to metallographic analyses. A rectangular section of the workpiece containing this particular hole was mounted in epoxy resin and metallographically cut from the midpoint plane along the hole's 25 mm depth. The sectioned plane, which is perpendicular to the top surface, was then polished with a 0.1  $\mu\text{m}$  diamond suspension. The sectioned surfaces were ultrasonically cleaned in ethanol and etched in 0.5% HF solution to reveal the cross-sectional microstructure of the threads being cut. Another section, which is parallel to the top surface, was also polished to obtain a hardness measurement. The metallographic cross-sections taken from the thread surfaces were coated using an electroless Ni solution at 95 °C for 2 hours prior to sectioning for subsurface hardness measurement, in order to preserve the morphology of the subsurface that



formed during tapping. A scanning electron microscope (JEOL 5400 SEM) was used to investigate the amount of aluminum adhesion to the thread pitches, and to study the formation of built-up edges (BUEs).

Thermal analysis was performed by means of a DSC (TGA Q600 TA Instruments, USA) analyser using a heating rate of 10 °C/min. Argon gas was used to prevent oxidation of the samples. After heating, nitrogen-cooling was used for all runs. The aim of the DSC studies was to determine the thermal degradation temperature of the lubricants used in tapping tests.

#### **4.2.6 Pin-on-Disk Tests**

Sliding wear tests were conducted using a pin-on-disk-type tribometer (CSM Instruments). Pins with a 4 mm radius, made from the same 319 Al used in tapping tests, were tested against uncoated HSS and DLC coated HSS coupons in dry sliding in ambient air for sliding cycles up to  $10^3$ . Additionally, uncoated HSS coupons were tested using FA-MQL fluid under boundary lubricated condition and flooded (MO) tap oil under hydrodynamic lubrication condition. All pin-on-disc wear tests were performed at a 0.12 m/s linear speed and a 5 N normal load.

### **4.3. EXPERIMENTAL RESULTS**

#### **4.3.1. Dry Tapping Using Uncoated HSS Taps**

While tapping, the test had to be stopped at only the 17<sup>th</sup> hole because the HSS tap became stuck to the 319 Al workpiece as a result of aluminum adhesion, and this condition was defined as tap failure. [Fig. 4.6](#) plots variations in the average forward torque and the number of

holes--showing the abrupt increase that occurred during HSS dry tapping. The average forward torque reached 3.18 N-m at the onset of failure. Meanwhile, the average backward torque also increased significantly from the 1<sup>st</sup> hole (-0.23 N-m) to the 17<sup>th</sup> hole (-1.63 N-m). This provided a sharp contrast to tapping using DLC-coated HSS tools and uncoated HSS in MQL and flooded tapping conditions, for which no tool failure occurred and the average torque values were low throughout the experiments.

The shapes of the torque curves generated during HSS dry tapping appear in [Fig. 4.7 \(a\)](#) in the sequence that the holes were formed. An investigation of the individual torque profile of each hole revealed that in most cases, an increase in torque was observed at increased hole depths--usually provoked by chip clogging. This corresponded to “forward torque spike” behaviour, as identified in [Fig. 4.7 \(a\)](#). A total of 25% of the holes exhibited forward torque spikes during HSS dry tapping. The maximum forward torque recorded was 5.32 N-m at the end of the tool’s life (17<sup>th</sup> hole). Backward torque spikes--spikes generated while the tap travelled out of the hole--were also noted at 40, 60 and 80 seconds ([Fig. 4.7a](#)). 18% of the holes that underwent HSS dry tapping produced backward torque spikes. The maximum backward torque recorded was -3.10 N-m at the 17<sup>th</sup> hole.

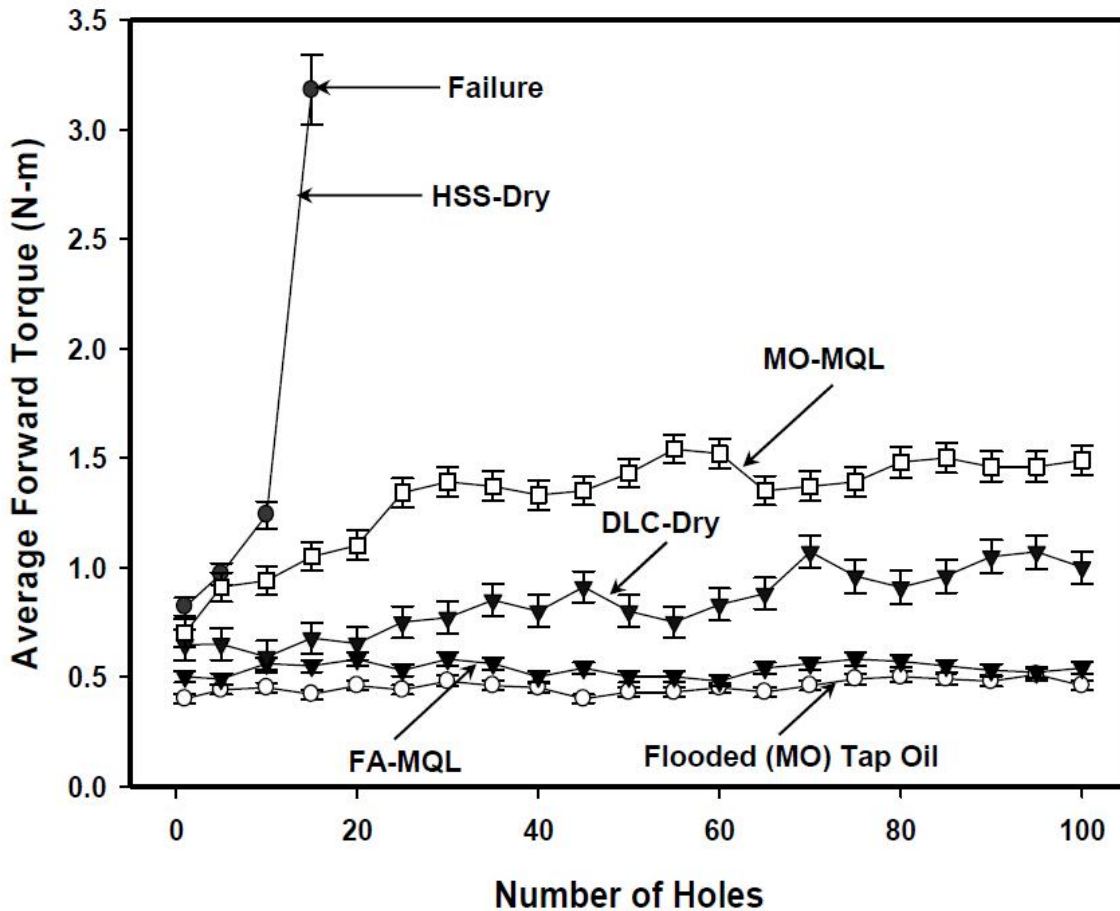


**Figure 4. 6** Average forward torques for dry tapping (uncoated HSS, DLC-coated HSS), MQL tapping using uncoated HSS (MO-, FA-MQL) and flooded drilling (MO tap oil) using uncoated HSS.

#### 4.3.2. Dry Tapping Using DLC-Coated Taps

According to Fig. 4.6, dry tapping with the DLC-coated HSS tap resulted in prolonged tool life. Fig. 4.7 (b) shows the DLC dry tapping torque responses for the first 16 holes. Generally, more uniform torque profiles were observed compared to those generated in HSS dry tapping, although some forward torque spikes were still observed. The holes tapped starting at 50, 60 and 70 seconds, for example, resulted in a total of 11% of the holes exhibiting forward torque spikes and 2% exhibiting backward torque spikes. The average forward torque (Fig. 4.6)

increased from 0.64 N-m at the 1<sup>st</sup> hole to only 1.01 N-m at the 100<sup>th</sup> hole, corresponding to an increase of 56%, which compares favourably with almost 300% for the HSS dry tapping. Consequently, the use of DLC-coated tools provided a few advantages during the dry tapping of 319 Al blocks. It was necessary to evaluate whether equal or better improvements could be achieved using the MQL tapping, in addition to how they would compare with the benchmark flooded tapping.

#### **4.3.3. MQL Tapping and Flooded Tapping**

Tapping that used uncoated HSS taps under MQL conditions during which conventional tap oil (MO-MQL) was supplied at a rate of 80 ml/h proved successful in preventing premature tool failure. In this case, higher average torque was evident compared to DLC dry drilling, as shown in [Fig. 4.6](#). The average torque increased from 0.71 N-m at the 1<sup>st</sup> hole, to 1.49 N-m at the 100<sup>th</sup> hole—an increase of 110%. In fact, for the majority of the experiments, the torque values appeared to maintain an average of torque of 1.45 N-m. According to [Fig. 4.6](#), the FA-MQL tapping induced an average cutting torque that was consistently low and remained more stable compared to the MO-MQL. An increase from 0.50 (1<sup>st</sup> hole) to 0.55 N-m (100<sup>th</sup> hole) can be observed—an almost insignificant increase of 10% that indicates a desirable steady-state behaviour throughout the entire range when using FA-MQL tapping. The sound performance of FA-MQL was attributed to the presence of extreme pressure additives in FA-MQL. The performance of FA-MQL is discussed in Section 4.3.

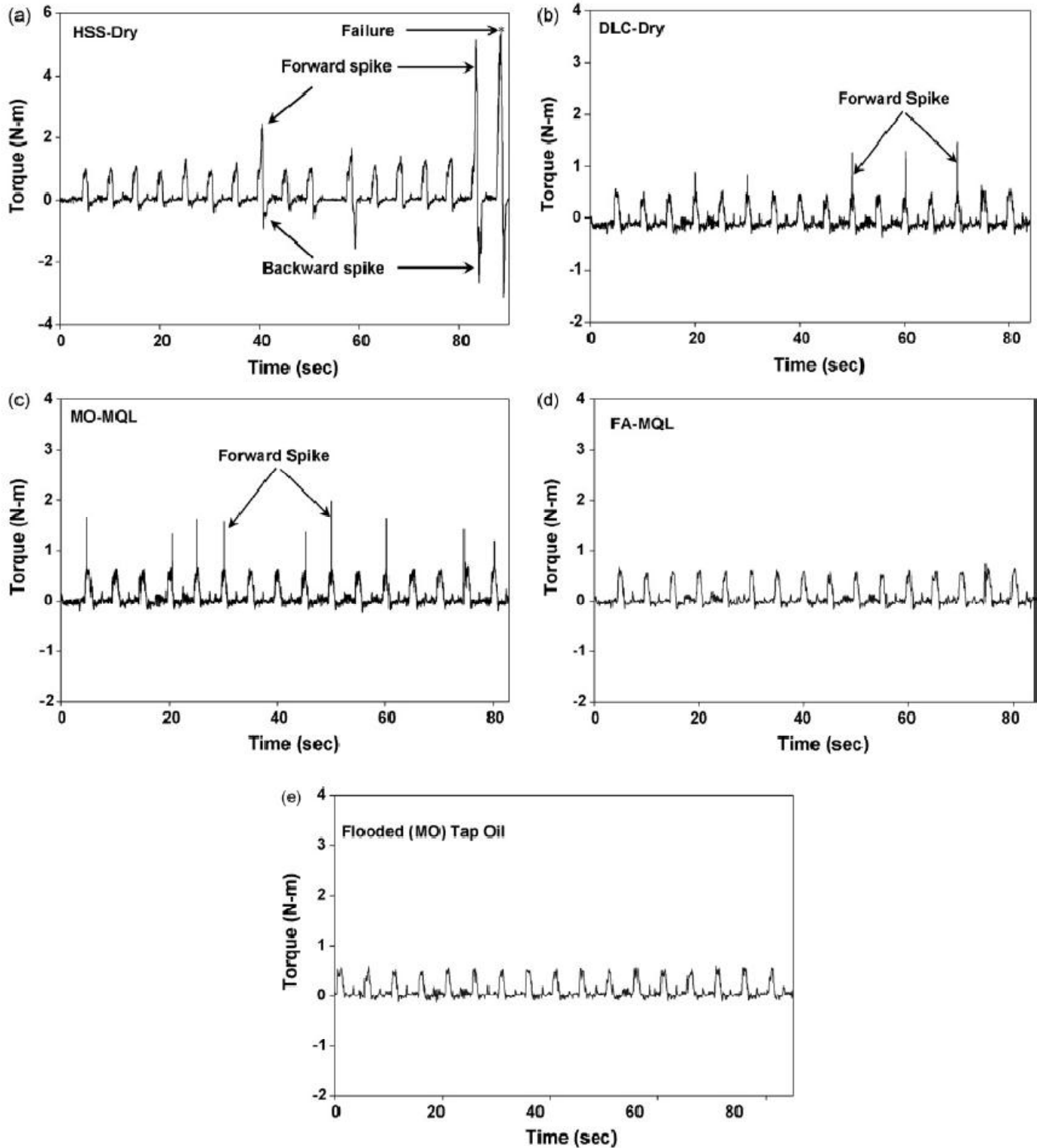


**Figure 4. 7** Variations of torques during the tapping of each hole with the time. (a) HSS-dry tapping; (b) DLC-coated HSS-dry tapping; (c) MO-MQL tapping with HSS; (d) FA-MQL tapping with HSS; (e) flooded tapping with HSS.

Figs. 4.7 (c) and (d) show the torque responses of the first 16 holes for each of the two MQL agents. Some forward torque spikes can be observed in the holes starting at 5, 25-35, 45, 55 and 60 seconds during MO-MQL tapping. 22% of the tapped holes exhibited forward torque spikes during MO-MQL tapping. As previously stated, a uniform torque response was observed throughout the entire range during FA-MQL tapping, a pattern that was also evident in Fig. 4.7 (d), which shows that no significant forward or backward torque spikes were observed during FA-MQL tapping.

The lowest average forward torque values were generated when the mineral-based tap oil (MO) was supplied at a rate of 10,000 ml/h i.e., in the case of flooded tapping. An increase in the average torque from 0.40 N-m for the 1<sup>st</sup> hole to 0.46 N-m over the course of the experiments corresponded to a modest increase of 15% (Fig. 4.6). According to Fig. 4.7 (e), no forward or backward torque spikes were observed during flooded tapping.

Since flooded tapping is the standard machining condition, it can be concluded that a comparable performance could be achieved using an 80 ml/h supply of the FA-MQL fluid. The use of the commercial tap oil as an MQL agent (MO-MQL) does not bring the same advantages. Hence, the emphasis in the remainder of this manuscript will be on further characterization of the FA-MQL tapping responsible for low average torques and a stable behaviour similar to the flooded tapping of 319 Al. Additionally, dry tapping using the DLC-coated tool will be given attention. An examination of chip morphology has shed further light on the details of these tapping processes, as described in **Section 3.4**.

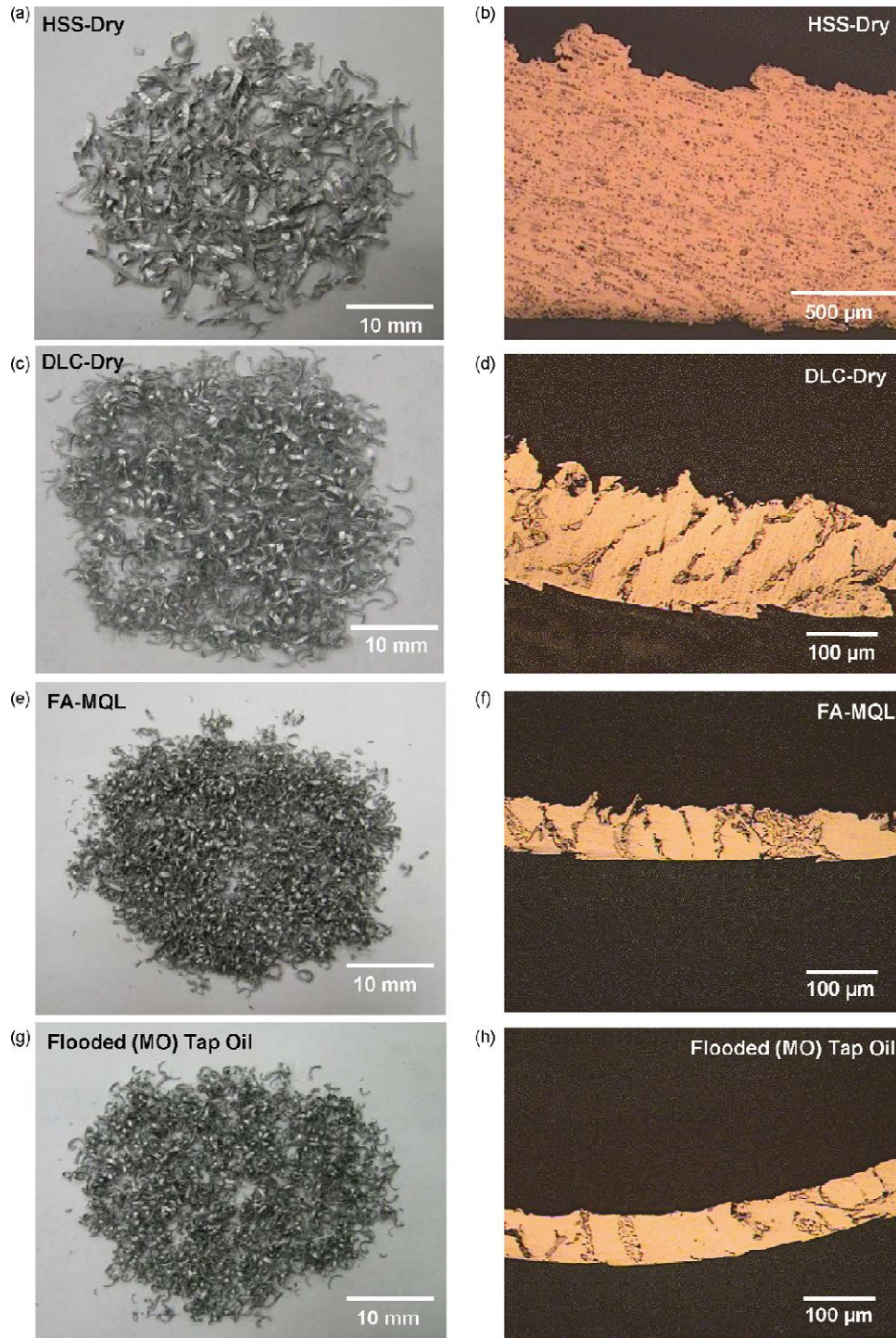


**Figure 4. 8** Typical chips generated during (a and b) HSS-dry tapping; (c and d) DLC-dry tapping; (e and f) FA-MQL tapping with HSS; (g and h) flooded tapping with HSS.

#### 4.3.4. Chip Morphology

Figs. 4.8 (a-d) display low magnification photographs that show the different chip morphologies generated under HSS dry, DLC dry, FA-MQL and flooded (MO) tapping conditions. Figs. 4.8 (e-h) provide corresponding higher-magnification cross-sectional micrographs taken after the chips had been polished. The average chip length was calculated by considering a sample size of about 50 chips collected from each set of tapping experiments. The longest average chip length was  $8.3 \pm 3.2$  mm, generated during HSS dry tapping. Meanwhile, the average chip length was measured as  $5.1 \pm 2.7$  mm during DLC dry tapping. Tapping using FA-MQL ( $3.3 \pm 0.5$  mm) and flooded (MO) tapping conditions ( $5.2 \pm 1.3$  mm) also produced short chip segments. The thickest chip-- $1,005 \pm 150$   $\mu\text{m}$ --resulted during HSS dry tapping, while the average chip thickness were  $125 \pm 11.3$   $\mu\text{m}$ ,  $43.9 \pm 7.1$   $\mu\text{m}$  and  $51.5 \pm 6.9$   $\mu\text{m}$  for DLC dry tapping, FA-MQL and flooded (MO) tapping conditions. It is worth noting that the thickness of the chips generated during HSS dry tapping were even larger than the taps' pitch length (1.25 mm), supporting the possibility of adhesion to the threads.

#### 4.3.5. Temperature Increase During Tapping

Figs. 4.9 (a-e) illustrated variations in the temperature generated during the tapping of individual holes within the cutting time, for uncoated HSS dry tapping, DLC dry tapping, FA-MQL and flooded (MO) tapping conditions. MO-MQL was included to provide a better understanding of the MQL tapping agents' effects. Fig. 4.9 (f) shows the highest temperatures recorded during the tapping of each hole until tool failure, for HSS dry tapping and for the first



50 holes of the other tapping conditions. The temperature during HSS dry tapping increased rapidly to 241 °C at the 17<sup>th</sup> hole, corresponding to the end of tool life. The recorded temperature did not exceed 75 °C during DLC dry tapping. During MO-MQL tapping with the HSS tap, the maximum temperature observed was 118 °C. Using the FA-MQL agent, the temperature profile remained almost constant throughout the tapping tests. The temperature increased by only 10% from the 1<sup>st</sup> hole (50 °C) to the 50<sup>th</sup> hole (55 °C). During the course of flooded tapping, the maximum temperature did not exceed 48 °C.

In summary, flooded (MO) tapping and FA-MQL conditions served to maintain the low temperatures conducive to mitigating aluminum adhesion. The DLC-coated tapping tool's performance was also remarkably good, compared to dry tapping with uncoated HSS taps, and consistent with the low torque response depicted in [Fig. 4.6](#).

[Table 4.1](#) summarizes the maximum and average forward and backward torques, maximum temperature, average chip length and average chip width obtained from the taps operated under HSS dry tapping, DLC dry tapping, FA-MQL and flooded (MO) conditions. A summary of the torque, temperature and chip size generated when MO-MQL media was used is also given.

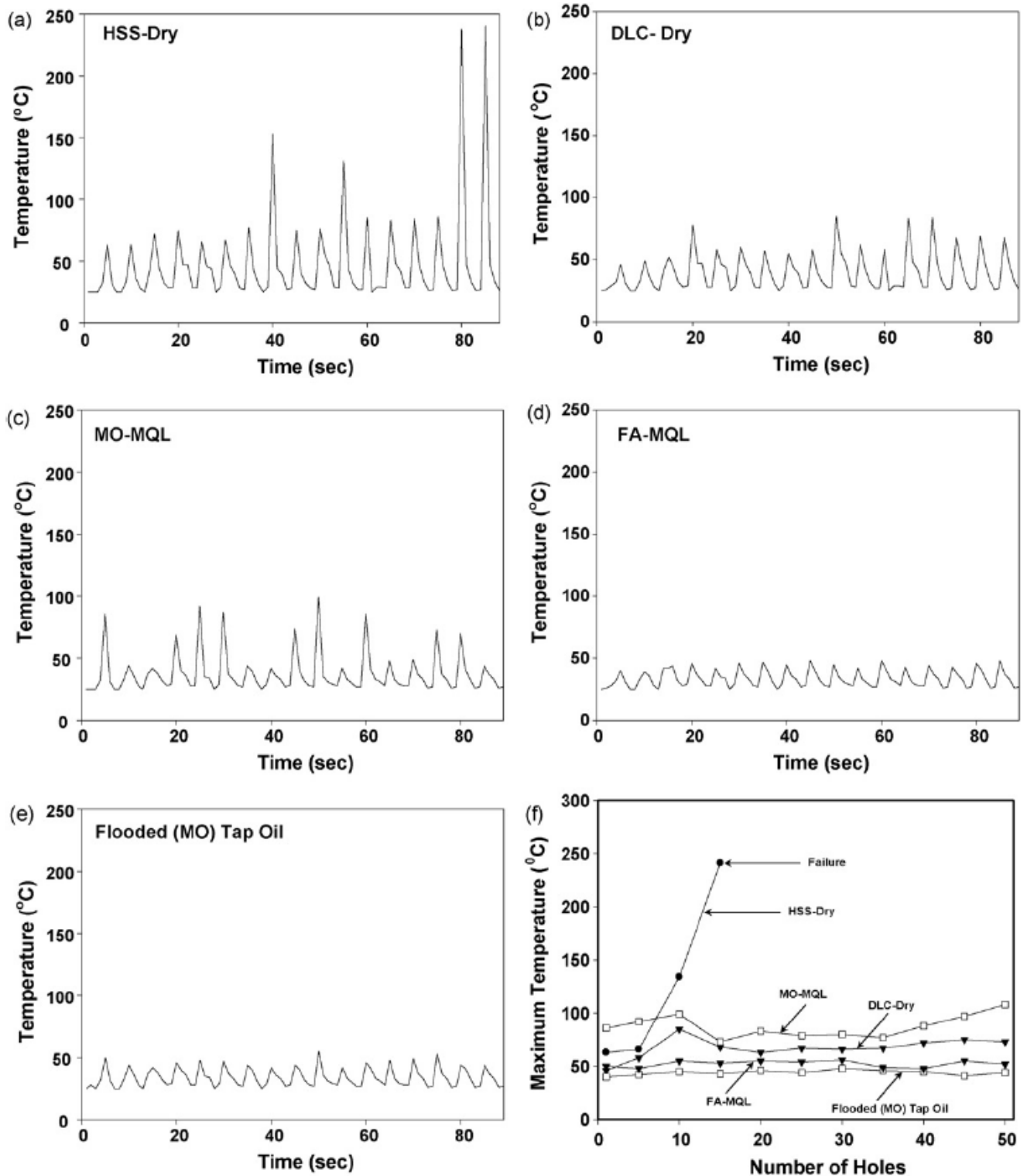


**Figure 4.9** Variation of workpiece temperatures during the tapping of each hole with the time. (a) HSS-dry tapping; (b) DLC-coated HSS-dry tapping; (c) MO-MQL tapping with HSS; (d) FA-MQL tapping with HSS; (e) flooded tapping with HSS. (f) Maximum temperature variations with number of holes.

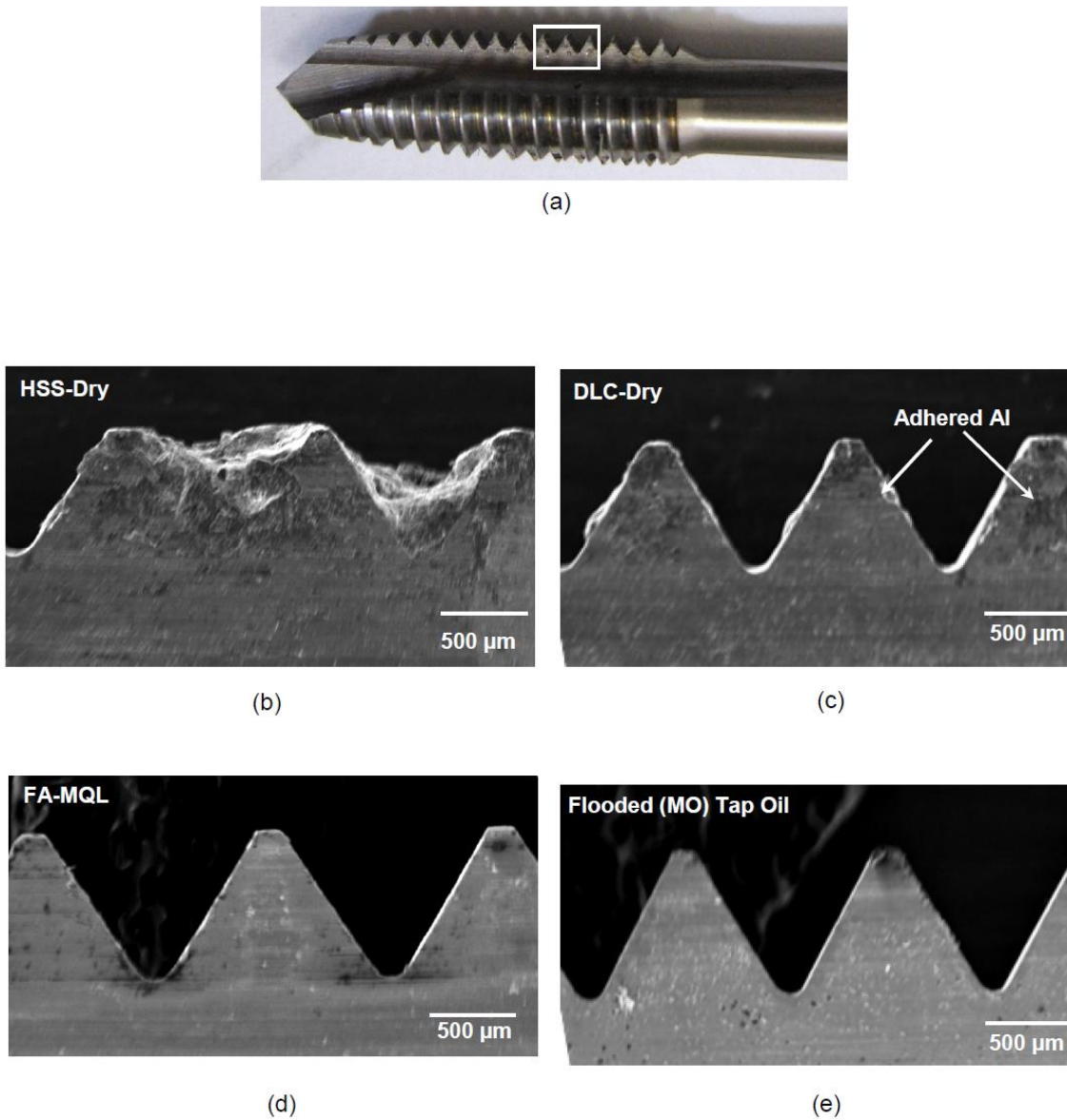


**Figure 4. 10** (a) A close-up view of the tap showing the area investigated. SEM secondary electron images showing adhesion of aluminum to the threads in (b) HSS-dry tapping, (c) DLC-dry tapping, (d) FA-MQL, and (e) flooded tapping with HSS.

#### 4.3.6 Aluminum Adhesion to Tool and Thread Quality

The scanning electron microscopy (SEM) performed on the cross-sections of the tap surfaces used in the HSS dry tapping, DLC dry tapping, FA-MQL and flooded (MO) tapping

experiments for the tap locations shown in Fig. 4.10 (a). As Fig. 4.10 (b) demonstrates, the workpiece material transferred to the pitches of the HSS tap threads during dry tapping, and the transferred aluminum covered almost the entire area of the thread pitches, causing a prominent BUE. During tapping experiments, the taps lost their geometrical accuracy as a more and more prominent BUE was developed (Venkatesh and Xue, 1996). Some patches of adhered aluminum were observed in dry tapping using the DLC-coated taps, consistent with occasional torque spikes (Fig 4.7b), but to a lesser extent compared to those produced by the HSS-dry tapping (Fig. 4.10c). BUE formation on taps was neither observed in FA-MQL (Fig. 4.10d), nor in conventional flooded (MO) tapping (Fig. 4.10e).

The fact that aluminum chips adhered to the taps was detrimental to the workpiece thread quality; severely damaging and breaking the threads of 319 Al --observed during HSS dry tapping and exemplified in Fig. 4.11 (a). As no significant BUE formation occurred on DLC-coated taps, the corresponding thread quality turned out to be very good (Fig. 4.11 b). This is a significant point in favour of dry tapping with the DLC-coated tools. As expected, MQL and flooded tap conditions produced excellent thread quality, as evident in Figs. 4.11 (c) and (d). The high thread quality in each of the last three conditions was maintained even when the threads were machined only a few micrometers away from large casting defects.

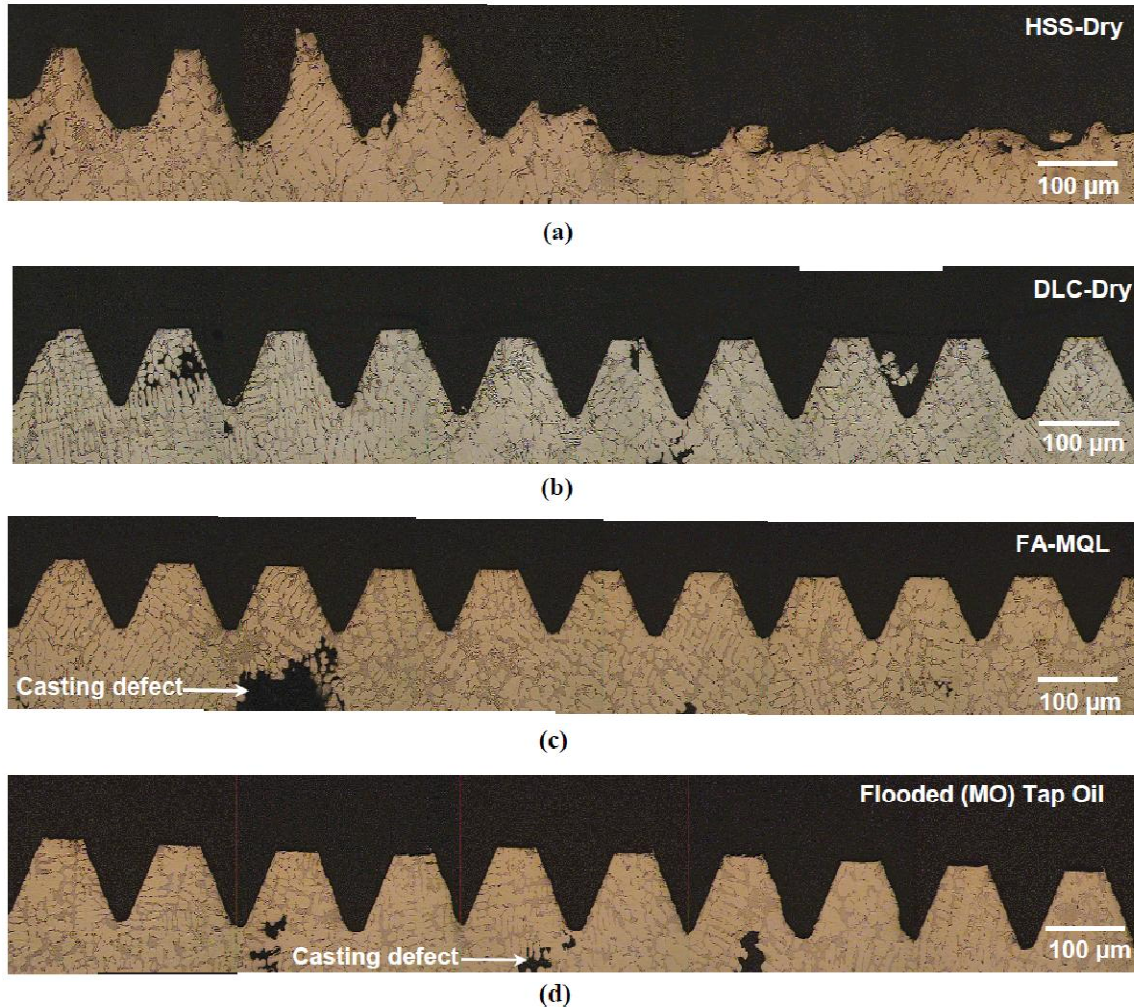


**Figure 4. 11** Optical micrograph showing the thread morphology for (a) HSS-dry tapping, (b) DLC-dry tapping, (c) FA-MQL and (d) flooded tapping with HSS.

#### 4.4. Discussion

This section discusses the mechanisms responsible for the improvements provided by DLC-coated tools, compared to dry tapping--considering the possible reasons behind the fact that FA-MQL tapping showed a performance comparable to flooded tapping. Temperature generation in the workpiece and the factors facilitating the transfer of aluminum to the taps--namely the role of the coefficient of friction (COF) are given particular attention. Lastly, the role that FA-MQL fluid composition plays in the reduction of adhesion is discussed.

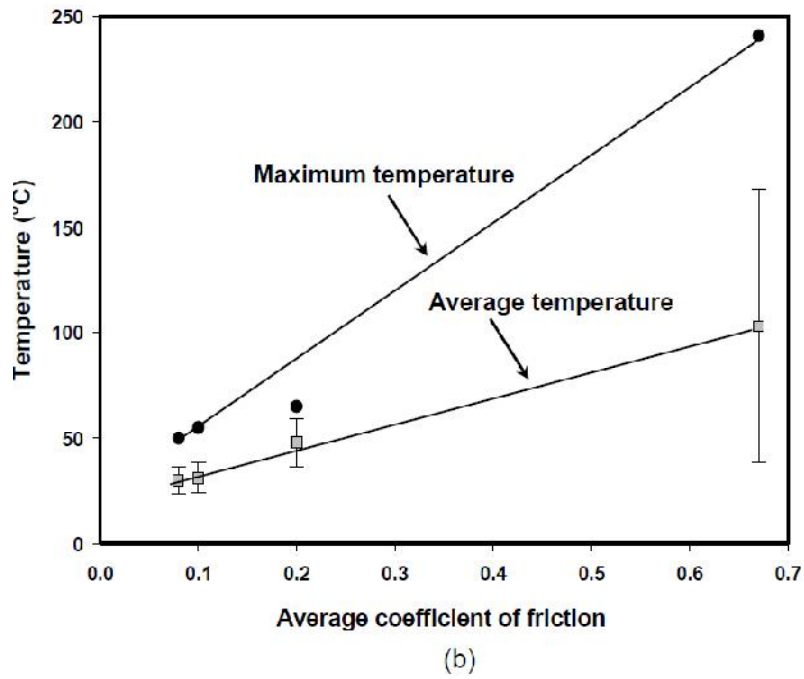
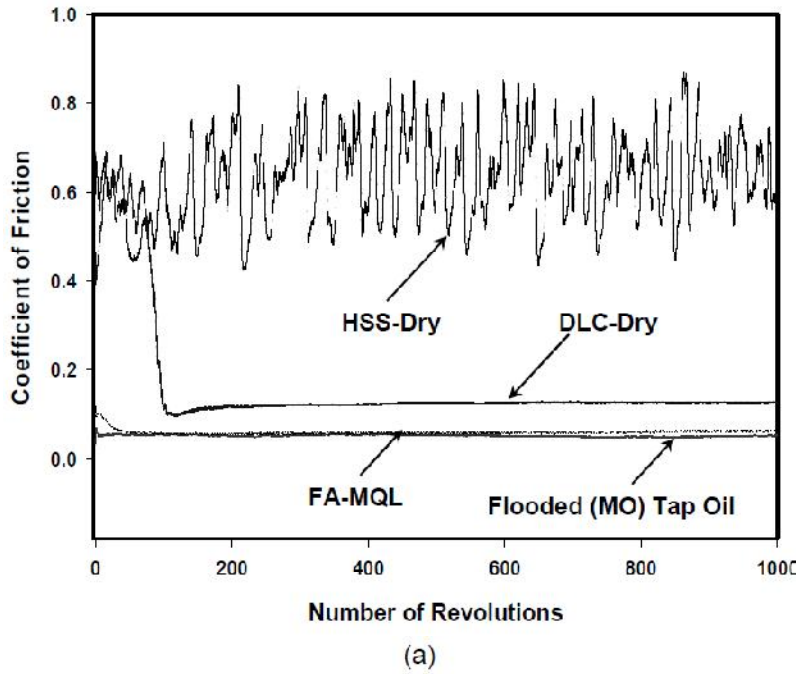


**Figure 4. 12** (a) COF vs. number of revolutions during pin-on-disc sliding tests. (b) COF plotted against the maximum and average tapping temperatures.

#### 4.4.1. The Role of COF

The experimental results presented in **Section 3** have clearly demonstrated an enhancement in the dry tapping performance of 319 aluminum alloys using DLC coated tools, in comparison to uncoated HSS tools. In addition to prolonging the tool life, reductions in average and maximum forward and backward torques were evident. These results are in agreement with the tribological test results on DLC against 319 Al, which indicated the much smaller tendency of aluminum to adhere to the DLC surface, compared to uncoated steel as noted by Konca et al. (2006). Thus, a more thorough understanding of the effect of DLC coatings against 319 Al can be gained from the examination of the COF values obtained using the pin-on-disc test. As shown in Fig. 4.12 (a), the average COF for DLC coatings tested against 319 Al had a low value of  $0.20 \pm 0.12$  in ambient air, whereas the average COF of uncoated HSS was  $0.63 \pm 0.10$ . The frictional temperature increase due to sliding between two contacting solids pressed together by a normal force  $F$ , sliding at a relative velocity  $v$  depends on the COF  $\mu$  between the surfaces in contact (Lim and Ashby, 1987). The heat generated  $q$ , per unit of nominal contact area  $A_n$ , per second can be expressed as follows:

$$q = \frac{\mu F v}{A_n} \quad (1)$$

The temperature  $T_b$ , at the contacting (e.g., tool-chip) interface--as a result of injection of the frictional heating across  $A_n$ --is related to the heat flux  $J$  through the thermal conductivity of aluminum  $K$  as shown below:

$$J = K \left( \frac{T_b - T_0}{L} \right) \quad (2)$$

where  $T_0$  is the ambient temperature and  $L$  is the equivalent linear heat diffusion distance as defined in Lim and Ashby (1987). From Equations (1) and (2), the COF  $\mu$  between the contacting surfaces is:

$$\mu = \frac{KA_n}{FvL} (T_b - T_0) \quad (3)$$

Using Equation 3, the COF can be correlated to the temperature generated during tapping. This is done in Fig. 4.12 (b), which shows a linear relationship between the sliding induced COF and the maximum tapping temperature, as well as the average temperature. A low COF between the tool and the workpiece materials restricts the contact surface temperature increase to low values, thus limiting aluminum adhesion to the tool in the case of dry tapping. The high COF between the 319Al and HSS surfaces in dry contact would lead to softening of aluminum (see Section 4.2) due to high temperature increase, promoting adhesion.

Meanwhile, a low COF ( $0.10 \pm 0.03$ ) was observed in flooded conditions, i.e., when the pin-on-disc tests were conducted using the 319Al pin against a HSS disc surface under hydrodynamic contact conditions using the MO tapping fluid (Fig. 4.12a). It was interesting to observe that the COF of  $0.08 \pm 0.05$ --generated when using FA-MQL fluid under boundary lubricated conditions in the pin-on-disc tests--provided the same COF. This implies that FA-MQL fluid could be as effective as flooded conditions in terms of reducing aluminum adhesion. This is consistent with the low temperature generation in Fig. 4.9 (f). The elimination of aluminum adhesion was also evident from the metallographic inspections of the tool surfaces, as discussed below.



#### 4.4.2. The Role of Subsurface Hardening

The high cutting temperatures generated during dry tapping of the 319 Al reaching as high as 241 °C (Fig. 4.9f) reduced the hardness of the material causing excessive adhesion of softer aluminum to the taps, and ensuring rapid tool failure. The effect that frictional contact-induced heating has on aluminum softening during tapping can be determined from an examination of the hardness profiles of the material layers immediately beneath the holes. Vickers microhardness indentations made for this purpose, starting from the edge of the hole surface and placed at intervals of 20 μm in a direction normal to this surface until a depth of approximately 225 μm below the surface, the hardness of the bulk material was attained. Fig. 4.13 (a) records the observed area for microhardness tests, while Fig. 4.13 (b) illustrates the variations in microhardness with the distance from the hole surface. After dry tapping, the aluminum hardness 20 μm below the hole surface ( $49 \pm 8$  HV) was about 30% lower than the bulk hardness of 319 Al ( $67.0 \pm 8.0$  HV), whereas the microhardness profiles obtained after FA-MQL and flooded tapping were characterized by an increase towards the hole surface. At 20 μm below the tapped surface, both FA-MQL tapping ( $70 \pm 4$  kg-mm<sup>-2</sup>) and flooded tapping ( $71 \pm 3$  kg-mm<sup>-2</sup>) produced higher hardness values compared to bulk hardness. In these cases, the temperature increase during tapping was not high enough to reduce hardening of material layers adjacent to the contact surface. Consequently, aluminum adhesion to the tool was at a minimum, leading to the small torques shown in Fig. 4.6.

#### 4.4.3 MQL Fluid Effects

Finally, it is instructive to comment on the role that the composition of the MQL agent used has on tapping performance. Enhanced tapping performance using FA-MQL can be attributed to the presence of extreme pressure additives in the MQL agent containing S and P. The presence of these elements in the MQL agent was confirmed by NMR tests (see **Section 2.2**), as well as electron diffraction spectroscopy (EDS) analyses ([Bhowmick et al., 2010](#)). The build up of a protective layer of those additives prevents direct contact between the interacting surfaces of the workpiece material and the tap surface, which minimizes aluminum adhesion. The protective layers can be formed either by the physical adsorption of the additives, or by the chemical reaction between the metal surface and the additives ([Rahman et al., 2002](#)). It has been noted that the formation of protective layers by adsorption occurs at temperatures up to 120 °C ([Trent and Wright, 2000](#)). Results of DSC analyses performed to evaluate the thermal stability of MQL and conventional (flooded) tap oil are represented in Chapter 8 (Section 3). The two exothermic peaks starting at 140 °C for conventional tap oil (MO) arise as a result of the thermal decomposition of hydrocarbon molecules in the tap oil ([Choi et al., 1997](#)). For FA-MQL, the first exothermic peak was observed at 206 °C, indicating the high thermal stability of FA-MQL. As reported in **Section 3.5**, the temperature generated during FA-MQL tapping was about 55 °C. Similarly, the temperature did not exceed 48 °C during flooded tapping, suggesting that the decomposition of MO tap oil during flooded tapping is unlikely. During MO-MQL tapping, however, the temperature exceeded 120 °C ([Fig. 4.9f](#)) and reached a temperature nearly equal to the decomposition temperature of MO tap oil. This led to an interpretation of the effectiveness of FA-MQL in maintaining stable and low torque values and providing an equal performance compared to flooded tapping conditions--based of the stability of the FA-MQL agent during the tapping operation.

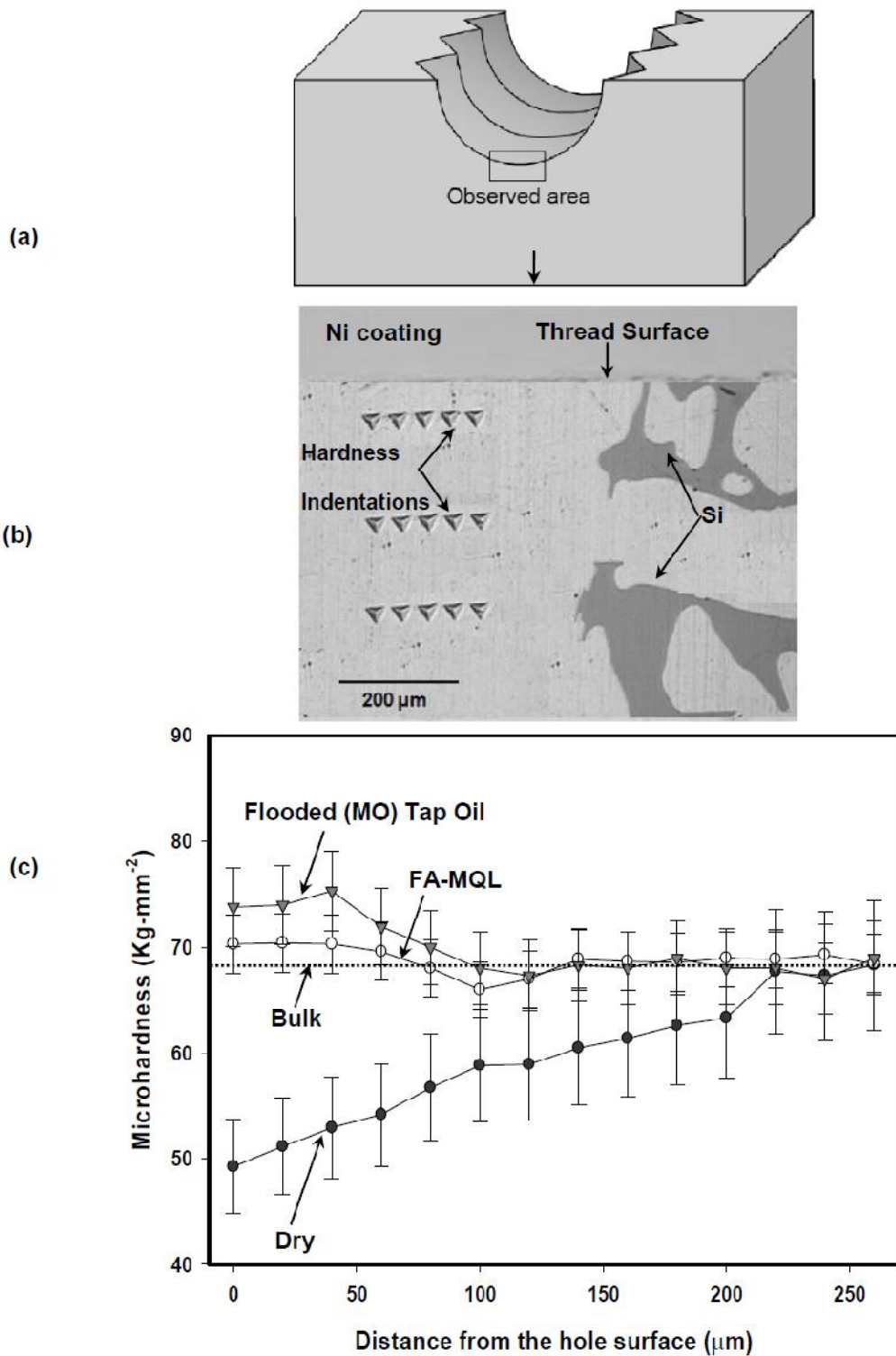


**Figure 4. 13** (a) Schematic diagram of a tapped hole showing the plane where microhardness indentations were made and (b) an optical micrograph showing the Vickers indentation impressions. (c) Subsurface hardness variation with the depth from the hole surface.

## 4.5. Conclusions

This study explored the tapping of a 319-grade Al-Si alloy using unconventional conditions—specifically dry and MQL machining. The main conclusions are as follows:

- (1) Dry tapping of a 319 Al alloy using an HSS tap led to immediate tool failure. HSS dry tapping suffered from extensive aluminum adhesion and resulted in abrupt increases in torque before tool failure. The use of DLC-coated taps prolonged the tool life and generated small, stable average torques due to the mitigation of aluminum adhesion. The resulting thread quality was enhanced considerably.
- (2) The high coefficient of friction (COF) between the 319Al and HSS interfaces led to high temperature increase during dry tapping, promoting adhesive aluminum transfer. A decrease in the hardness of the materials adjacent to the threads also occurred. A low COF between the workpiece and the DLC-coated tool restricted temperature increase, limiting aluminum adhesion to the tap surface. The low COF of DLC against aluminum was responsible for preventing built-up edge (BUE) formation on the taps and in improving the thread quality of tapped holes.
- (3) Tapping using 80 ml/h fatty acid-based MQL fluid provided a performance equal to that of flooded tapping with a high thread quality. The use of MQL was effective in restricting temperature increase during tapping, ensuring minimal aluminum adhesion to the tap that resulted in low torques. The presence of sulphur and phosphorus-based additives in the MQL fluids helped prevent aluminum adhesion.

## List of References

Bhowmick, S., Alpas, A.T., 2008. The performance of hydrogenated and non-hydrogenated diamond-like carbon tool coatings during the dry drilling of 319 Al. *International Journal of Machine Tools and Manufacture*. 48, 802–814.

Bhowmick, S., Alpas, A.T., 2008. Minimum quantity lubrication drilling of aluminum–silicon alloys in water using diamond like carbon coated drills. *International Journal of Machine Tools and Manufacture*. 48, 1429-1443.

Bhowmick, S., Lukitsch, M.J., Alpas, A.T., 2010. Dry and minimum quantity lubrication drilling of cast magnesium alloy (AM60). *International Journal of Machine Tools and Manufacture*. 50, 444-457.

Boothroyd, G., Knight, W.A., 2006. *Fundamentals of machining and machine tools*. CRC Press, Taylor and Francis. p. 190.

Braga, D.U., Diniz, A.E., Miranda, G.W.A., Coppini, N.L., 2002. Using a minimum quantity of lubricant (MQL) and a diamond coated tool in the drilling of aluminum–silicon alloys. *Journal of Materials Processing Technology*. 122, 127-138.

Chen, M., Liu, G., Zhang, X., 2007. Optimization studies on hole-making tools for high-performance cutting austenitic stainless steel. *Machining Science and Technology*. 11, 183-200.

Choi, U.S., Ahn, B.G., Kwon, O.K., Chun, Y.J., 1997. Tribological behaviour of some antiwear additives in vegetable oils. *Tribology International*, 30, 677-683.

Dasch, J.M., Ang, C.C., Wong, C.A., Cheng, Y.-T., Weiner, A.M., Lev, L.C., Konca, E., 2006. A comparison of five categories of carbon-based tool coatings for dry drilling of aluminum. *Surface and Coatings Technology*. 200, 2970-2977.

Dosbaeva, J., Fox-Rabinovich, G., Dasch, J.M., Veldhuis, S., 2008. Enhancement of wet- and MQL- based machining of automotive alloys using cutting tools with DLC/polymer surface treatments. *Journal of Materials Engineering and Performance*. 17, 346-351.

Isakov, E., 2003. *Engineering formulas for metal cutting*, Industrial Press. Inc., 1<sup>st</sup> Edition, New York, p. 176.

Kelly, J.F., Cotterell, M.G., 2002. Minimal lubrication machining of aluminum alloys. *Journal of Materials Processing Technology*. 120, 327-334.

Klocke, F., Eisenblaetter, G., 1997. Dry cutting. *CIRP Annals—Manufacturing Technology*. 46, 519–526.

- Konca, E., Cheng, Y.-T., Weiner, A.M., Dasch, J.M., Alpas, A.T., 2006. Elevated temperature tribological behaviour of non-hydrogenated diamond-like carbon coatings against 319 aluminum alloy. *Surface & Coatings Technology*. 200, 3996 – 4005.
- Lim, S.C., Ashby, M.F., 1987. Wear- mechanism maps. *Acta Metallurgica*. 35, 1-24.
- Rahman, M., Kumar, A.S., Salam, M.U., 2002. Experimental evaluation on the effect of minimal quantities of lubricant in milling. *International Journal of Machine Tools and Manufacture*. 42, 539-547.
- Reiter, A.E., Brunner, B., Ante, M., Rechberger, J., 2006. Investigation of several PVD coatings for blind hole tapping in austenitic stainless steel. *Surface and Coatings Technology*. 200, 5532-5541.
- Srivastava, A.K., Finn, M.E., Kinney, M.A., 2004, Tool/work material/cutting fluid interaction while tapping into AA-319 and AA-A356 T6 lost foam aluminum castings. *Transaction of NAMRI/SME*. 32, 263-270.
- Sullivan, D.O', Cotterell, M., 2001. Temperature measurement in single point turning. *Journal of Materials Processing Technology*. 118, 301-308.
- Trent, E., Wright, P., 2000, *Metal cutting*. 4<sup>th</sup> Edition, Butterworth–Heinemann publications, London, p 328.
- Veldhuis, S.C., Dosbaeva, G.K., Benga, G., 2007. Application of ultra-thin fluorine-content lubricating films to reduce tool/workpiece adhesive interaction during thread cutting operations. *International Journal of Machine Tools and Manufacture*. 47, 521-528.
- Venkatesh, V.C., Xue, W., 1996. A study of the built- up edge in tapping with indexable coated carbide inserts. *Journal of Materials Processing Technology*. 58, 379-384.
- Warrington, C., Kapoor, S., DeVor, R., 2005. Experimental investigation of thread formation in form tapping. *Journal of Manufacturing Science and Engineering*. 127, 829-836.
- Zedan, Y., Samuel, F.H., Samuel, A.M., Doty, H.W., 2010. Effects of Fe intermetallics on the machinability of heat-treated Al- (7-11)% Si alloys. *Journal of Materials Processing Technology*. 210, 245-257.

## TABLE

**Table 4.1:** Torque, temperature, chip length and chip width during HSS-dry, DLC-dry, MO-MQL, FA-MQL and flooded tapping of 319 Al.

<b>Characteristic parameters</b>	<b>HSS- Dry</b>	<b>DLC- Dry</b>	<b>MO-MQL</b>	<b>FA-MQL</b>	<b>Flooded</b>
Maximum forward torque (N-m)	5.32	1.46	1.96	0.61	0.56
Maximum backward torque (N-m)	3.10	0.56	0.91	-	-
Range of forward average torque (N-m)	0.82-3.18	0.64-1.01	0.71-1.49	0.50-0.55	0.40-0.46
Range of backward average torque (N-m)	0.23-1.53	0.13-0.29	0.17-0.56	-	-
Maximum temperature (°C)	241	75	118	55	48
Average chip length (mm)	8.25 ± 3.21	5.05 ± 2.76	6.28 ± 2.33	3.28 ± 0.5	5.2 ± 1.3
Average chip width (µm)	1005.21 ± 150.33	125.13 ± 11.31	77.20 ± 8.35	43.90 ± 7.11	51.51 ± 6.92

## CHAPTER 5

### **Dry and Minimum Quantity Lubrication Drilling of Cast Magnesium Alloy (AM60)**

Dry and minimum quantity lubrication (MQL) drilling of cast magnesium alloy AM60 used in the manufacturing of lightweight automotive components is discussed in this chapter. The experimental approach and analyses are discussed in Section 5.2. Tool life during dry drilling was inadequately short, due to excessive magnesium transfer and adhesion to the (HSS steel) drill causing drill failure in less than 80 holes, which is discussed in Section 5.3.1.1. The use of MQL reduced magnesium adhesion and built-up edge formation, resulting in an increase in tool life as well as reductions in both average torque and thrust forces—prompting a performance similar to that of flooded drilling, which is discussed in Section 5.3.1.2 to 5.3.1.3. The temperature increases in dry, MQL and flooded drilling are discussed in Section 5.3.2. Surface roughness and chip shapes formed under dry, MQL and flooded conditions are discussed in Section 5.3.3 and 5.3.4. The mechanical properties of the material adjacent to drilled holes, as evaluated through plastic strain and hardness measurements near the holes, revealed a notable softening in the case of dry drilling, but not for MQL drilling are discussed in Section 5.4. The summaries of the Chapter 5 are written in Section 5.5.

#### **5.1. Introduction**

The high strength-to-mass ratio of aluminum and magnesium alloys provide automotive and aerospace engineers with an opportunity to replace the traditional role of steel and cast iron components used in the transportation industry with these lightweight substitutes. Automotive



powertrain components made of cast aluminum and magnesium alloys effectively decrease fuel consumption by reducing the total mass per vehicle. As such, a magnesium-6% aluminum alloy (AM60) with applications in steering wheel frames and gear boxes is of increasing interest in the manufacturing of powertrain components for which drilling is one of the most critical machining processes. The machinability of magnesium alloys using metal removal fluids (MRF) has not proved problematic, and has been characterised by low cutting forces and finely broken chips [5.1], but the use of MRF is apprehensive from an environmental perspective [5.2]. With this in mind, it makes economical and ecological sense to develop environmentally sustainable machining processes for these new alloys that do not rely on MRF. The use of dry machining, examined by several research groups [5.3-5.6], is a possible consideration, but the dry machining of cast aluminum alloys remains problematic due to aluminum's strong tendency to adhere to the cutting tool, causing premature drill failure. Studies found that less than fifty holes could be drilled in a 319 grade aluminum- 6% silicon alloy using the standard, high speed steel (HSS) drills [5.7-5.8]. In addition, formation of -adhesive layers and a built-up edge (BUE) on the tool tip during dry machining reduces the quality of the machined surface [5.9-5.10]. Like aluminum alloys, chips formed during the dry drilling of magnesium alloys can readily adhere to the cutting tools. Gariboldi [5.11] investigated dry drilling in a AM60 magnesium alloy using HSS and TiN-coated HSS drills, and observed that all the drills exhibited short tool lives--failing as a result of extensive magnesium adhesion to their cutting edges and drill flutes. Tonshoff and Winkler [5.12] studied the dry turning of a magnesium-9% aluminum (AZ91) alloy with drills coated by polycrystalline diamond, and reported a uniform force response with no significant BUE formation.

A relatively new technique consisting of feeding only a few milliliters of fluid to the tool's cutting edge, namely minimum quantity of lubrication or MQL, has emerged as an environmentally friendly alternative to completely dry machining. The MQL fluid is atomized in a nozzle to form extremely fine droplets, which are then fed to the machining point in the form of an aerosol spray at a rate not exceeding 100 ml/h [5.13]. To the authors' knowledge, there is no work in the open literature on the MQL drilling of magnesium castings. Some research has been conducted on the application of MQL to the machining of aluminum alloys, and reviewing the available literature on the MQL machining of aluminum is instructive.

Davim et al. [5.14] studied the dry drilling of commercial purity aluminum (AA1050) compared with MQL drilling, for which an emulsion oil was applied at a rate of 250 ml/h, and flooded drilling, using the same fluid at a rate of 1,200 l/h. Dry drilling in all speed and feed rate combinations was characterized by the generation of high cutting power and thrust force (3000 MPa), while MQL and flooded drilling reduced the thrust forces to a similar level of 2,000 MPa. No difference in hole surface roughness was observed between MQL and flooded drilling. Klocke et al. [5.15] studied the effect of MQL on the drilling of a cast aluminum- 9% silicon alloy (380 Al) using a synthetic, ester-based fluid supplied at a rate of 10 ml/h. The holes displayed less surface roughness with MQL (25  $\mu\text{m}$ ) when compared to dry cutting (45  $\mu\text{m}$ ). MQL provided a lower maximum cutting torque of  $\sim 3$  N-m, compared to dry drilling ( $\sim 10$  N-m). Kelly and Cotterell [5.16] compared the flooded drilling of an aluminum-4.5% magnesium alloy (5080 Al) using mineral soluble oil supplied at a rate of 5,200 ml/min with the MQL drilling using a vegetable oil supplied at 20 ml/h, and dry drilling. The maximum torque generated during MQL drilling (2.2 N-m) was lower than that of the dry drilling, which generated a maximum torque of 3.8 N-m. MQL appeared to perform slightly better than the flooded

conditions, for which the highest torque was 2.4 N-m. In addition, a lower feed force of 400 N was measured for MQL drilling, compared to flooded drilling (450 N). Braga et al. [5.17] compared mineral oil MQL drilling, supplied at a rate of 10 ml/h and soluble oil flooded drilling supplied at a rate of 2,400 l/h of A356 aluminum-silicon alloys using a carbide drill. MQL drilling generated a maximum feed force of 1,260 N, which was very similar to the 1,250 N measured during flooded drilling.

Bardetsky et al. [5.18] reported on the other hand that the flooded mineral oil supplied at a rate of 40 l/min outperformed the MQL (synthetic phosphate ester) supplied at a rate of 10 ml/h during the high speed milling of 319 Al alloys using cemented carbide inserts. Specifically, a lower resultant cutting force of 300 N was measured in the case of the flooded cooling, compared to 350 N for the MQL. The authors [5.18] emphasized the benefits of anti-wear additives consisting of organic phosphates and extreme pressure additives consisting of sulfurized hydrocarbons in the cutting fluid. The effectiveness of these additives in flooded lubricant was attributed to the formation of a protective layer on the freshly cut metal surfaces.

There exists some work that examines the efficiency of MQL when used in combination with adhesion mitigating tool coatings. Dosbaeva et al. [5.19] used diamond-like carbon (DLC) coated drills and compared the effect of vegetable oil-based MQL with conventional flooded conditions when drilling 319 Al. The average torque of 3.71 N-m measured for the flooded drilling was very close to that recorded for MQL drilling. The cutting performance of DLC coated HSS drills using an MQL agent of distilled water spray (30 ml/h) was also examined [5.20]. Two types of DLC drill coatings--non-hydrogenated and 40 at % hydrogen--were used. The aqueous H<sub>2</sub>O-MQL cutting of 319 Al using both types of DLC-coated drills reduced the average drilling torque to 1.65 N-m, compared to dry drilling (4.11 N-m)--a level not unlike

performance under flooded conditions (1.75 N-m). H<sub>2</sub>O-MQL cutting using non-hydrogenated DLC was preferred to hydrogenated DLC, because the latter resulted in less drill flute aluminum adhesion, which required smaller torque and thrust force for drilling.

The studies reviewed above emphasize the benefits of using MQL machining for aluminum alloys, and suggest an almost equal performance to that of the conventional flooded machining. The feasibility of MQL machining of magnesium alloys used for automotive and aerospace castings has yet to be determined. Accordingly, the objective of this work is to assess whether or not the MQL drilling of magnesium alloys is superior to dry drilling, and to consider whether it demonstrates a comparable performance to flooded drilling. An AM60 grade magnesium alloy was selected, due to its growing use in automotive powertrain components. The drilling performance of this alloy was investigated by measuring the torque and thrust force, then providing statistical analyses of the various types of torque and force curves encountered. Temperature increases in the workpiece material were also measured, and results were discussed in light of metallographic analyses consisting of plastic strain estimation and the generation of hardness gradients during drilling, as well as by quantitatively determining the amount and composition of material transferred to the tool.

## **5.2. Experimental procedures and analyses**

### **5.2.1. Workpiece Material and Cutting Tool**

A die cast magnesium AM60 alloy in the form of  $60 \times 10.16 \times 7.62 \text{ cm}^3$  plates was used as the workpiece. The AM60 magnesium contained 6.0 wt.% Al, while the other elements found in the alloy's composition were 0.1 wt. % Si, 0.2 wt.% Zn, 0.3 wt.% Cu, 0.6 wt.% Mn, 0.01 wt.% Ni and the balance Mg. The hardness of the alloy was  $67 \pm 8.0 \text{ kg-mm}^{-2}$  on a Brinell

hardness scale. Quantitative metallographic analyses of the grain size were conducted using approximately 100 grains, and the maximum and minimum dimensions of each grain were measured. The mean value of magnesium grain length, determined in this way, was  $251 \pm 146$   $\mu\text{m}$ . The mean grain width was measured as  $243 \pm 23$   $\mu\text{m}$ , suggesting that the alloy had coarse grains with an equiaxed morphology (aspect ratio of 1.03). Careful metallographic characterization of the microstructure was important because the grain boundaries were used as metallographic markers to determine the plastic strain gradients generated near the holes drilled in the workpiece (see Section 4).

The cutting tools used for the drilling tests were  $6.35 \pm 0.01$  mm-diameter HSS twist drills with a composition of 0.95 wt.% C, 6.00 wt.% W, 5.00 wt.% Mo, 4.20 wt.% Cr, 2.00 wt.% V, and the balance Fe. The average hardness of the HSS steel drills was  $64 \pm 2.50$  HRC (Rockwell Hardness C Scale). The characteristic features of the twist drills have been described previously [5.8]. A single drill was used for each set of experiments, during which 150 holes were drilled.

### **5.2.2. Drilling Tests**

Drilling experiments were carried out using a vertical CNC milling machine equipped with an external MQL system. A schematic diagram of the experimental set-up is shown in Fig. 5.1 (a). During the drilling of each hole, the torque and thrust force generated were measured simultaneously using a non-contact, magneto-static torque sensor consisting of a stator placed about 5 mm away from the rotor and mounted to the base of the drill, as shown in Fig. 5.1 (b). The MQL nozzle and infrared thermometer used to take temperature measurements are also shown in Fig. 5.1 (b).

Dry drilling tests were carried out in an ambient atmosphere. Two types of MQL agents were applied. These were i) a distilled water spray referred to as H<sub>2</sub>O-MQL, and ii) a fatty acid-based MQL agent (Vogel, Germany) referred as FA-MQL, with a density of 0.84 mg/m<sup>3</sup> measured at 25 °C and a viscosity of 75 mm<sup>2</sup>/s also measured at 25 °C. The FA-MQL fluid contained sulphur and phosphorous, as determined by the energy dispersive spectroscopy (EDS) analyses. The MQL agents were applied to the drill tip at a flow rate of 10 ml/h. The optimum MQL supply rate was determined based on the experiments described in Section 5.2.4. Tests were also carried out using flooded drilling conditions, during which a conventional, mineral oil-based MRF was applied at the rate of 30.0 l/h. The density and viscosity of the mineral oil were determined to be 0.78 mg/m<sup>3</sup> and 72 mm<sup>2</sup>/s at 25 °C.

Drilling experiments were conducted using a cutting speed of 2,500 rpm (50 m/min) and a feed rate of 0.25 mm/rev. During each drilling cycle, a fresh 19 mm deep (~3 x drill diameter) blind hole was drilled in the AM60 magnesium alloy workpiece, with a horizontal, center-to-center spacing of 10 mm maintained between adjacent holes. The same distance was maintained between each row.

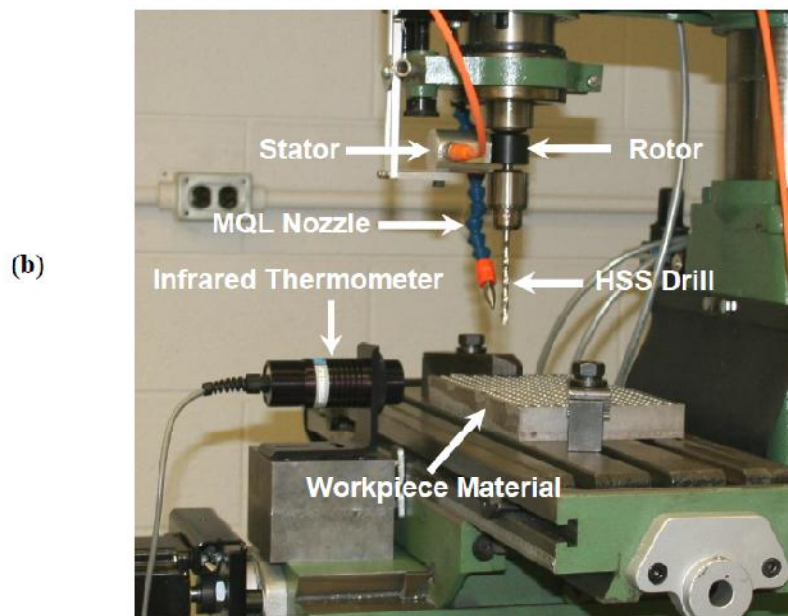
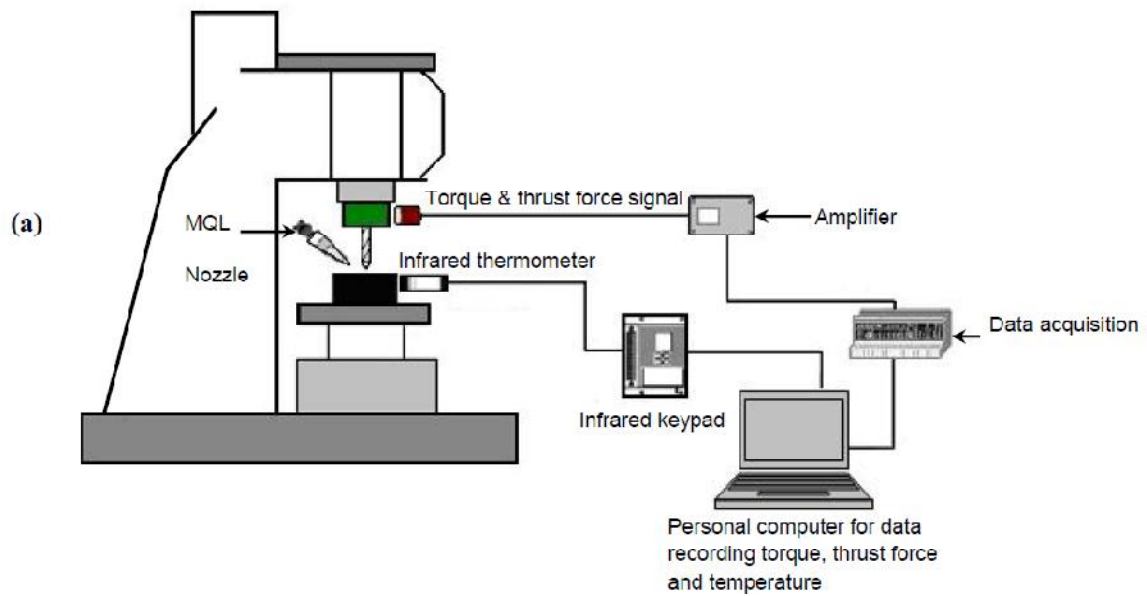


**Figure 5. 1** (a) Schematic diagram showing the experimental set-up, (b) close-up view showing the non-contact torque and thrust force sensor (rotor and stator), MQL nozzle, infrared thermometer and AM60 magnesium alloy workpiece.

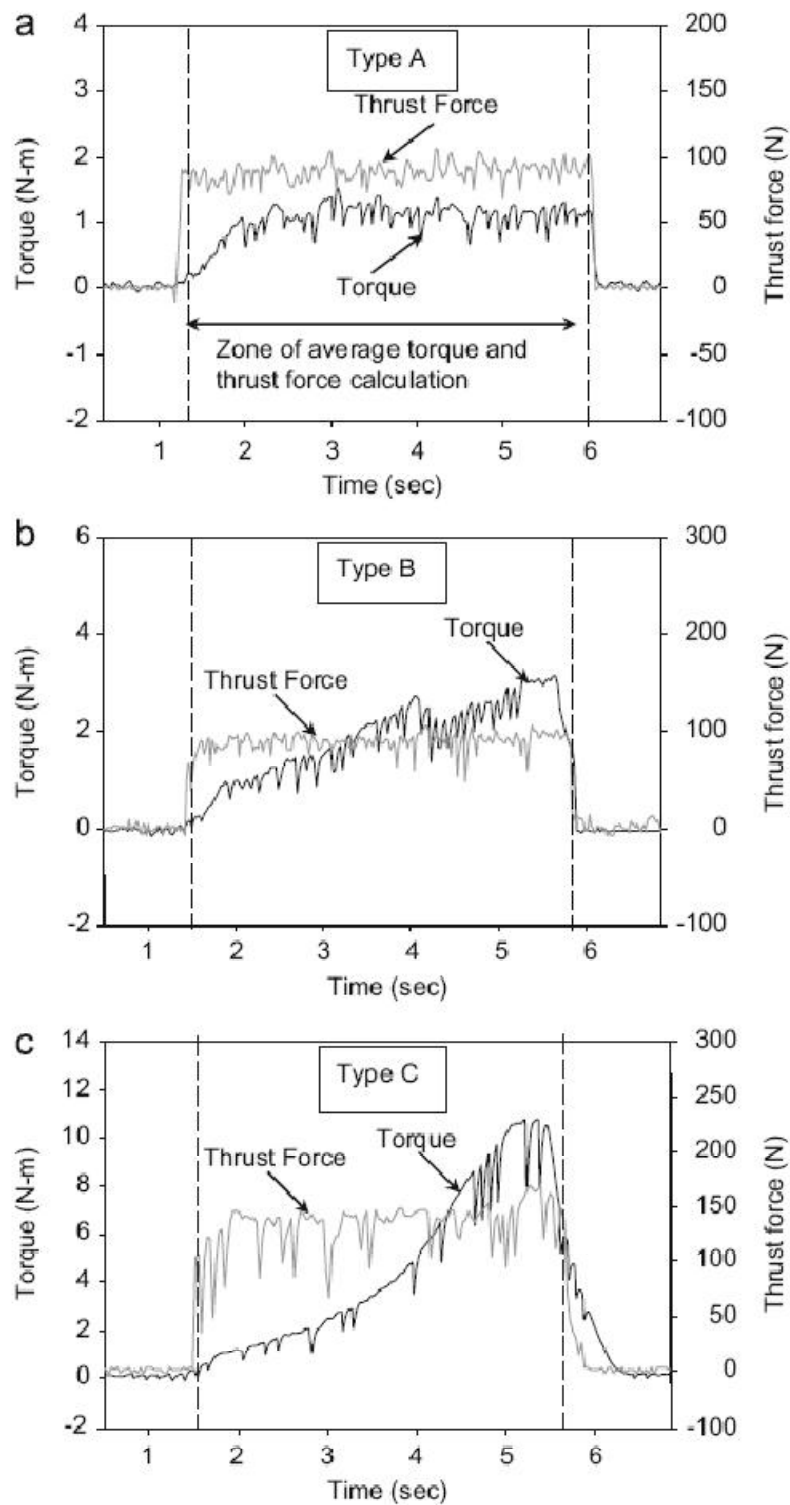


**Figure 5. 2** The three types of torque (black) and thrust force (grey) curves generated during drilling: (a) ‘Type A’: a uniform (steady-state) torque and thrust force curve observed in both H<sub>2</sub>O-MQL and FA-MQL drilling; (b) ‘Type B’: characterized by a continuous increase in torque and (c) ‘Type C’: a torque curve that showed an abrupt increase in torque, indicating chip clogging at the end of the drilling cycle—typically encountered during dry drilling.



Tool life was evaluated by determining the total number of holes drilled before drill failure occurred, as in the case of dry drilling. In other cases, drilling was continued until 150 holes were formed in succession without failure, and the amount of adhesion to the tool tip as well as the hole surface quality were examined for the last hole drilled. In addition, the average torque and thrust force values for each drilled hole were determined. The drilling performances of dry, MQL and flooded conditions were further analysed and compared by providing statistical analyses of the different torque response patterns observed, as described in Section 5.2.3.

### **5.2.3. Average Cutting Torque and Thrust Force**

The average torque (in N-m) and thrust force (in N) generated during the drilling of each individual hole were calculated within the time period corresponding to the drill's first contact with the workpiece surface and its complete retraction at the end of the drilling cycle, as indicated in Fig. 5.2. To calculate the average torque and thrust force, arithmetic means of recorded torque and force signals were determined within this specific time period.

The torque curves generated throughout the drilling experiments showed common profiles that could be classified in three distinct types. The first was a torque curve that exhibited a steady-state drilling behaviour (with values fluctuating around a constant, mean torque value (Fig. 5.2a) is classified as 'Type A'. This was the most common type of torque behaviour encountered during MQL drilling. This behaviour usually corresponds to the smallest amount of magnesium adhesion to the tool.

The second type of torque behaviour was characterized by a continuous increase in torque, as shown in Fig. 5.2 (b), and classified as 'Type B'. Flooded drilling generated the characteristic 'Type B' response more often than the other conditions. During MQL drilling,

with an increase in the number of holes drilled, ‘Type A’ torque behaviour was replaced by ‘Type B’ behaviour, which was attributed to magnesium’s increased tendency to adhere to the drill, requiring higher torque to drive it out of the hole.

‘Type C’ torque behaviour (Fig. 5.2c) was observed during dry drilling. This behaviour was associated with a prominent torque peak at the end of the drilling cycle. The formation of a built-up edge (BUE) accompanying magnesium adhesion to the tool was considered responsible for the increase in maximum torque value to levels higher than those observed in the ‘Type A’ and ‘Type B’ behaviours. The associated torque peak formed during drill retraction was reminiscent of the large ‘torque spikes’ encountered in the dry drilling of cast aluminum alloys [5.20]. Thrust force curves that correspond to each of these torque types are depicted in Figs. 5.2 (a-c), and it is noted that large, instantaneous force fluctuations around the mean characterized the thrust force curves associated with ‘Type C’ behaviour.

#### **5.2.4. Selection of MQL Flow Rate**

Preliminary experiments have shown that there was no significant difference in average torque responses when MQL fluids were supplied at the rates of 10, 20 and 30 ml/h (Fig. 5.3). The average torque increased when an MQL stream lower than 10 ml/h was used, as evident from the 30% increase when a flow of 5 ml/h MQL was employed. The experiments shown in Fig. 5.3 were for FA-MQL drilling, but a similar trend was observed when H<sub>2</sub>O-MQL drilling was used although the average torques for H<sub>2</sub>O-MQL drilling were generally 5-10% higher than those observed during FA-MQL drilling. Consequently, both MQL fluids were applied at the rate of 10 ml/h throughout the rest of the experiments. The differences noted between the drilling responses of different types of MQL agents will be described in detail in Sections 3 and 4.

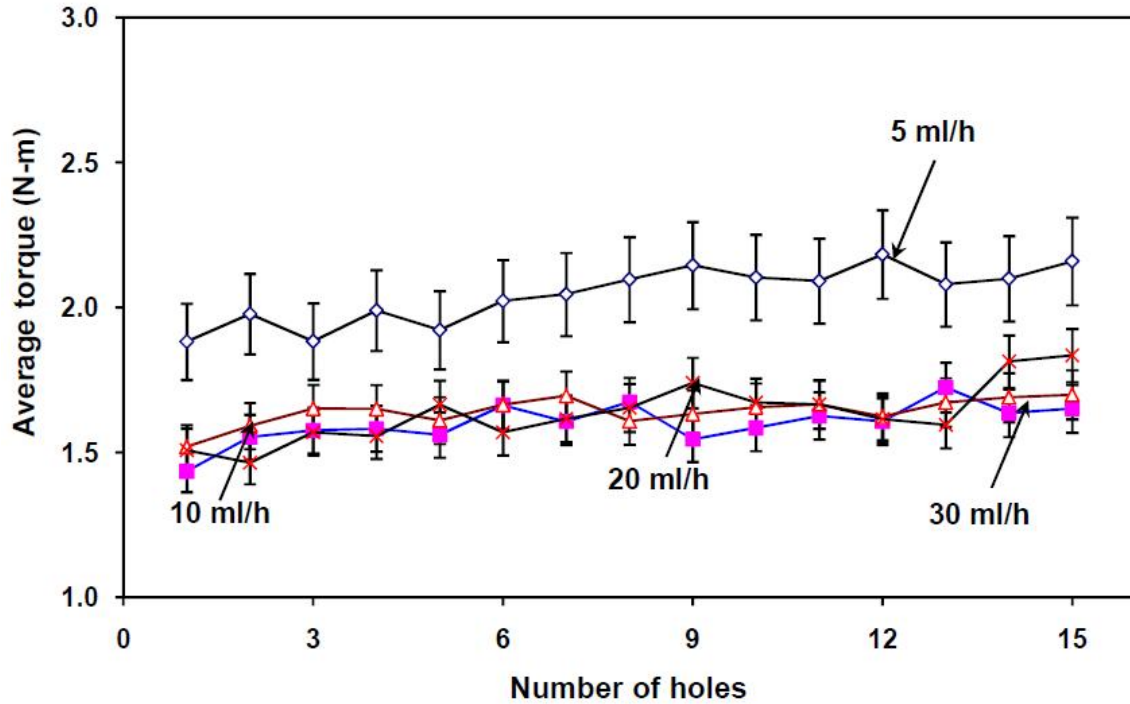


**Figure 5.3** Calibration experiments performed to determine the optimum MQL rate. Average torque variation is plotted against the number of holes for different rates of FA-MQL supply. No significant difference was observed between flow rates of 30, 20 and 10 ml/h, while using a flow rate of 5 ml/h resulted in higher torques. The error bar indicates the standard deviation of torque data for each hole.

### 5.2.5. Temperature Measurements

The temperature generated in the workpiece material during the drilling of the first 25 holes (the first row) was measured using a non-contact, infrared thermometer with its beam placed perpendicular to the long side of the test block, 3 mm away from the hole being drilled (Fig. 5.1b). The infrared thermometer calculates the temperature using the following equation:

$I = \varepsilon \sigma (T^4 - T_a^4)$  where  $I$  is the thermal power in  $W/m^2$ ,  $\sigma$  is the Steffen-Boltzman constant ( $5.67 \times 10^{-8} W/m^2K^4$ ),  $T$  and  $T_a$  are the temperature of the object and ambient surroundings in Kelvin and  $\varepsilon$  is the emissivity of the material. The emissivity of the AM60 magnesium alloy was determined by heating the alloy in a furnace to a known temperature (150 °C) measured by a

thermocouple attached to its surface, then adjusting the emissivity value until the infrared thermometer's reading equalled the known temperature. In this way, the emissivity of AM60 magnesium was determined to be  $\varepsilon = 0.24$ .

### **5.2.6. Metallography of Hole Microstructure, Surface Roughness and Tool Tips**

The last holes drilled before tool failure, and upon completion of the predetermined numbers of test cycles for MQL and flooded conditions, were selected for metallographic analyses. A rectangular section of the workpiece containing this particular hole was metallographically mounted in epoxy resin, and sectioned in the middle of the total hole depth. The sectioned plane parallel to the top surface was then polished with a 0.1  $\mu\text{m}$  diamond suspension. The samples were ultrasonically cleaned in ethanol and etched in Picral solutions containing 5 ml acetic acid, 6 g picric acid, 10 ml  $\text{H}_2\text{O}$  and 100 ml ethanol to analyze the microstructure of the material adjacent to the surface of the drilled hole. The amount of deformation induced by drilling was estimated by studying the displacement of magnesium grain boundaries adjacent to the sectioned hole surface, using an optical microscope. This technique was adopted from sliding wear experiments, for which the sub-surface displacement gradients were determined using the grain boundaries as metallographic markers [5.21, 5.22].

The surface morphologies of drilled holes were observed using a non contact, optical surface profilometer (WYKO NT 1100), which was used in the vertical scanning interferometry (VSI) mode to determine the three-dimensional representation of surface profiles and hence, the average surface roughness,  $R_a$ .

A scanning electron microscope (JEOL 5400 SEM) was used to investigate the amount of magnesium adhesion to the drill flutes, and to study the formation of built-up edges (BUEs). Semi-quantitative chemical analyses of the drill flutes were performed using energy dispersive analyses, EDS (EDAX-Genesis) to determine the composition of the adhered material.

## 5.3. RESULTS AND ANALYSES

### 5.3.1. Torque and Thrust Force Curves

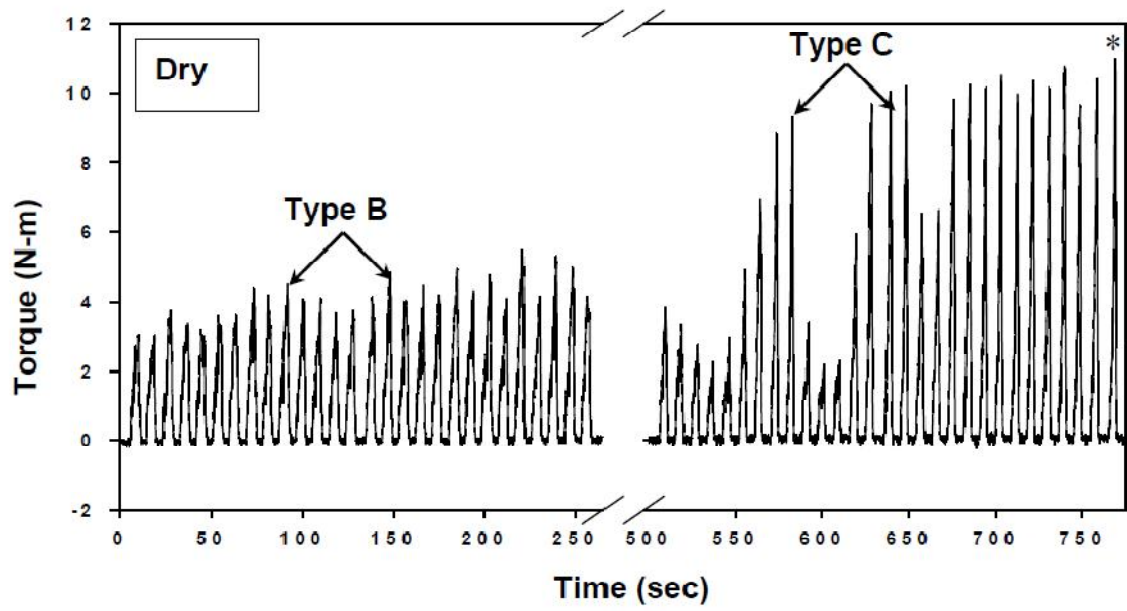
#### 5.3.1.1. Dry Drilling

It quickly became clear during the dry drilling of the magnesium alloy that the tool life was very short--limited to less than eighty holes. The torque responses generated during the course of drilling the individual holes is shown in [Fig. 5.4 \(a\)](#). While drilling the 79<sup>th</sup> hole, the drill seized to the magnesium workpiece and could no longer be retrieved. Hence, this condition is defined as drill failure. A closer inspection of the torque curves generated during the drilling of the first 25 holes and last 25 (54<sup>th</sup>-78<sup>th</sup>) holes ([Fig. 5.4a](#)) revealed that two typical torque patterns were depicted. Initially, the ‘Type B’ torque curve behaviour ([Fig. 5.2b](#)) was commonly observed. As the number of successive holes drilled increased, ‘Type C’ torque behaviour ([Fig. 5.2c](#)) became distinctive, as a result of increasingly frequent hole clogging events at the end of each individual hole drilling cycle. The maximum torque recorded exceeded 8.00 N-m for a large number of holes (exhibiting ‘Type C’ behaviour), and reached 10.85 N-m at the 78<sup>th</sup> hole at the onset of drill failure. Overall, a total of 58 holes exhibited ‘Type C’ torque behaviour, corresponding to 73% of the holes drilled. The data pertaining to statistical analyses of the typical torque types encountered during dry drilling is represented in [Fig. 5.5](#), compared with

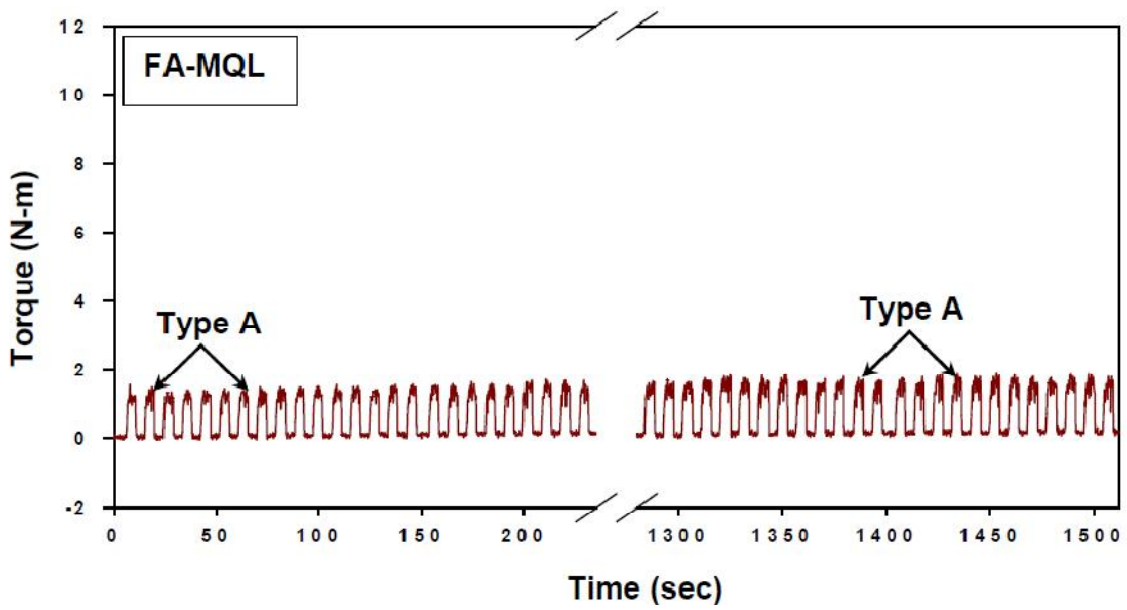
MQL and flooded conditions. Thus, not only the tool life was too brief but dry drilling also required the application of high torques, and was not smooth, with only 2% of the total number of holes drilled revealing 'Type A' behaviour.

Variations in the average torque in relation to the number of dry drilled holes are plotted in [Fig. 5.6](#). The average torque was calculated to be 2.28 N-m for the first hole, and 9.32 N-m for the 78<sup>th</sup> hole, corresponding to a large increase of 309% at the onset of drill failure. The average torque variations were more or less uniform up to the 45<sup>th</sup> hole, corresponding to 'Type B' behaviour, but then a rapid increase ensued. The increase in average torque did not always continue with an increase in the number of holes. For example, a decrease was evident around the 28<sup>th</sup> hole, implying the occasional peeling away of the adhered magnesium chips from the tip of the drill. The factors leading to magnesium adhesion will be discussed in detail in Section 4 by means of metallographic analyses.

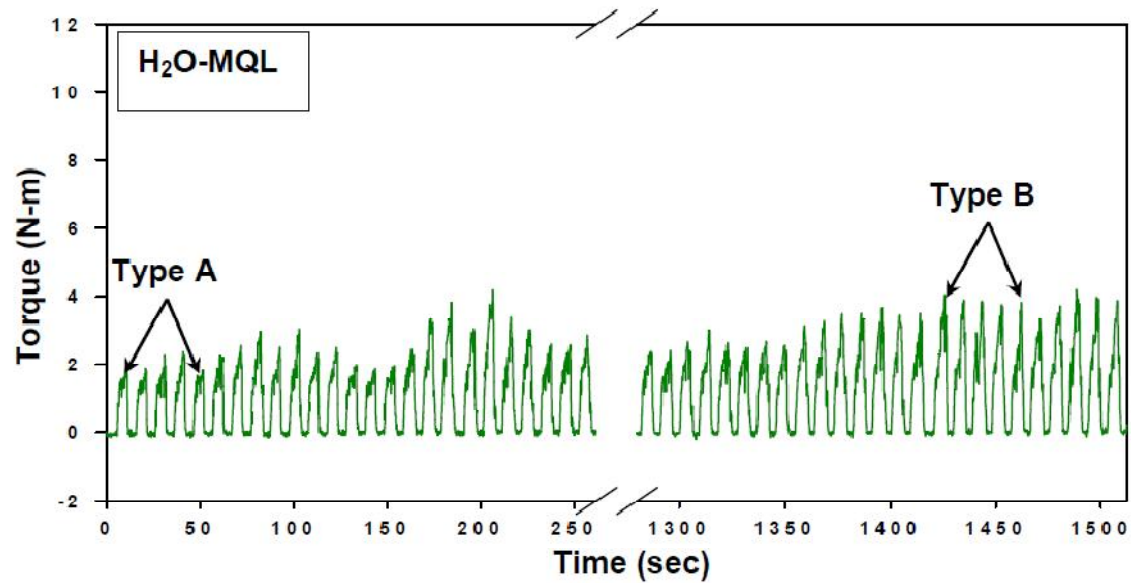
The thrust force was measured simultaneously with the torque response of each hole. The average thrust forces were high, and increased from 102 N for the 1<sup>st</sup> hole, to 165 N at the 78<sup>th</sup> hole, corresponding to a total increase of 62% ([Fig. 5.7](#)).



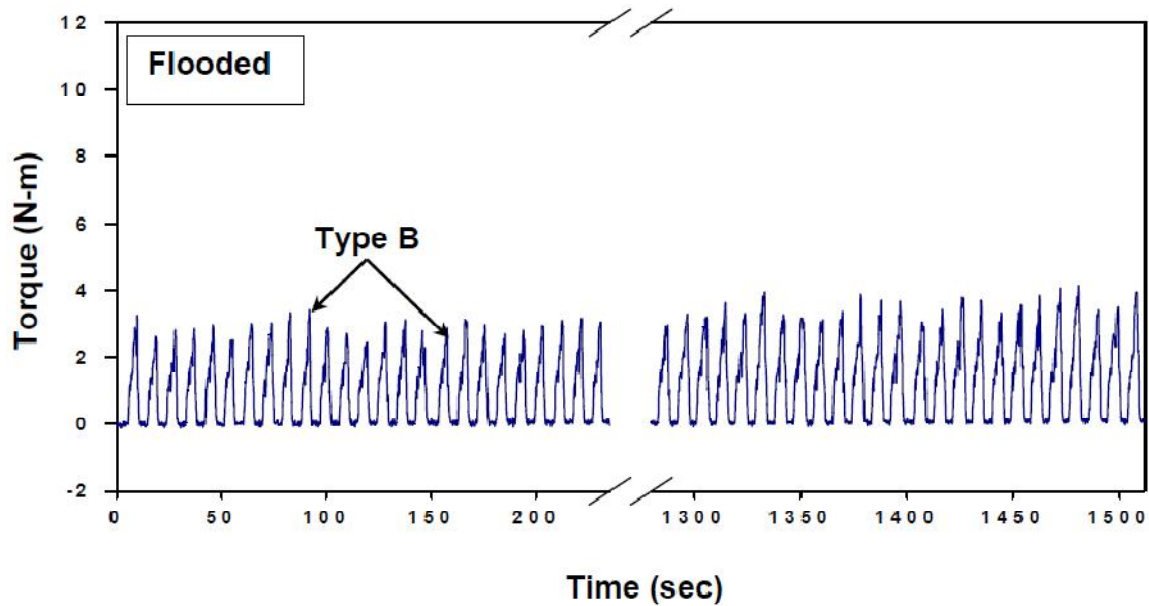
(a)



(b)



(c)



(d)

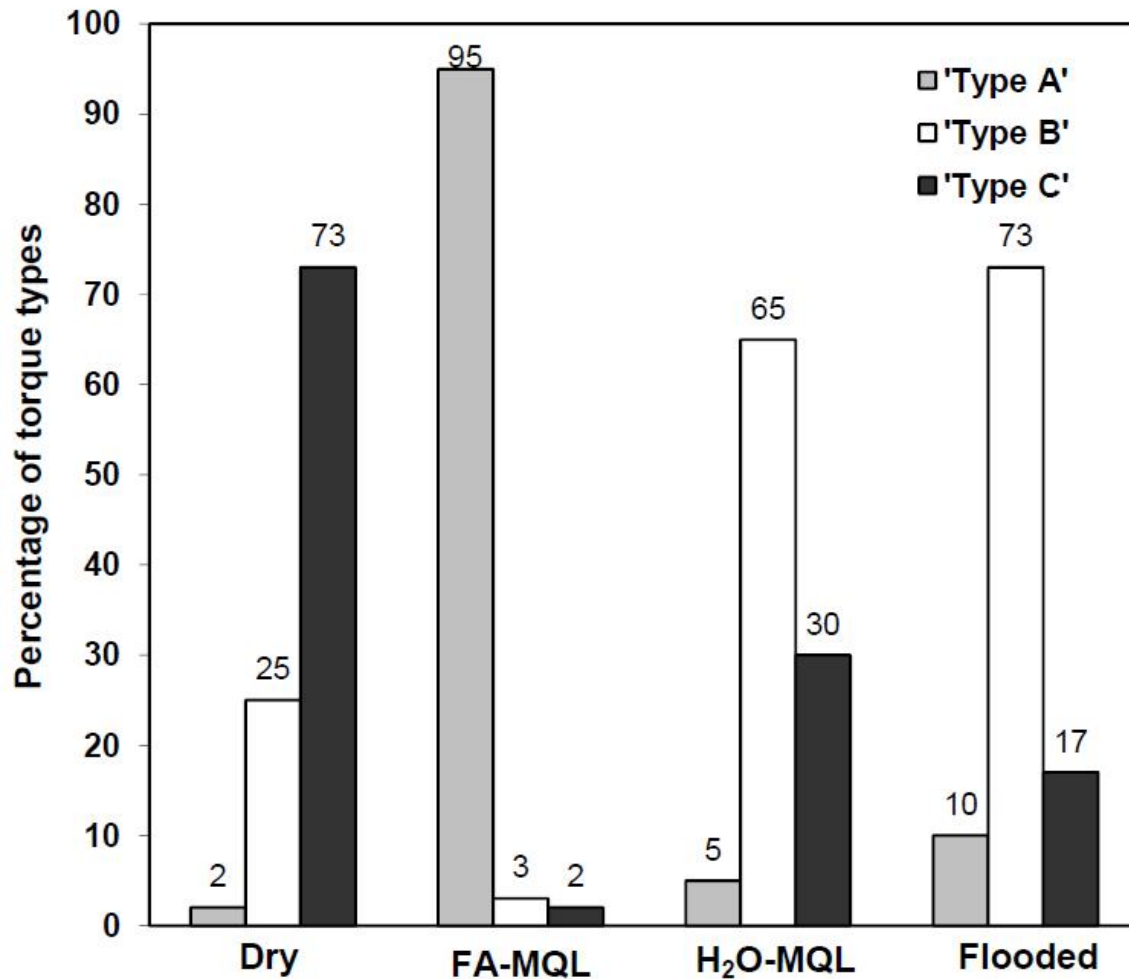
**Figure 5. 4** Variations in the torque profiles generated during the drilling of each hole with the time. (a) Torque data representing the first 25 (1st–25th) and last 25 (54th–78th) holes under dry drilling conditions. The last hole drilled before drill failure is identified by an asterisk. (b) Torque responses for the first 25 and last 25 (126th–150th) holes drilled using FA-MQL.(c) Torque responses for the first 25 and last 25 (126th–150th) holes drilled using H<sub>2</sub>O-MQL. (d)Torque responses for the first 25 and last 25 (126th–150th) holes drilled using flooded conditions.



### 5.3.1.2. MQL Drilling

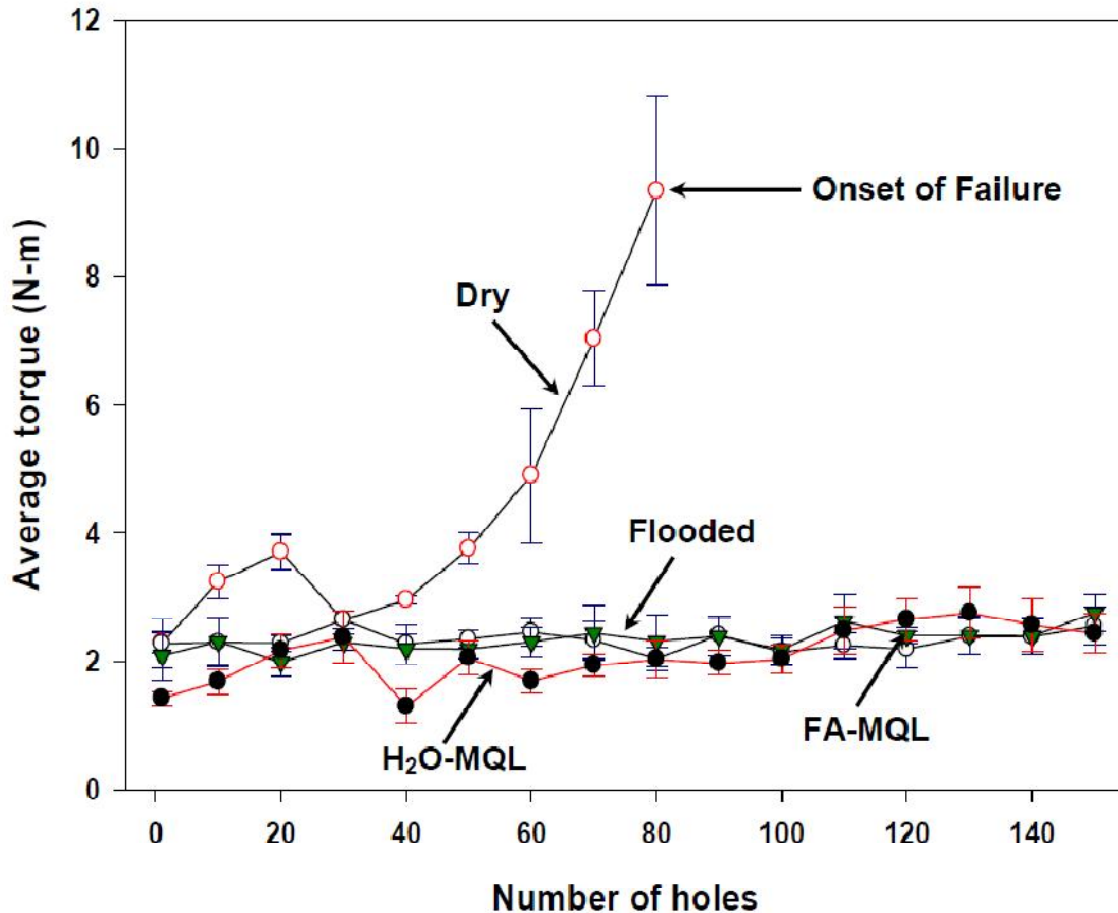
Both types of MQL agents used (FA-MQL and H<sub>2</sub>O-MQL), successfully increased tool life, compared to dry drilling. No drill failure occurred due to magnesium adhesion and seizure during the tests, which consisted of 150 holes. The maximum and average torque and thrust force values were consistently lower than those generated during dry drilling, and remained stable during MQL drilling. There were, however, differences in drilling behaviour, depending on the MQL agent used.

Fig. 5.4 (b) shows the torque responses of the first 25 holes, and the last 25 (126<sup>th</sup>-150<sup>th</sup>) drilled in the magnesium alloy block using the FA-MQL fluid. The maximum torque did not exceed 2.00 N-m during the drilling of any holes, and a uniform torque response consisting predominantly of ‘Type A’ behaviour, characterized the entire drilling range. Specifically, a total of 142 holes (95% of the 150 holes drilled) exhibited ‘Type A’ torque behaviour (Fig. 5.5). H<sub>2</sub>O-MQL drilling also decreased the maximum torque values (Fig. 5.4c), but exhibited differences from FA-MQL when the observed torque patterns were analysed. Specifically, the percentage of holes with ‘Type A’ behaviour was much lower, at 5%. The rest exhibited either ‘Type B’, which corresponded to 65% of total holes, or ‘Type C’ behaviour (Fig. 5.5). The highest torque values observed during H<sub>2</sub>O-MQL drilling were consistently lower than those obtained during dry drilling. This is clear from a comparison of the magnitude of ‘Type B’ curves in Figs. 5.4 (a) and 5.4 (c). On the other hand, Figs. 5.4 (b) and 4 (d) show that the maximum torque values reached during H<sub>2</sub>O-MQL drilling were in the range of 3.50-4.00 N-m--higher than during FA-MQL drilling.



**Figure 5. 5** Percentage of holes that exhibited different types of torque responses (Types A–C) using dry, FA-MQL, H<sub>2</sub>O-MQL and flooded drilling conditions.

Variations between the average torque and the number of holes drilled are plotted in [Fig. 5.6](#), which emphasizes the advantages of MQL drilling over dry drilling. The use of both FA-MQL and H<sub>2</sub>O-MQL drilling resulted in low average torque values that remained within a narrow range of 2.00 - 2.50 N-m. More specifically, the average torque values for FA-MQL drilling varied between 2.27 for the 1<sup>st</sup> hole and 2.55 N-m for the 150<sup>th</sup>. The average torque range for H<sub>2</sub>O-MQL drilling was wider (1.42 N-m in the 1<sup>st</sup> hole and 2.43 in the 150<sup>th</sup> hole).



**Figure 5. 6** A comparison of average torques under dry, FA-MQL, H<sub>2</sub>O-MQL and flooded drilling conditions. The figure shows reduced data for clarity. The error bars indicate the standard deviation of torque data for each hole.

Thrust force variation was uniform throughout FA-MQL drilling, with a maximum thrust force of 125 N. The average thrust force increased only 28% between the 1<sup>st</sup> hole (88 N) and the 150<sup>th</sup> hole (112 N) (Fig. 5.7). The H<sub>2</sub>O-MQL drilling caused an increase in the average thrust within a similar range, from 80 N in the 1<sup>st</sup> hole to 154 N in the 150<sup>th</sup> (Fig. 5.7). These observed differences between the performances of MQL media are discussed in Section 4. Of note was the fact that the performance achieved by MQL drilling using either fluid at a rate of 10 ml/h, was at least equal to that of flooded drilling, which will be described in the next section.

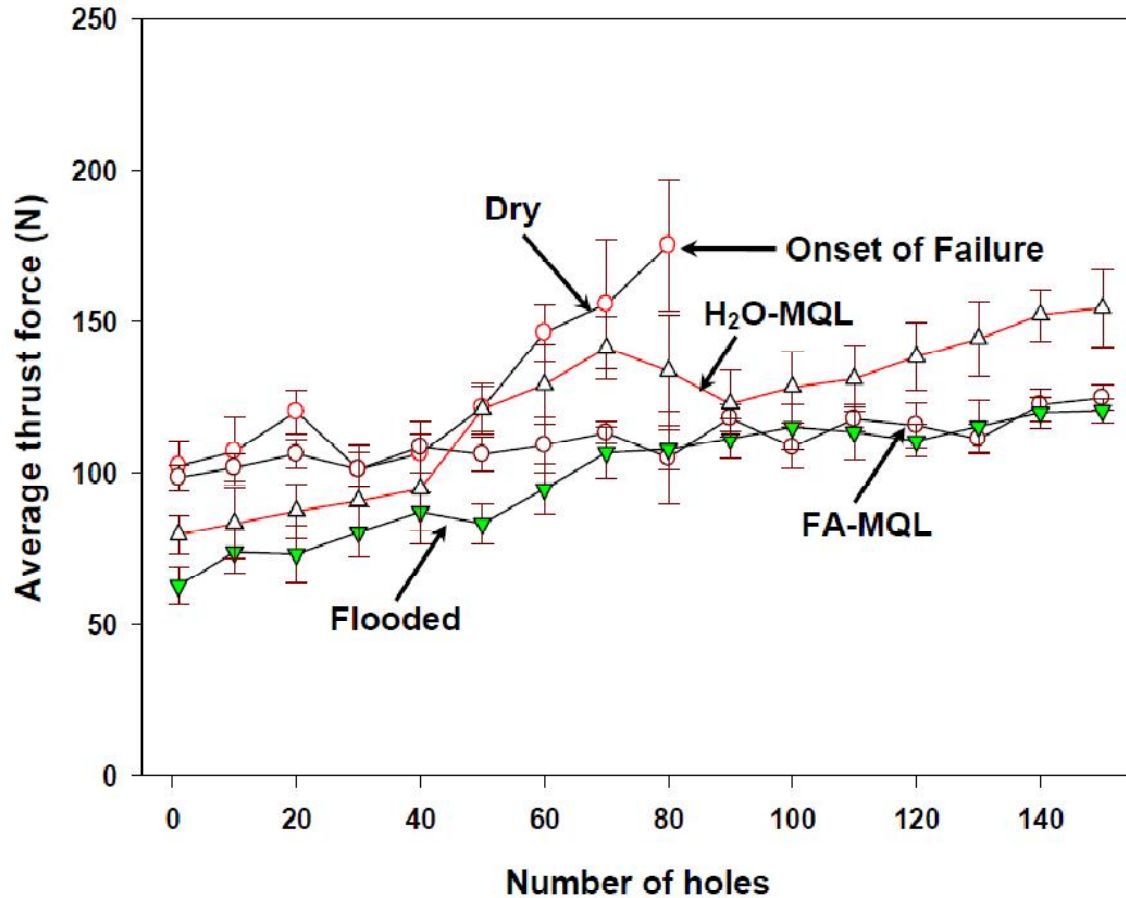


**Figure 5. 7** A comparison of the average thrust forces under dry, FA-MQL, H<sub>2</sub>O-MQL and flooded drilling conditions. The error bars indicate the standard deviation of thrust force data for each hole.

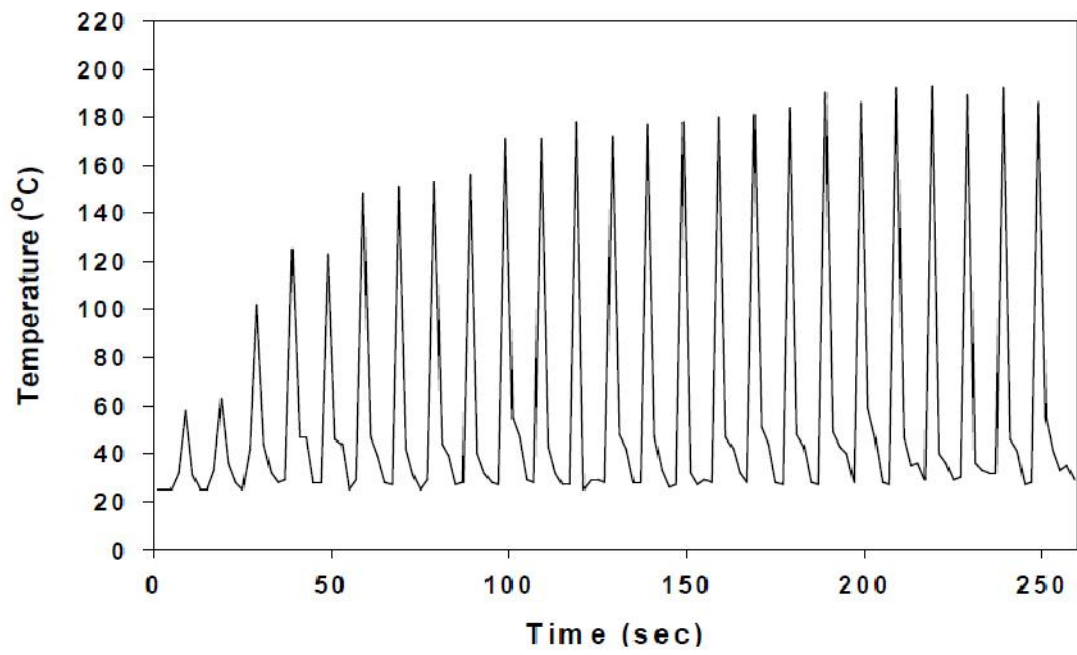
### 5.3.1.3. Flooded Drilling

The experiments and analyses in Sections 3.1.1 and 3.1.2 established that the MQL drilling of magnesium alloys led to considerable improvements when compared to dry drilling. Nonetheless, a comparison with conventional flooded drilling was necessary to assess the extent of the improvements achieved through MQL drilling. For this reason, drilling experiments were conducted using a mineral oil-based metal removal fluid supplied at a rate of 30,0 l/h under the same experimental conditions employed for dry and MQL drilling. The results of these flooded

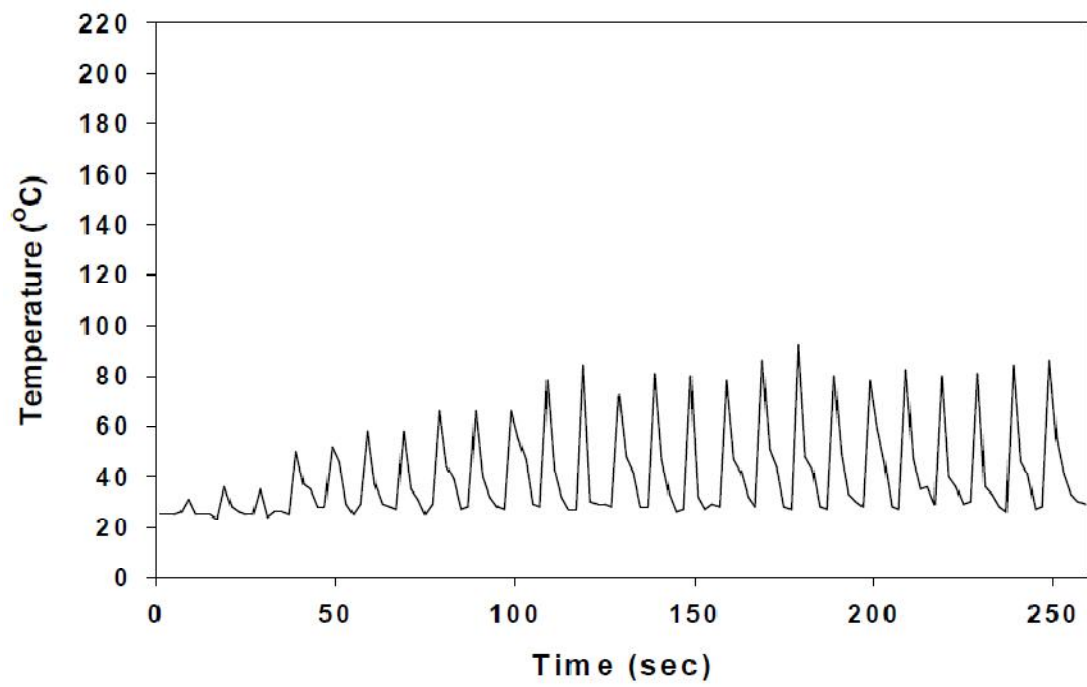
drilling experiments appear in Fig. 5.4 (d). As expected, no indication of tool failure was observed. 10% of the total holes drilled displayed ‘Type A’ torque behaviour, while 73% exhibited ‘Type B’ and 17% ‘Type C’ behaviour (Fig. 5.5). In this respect, flooded drilling performed much like H<sub>2</sub>O-MQL drilling. Compared to FA-MQL, which was primarily characterized by ‘Type A’ torque behaviour, more frequent occurrences of ‘Type B’ and ‘Type C’ curves were noted.

When the average torque behaviour of the holes were considered (Fig. 5.6), no discernible difference between flooded drilling and MQL drilling could be detected. The average torque during flooded drilling increased from 2.08 N-m for the 1<sup>st</sup> hole, to 2.75 N-m for the 150<sup>th</sup> hole. These values were within the same range as the average torque values for MQL drilling. The same comparison holds for the average thrust force values of flooded drilling, for which the initially low force (e.g. 63 N for the 1<sup>st</sup> hole) increased to 121 N on the last hole drilled (Fig. 5.7). While the increase in average thrust force seemed to be faster (92%) compared to MQL drilling when the entire number of holes drilled was considered, it is difficult to statistically argue that a real difference between MQL and flooded drilling exists, based on these average values.

One observation that initially appeared counterintuitive emerged when Figs. 5.4 (b) and 5.4 (d) were compared, indicating that the maximum torque values reached while using FA-MQL were lower than those achieved during flooded drilling. There was a stronger correlation between flooded and H<sub>2</sub>O-MQL drilling in terms of similarities in the peak torque values and torque types statistics (both dominated by Type B). Considering the maximum thrust forces, FA-MQL (125 N) also compared favourably to flooded drilling, for which the highest force was 145 N.



(a)



(b)

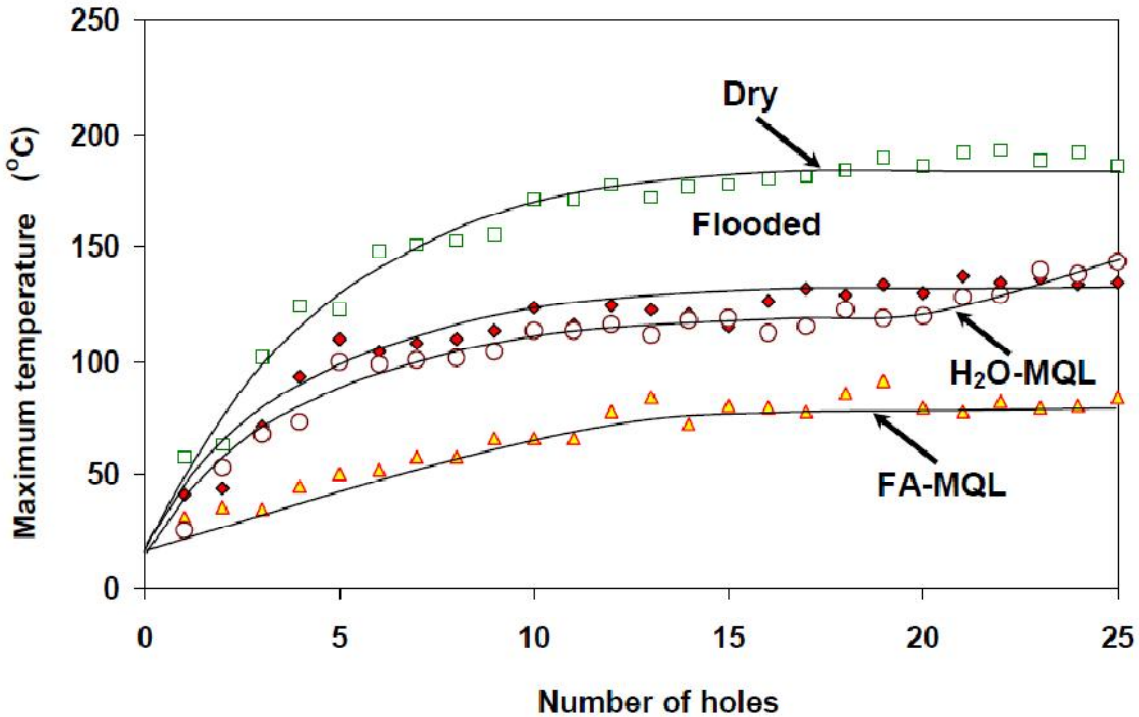


**Figure 5. 8** Workpiece temperature increase with the drilling time for: (a) dry drilling, (b) FA-MQL drilling, and (c) maximum temperature variations for the first 25 holes drilled using dry, FA-MQL, H<sub>2</sub>O-MQL and flooded conditions.

### 5.3.2. Temperature Increases During Drilling

Figs. 5.8 (a) and (b) show the temperature variations generated during the drilling of individual holes within the cutting time for the first 25 holes in dry and FA-MQL drilling. The maximum temperatures reached during the drilling of each hole are plotted in Fig. 5.8 (c) for all drilling conditions used. The temperature during dry drilling increased rapidly above 150 °C after drilling the first 10 holes, although the rate of temperature increase actually slowed down afterwards, but temperatures just under 200 °C were still reached. During the course of FA-MQL drilling, an initial temperature increase to 50 °C was observed, but the maximum temperature did not exceed 86 °C, and a plateau with a mean of about 60 °C was reached after drilling the first 15 holes (Fig. 5.8c). The maximum temperatures were lower compared to the measurements taken

during flooded drilling, which correlated well with the lower torque and thrust forces observed during FA-MQL drilling. For H<sub>2</sub>O-MQL drilling, the temperature profile again consisted of a relatively fast initial increase, followed by a plateau after 10 holes. The mean plateau temperature stabilized at a high temperature of about 100 °C, and reached 134 °C at the end of the test. In summary, the maximum temperatures attained during H<sub>2</sub>O-MQL drilling followed trend that was similar to that of flooded drilling, consistent with the torque and thrust force results obtained for these two conditions.

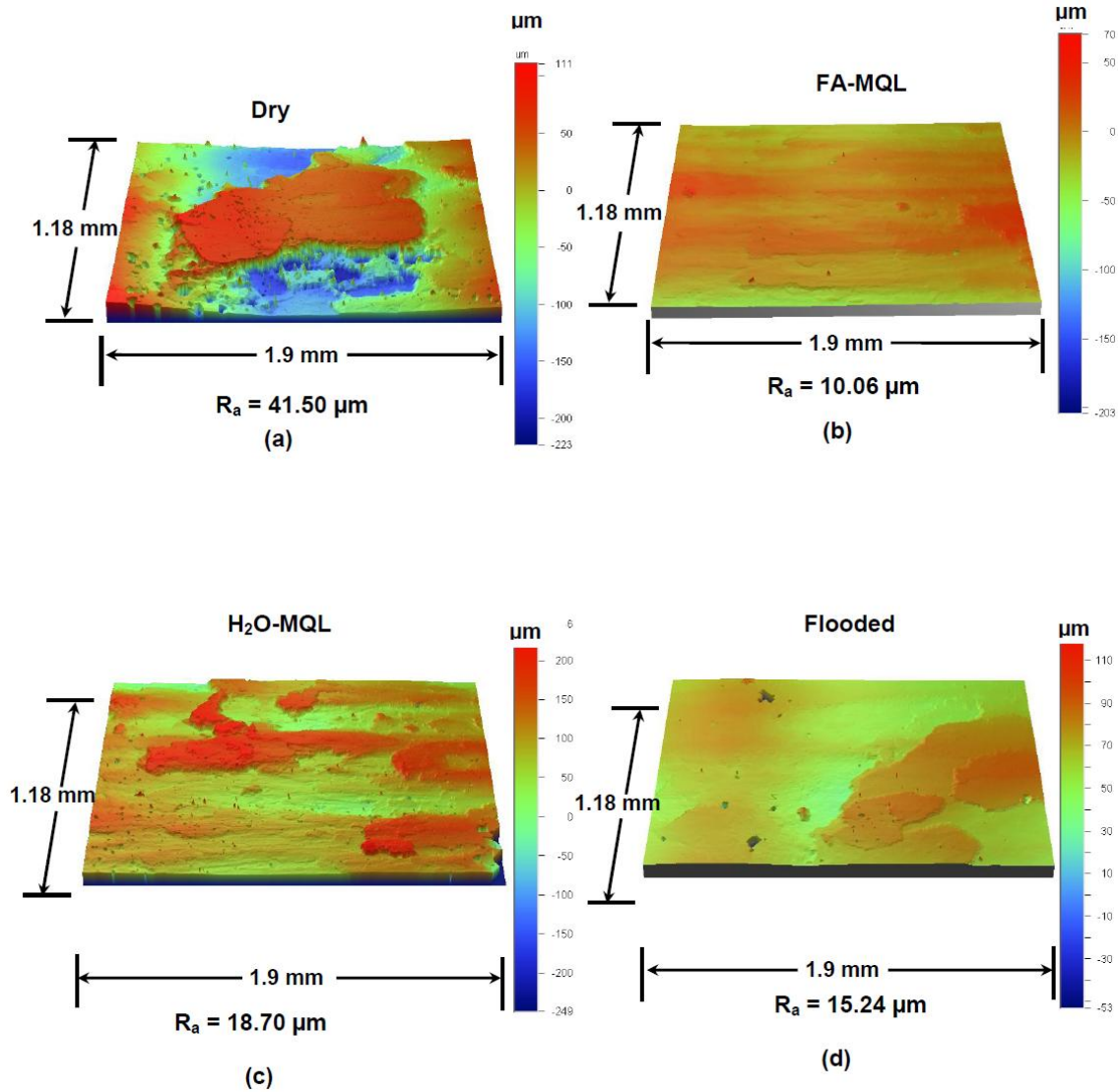
### 5.3.3. Surface Roughness

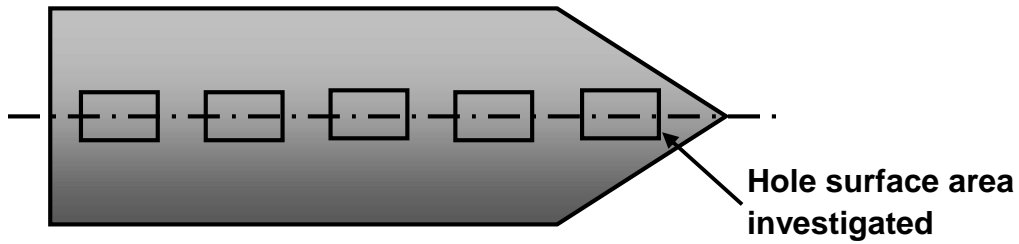
In order to explore the effect of dry and MQL drilling on the finish quality of the hole surface, the morphologies of these surfaces were investigated using a non-contact, optical surface profilometer. Three-dimensional profiles of typical sections of the drilled hole surfaces are shown in Figs. 5.9 (a-d) for all four drilling conditions. Sections were taken from the location shown in Fig. 5.9 (e) on the drilled hole surface. The dry drilled hole surface exhibits the roughest topography (Fig. 5.9a), while other drilling conditions produced smoother surfaces (Figs. 5.9 (b-d)). The average RMS surface roughness ( $R_a$ ) of each hole was obtained from the average  $R_a$  values collected from each of the five locations shown in Fig. 5.9 (e).

The change in surface roughness ( $R_a$ ) values with the number of holes produced in different drilling conditions is plotted in Fig. 5.9 (f). The initial surface roughness after drilling the first hole was  $11.2 \pm 2.2 \mu\text{m}$ , regardless of the drilling conditions. The highest surface roughness value recorded was  $46.8 \pm 25.3 \mu\text{m}$  at the onset of drill failure during dry drilling, where  $R_a$  increased along with the number of holes drilled. The  $R_a$  values were  $11.8 \pm 2.2 \mu\text{m}$ ,  $17.2 \pm 2.4 \mu\text{m}$  and  $12.9 \pm 2.9 \mu\text{m}$  for FA-MQL, H<sub>2</sub>O-MQL and flooded conditions, respectively,

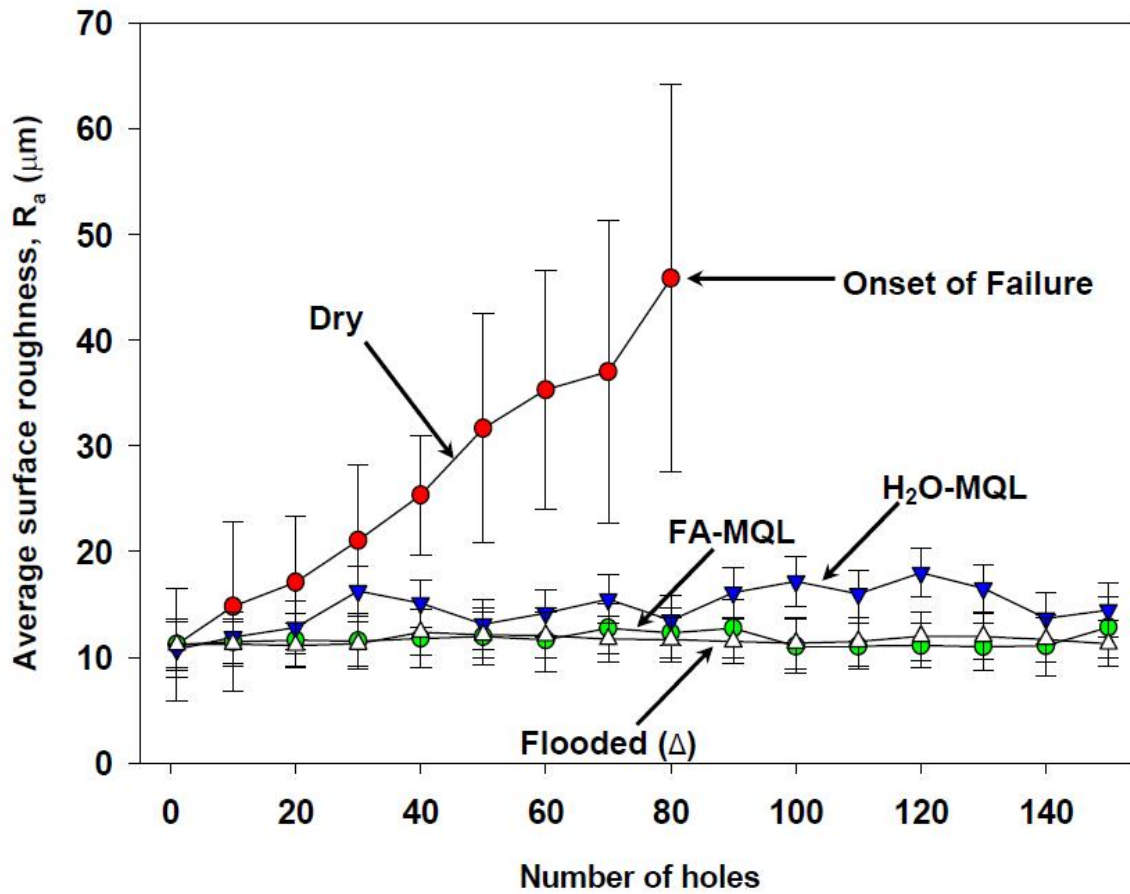


and did not increase with the number of holes drilled. This suggests that they were within the margin of experimental error, although it can be argued that H<sub>2</sub>O-MQL drilling produced slightly rougher surfaces.





(e)



(f)

**Figure 5. 9** Three-dimensional optical surface profilometry images of typical surfaces for (a) dry drilling, (b) FA-MQL drilling, (c) H<sub>2</sub>O-MQL drilling, (d) flooded drilling and (e) schematic diagram of a longitudinal cross-section of a drilled hole, identifying the locations of five areas on hole surface from which the average surface roughness,  $R_a$ , was calculated. The topographical images shown in (a)–(d) are taken from the same location—closest to the drill tip. (f) Comparison of average surface roughness variations under dry, FA-MQL, H<sub>2</sub>O-MQL and flooded drilling conditions.

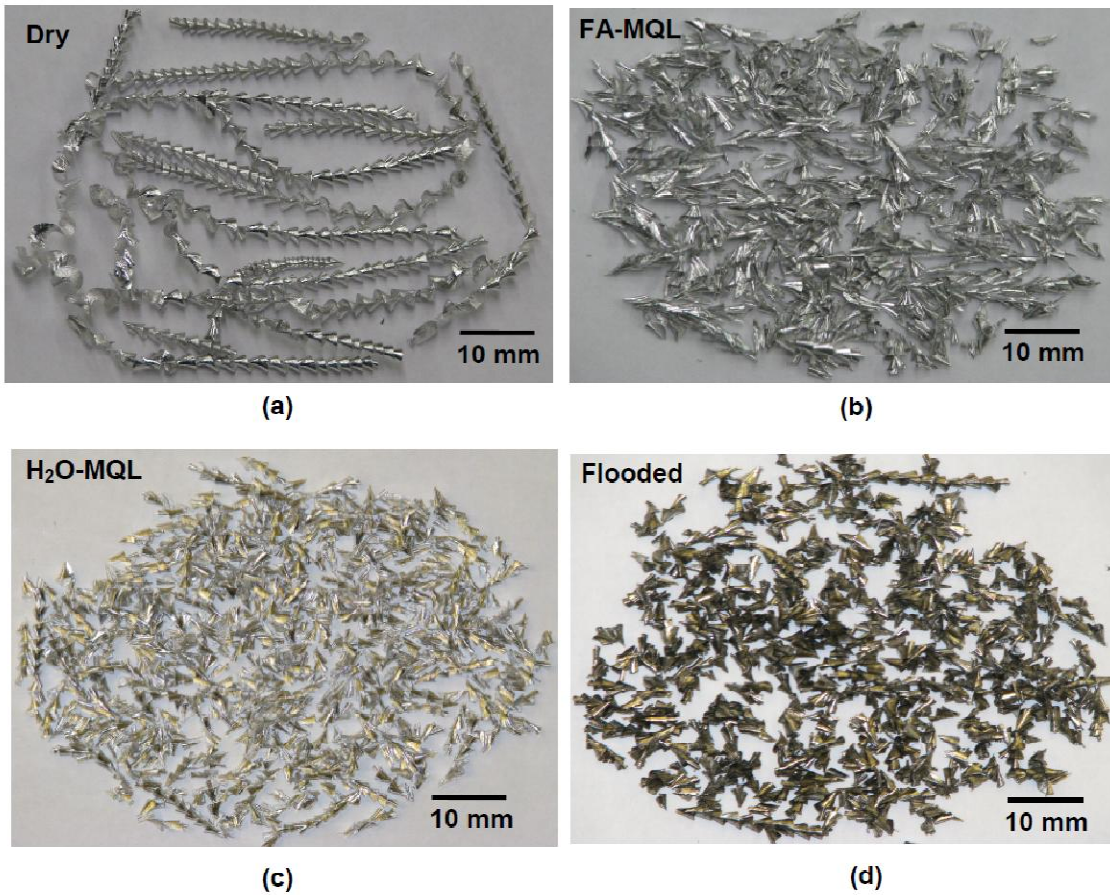


**Figure 5. 10** Low magnification optical images showing typical chip shape for (a) dry, (b) FA-MQL, (c) H<sub>2</sub>O-MQL and (d) flooded conditions.

#### 5.3.4. Chip Morphology

Figs. 5.10 (a) - (d) illustrate the different chip shapes formed under dry, FA-MQL, H<sub>2</sub>O-MQL and flooded conditions. The average chip length was calculated by considering more than 50 chips from each drilling experiment. The longest average chip length was  $246.5 \pm 32.0$  mm, generated under dry drilling conditions. Drilling using FA-MQL ( $6.2 \pm 0.5$  mm), H<sub>2</sub>O-MQL ( $7.2 \pm 1.5$  mm) and flooded conditions ( $7.2 \pm 1.6$  mm) produced short chip segments of almost equal

lengths. The chips were mounted in epoxy resin and polished using standard metallographic procedures before measuring their width. The widest chip of  $86.3 \pm 12.2 \mu\text{m}$  resulted from dry drilling, while the average chip widths were  $13.9 \pm 2.1 \mu\text{m}$  and  $31.5 \pm 6.9 \mu\text{m}$  for FA-MQL and H<sub>2</sub>O-MQL not unlike the chip width of  $26.1 \pm 1.5 \mu\text{m}$  that was produced during flooded drilling.

[Table 5.1](#) provides a general summary of all the results given in the above sections, and lists the average and maximum torque and thrust force responses obtained from the drills operating under different conditions. The maximum temperature reached for each condition is also indicated. The table also summarizes data on average surface roughness and chip dimensions.

## 5.4. Discussion

The observations and analyses presented in Section 3 demonstrate improvements in the performance of MQL drilling over the dry drilling of magnesium alloy AM60, including prolonged tool life as well as a reduction in the average and maximum torque and thrust force values. The results also suggest that MQL drilling can be as effective as flooded drilling. This section discusses the possible mechanisms responsible for the improvements attributed to MQL drilling over dry drilling--through the consideration of the plastic strains and hardness variations of magnesium during the drilling of the holes. Correlations between the temperature increase during drilling and magnesium adhesion to the tool are established using mechanical property changes.

It is well established that the use of MRF's facilitate the removal of chips and provide lubrication to the tool-workpiece interface and decrease the cutting temperature. The generation of high cutting temperatures during the dry drilling of the magnesium alloy soaring to 193 °C

(Fig. 5.8) reduce the hardness of the material and promote the adhesion of softer material to the drills. Consequently, rapid drill failure occurs, as shown in Fig. 5.4 (a). The effects of drilling-induced temperature increase on magnesium's softening behaviour can be understood by examining the hardness profiles of the material in the vicinity of the drilled holes. For this purpose, Vickers microhardness indentations were made on the metallographic cross-sections, in a direction normal to the edge of the drilled surface at 10  $\mu\text{m}$  intervals (Fig. 5.11a). As shown in Fig. 5.11 (b) in a region of 5-90  $\mu\text{m}$  below the dry drilled hole surface magnesium's hardness decreased by 30% to about  $35 \pm 2 \text{ kg}\cdot\text{mm}^{-2}$  when compared to the alloy's bulk hardness of  $50 \pm 6 \text{ kg}\cdot\text{mm}^{-2}$ . Contrary to the dry drilled material, a 62% increase to  $81 \pm 4 \text{ kg}\cdot\text{mm}^{-2}$  occurred during FA-MQL drilling and a 34% increase to  $67 \pm 3 \text{ kg}\cdot\text{mm}^{-2}$  was noted during flooded drilling. As shown in Fig. 5.8 temperatures generated during the MQL and flooded drilling of magnesium were lower than those generated during dry drilling. Thus, for MQL and flooded drilling any temperature related softening effect was compensated by the strain hardening of the material layers adjacent to the drilled holes. To confirm the extent of material's hardening in these cases, the plastic strains produced near the hole surfaces were determined. Using the boundaries between two etched magnesium grains adjacent to the hole surface as metallographic markers (see Section 2.6), the grain boundary displacement that occurred to accommodate the plastic strains induced during drilling were estimated as shown in Figs. 5.12 (a and b). The local shear strain  $\gamma$  at a given distance from the drilled surface was estimated from the deformation angle  $\theta$  between the tangent to a grain boundary and a surface normal to the drilled surface using  $\gamma = \tan \theta$  [5.21, 5.22]. The largest shear strain  $\gamma$  was attained near the hole surface (Fig. 5.12c) and was as high as 11.0 in case of dry drilling. The maximum shear strains reached in magnesium were much smaller for MQL and flooded drilling (i.e., 0.9, for FA-MQL, 1.8 for

H<sub>2</sub>O-MQL and 1.5 for flooded drilling), confirming that the magnesium drilled using MQL and flooded conditions was less susceptible to shear deformation.

The softened magnesium that experienced severe plastic deformation during dry drilling spontaneously transferred to the drill tip, and adhered to the drill flutes as shown in Fig. 5.13 (a). The adhered magnesium layer covered the entire drill tip surface, and was as thick as 50 mm in height at the cutting edge. Hence, a prominent BUE was formed, which altered the geometry of the drill by increasing its diameter, prompting the feed rate to increase [5.23, 5.24]. Accordingly, the torque and cutting forces both increased during dry drilling in agreement with the data presented in Figs. (5.6) and (5.7). Additionally, the transferred magnesium provided an obstacle to the ejection of the chips, causing ‘Type C’ torque behaviour--characterized by an abrupt increase in torque at the end of each drilling cycle--to dominate, as shown in Fig. 5.4 (a). No notable BUE formation was observed after drilling using FA-MQL, although some spots on the drill flute were identified as displaying transferred magnesium (Fig. 5.13b). A small BUE was observed in H<sub>2</sub>O-MQL (Fig. 5.13c) and flooded conditions as well (Fig. 5.13d). The percentages of area covered by magnesium were estimated at  $13 \pm 6$  % for H<sub>2</sub>O-MQL and  $14 \pm 11$  % for flooded drilling (Fig. 5.13e), making chip evacuation through the drill flutes easier compared to dry drilling. The lowest magnesium coverage of the drill was under FA-MQL conditions, at  $8 \pm 4$ %, which correlates well with the most stable torque behaviour observed in these conditions--characterized predominantly by ‘Type A’ behaviour as shown in Fig 5.4b.

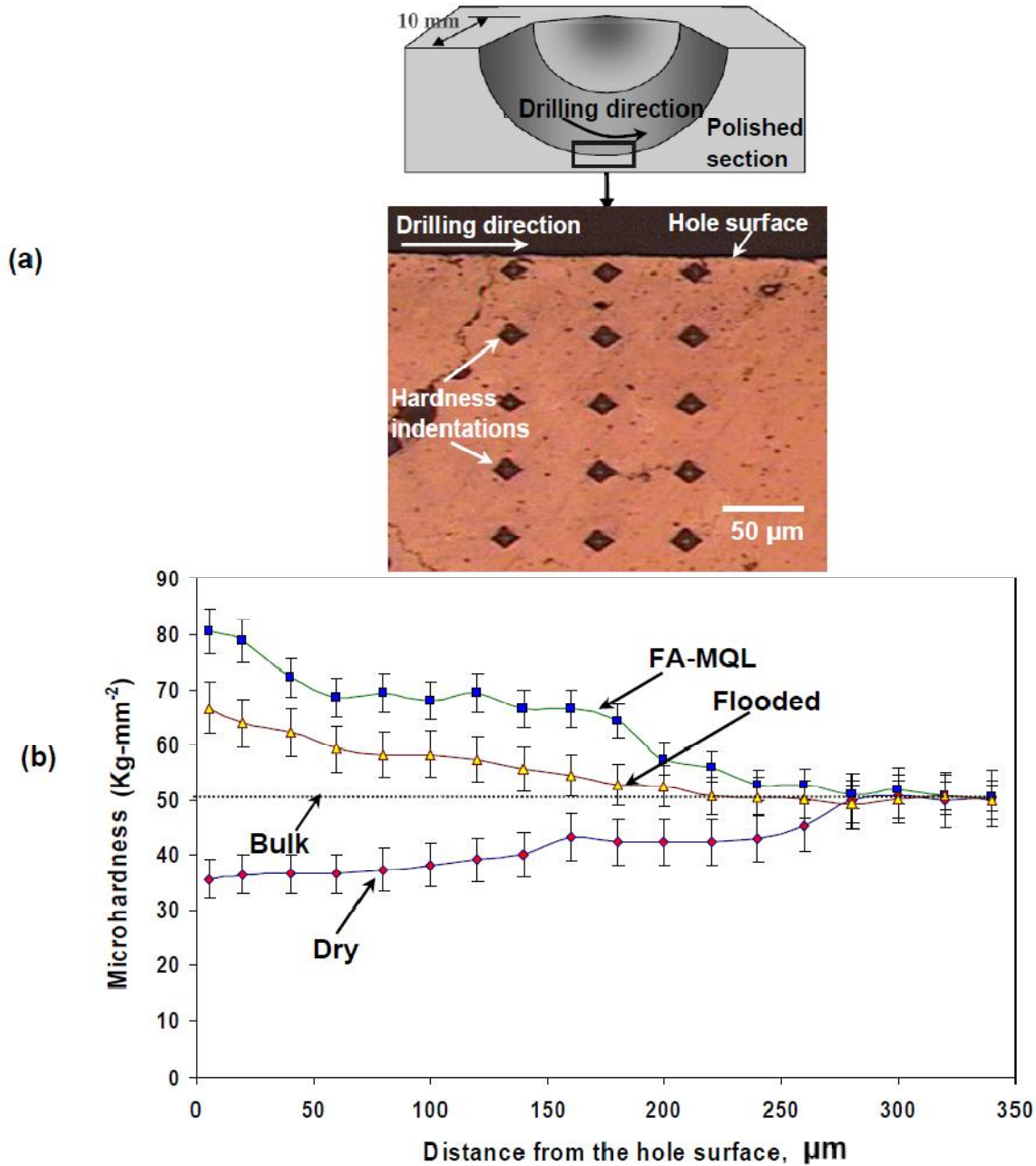


**Figure 5. 11** (a) Schematic diagram of a quarter section of a drilled hole showing the plane (mid-section of the hole parallel to the workpiece surface) where microhardness indentations were made, and an optical micrograph of this section with the Vickers indentation impressions. Indentations were made in a direction normal to the hole surface, and to a depth of approximately 300  $\mu\text{m}$  below the surface, where the hardness of the bulk material (unaffected by the heat) could be attained. Measurements were taken three times at each depth. (b) Average hole sub-surface hardness variations with increasing the depth from the hole surface for dry, FA-MQL and flooded conditions.

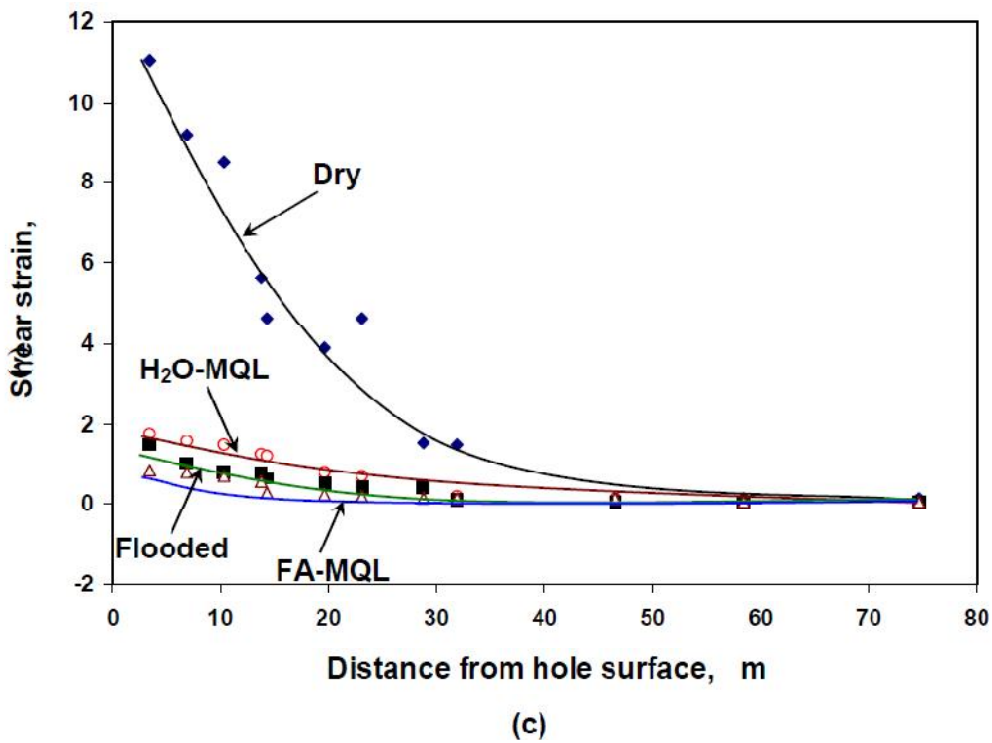
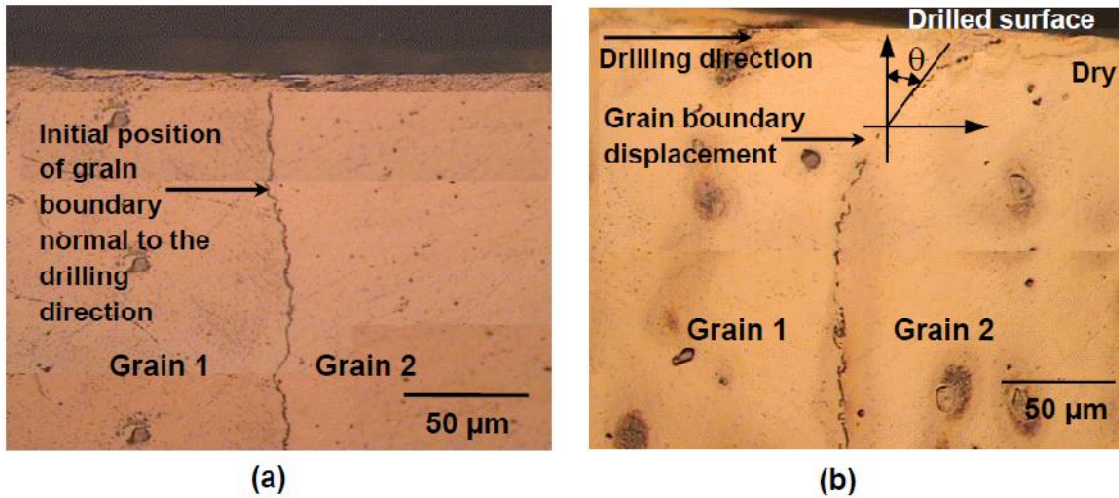


**Figure 5. 12** Cross-sectional optical micrographs showing (a) the initial position of a grain boundary between two adjacent grains. Grain boundaries were assumed to be perpendicular to the hole surface. (b) The displacement of the grain boundary after drilling and a schematic diagram showing the determination of deformation angle  $\theta$  from the slope of the deformed grain boundary. (c) Variation of the shear strain with depth for dry, FA-MQL, H<sub>2</sub>O-MQL and flooded drilling conditions.



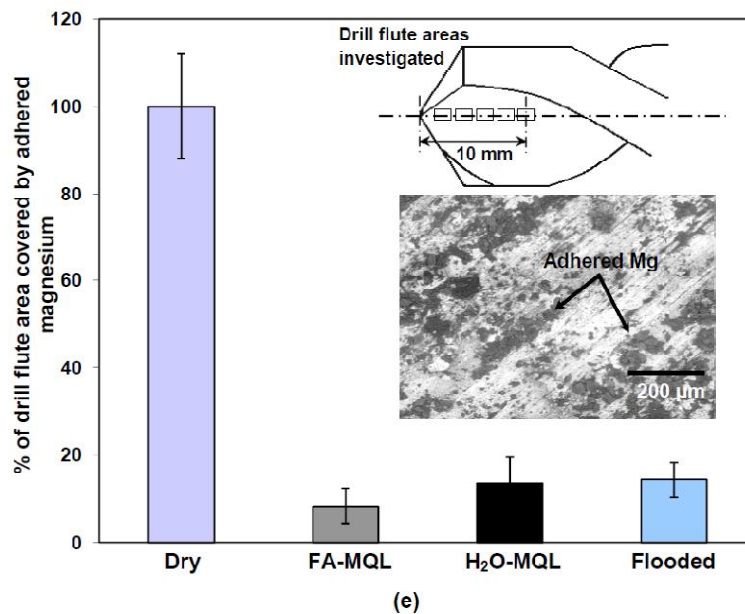
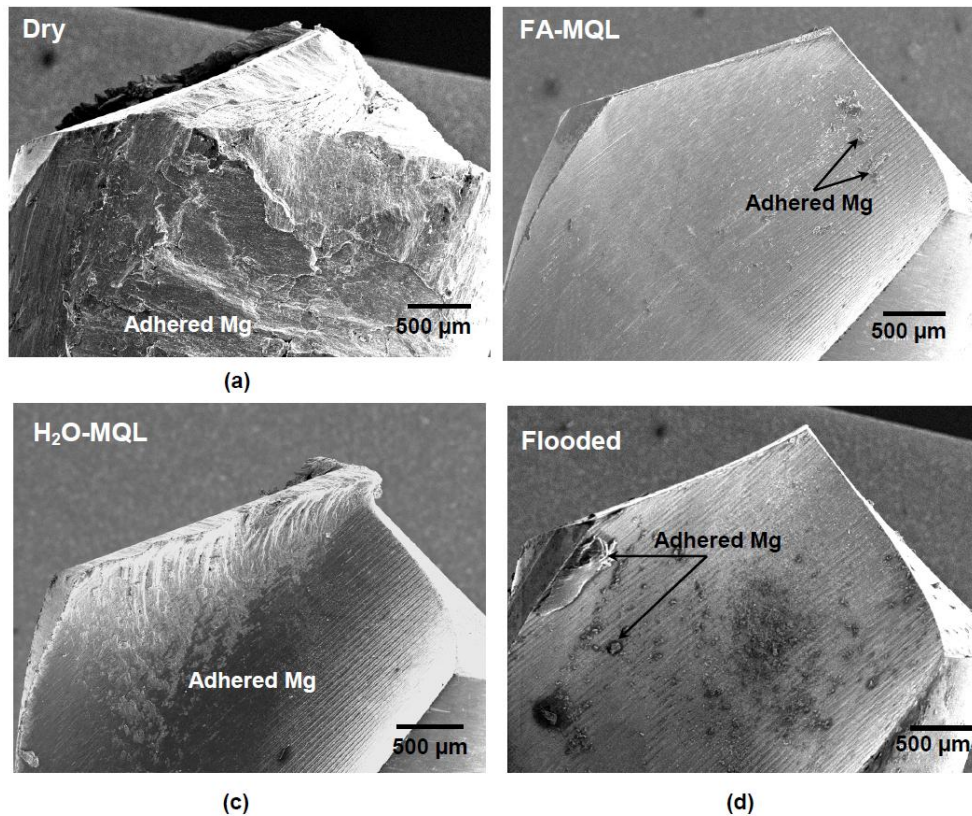


**Figure 5. 13** SEM secondary electron images showing the adhesion of magnesium to the drill flutes: (a) dry, (b) FA-MQL, (c) H<sub>2</sub>O-MQL and (d) flooded conditions. (e) Percentage of the drill flute surface area covered by adhered magnesium for all drilling conditions. The locations of the SEM images taken on the drill flute and a back-scattered electron image of a section of the drill flute tested under dry conditions are also shown. The reported values are the averages of values obtained from five images of each drill.

Lastly, the differences between the effectiveness of the two MQL agents used warrant more exploration. The results presented in Section 3 suggested that H<sub>2</sub>O-MQL drilling was as efficient as flooded drilling. The use of water in large quantities as MRF has traditionally been avoided during the flooded drilling of magnesium because magnesium chips can react with water and form Mg(OH)<sub>2</sub> and free H<sub>2</sub> [5.25]. The use of small quantities of water in MQL may not be unfavourable, but long term drilling performance assessments are needed to confirm this. It was noted that the use of FA-MQL agent led to several key improvements compared to H<sub>2</sub>O-MQL (and flooded) drilling. The electron diffraction spectroscopy (EDS) analyses performed on the drills examined after the tests (Figs. 5.14 a-c) provided evidence of the existence of elements like phosphorous and sulphur on the drill surfaces used for drilling under FA-MQL conditions (Fig. 5.14a) but not on the drills tested under other conditions (Figs. 5.14 b, c). These elements are associated with the compounds known as ‘extreme pressure additives’ [5.16, 5.24] in the surface layers that are used to prevent metal-to-metal contacts in tribological applications [5.26, 5.27]. It was suggested that [5.28] the layers can be formed by the physical adsorption of the additives within a temperature range not exceeding 120°C, which is compatible with the current experiments. The effectiveness of the FA-MQL drilling may thus be attributed to the formation of protective layers on the drill surfaces, which reduces magnesium’s adhesion tendency to the tool and therefore resulting in the lowest drilling temperatures among the conditions considered as well as stable torque and thrust force patterns.

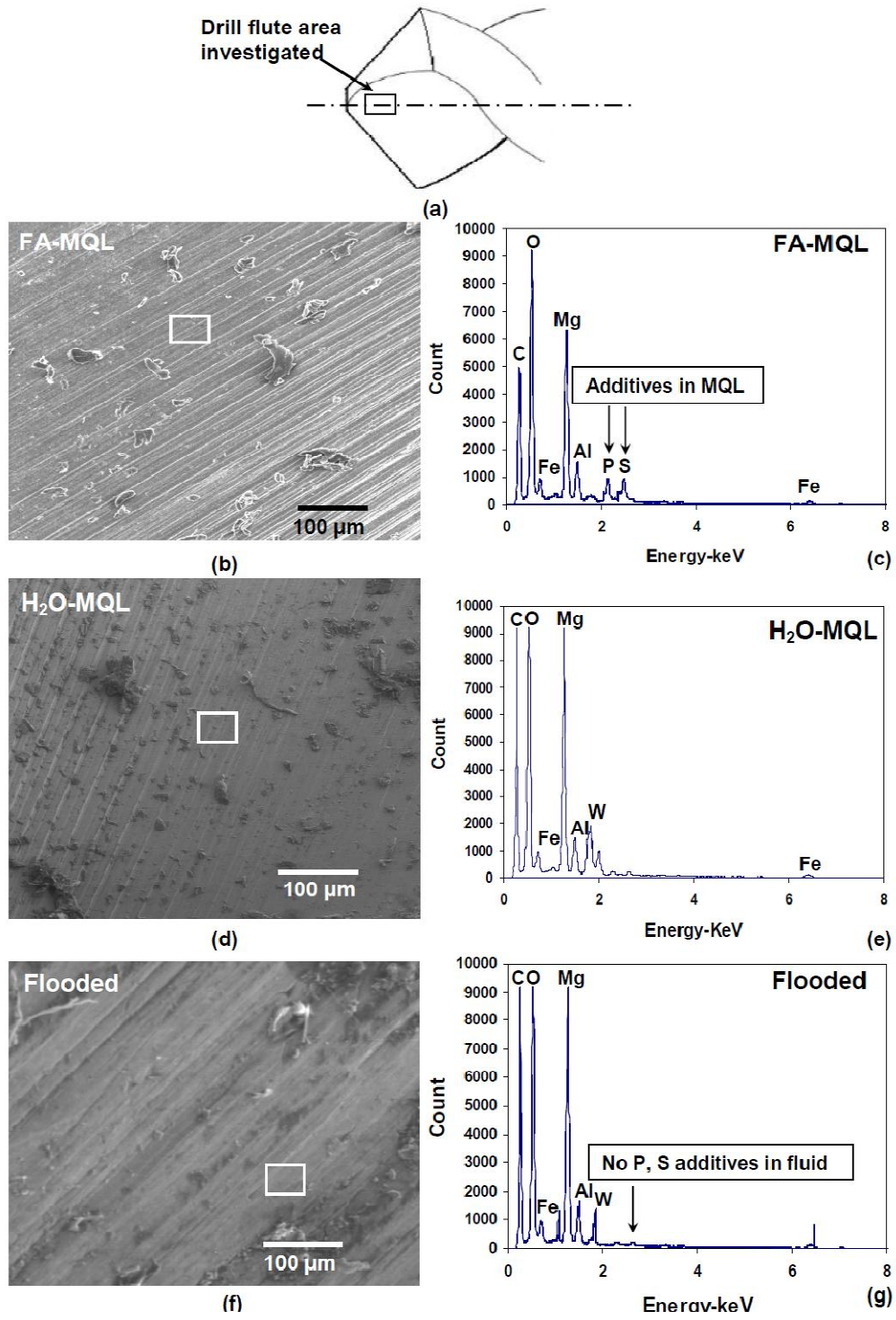


**Figure 5. 14** (a) Schematic representation of drill flute showing the area on which EDS compositional analyses were performed. (b) SEM image of the drill flute in FA-MQL conditions. (c) EDS spectra of insert in plate (b). (d) SEM image of the drill flute in H<sub>2</sub>O-MQL conditions. (e) EDS spectra of insert in plate (d). (f) SEM image of the drill flute in flooded conditions. (g) EDS spectra of insert in plate (f).

## 5.5. Conclusions

Experiments and analyses were conducted to assess the efficiency of MQL drilling when applied to a lightweight AM60 magnesium alloy, tested using both aqueous (H<sub>2</sub>O-MQL) and fatty acid-based (FA-MQL) fluids. Improvements over dry drilling were noted, while flooded drilling was used to benchmark the MQL drilling performance. The following conclusions can be drawn from the results presented:

(4) Dry drilling an AM60 magnesium alloy using a HSS drill led to abrupt drill failure before drilling eighty holes. Dry drilling increased the temperature of the material adjacent to the hole surface, and caused to a notable decrease in the hardness of the material and generation of large plastic strains in the vicinity of the hole. The transfer of soft magnesium to the tool tip resulted in the formation of a prominent BUE and consequently high torques and thrust forces were generated.

(5) The cutting performance of the MQL revealed significant improvements over dry drilling. Uniform torque and thrust force responses were observed in both H<sub>2</sub>O-MQL and FA-MQL drilling, with no abrupt increase in torque during each drilling cycle. Small, discontinuous chips formed while drilling using either H<sub>2</sub>O-MQL or FA-MQL. The attainment of a smooth hole surface was an additional benefit of MQL drilling. In these respects, the MQL drilling performance matched that of flooded drilling.

(6) The maximum temperature generated in the workpiece during MQL drilling did not exceed that produced during flooded drilling. Consequently, there was no softening of the material around the holes during the course of drilling. In turn, the amount of magnesium transferred to the drill flutes and BUE formation at the drill's cutting edge were both significantly reduced, resulting in lower torque and thrust force requirements for drilling.

## List of references

- [5.1] H.J. Morales, Magnesium, machinability and safety, SAE Technical paper No.800418, SAE, Detroit, Michigan, 1980.
- [5.2] Occupational exposure to metalworking fluids: a criteria for a recommended standard, US National Institute for Occupational Safety and Health Publication, 98-102 (1998) 1, 2, 44, 143.
- [5.3] G. Byrne, D. Dornfeld, B. Denkena, Advancing cutting technology, Annals of the CIRP 52 (2003) 483-507.
- [5.4] S. Kalidas, R.E. Devor, S.G. Kapoor, Experimental investigation of the effect of drill coatings on hole quality under dry and wet drilling conditions, Surface and Coatings Technology 148 (2001) 117 – 128.
- [5.5] M. Lahres, P. Muller-Hummel, O. Doerfel, Applicability of different hard coatings in dry milling of aluminum alloys, Surface and Coatings Technology 91 (1997) 116 – 121.
- [5.6] M. Nouari, G. List, F. Girot, D. Coupard, Experimental analysis and optimisation of tool wear in dry machining of aluminium alloys, Wear 255 (2003) 1359–1368.
- [5.7] J.M. Dasch, C.C. Anga, C.A. Wong, Y.-T. Cheng, A.M. Weiner, L.C. Lev, E. Konca, A comparison of five categories of carbon-based tool coatings for dry drilling of aluminum, Surface and Coatings Technology 200 (2006) 2970 – 2977.
- [5.8] S. Bhowmick, A.T. Alpas, The performance of hydrogenated and non-hydrogenated diamond-like carbon tool coatings during the dry drilling of 319 Al, International Journal of Machine Tools and Manufacture 48 (2008) 802–814.
- [5.9] A.A. Bezerra, A.R. Machado, A.M. Souza Jr., E.O. Ezugwu, Effects of machining parameters when reaming aluminum-silicon (SAE 322) alloy, Journal of Materials Processing Technology 112 (2001) 185-198.
- [5.10] M.S. Carrilero, R. Bienvenido, J.M. Sanchez, M. Alvarez, A. Gonzalez, M. Marcos, A SEM and EDS insight in to the BUL and BUE differences in the turning processes of AA2024 Al-Cu alloy, International Journal of Machine Tools and Manufacture 42 (2002) 215–220.

- [5.11] E. Gariboldi, Drilling a magnesium alloy using PVD coated twist drills, *Journal of Materials Processing Technology* 134 (2003) 287-295.
- [5.12] H.K. Tonshoff, J. Winkler, The influence of tool coatings in machining of magnesium, *Surface and Coatings Technology* 94-95 (1997) 610-616.
- [5.13] K. Weinert, I. Inasaki, J.W. Sutherland, T. Wakabayashi, Dry machining and minimum quantity lubrication, *CIRP Annals—Manufacturing Technology* 53 (2004) 511-537.
- [5.14] J.P. Davim, P.S. Sreejith, R. Gomes, C. Peixoto, Experimental studies on drilling of aluminum (AA1050) under dry, minimum quantity of lubricant, and flood-lubricated conditions, *Proc. IMechE Vol. 220 Part B: J. Engineering Manufacture* 220 (2006) 1605-1611.
- [5.15] F. Klocke, G. Eisenblaetter, Dry cutting, *CIRP Annals—Manufacturing Technology* 46 (1997) 519–526.
- [5.16] J.F. Kelly, M.G. Cotterell, Minimal lubrication machining of aluminum alloys, *Journal of Materials Processing Technology* 120 (2002) 327-334.
- [5.17] D.U. Braga, A.E. Diniz, G.W.A. Miranda, N.L. Coppini, Using a minimum quantity of lubricant (MQL) and a diamond coated tool in the drilling of aluminum–silicon alloys, *Journal of Materials Processing Technology* 122 (2002) 127-138.
- [5.18] A. Bardetsky, H. Attia, M. Elbestawi, Evaluating of tool wear suppressive ability of lubricants used in minimum quantity of lubrication application in high speed machining of cast aluminum alloys, *American Society of Mechanical Engineers, Manufacturing Engineering Division* 16 (2005) 23-29.
- [5.19] J. Dosbaeva, G. Fox-Rabinovich, J. Dasch, S. Veldhuis, Enhancement of wet- and MQL-based machining of automotive alloys using cutting tools with DLC/polymer surface treatments, *Journal of Materials Engineering and Performance* 17 (2008) 346-351.
- [5.20] S. Bhowmick, A.T. Alpas, Minimum quantity lubrication drilling of aluminum–silicon alloys in water using diamond like carbon coated drills, *International Journal of Machine Tools and Manufacture* 48 (2008) 1429-1443.

[5.21] J.H. Dautzenberg, J.H. Zaat, Quantitative determination of deformation by sliding wear, *Wear* 23 (1973) 9-19.

[5.22] C. Perrin, W.M. Rainforth, Work hardening behaviour at the worn surface of Al-Cu and Al-Si alloys, *Wear* 203-204 (1997) 171-179.

[5.23] V.C. Venkatesh, W. Xue, A study of the built- up edge in drilling with indexable coated carbide inserts, *Journal of Materials Processing Technology* 58 (1996) 379-384.

[5.24] P. Matthew, P.L.B. Oxley, Predicting the cutting conditions at which built- up edge disappear when machining plain carbon steels, *Annals of the CIRP* 29 (1980) 11-16.

[5.25] D.A. Stephenson, J.S. Agapiou, *Metal cutting theory and practice*, Second edition, CRC Taylor and Francis, USA, 593.

[5.26] M. Rahman, A.S. Kumar, M.U. Salam, Experimental evaluation on the effect of minimal quantities of lubricant in milling, *International Journal of Machine Tools and Manufacture* 42 (2002) 539-547.

[5.27] E. Trent, P. Wright, *Metal cutting*, 4<sup>th</sup> Edition, Butterworth–Heinemann publications, London, 328.

[5.28] V. Stepina, V. Vesely, *Lubricants and special fluids*, Elsevier Scientific Publishing Company, Amsterdam, 1992.

**TABLE**

**Table 5.1:** Torque, thrust force, temperature, surface roughness, chip length, chip width and percentage of area covered by adhered magnesium during dry, FA-MQL, H<sub>2</sub>O-MQL and flooded drilling of AM60 magnesium alloy.

<b>Characteristic Parameters</b>	<b>Drilling Conditions</b>			
	<b>Dry</b>	<b>H<sub>2</sub>O-MQL</b>	<b>FA-MQL</b>	<b>Flooded</b>
Maximum torque (N-m)	10.85	4.14	1.92	4.48
Maximum thrust force (N)	205.22	134.12	125.10	145.21
Range of average torque (N-m)	2.28-9.32	1.42-2.43	2.27-2.55	2.08-2.75
Range of average thrust force (N)	102.05-165.11	80.10-145.21	88.13-112.18	63.09-121.33
Maximum temperature (°C)	193	134	86	129
Average plateau temperature (°C)	150 ± 15	100 ± 10	60 ± 7	110 ± 9
Average surface roughness, R <sub>a</sub> (μm)	46.80 ± 25.31	17.20 ± 2.35	11.80 ± 2.20	12.91 ± 2.85
Average chip length (mm)	246.31 ± 32.11	7.25 ± 1.50	5.23 ± 0.31	7.15 ± 1.64
Average chip width (μm)	86.31 ± 12.20	31.51 ± 6.92	13.89 ± 2.10	26.12 ± 1.47
Percentage of area covered by adhered Mg (%)	100 ± 11	13 ± 6	8 ± 4	14 ± 11



## CHAPTER 6

### **The role of diamond-like carbon coated drills on minimum quantity lubrication drilling of magnesium alloys**

Minimum quantity water lubrication (H<sub>2</sub>O-MQL) and dry drilling behaviour of a cast magnesium alloy (AZ91) using non-hydrogenated diamond-like carbon (NH-DLC) coated HSS drills are discussed in this chapter. A comprehensive literature review is provided in Section 6.1, which envelops recent progresses in both drilling (flooded, dry, near-dry) of diamond-like carbon coatings for aluminum and magnesium alloys. The experimental approach and analyzes are discussed in Section 6.2. Due to adhesion of magnesium to the drills that caused rapid drill failure neither uncoated HSS nor NH-DLC coated drills could be used in dry drilling of AZ91 is discussed in Section 6.3.1. Temperature increase in drilling using uncoated and DLC coated HSS in different drilling conditions (dry, MQL and flooded) is discussed in Section 6.3.2. The machining experiments were supported by tribological experiments as well as microstructural characterizations of material around the drilled holes are discussed in Section 4. The conclusions of the Chapter 6 are written in Section 6.5.

#### **6.1. Introduction**

Carbon based tool coatings, particularly diamond like carbon (DLC) coatings have shown low coefficient of friction (COF) and allowed minimal amounts of aluminum and magnesium adhesion to their surfaces under ambient tribological testing conditions [6.1]. Due to these

favourable tribological properties these coatings are being considered as tool coatings for dry machining of lightweight aluminum and magnesium alloys. One of the primary uses of these lightweight alloys is in the automotive components made of cast aluminum and magnesium alloys to reduce the vehicle's fuel consumption by reducing its total mass. An important consideration in drilling of the cast aluminum and magnesium components without the use of metal removal fluids is however the adhesion of metallic chips to the drill flutes leading to rapid tool failure [6.2]. Development and characterization of tool coatings that minimize adhesion of aluminum and magnesium to the tools is an active research area. Meanwhile, an environmentally friendly technique that feeds minimal quantities of lubricant i.e. 10-100 ml/h to the cutting edge of the tool---a method known as minimum quantity lubrication (MQL) is promising and could be used in conjunction with the DLC coated drills. The current work investigates the application of DLC coatings in the MQL drilling of AZ91 magnesium alloys. The AZ91 alloy has found applications in engine crankcases, gear boxes and other powertrain components for which drilling is an important machining processes. In this work, the effects of the drilling with aqueous MQL (H<sub>2</sub>O-MQL) process were considered not only because water provides naturally an environmentally sustainable MQL fluid, but also because the non hydrogenated DLC coatings revealed fine tribological properties (low wear and friction, minimum adhesion) under high humidity atmospheres. The existing literature pertaining to the friction and wear of DLC coatings in water and high humidity is reviewed in the following paragraphs.

Ronkainen et al. [6.3] compared the tribological performance of hydrogenated DLC (H-DLC) and non-hydrogenated DLC (NH-DLC) in water against alumina balls. The H-DLC coating performed poorly under water lubricated conditions, resulting in rapid wear. The

coefficient of friction (COF) of H-DLC, which wore through, was high (0.7), but for the NH-DLC coatings the COF values were low, in the range of 0.04–0.05. The authors attributed the low COF of NH-DLC to the formation of the carbonaceous transfer film on the counterface materials. Anderson et al. [6.4] studied the effects of water vapour on the friction behaviour of H- and NH-DLC coatings against M50 grade steel ball. The COF values for the NH-DLC and H-DLC coatings tested in vacuum were 0.60 and 0.01, respectively. When water vapour was introduced into the test chamber, however, the DLC coatings exhibited opposite COF friction trends. Specifically, the COF of the NH-DLC decreased to 0.07 while that of the H-DLC increased slightly to 0.08 in water vapour environment. The authors suggested that the decreasing COF of the NH-DLC coatings was caused by the passivation of dangling carbon bonds on the coating surface by the adsorbed water molecules. The increase in the COF of H-DLC was attributed to the dipole like interactions between the counterfaces induced by adsorbed water vapour. Konca et al. [6.5] studied the effects of testing atmosphere on the tribological behaviour of the NH-DLC against the 319 Al (Al-6.5% Si) alloy and measured high COFs (0.46, 0.47, and 0.44) and high wear rates ( $2.48 \times 10^{-4}$ ,  $3.60 \times 10^{-4}$  and  $6.64 \times 10^{-5}$  mm<sup>3</sup>/m) for the NH-DLC coatings in vacuum, nitrogen and dry air (0% relative humidity, RH). The lowest COF (0.08) and wear rate ( $4.38 \times 10^{-7}$  mm<sup>3</sup>/m), however, were observed in air with an 85% RH. It was generally thought that the presence of hydrogen in water promotes the formation of C-H bonds, which helps to passivate the carbon bonds on DLC surfaces. Liu et al. [6.6] compared the friction behaviour of diamond to H-DLC and NH-DLC against alumina ball. The resulting COF decreased from 0.09 to 0.03 as the RH increased from 10% to 85%, for the diamond surface. Similar behaviour was observed for NH-DLC; As the RH increased from 5% to 90%, the COF decreased from 0.10 to 0.04. H-DLC, however, behaved contrarily to diamond and NH-DLC,

with the COF increasing from 0.07 to 0.13 as the RH increased from 5% to 85%. Bhowmick and Alpas [6.2] examined cutting performances of H-DLC and NH-DLC coated HSS drills using H<sub>2</sub>O-MQL supplied at a rate of 30 ml/h. During H<sub>2</sub>O-MQL drilling of 319 Al using NH-DLC-coated drills an average drilling torque of 1.65 N-m was measured, much alike to drilling using conventional flooded condition with an average torque of 1.75 N-m. This represented a significant reduction compared to dry drilling that generated a torque of 4.11 N-m. Konca et al. [6.1] studied the dry sliding wear behaviour of NH-DLC coatings against pure Mg (99.9 wt.%). Tests were performed in ambient air (28% RH) and in an argon atmosphere. In argon, the NH-DLC coatings showed a very low COF of 0.05 after an initial running-in period. Carbonaceous material transfer from the NH-DLC to the contact surface of the Mg pin was observed in argon. Changing the test atmosphere from argon to ambient air increased the COF to 0.40, which was accompanied by the formation of oxidized Mg debris and an increased wear rate.

Only a few studies reported the machining of magnesium alloys and these studies have focussed on the use of conventional hard coatings and polycrystalline diamond as the tool material. Tonshoff and Winkler [6.7] studied dry turning of an AZ91 alloy with carbide drills coated by TiN for which flank built-up edge (BUE) formation was observed during cutting, while no significant BUE occurred during machining with polycrystalline diamond-coated tools. Gariboldi [6.8] investigated dry drilling of an AM60 alloy (Mg- 6% Al) using uncoated and TiNcoated HSS drills and found that all the drills exhibited short tool lives and failed as a result of magnesium adhesion to the cutting edges and drill flutes. Thus, the existing studies emphasize that the difficulty in dry machining of magnesium arise from the adhesion of magnesium to the tool. To minimize the adhesion of magnesium to the drills, the feasibility of using MQL drilling of AM60 was investigated by Bhowmick et al. [6.9] using water and fatty acid-based MQL

agents (FA-MQL) and uncoated HSS drills. The highest torque values observed during H<sub>2</sub>O-MQL (2.43 N-m) drilling were consistently lower than those obtained during dry drilling (9.32 N-m). A lower resultant torque (2.55 N-m) and better surface quality was observed when using FA-MQL compared dry (9.32 N-m) drilling. The overall performance of FA-MQL was similar to the conventional flooded drilling.

The literature suggests the positive role of water in reducing the friction of NH-DLC. Accordingly, the objective of this work was to study H<sub>2</sub>O-MQL performances of the NH-DLC coated tools in drilling of a common magnesium alloy AZ91 used in lightweight cast components and assess whether they would demonstrate a comparable performance to flooded drilling. Drilling performances of NH-DLC coated and uncoated drills were assessed by measuring torques and temperatures generated in the AZ91 workpiece under dry and H<sub>2</sub>O-MQL drilling conditions. Pin-on-disk type tribological tests were undertaken to determine the COF of AZ91 under dry and water environments. Metallographic analyses consisting of determination of subsurface deformation, drill wear and the amount of material transferred to the tool were conducted.

## **6.2. Experimental Details**

### **6.2.1. Workpiece materials: AZ91 Mg and DLC Coatings on Drills**

The workpiece material used for drilling tests was an AZ91 Mg-Al-Zn alloy in the form of  $60 \times 10.16 \times 7.62$ -cm<sup>3</sup> plates. The composition of the AZ91 was (in wt. %): 8.90% Al, 0.91% Zn, 0.20% Mn, 0.0025% Fe, <0.0007% Cu, <0.0006% Ni, 0.005% Si and the balance Mg. The hardness of the alloy, measured with a Vickers microhardness tester, was HV<sub>10</sub> 65 ± 4.2 (63 ± 6.0 measured on Brinell hardness scale). The microstructure of the AZ91 consisted of α-Mg

grains with an average grain size of  $318 \pm 54 \mu\text{m}$  and a eutectic mixture of Mg and  $\text{Mg}_{17}\text{Al}_{12}$  at some grain boundaries.

The cutting tools used for the drilling tests performed on AZ91 were  $6.35 \pm 0.01 \text{ mm}$ -diameter high-speed steel (HSS) twist drills. The drill consists of two flutes with high helix angle of  $37^\circ$  and point angle of  $118^\circ$ . The hardness of the HSS twist drills used was 64 HRC.

The literature survey presented in Section 1 has indicated that tribological properties of non-hydrogenated DLC, NH-DLC, coatings in water and under high humidity environments are characterised by low COF. Accordingly, in this work NH-DLC coatings were considered as the drill coatings. NH- DLC coatings were deposited on the HSS twist drills using a closed field unbalanced magnetron sputter ion plating system. The NH-DLC coated drills deposited in this way by Teer Coatings Ltd. (Worcestershire, UK) for this work. The thickness of the NH-DLC coatings was  $2.5 \mu\text{m}$ . Their nano-hardness was measured as 13 GPa (1400 VHN) using Hysitron TI 900 Triboindenter equipped with a Berkovich nano-indenter. The coating deposition parameters as well as details of coatings' properties can be found elsewhere [\[6.10\]](#).

### **6.2.3. Dry, MQL and Flooded Drilling Tests**

All drilling tests were performed using a CNC (CNC Master, USA) drill press equipped with a non-contact torque measurement transducer. Preliminary experiments were carried out in order to select the drilling speed and the feed rate used for the rest of the experiments. For this purpose, a series of initial drilling tests were conducted at speeds of 1000, 1500, 2000 and 2500 rpm and feed rates of 0.10, 0.15, 0.20 and 0.25 mm/rev. under dry conditions using uncoated HSS drills. The results indicated that the average torque was higher at high speed and feed rate

combinations. Considering that machining at high speeds and feed rates increases industrial productivity, the highest speed and feed rate were selected so that the drilling tests were performed at a cutting speed of 2500 rpm (50 m/min) using a feed rate of 0.25 mm/rev. Each (blind) hole drilled was 19 mm in depth corresponding to  $\sim 3 \times$  drill diameter. The tool life was evaluated by determining the total number of holes drilled until drill failure that occurred due to either i) jamming of the drill bit due to magnesium adhesion-- as in the case of dry drilling by uncoated HSS drills or ii) attainment of the flank wear to 100  $\mu\text{m}$  in depth-- as in the case of dry drilling using NH-DLC coated drills [6.11]. In other cases drilling process was continued until 1000 holes were drilled in succession without tool failure. The holes were drilled in lines with a horizontal center-to-center spacing of 10 mm maintained between them.

The torque generated during drilling was measured using a non-contact magneto-static torque sensor. The torque required to drill each hole was measured individually as a function of drilling time. Each drilling cycle, i.e., duration between the initial contact and the complete retraction of the drill bit was approximately 5 seconds. The average torque (in N-m) was calculated for this time span, as described in [6.9]. The temperature increase in the AZ91 workpiece was measured by means of a non-contact, infrared thermometer from one side of the workpiece--3 mm away from the first row of holes (25 holes) being drilled. A detailed explanation of the measurement technique using an infrared thermometer can be found in [6.9].

Drilling tests were carried out without the use of any metal removal fluid, i.e. under the dry drilling condition, as well as MQL and flooded conditions. Distilled water used as the MQL agent was directed to the drill tip by means of an external MQL system, at a rate of 30 ml/h. Preliminary experiments have detected no significant difference in average torque responses when MQL fluids were supplied at the rates of 30, 40 and 50 ml/h but at lower MQL supply rates

the torque increased. For example, the average torque increased when an MQL stream lower than 30 ml/h was used, as evident from the 30% increase when a flow of 20 ml/h MQL was employed. Thus, an MQL flow rate of 30 ml/h was used during the drilling test. A commercially available mineral oil supplied at a flow rate of 30,000 ml/h was used for the flooded drilling tests.

#### **6.2.4. Microstructures of Drilled Holes and Drill Tips**

The last holes drilled before the tool failure or upon completion of the predetermined numbers of test cycles (1000), were selected for metallographic analyses. A rectangular section of the workpiece containing this particular hole was metallographically mounted in epoxy resin, and cut along its mid-section parallel to the hole surface. The sectioned plane was then polished using a 0.1  $\mu\text{m}$  diamond suspension. The samples were ultrasonically cleaned in ethanol and etched in Picral solutions containing 5 ml acetic acid, 6 g picric acid, 10 ml  $\text{H}_2\text{O}$  and 100 ml ethanol. The metallographically prepared sections were examined using optical microscope (OM). To investigate the amount of magnesium adhesion to the drill flutes and to study the drill wear a scanning electron microscope (JEOL 5400 SEM) was used.

#### **6.2.5. Measurement of Coefficient of Friction by Pin-on-disk Tests**

Tribological tests were used to determine the coefficient of friction (COFs) of AZ91 pins and flat NH-DLC samples. The pin-on-disk type tribological tests were conducted under dry sliding as well as water spray condition in order to simulate friction during  $\text{H}_2\text{O}$ -MQL cutting. AZ91 pins rounded to have a 4 mm radius at one end were tested against the NH-DLC coated M2 steel coupons. A constant load of 5 N was applied to the other end of the pin and a sliding



speed of 0.12 m/s was used. During the course of the pin-on-disk tests distilled water was supplied at a rate of 30 ml/h, same as that was used in drilling tests. The contact geometry during pin-on-disk tests differ from those of the drilling tests. But as will be discussed later, the measured COF was helpful to rationalise the mechanisms of drill wear and magnesium transfer to the tools. The wear rate of the coating after each test was calculated from the volume of the material removed by measuring the cross sectional area of the wear track at 12 different locations along the circumference of the wear track using an optical surface profilometer (Wyko NT 1100). The details of measurement technique can be found in [6.5].

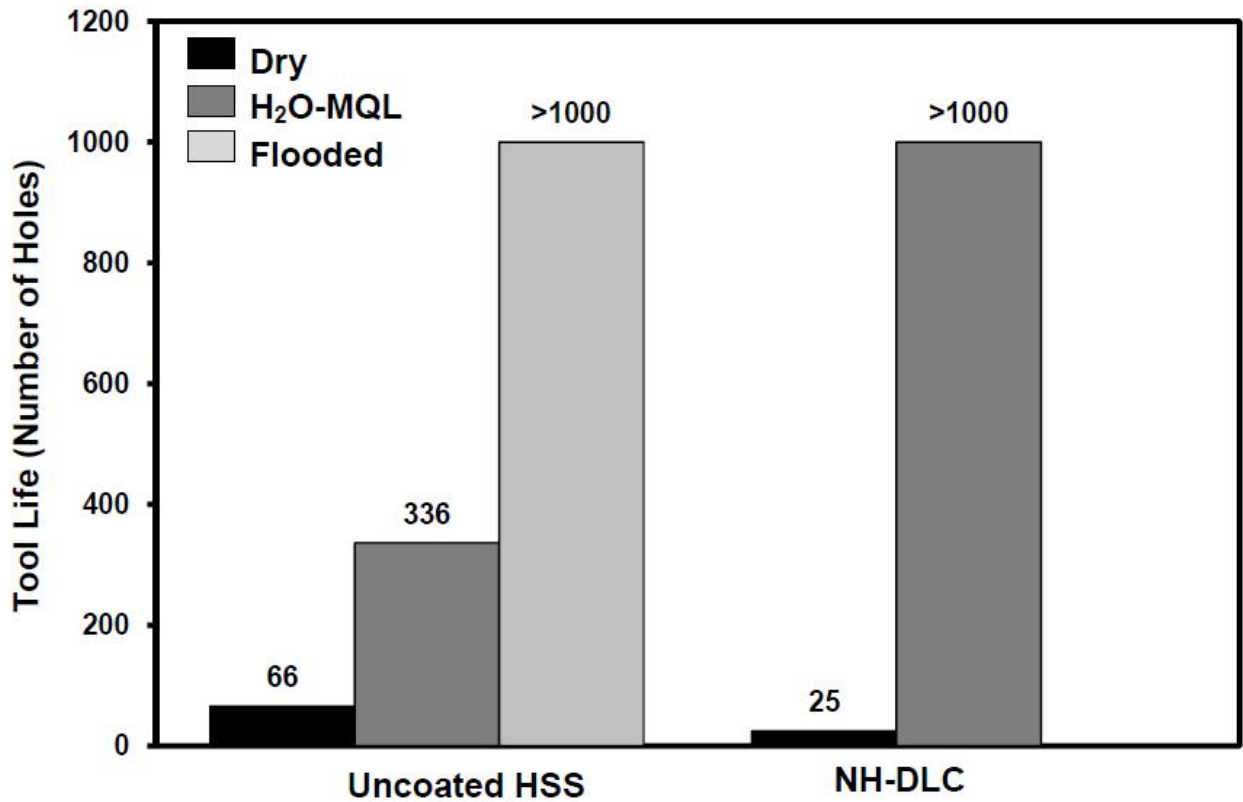


**Figure 6. 1** Tool life comparisons of uncoated HSS drills in dry, H<sub>2</sub>O-MQL and flooded conditions and NH-DLC-coated HSS drills in dry and H<sub>2</sub>O-MQL conditions. The drills did not fail in HSS/flooded and NH-DLC/H<sub>2</sub>O-MQL conditions.

## 6.3. Experimental Results

### 6.3.1. Tool Life and Torque Generated During Drilling

During dry drilling of AZ91 using the uncoated HSS drill, tool failure occurred as a result of extensive magnesium adhesion almost immediately after the drilling test started; the tool life was limited to drilling only 66 holes (Fig. 6.1). The torque-time signal profiles recorded during the course of dry drilling of the individual holes using the HSS drills are shown in Fig. 6.2 (a) for the 25 holes preceding the tool failure (41<sup>th</sup>-66<sup>th</sup> holes). The torques generated were high, usually exceeding 4 N-m. Especially those exceeding 10 N-m at the onset of tool failure were evident. When the average values of the torques were considered for the entire experiment, it was noted that they increased abruptly from 1.60 N-m for the 1<sup>st</sup> hole, to 8.65 N-m for the 66<sup>th</sup> hole (Fig. 6.3).

In contrast, during H<sub>2</sub>O-MQL drilling with the HSS drills drill failure was delayed until the 336<sup>th</sup> hole as depicted in Fig. 6.1. The torques were high and fluctuated widely towards the end of tool life shown in Fig. 6.2 (b) for last 25 holes (311<sup>th</sup> to 336<sup>th</sup> holes) for which values greater than 10 N-m were recorded. The average torque increased by 126% from the 1<sup>st</sup> hole (2.77 N-m) to the 336<sup>th</sup> hole (6.25 N-m) (Fig. 6.3). Thus although an increase in tool life was recorded for H<sub>2</sub>O-MQL drilling, the torque response could not be said to have been improved significantly. In addition, the use of water, albeit in small quantities in conjunction with steel drills and Mg alloys require attention. The use of water has traditionally been avoided during Mg drilling because Mg can react with water vapour or steam to form Mg(OH)<sub>2</sub> and free H<sub>2</sub> [6.12]. This is a concern during H<sub>2</sub>O-MQL drilling using HSS drills, as the temperature reached near the boiling temperature of water (Section 3.2). Galvanic corrosion where magnesium can

act as an anode and HSS can be considered as a cathode in the presence of water as an electrolyte [6.13] is an additional issue. Thus, because of these complications, H<sub>2</sub>O-MQL drilling with the HSS drills would be implausible in practice and, the H<sub>2</sub>O-MQL drilling using HSS was not given further consideration in this manuscript. On the other hand, DLC coatings are highly corrosion resistant in the water environment. In fact DLC coatings have been used to protect the magnesium from corrosion [6.14]. Also as will be shown later in limit the drilling temperature increase to less than 52 °C, therefore there H<sub>2</sub> formation is avoided.

Using conventional flooded drilling at least 1,000 holes were drilled and the tool life exceeded the maximum number of holes drilled (Fig. 6.1). Fig. 6.2 (b) shows the torque responses of the last 25 holes drilled in flooded conditions, where the maximum torque remained less than 4 N-m. The average torque for the first hole drilled was 1.93 N-m and increased slightly to 2.42 N-m at the 1000<sup>th</sup> hole (Fig. 6.3). Hence, it is desirable to achieve a similar performance using NH-DLC coated drills.

The performance of NH-DLC coated HSS drills was highly sensitive to the drilling conditions. It was found that the dry drilling performance of the NH-DLC coated drills was even less satisfactory than that of the uncoated HSS drills. Dry drilling with the NH-DLC coated drills induced tool failure as soon as the test started i.e., at the 25<sup>th</sup> hole as shown in Fig. 6.1. The measured torque values (Fig. 6.2c) were as high as those generated during HSS dry drilling. As illustrated in Fig. 6.3, the average torque abruptly increased by almost 500% from the 1<sup>st</sup> hole (1.27 N-m) to the last hole (7.67 N-m). The NH-DLC coated drill failure while drilling the AZ91 alloy was due to the combination of two factors, namely adhesion of magnesium to the drill flutes and wear to the cutting edges of the tools, which will also be discussed in more detail in Section 4.

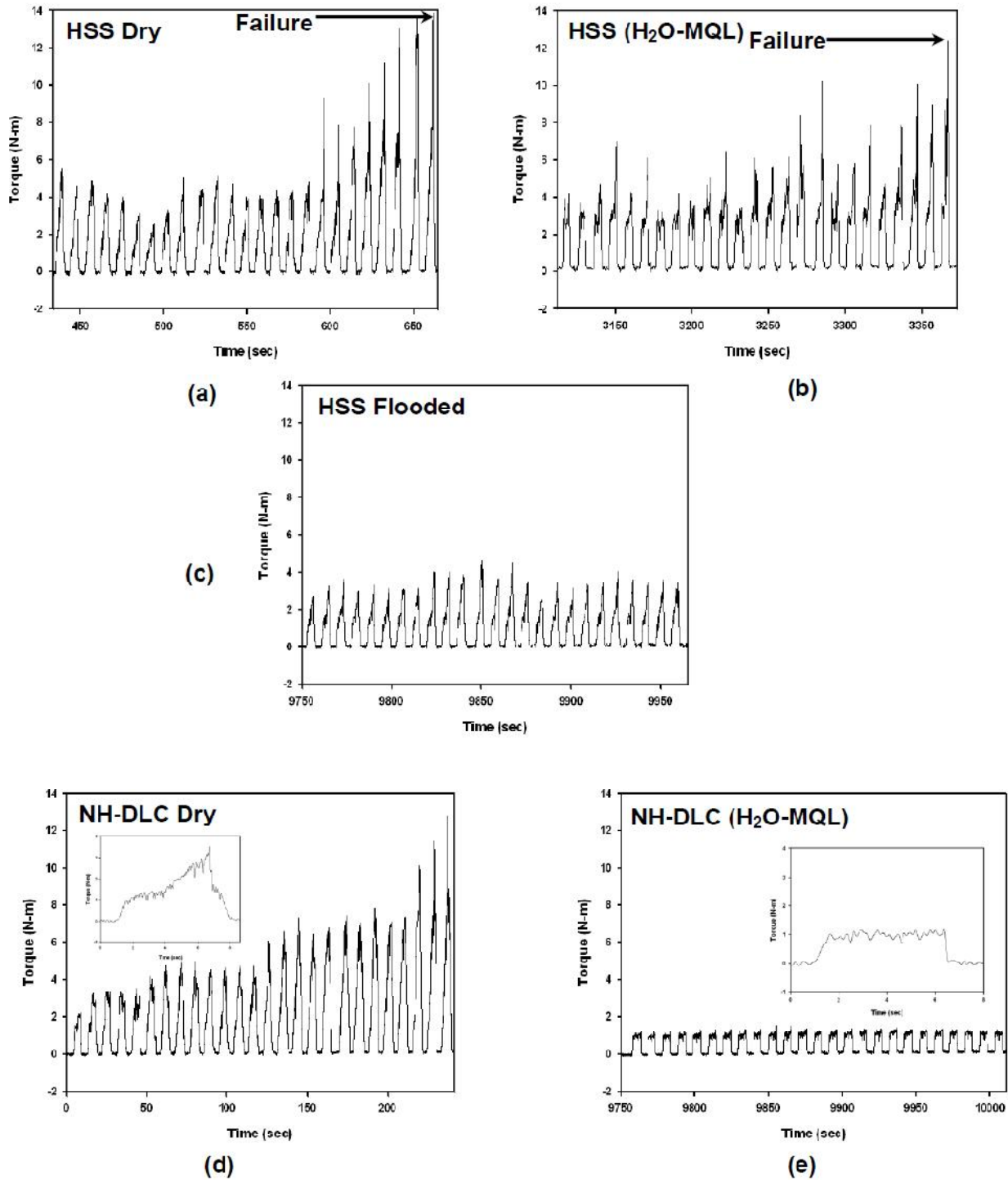


**Figure 6. 2** Torque variations for (a) HSS/dry of last 25 holes; (b) HSS/flooded of last 25 holes; (c) entire drilling cycle for NH-DLC/dry and (d) NH-DLC/H<sub>2</sub>O-MQL of last 25 holes. Typical torque curves for NH-DLC/dry and NH-DLC/H<sub>2</sub>O-MQL are shown in the insets of Fig. 2 (c) and Fig. 2 (d).

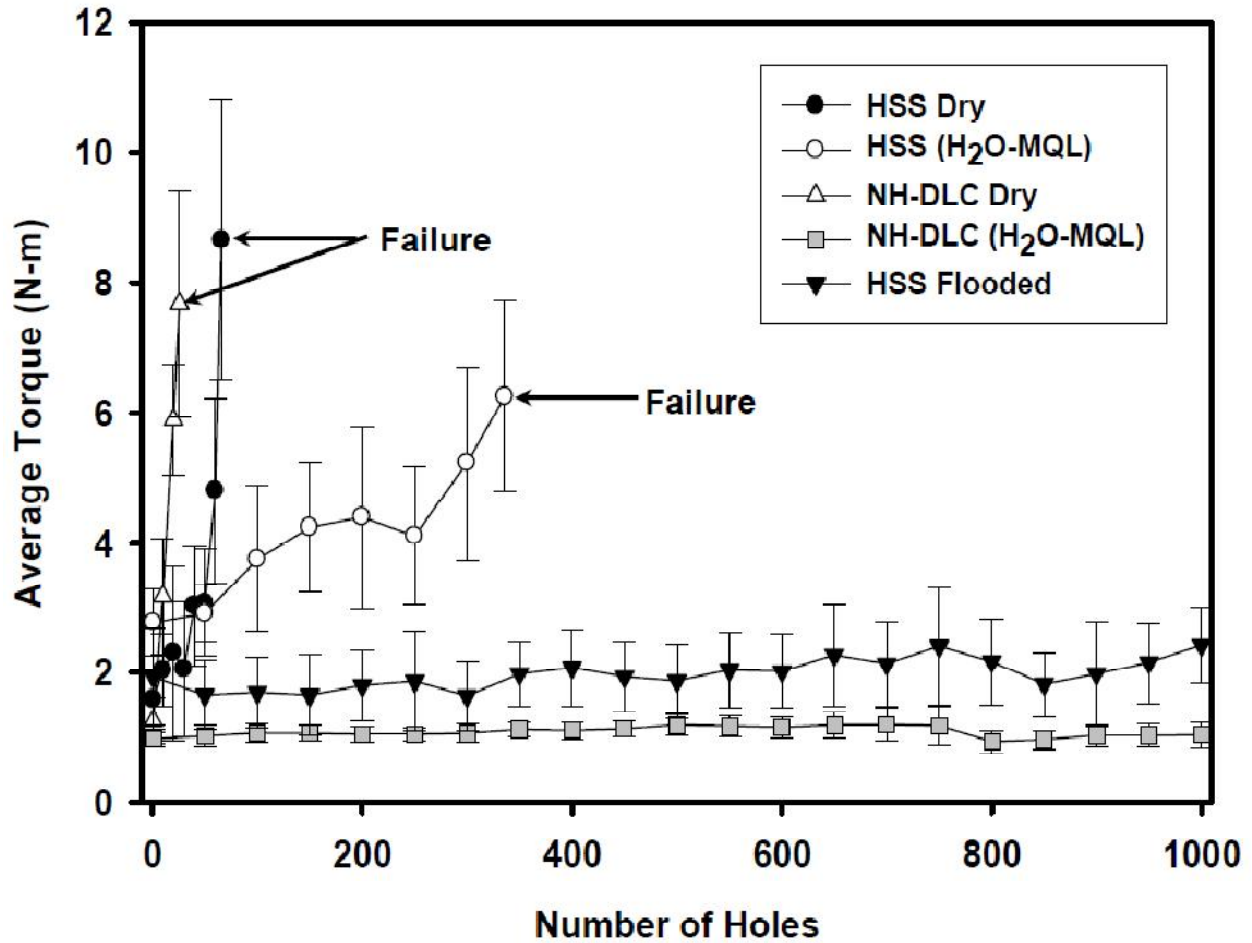


**Figure 6. 3** The average torque comparisons for uncoated HSS in dry and flooded conditions and NH-DLC-coated drills in dry and H<sub>2</sub>O-MQL conditions.

A notable improvement in both tool life and torque response occurred when NH-DLC-coated drills were used under H<sub>2</sub>O-MQL conditions; a significantly higher tool life was achieved while maintaining torque values whose maxima did not reach 1.5 N-m throughout the experiments. At least 1000 holes were drilled in succession (Fig. 6.1) without evidence of tool wear or magnesium adhesion. There was no difference between the torque signal amplitude and shape at the entrances and exits of the holes, as shown in the inset of Fig. 6.2 (d), indicating easy chip removal (in contrast to the increasing torque observed during chip removal when dry

drilling (Fig. 6.2c). The same figure indicates that the average torque variation from the first hole (0.99 N-m) to the last (1.05 N-m) was uniform, and displayed only a 6% increase throughout the entire range of the experiments.

In summary, the use of NH-DLC coated tools in conjunction with the H<sub>2</sub>O-MQL drilling of AZ91 alloy resulted in a performance similar to conventional flooded drilling.

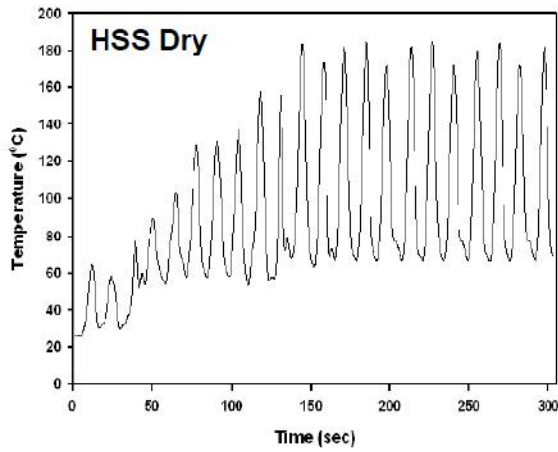
### 6.3.2. Temperature Increase During Drilling

Figs. 6.4 (a-e) show the workpiece temperatures generated during the drilling of the first 25 holes measured as a function of time for each drilling condition. The highest temperatures recorded during the drilling of each successive hole are plotted in Fig. 6.5. Accordingly, during flooded drilling the temperature increase was limited to 64 °C, whereas the maximum temperature recorded during the dry drilling of AZ91 alloy using an uncoated HSS drill was 175 °C and continued to increase with the increasing number of drilled holes. The use of HSS drills during the application H<sub>2</sub>O-MQL reduced the workpiece temperature significantly to 85 °C, but the slope of the temperature curve in Fig. 6.5 for this condition continued to increase. As mentioned previously in **Section 3.1** the formation of steam and hydrogen gas with the negative consequences appeared to be likely.

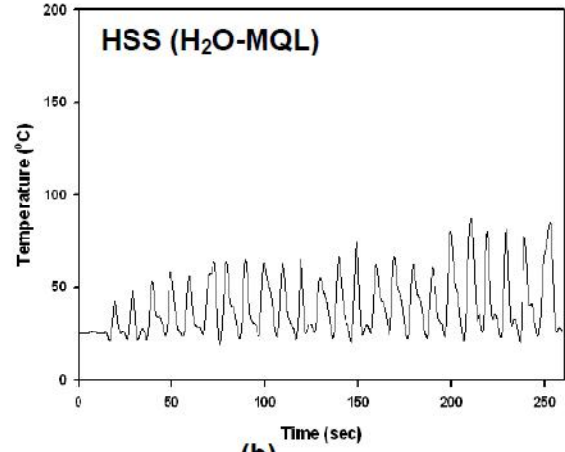
Dry drilling using NH-DLC coated drills produced temperatures as high as 271 °C that surprisingly well exceeded those generated during HSS dry drilling. It was interesting to observe that when the same drilling experiments were conducted with the NH-DLC coated drills under the H<sub>2</sub>O-MQL condition, a very different trend was observed; in this case the use of NH-DLC coated drills limited the temperature increase to a maximum of 52 °C. The temperature profile

was similar to that achieved in HSS flooded conditions. During H<sub>2</sub>O-MQL drilling with NH-DLC coated tools (Fig. 6.4d) and in the cases of flooded drilling (Fig. 6.4b), the workpiece temperature was reduced to 25 °C immediately after the drill was retracted upon completion of drilling of an individual hole. (Figs. 6.4 [a, c]).

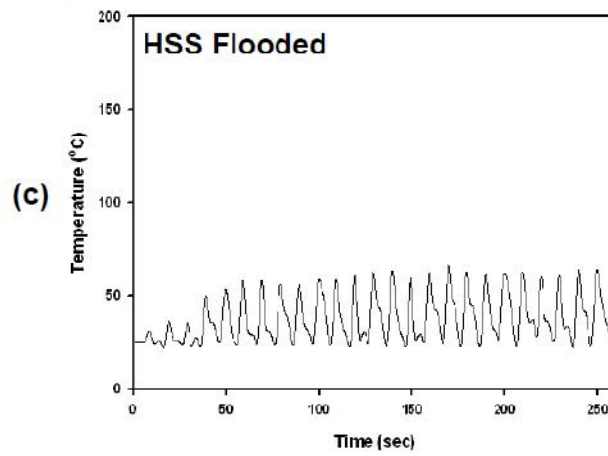
The salient test results pertaining temperature measurements made during drilling under various conditions are summarized in Table 6.1. The tool life, maximum torque, range of average torque and the maximum temperature, average coefficient of friction and average wear rate values are listed for each drilling condition, for direct comparison. These observations revealed several important points that could be summarized as follows: i) the dry drilling of AZ91 led to rapid tool failure and high torques and temperature increases, regardless whether uncoated HSS or NH-DLC coated HSS drills were used, but ii) a substantial improvement was achieved when NH-DLC coated drills were used under the H<sub>2</sub>O-MQL condition; not only was the tool life prolonged, but the drilling torques were reduced to low and stable levels. In addition, NH-DLC coatings, the workpiece temperature remained low and hence resulting in a performance much like that encountered during flooded drilling.



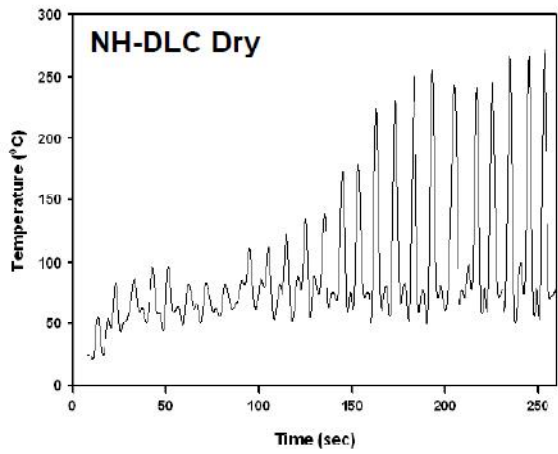
(a)



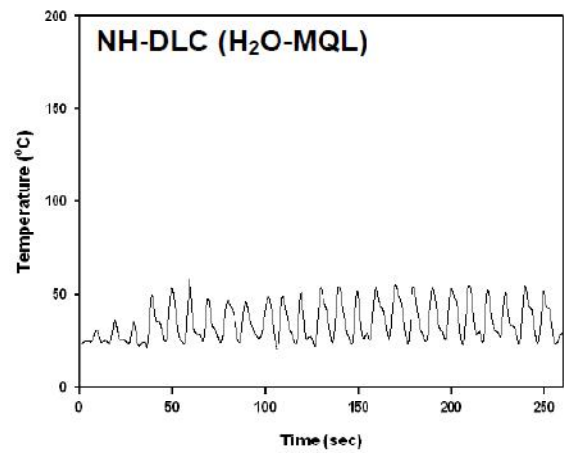
(b)



(c)



(d)



(e)

**Figure 6. 4** Temperature profiles of the first 25 holes for (a) HSS/dry; (b) HSS/flooded; (c) NH-DLC/dry and (d) NH-DLC/H<sub>2</sub>O-MQL.



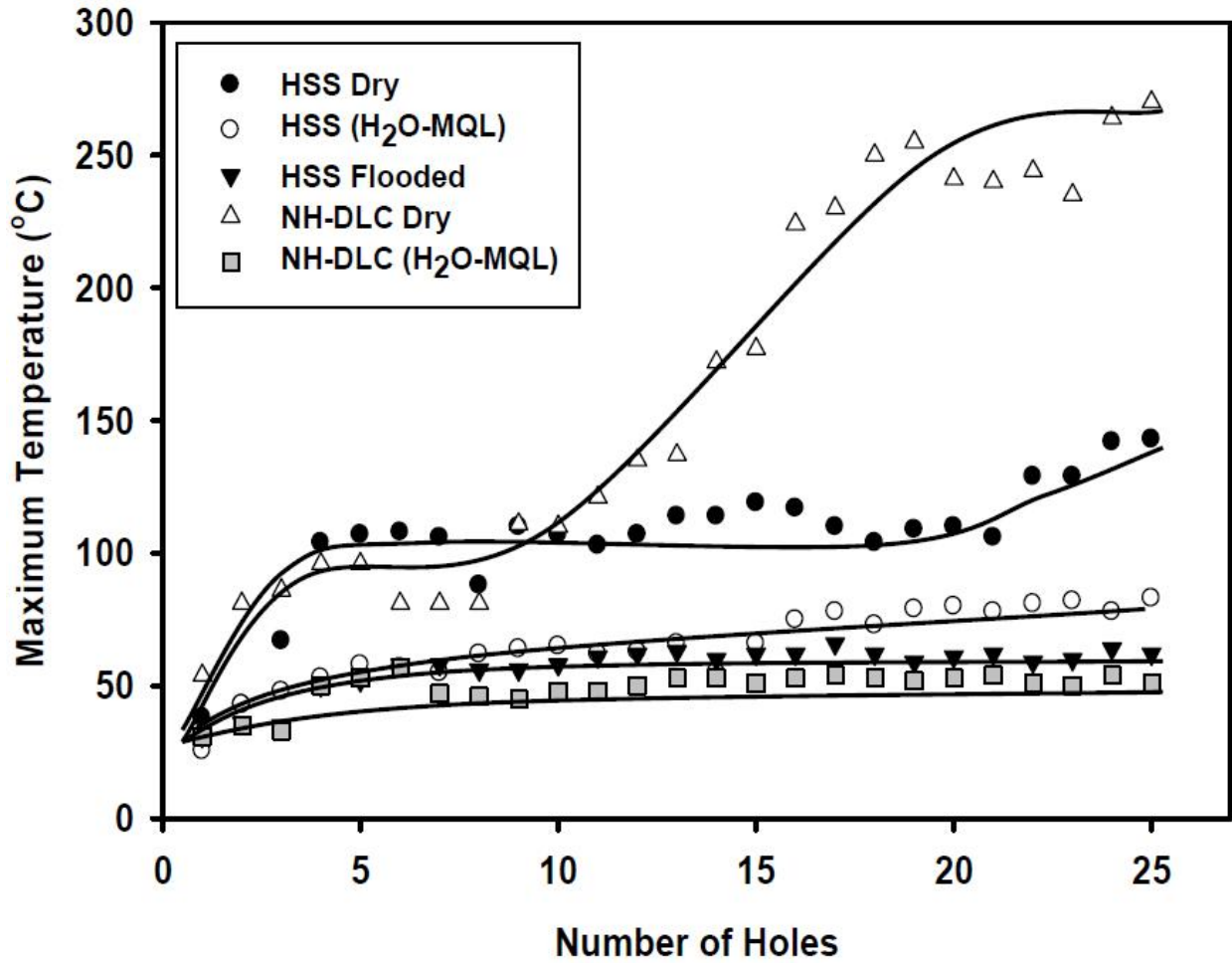
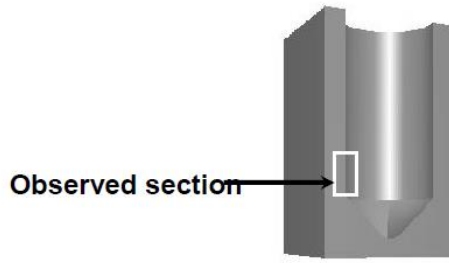


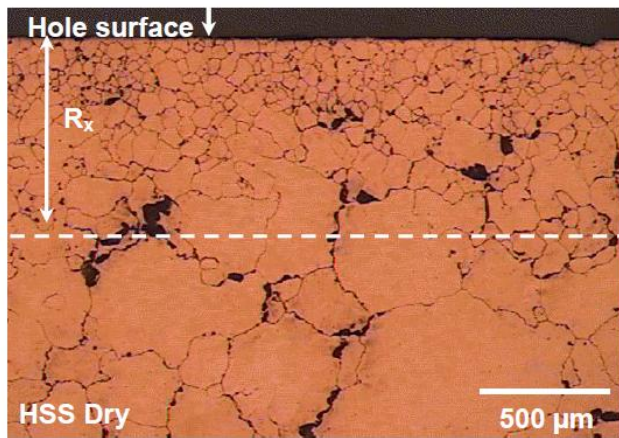
**Figure 6. 5** Maximum temperature variations for the first 25 holes during drilling in dry, H<sub>2</sub>O-MQL and flooded conditions using uncoated, dry, H<sub>2</sub>O-MQL conditions with NH-DLC-coated HSS drills.

### 6.4. Discussion

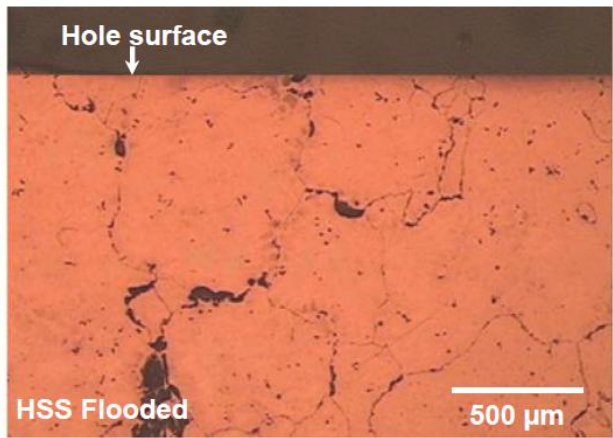
This section focuses on the analyses of mechanical and tribological properties of the interfaces between the AZ91 workpiece and the drill surface. The observed improvements when MQL drilling with NH-DLC coated drills will be discussed in terms of these properties. The changes that occurred in the AZ91 alloy’s microstructure during the drilling of the holes are also explored and related to drilling performance under different conditions.



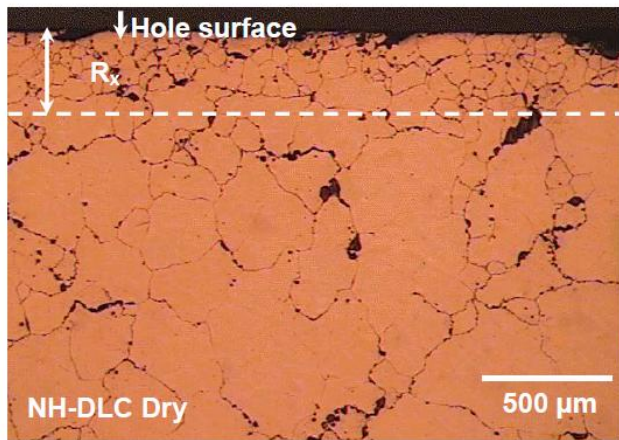
(a)



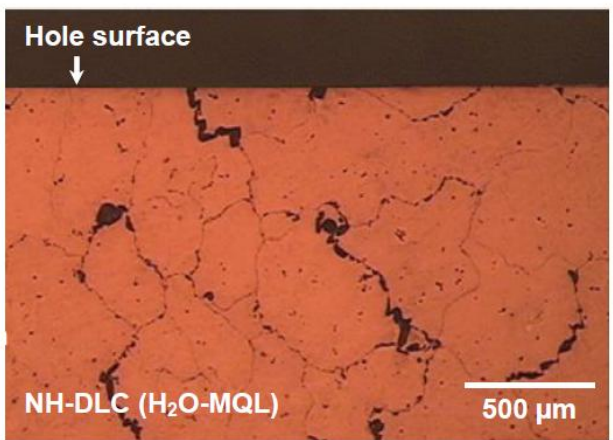
(b)



(c)

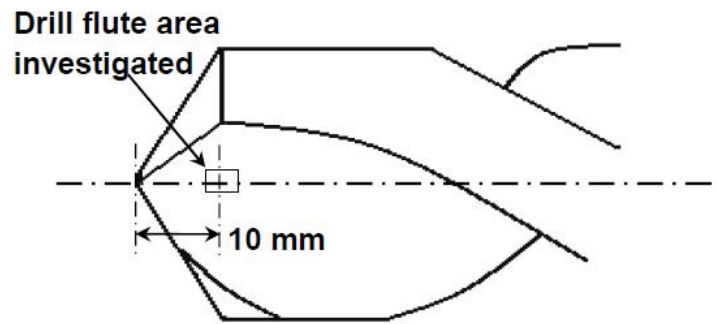


(d)

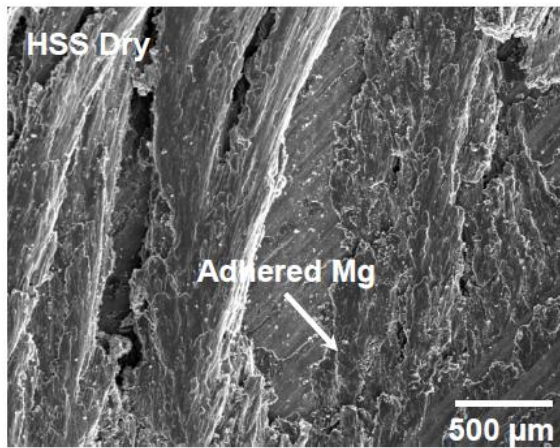


(e)

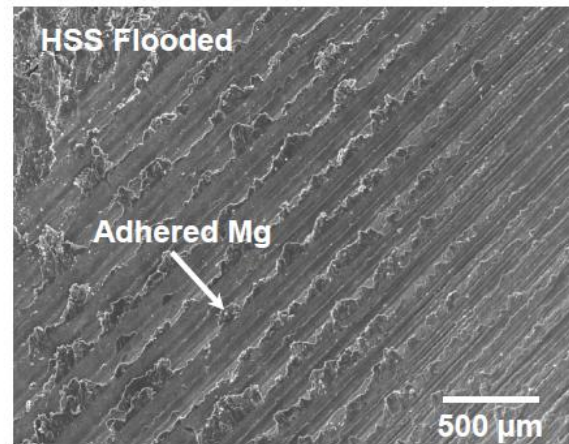
**Figure 6. 6** (a) Schematic diagram of half a drilled hole showing the plane where microstructures were observed. Subsurface microstructures of the last hole for (b) HSS/dry; (c) HSS/flooded; (d) NH-DLC/dry and (e) NH-DLC/H<sub>2</sub>O-MQL.  $R_x$  indicates recrystallized Mg grains.



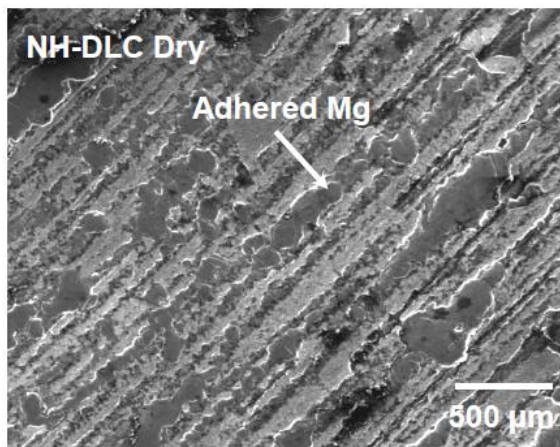
(a)



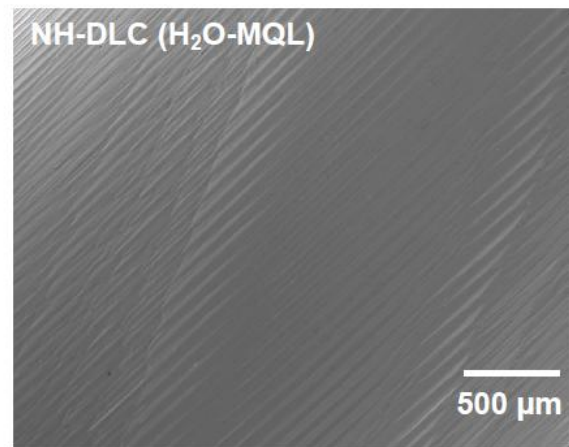
(b)



(c)



(d)



(e)

**Figure 6. 7** (a) Locations of SEM images taken on the drill flute. SEM images showing magnesium adhesion to drill flutes: (b) HSS/dry; (c) HSS/flooded; (d) NH-DLC/dry and (e) NH-DLC/H<sub>2</sub>O-MQL.

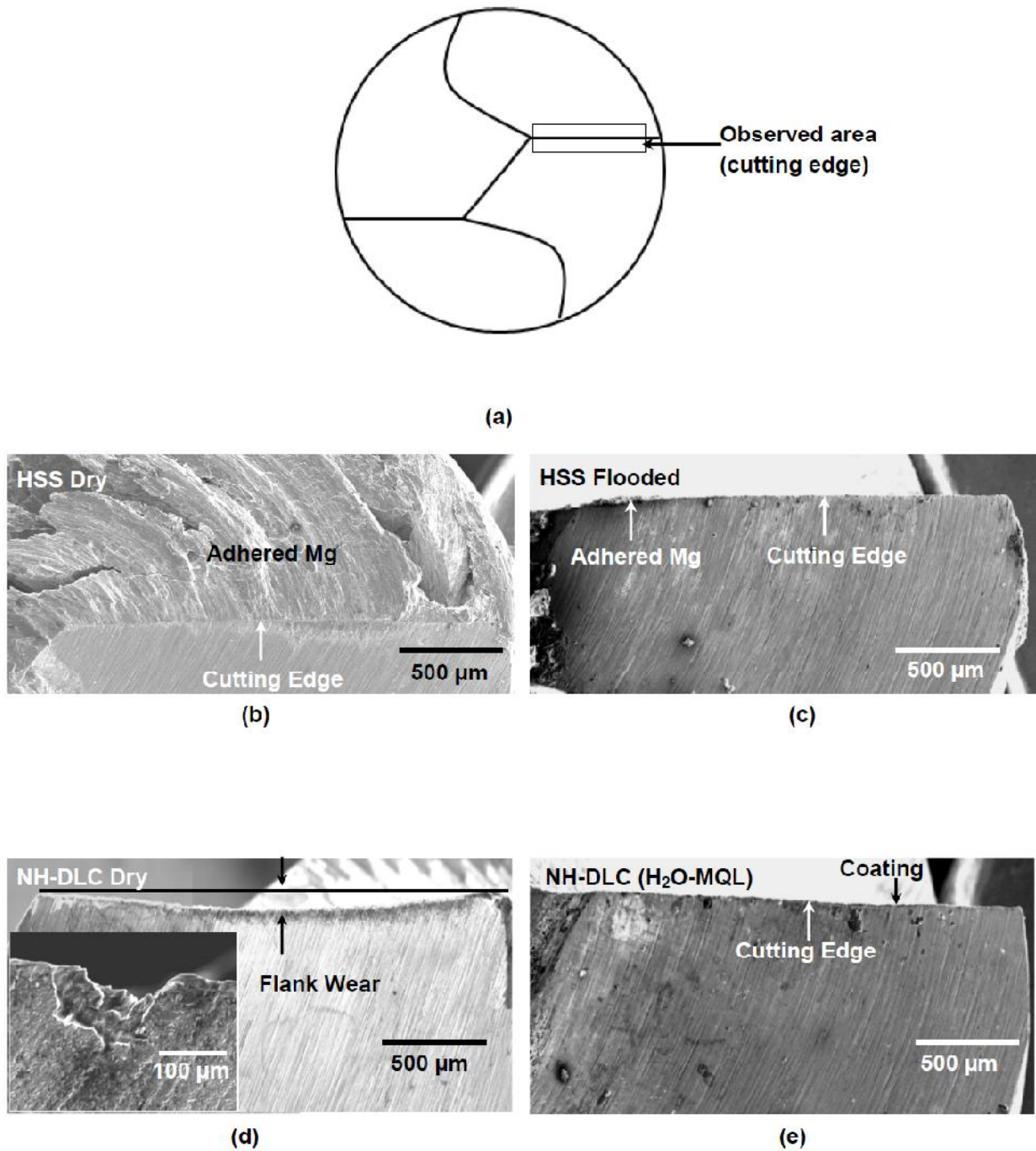


**Figure 6. 8** (a) Locations of SEM images taken on the drill cutting edge. SEM images of the cutting edge for (b) HSS/dry; (c) HSS/flooded; (f) NH-DLC/dry and (g) NH-DLC/H<sub>2</sub>O-MQL.

The workpiece microstructures developed near the drilled holes during dry, MQL and flooded drilling depended on workpiece temperatures. The microstructures of the last holes

drilled in each drilling condition, as obtained from the location indicated in Fig. 6.6 (a), are shown in Fig. 6.6 (b-e). It is noted that on the section taken from the workpiece subjected to dry drilling using uncoated HSS, Fig. 6.6 (b), the size of the subsurface grains within a zone of 600-900  $\mu\text{m}$  below the tool-workpiece contact surface were smaller ( $70 \pm 10 \mu\text{m}$ ) than those of the original grains--with an average size of  $318 \pm 54 \mu\text{m}$ . This indicates the occurrence of grain recrystallization during dry drilling.

The presence of recrystallized grains at the subsurface of the AZ91 drilled using NH-DLC coated drills under dry conditions is evident in Fig. 6.6 (d). The presence of a large, subsurface zone of recrystallized grains in ( $R_x$ ) extending to a depth of 600-1000  $\mu\text{m}$  is consistent with the fact that the drilling induced temperatures that exceeded  $270 \text{ }^\circ\text{C}$ , which corresponds to  $0.4 T_m$  where  $T_m$  is the melting temperature of AZ91 [6.15]. There was no evidence of significant recrystallization in the subsurface region during flooded drilling (Fig. 6.6d). Similarly, when MQL drilling was used with NH-DLC coated tools, no recrystallization occurred (Fig. 6.6e) because the workpiece temperature remained lower than  $50 \text{ }^\circ\text{C}$  (Fig. 6.5) and the hardness of the material underneath the hole was similar to AZ91's original hardness--hence no softening occurred in the case of flooded drilling. On the other hand the microhardness of the recrystallized grains was  $40 \pm 6 \text{ kg}\cdot\text{mm}^{-2}$  (38% lower than the original hardness of AZ91). Thus, heating the AZ91 alloy during drilling resulted in the reduction of the alloy's hardness and promoted adhesion of softened material to the drill flutes, leading to the formation of a large BUE at the tool tip. Magnesium transfer to the drill flutes can be seen in Figs. 6.7 (b-e), which present SEM micrographs taken from the location shown in Fig. 6.7 (a). The drill flutes displayed significant amounts of transferred magnesium after dry drilling using the uncoated HSS drills (Fig. 6.7b). NH-DLC coated drills also exhibited magnesium transfer in dry drilling

conditions (Fig. 6.7c). A small amount of magnesium was observed on the drill flutes examined after flooded drilling (Fig. 6.7d). But no evidence of magnesium transfer was found on the drill flutes after H<sub>2</sub>O-MQL drilling using NH-DLC coated tools (Fig. 6.7e).

The role of adhesion on BUE formation was examined at the drill tip as shown in Fig. 6.8 (a). Dry drilling using the uncoated HSS drills led to the formation of a prominent BUE at the tool tip (Fig. 6.8b). The formation of this bulky BUE is believed to be the main reason for the rapid failure of the uncoated drills. A different type of drill failure mechanism was observed in the NH-DLC coated drills which consisted of wear of the cutting edge or flank wear, as illustrated in Fig. 6.8 (c). The flank wear during dry drilling using NH-DLC coated drills was substantial i.e., about a 100 µm depth (Fig. 6.8c). At higher magnification SEM images, there existed evidence that flank wear was due to the micro-chipping of the cutting edge (Fig. 6.8c). During flooded drilling, a BUE was formed on the cutting edge, but this was discontinuous and apparent only in a few local spots (Fig. 6.8d). Flank wear was also a characteristic feature of the NH-DLC coated drills used under H<sub>2</sub>O-MQL condition, but as the Fig. 6.8 (e) indicates its intensity was much less than compared to dry drilling.

The wear of the NH-DLC coated tool can be explained by considering the tribological behaviour of NH-DLC coatings at elevated temperatures. The wear resistances of the NH-DLC coatings have been found to deteriorate at elevated temperatures when tested against aluminum. No Significant wear was observed at temperatures below 120 °C but at higher temperatures severe wear occurred [6.1]. It was reported that The H-DLC's wear rate increased by almost an order of magnitude from  $2.9 \times 10^{-7} \text{ mm}^3/\text{m.N}$  to  $1.5 \times 10^{-6} \text{ mm}^3/\text{m.N}$ , when the test temperature increased from 25° to 240 °C. The wear rate of NH-DLC increased more drastically from  $2.1 \times 10^{-7} \text{ mm}^3/\text{m.N}$  to  $5.8 \times 10^{-5} \text{ mm}^3/\text{m.N}$  when tested in the similar temperature range [6.16]. The

reasons for the rapid wear were not entirely clear but graphitization of the DLC's original amorphous ( $sp^2/sp^3$  hybrid) structure was proposed as a possible wear mechanism [6.17]. As the temperature generated using NH-DLC coated drills during dry drilling exceeded  $270\text{ }^\circ\text{C}$  (Fig. 6.5), the coatings' wear resistance deteriorated during contact with the workpiece.

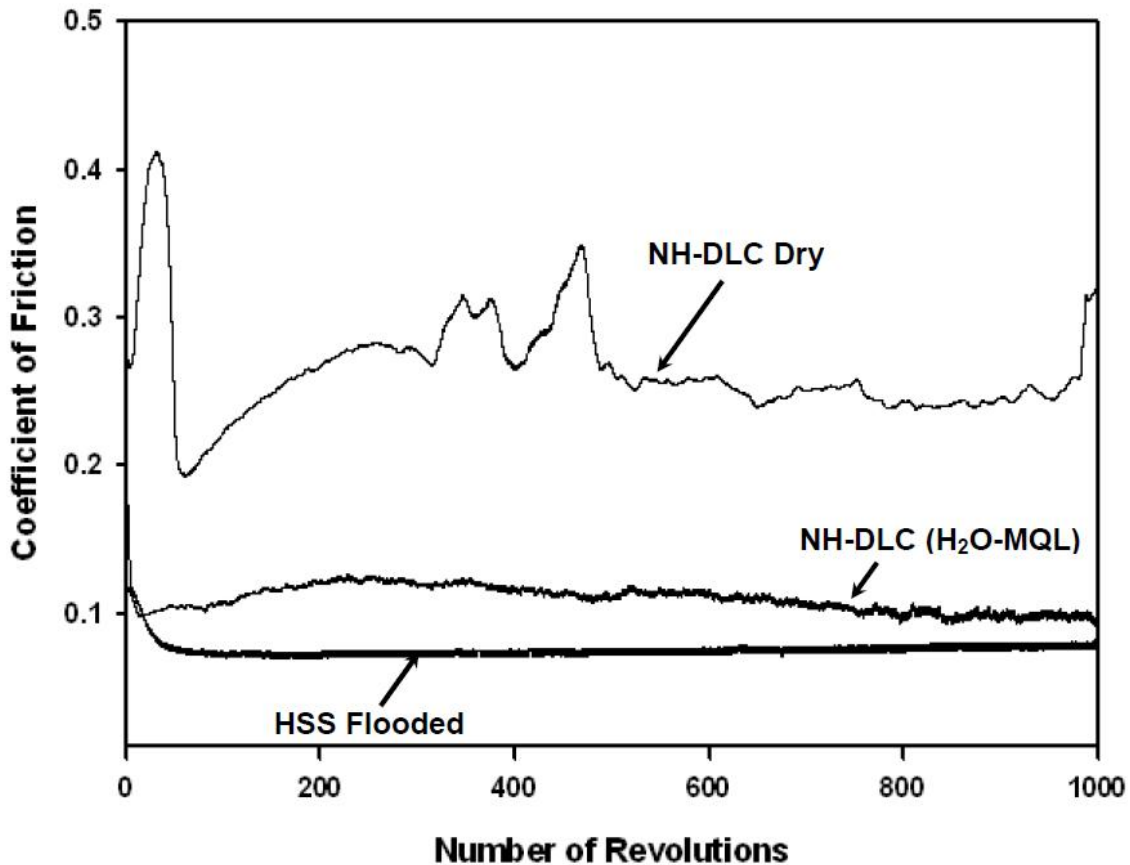


**Figure 6. 9** COF curves with number of revolutions during the sliding of AZ91 pin against NH-DLC-coated disks in dry and H<sub>2</sub>O-MQL conditions and uncoated HSS in flooded conditions.

Tool wear was significantly reduced when H<sub>2</sub>O-MQL drilling was used in conjunction with the NH-DLC coated drills. The high wear resistance of NH-DLC in H<sub>2</sub>O-MQL compared to NH-DLC in dry conditions ensured that the coating remained intact on the tool and, consequently, the beneficial —machining properties such as low drilling torque and long tool life were observed. Thus preventing the temperature rise during drilling is critical to reduce tool wear

and the contact temperature generated during tool-workpiece interaction should be related to the frictional properties of the coatings in machining environment, namely air and water. In order to better understand the tribological behaviour of NH-DLC coatings under water and air environments, tribological tests were conducted using a pin-on-disk configuration as described in Section 2.5. During dry sliding (ambient air with 45% RH), an average COF value of  $0.24 \pm 0.06$  was measured. The average COF decreased to  $0.11 \pm 0.01$  when the sliding tests were conducted using a distilled water spray of 30 ml/hr (Fig. 6.9). The uncoated M2 tool steel tested under fully lubricated conditions, as a reference; using the same mineral oil used for the flooded drilling tests resulted in a COF of  $0.08 \pm 0.01$ . The low COF obtained when the water spray was used on NH-DLC coatings may be attributed to the passivation of carbon bonds by -OH and -H that become dissociated from H<sub>2</sub>O. Theoretical and experimental studies have shown that water effectively passivates the free (or dangling) carbon bonds on the NH-DLC's surface as more H and -OH are provided to these free carbon atoms [6.4]. Qi et al. [6.18] used first principles calculations to show how H<sub>2</sub>O would dissociate at the diamond and DLC surfaces into -OH and H and how where chemical bonding between these surfaces and -OH is then established. The H atom serves as a bridge between the two carbon atoms. A counterface atom such as aluminum that would transfer to a clean NH-DLC surface will not transfer readily to H or -OH passivated surfaces because these surfaces have a much smaller work of separation compared to a non-passivated carbon interface. Consequently, it is conceivable that the passivation of NH-DLC surfaces in the presence of H<sub>2</sub>O-MQL would prevent adhesion between the magnesium and the drill bit coated with NH-DLC, resulting in a performance comparable to flooded drilling with HSS. Therefore, NH-DLC-coated drills used under H<sub>2</sub>O-MQL drilling conditions may be an environmentally sustainable alternative to the flooded drilling of AZ91 alloys.



## **6.5. Conclusions**

- [1] During the dry drilling of AZ91, neither uncoated HSS nor NH-DLC coated drills showed tool life longer than 70 holes.
- [2] The high temperature generated during dry drilling using HSS and NH-DLC coatings initiated recrystallization of AZ91 surfaces. Softened magnesium promoted adhesion and BUE formation in case of HSS, and flank wear when NH-DLC coatings were used, with both processes resulting in high drilling torque.
- [3] The application of 30 ml/h H<sub>2</sub>O-MQL with NH-DLC coated drills led to significant improvement in tool life, as well as reduction in drilling torque.
- [4] The low COF of NH-DLC under H<sub>2</sub>O-MQL conditions restricted the temperature increase, which limited magnesium adhesion and no significant drill wear occurred. Consequently, NH-DLC in H<sub>2</sub>O-MQL generated low drilling torques.
- [5] The performance of NH-DLC-coated tools during H<sub>2</sub>O-MQL drilling was as efficient as flooded drilling by HSS drills using mineral oil. The use of NH-DLC-coated drills under these conditions can provide a viable substitute to the conventional flooded drilling of AZ91.

## **List of References:**

- [6.1] E. Konca, Y.-T. Cheng, A.T. Alpas, Sliding wear of non-hydrogenated diamond-like carbon coatings against magnesium, *Surface & Coatings Technology* 201 (2006) 4352–4356.
- [6.2] S. Bhowmick, A.T. Alpas, Minimum quantity lubrication drilling of aluminum–silicon alloys in water using diamond like carbon coated drills, *International Journal of Machine Tools and Manufacture* 48 (2008) 1429– 1443.
- [6.3] H. Ronkainen, S. Varjus, K. Holmberg, Tribological performance of different DLC coatings in water-lubricated conditions, *Wear* 249 (2001) 267- 271.
- [6.4] J. Andersson, R.A. Erck, A. Erdemir, Friction of diamond-like carbon films in different atmospheres, *Wear* 254 (2003) 1070- 1075.
- [6.5] E. Konca, Y.-T. Cheng, A.M. Weiner, J.M. Dasch, A.T. Alpas, Effect of test atmosphere on the tribological behaviour of the non-hydrogenated diamond-like carbon coatings against 319 aluminum alloy and tungsten carbide, *Surface & Coatings Technology* 200 (2005) 1783 – 1791.
- [6.6] E. Liu, Y.F. Ding, L. Li, B. Blanpain, J.-P. Celis, Influence of humidity on the friction of diamond and diamond-like carbon materials, *Tribology International* 40 (2007) 216-219.
- [6.7] H.K. Tonshoff, J. Winkler, The influence of tool coatings in machining of magnesium, *Surface & Coatings Technology* 94-95 (1997) 610-616.
- [6.8] E. Gariboldi, Drilling a magnesium alloy using PVD coated twist drills, *Journal of Materials Processing Technology* 134 (2003) 287-295.
- [6.9] S. Bhowmick, M.J. Lukitsch, A.T. Alpas, Dry and minimum quantity lubrication drilling of cast magnesium alloy (AM60), *International Journal of Machine Tools and Manufacture* 50 (2010) 444–457.
- [6.10] J. Stallard, D.G. Teer, A study of the tribological behaviour of CrN, Graphit-iC and Dymon-iC coatings under oil lubrication, *Surface & Coatings Technology* 188–189 (2004) 525– 529.
- [6.11] I.S. Shyha, D.K. Aspinwall, S.L. Soo, S. Bradley, Drill geometry and operating effects when cutting small diameter holes in CFRP, *International Journal of Machine Tools & Manufacture* 49 (2009) 1008–1014.
- [6.12] D.A. Stephenson, J.S. Agapiou, *Metal cutting theory and practice* (second ed), CRC Taylor and Francis, USA (2006) p. 593.

- [6.13] G. Song, A. Atrens, Corrosion mechanisms of magnesium alloys, *Advanced Engineering Materials* 1 (1999) 11-33.
- [6.14] N. Yamauchi, K. Demizu, N. Ueda, T. Sone, M. Tsujikawa, Y. Hirose, Effect of peening as pretreatment for DLC coatings on magnesium alloy, *Thin Solid Films* 506– 507 (2006) 378 – 383.
- [6.15] S. Das, A.T. Morales, A.T. Alpas, Microstructural evolution during high temperature sliding wear of Mg–3% Al–1% Zn (AZ31) alloy, *Wear* 268 (2010) 94–103.
- [6.16] W. Ni, Y.-T. Cheng, A.M. Weiner, T.A. Perry, Tribological behavior of diamond-like-carbon (DLC) coatings against aluminum alloys at elevated temperatures, *Surface & Coatings Technology* 201 (2006) 3229– 3234.
- [6.17] A.A. Gharam, M.J. Lukitsch, M.P. Balogh, A.T. Alpas, High temperature tribological behaviour of carbon based (B<sub>4</sub>C and DLC) coatings in sliding contact with aluminum, *Thin Solid Films* 519 (2010) 1611- 1617.
- [6.18] Y. Qi. E. Konca, A.T. Alpas, Atmospheric effects on the adhesion and friction between non-hydrogenated diamond-like carbon (DLC) coating and aluminum – A first principles investigation, *Surface Science* 600 (2006) 2955–2965.

**Table 6.1:** Maximum torque, range of average torque and maximum temperature during drilling of AZ91 alloy using uncoated and NH-DLC coated HSS drill in different conditions. Average coefficient of friction and average wear rate during sliding of AZ91 against uncoated M2 steel in dry, H<sub>2</sub>O-MQL and flooded conditions and NH-DLC coated M2 steel in dry and H<sub>2</sub>O-MQL conditions.

<b>Drilling and Sliding Conditions</b>					
<b>Characteristic Parameters</b>	<b>HSS Dry</b>	<b>HSS H<sub>2</sub>O-MQL</b>	<b>HSS Flooded</b>	<b>NH-DLC Dry</b>	<b>NH-DLC H<sub>2</sub>O-MQL</b>
Tool life (number of holes)	66	336	> 1000	25	>1000
Maximum torque (N-m)	11.22	4.69	4.71	12.73	1.46
Range of average torque (N-m)	1.60-8.65	1.53-5.24	1.93-2.42	1.27-7.67	0.98-1.05
Maximum temperature (°C)	175	83	64	271	52
Average coefficient of friction	$0.39 \pm 0.02$	$0.28 \pm 0.10$	$0.08 \pm 0.01$	$0.27 \pm 0.06$	$0.11 \pm 0.01$
Average wear rate (10 <sup>-6</sup> mm <sup>3</sup> /m)	$309.15 \pm 31.25$	$108 \pm 26.21$	$0.81 \pm 0.73$	$19.19 \pm 7.37$	$1.71 \pm 0.62$

## CHAPTER 7

### **Minimum quantity lubrication drilling of lightweight aluminum and magnesium alloys used in automotive components**

In this chapter drilling performances of cast magnesium and aluminum alloys using the minimum quantity lubrication (MQL) as a potential environmentally sustainable machining technology are discussed. A comprehensive literature review in Section 7.1 is provided, which envelops recent progresses in MQL drilling for both aluminum and magnesium alloys. The experimental approach consists of the measurement of cutting torques and the thrust forces as well as the temperature generated in the workpiece are discussed in Section 7.2. The use of a fatty acid based MQL reduced the adhesion of aluminum and magnesium to the drill flutes and hence decreased torque and thrust forces as compared with H<sub>2</sub>O-MQL and flooded conditions is discussed in Section 7.3 to 7.4. The conclusions of the experimental results are written in Section 7.5.

#### **7.1. Introduction**

Aluminum and magnesium alloys are the substitutes of the traditional role of steel and cast iron components used in the transportation industry due to their low density (2.7, 1.74 vs 7.8 g/cm<sup>3</sup>). Hence, automotive power train components made of cast aluminum and magnesium alloys provide an effective way to reduce the fuel consumption by reducing the total mass per vehicle. For an example, 319 Al (6.0% Si, 3.5% Cu) is extensively used in automotive engine

blocks and heads and AM60 magnesium alloy has found applications in steering wheel frames and gear boxes, where drilling is one of the most vital machining processes. Elimination of cutting fluids during machining has multiple advantages including reducing hazards to human health, pollution to the environment, and disposal costs of the metal removal fluids. Dry machining of cast aluminum-silicon alloys however, is problematic due to aluminum's tendency to adhere to the cutting tool causing premature drill failure. Similarly, the hot chips that form during dry drilling of magnesium alloys can adhere to the drill tips. The reaction between magnesium and atmospheric air, causing ignition of chips, is also an issue.

During dry machining of aluminum alloys, the tool failure is commonly caused by the formation of an adhesive layer and built up edge, which reduces the quality of the machined surface [Weinert, et. al, 2004]. Among the machining operations, dry drilling of aluminum is the most challenging as the chips already adhered to the steel or carbide drill provide obstacles to extricate the chips through the drill flutes. An average of 45 holes could be dry-drilled in 319 Al using uncoated HSS; however,  $1 \times 10^3$  holes were made using metal removing fluids [Bhowmick and Alpas, 2008].

The effect of MQL on the drilling of cast Al-9%Si was studied using synthetic ester supplied at a flow rate of 10 ml/h by Klocke et al. [2000]. The holes displayed better surface roughness with MQL when compared to dry cutting. Cutting power and forces generated during the drilling of commercial purity aluminum in dry, MQL (250 ml/h) and flooded-lubricated conditions were investigated by Davim et al. [2006]. Higher cutting power and specific cutting force were observed during dry drilling in all speed and feed rate combinations, whereas differences between MQL and flooded-lubricated conditions were small. Surface roughness's of workpieces drilled using MQL and fully lubricated were similar for all feed and speed combinations.

Bardetsky et al. [2005] studied MQL effect during the high speed milling of Al-6% Si (319 Al) and observed a significant amount of material adhesion to the flank, clearance and rake faces during dry machining produced. In the case of MQL drilling, moderate adhesion was found on the flank, rake and clearance surfaces. Kelly and Cotterell [2002] compared the effects of flooded drilling using mineral soluble oil, MQL drilling using vegetable oil (20 ml/h), and dry on feed force, torque and surface roughness of cast Al-4.5% Mg. A reduction in torque and feed force were obtained for all methods of coolant application with an increase in cutting speed and feed rate using a HSS drill. In torque responses, MQL drilling (2.2 N-m) resulted in slightly lower torque than flooded (2.4 N-m), and dry (3.8 N- m) conditions. Braga et al. [2002] studied the drilling performance of the uncoated and diamond coated carbide drills under both MQL (mineral oil, 10 ml/h) and flooded of soluble oil lubrication conditions in the drilling of A356 alloy. Their evaluations showed that the performance of the drilling in terms of feed forces when using MQL (max. thrust force 1.26 kN) was analogous to that found using a high amount of flooded soluble oil (max. thrust force 1.25 kN). The power consumed when using flooded soluble oil (max. consumed power 0.86 kW) was higher than when using MQL (0.80 kW) for uncoated carbide drills, inferring that MQL could be a feasible alternative to conventional flooded condition. Bhowmick and Alpas [2008] investigated the cutting performance of diamond like carbon coated HSS drills in a distilled water spray (30 ml/h) used as the MQL agent. Two types of diamond-like carbon coatings, DLCs (non-hydrogenated and hydrogenated-40% H) were considered as these coatings were proven to have aluminum adhesion mitigating properties during tribological tests. The aqueous (distilled water) H<sub>2</sub>O-MQL cutting of 319 Al using either type of DLC-coated drills reduced the average drilling torque (1.65 N-m) compared to dry drilling (4.11 N-m) to a level similar to the performance under the flooded condition (1.75 N-m).

H<sub>2</sub>O-MQL drilling was more stable than the dry drilling; a smaller percentage of drilled holes exhibited “torque spikes”. H<sub>2</sub>O-MQL cutting using non-hydrogenated DLC was preferred to hydrogenated DLC because it resulted in less drill flute aluminum adhesion, resulting in less torque and thrust force being required during drilling.

The feasibility of MQL was also studied on the drilling of magnesium alloys. Bhowmick et al. [2010] studied the MQL drilling of cast magnesium (AM60) alloys using water (H<sub>2</sub>O-MQL) and fatty acid-based MQL (FA-MQL) agents. A lower resultant torque and better surface quality was observed in the case of FA-MQL, compared to those for H<sub>2</sub>O-MQL. The authors also emphasised the benefits of including extreme pressure additives consisting of sulphur and phosphorus-based hydrocarbons in the FA-MQL. The effectiveness of the FA-MQL was attributed to the formation of a protective layer on the tool surface.

In this study a systematic investigation of the effects of torques, thrust forces and the resulting temperatures were performed to assess MQL drilling performances of two technologically important lightweight alloys, namely 319 Al and AM60 Mg. The work also addresses the need to elucidate the role of different MQL fluids on drilling of these alloys including the use of distilled water. Metallographic analyses were undertaken to establish correlations between torque and thrust forces, and aluminum and magnesium transfer to the drills. Vis-a-vis comparison of the drilling performances of typical Al and Mg based lightweight alloys that are used in similar applications will assist to make a selection of the appropriate alloy based on their machining performance.



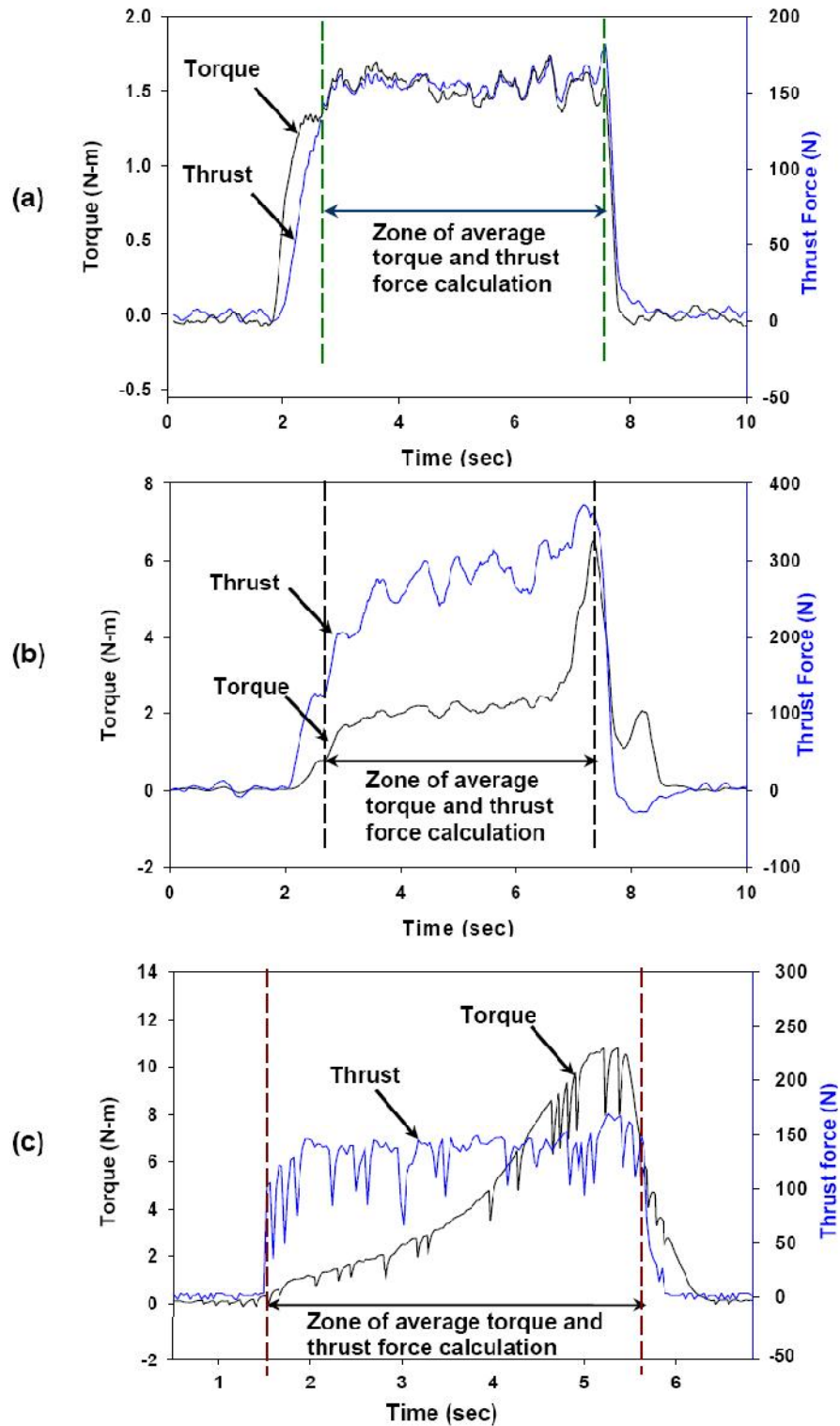


**Figure 7. 1** (a) A uniform torque curve generated during drilling in FA-MQL. Typical torque curve with a spike (b) 319 Al; (c) AM60 Mg. To calculate the average torque and thrust forces, data was taken from the onset of chip clogging to the retraction of the drill.

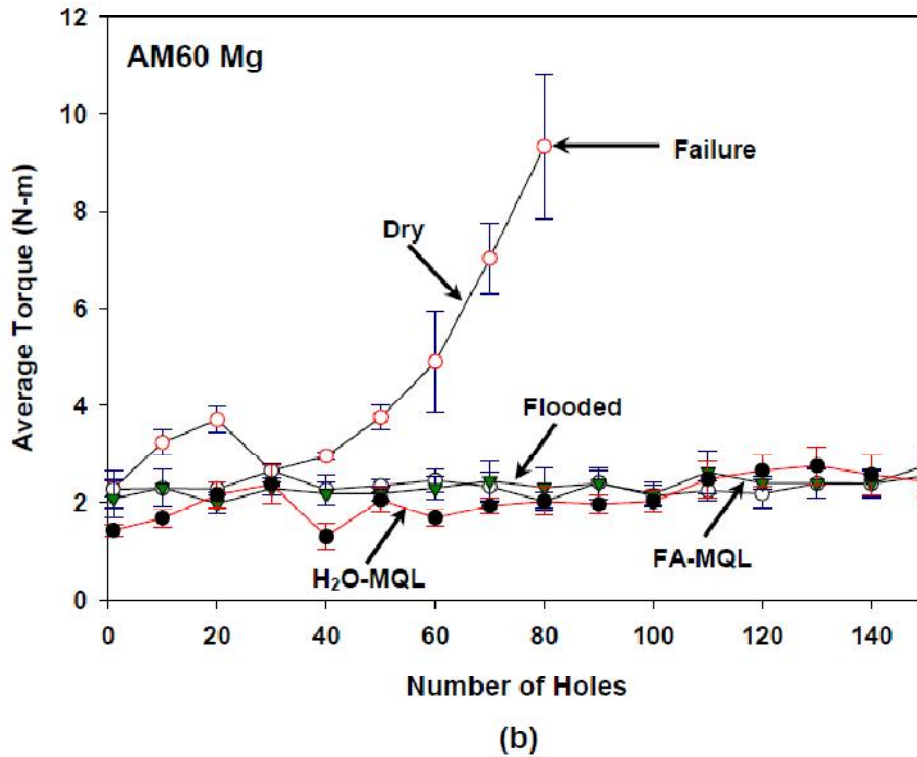
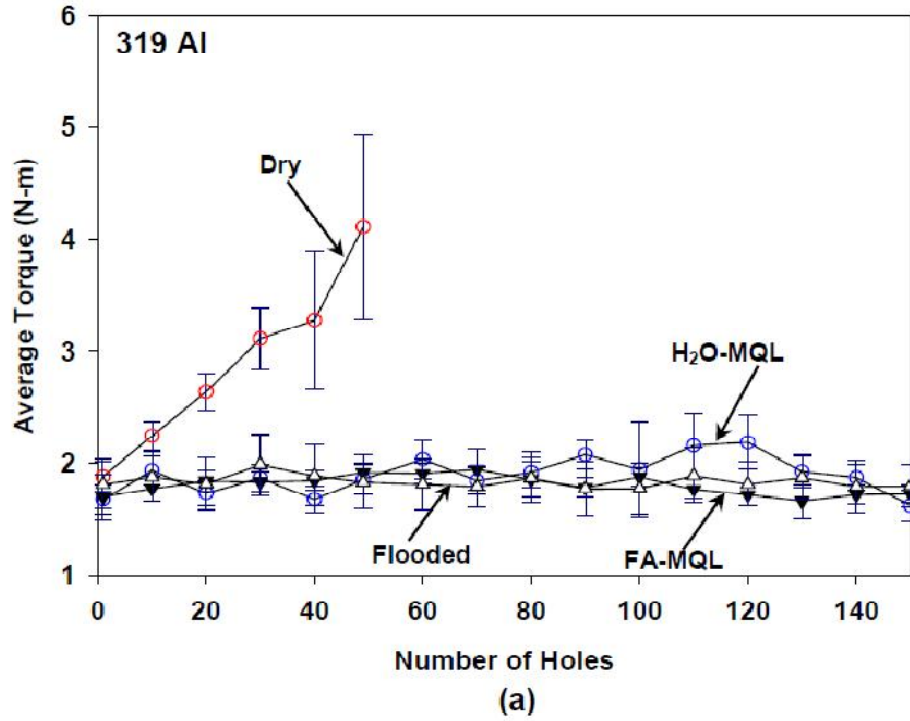


**Figure 7. 2** The average torque variations of the first 49 holes for dry and first 150 holes for H<sub>2</sub>O-MQL, FA-MQL and flooded conditions for (a) 319 Al; (b) AM60 Mg.

## **7.2. Experimental approach**

### **7.2.1. Workpiece Materials: 319 Al and AM60 Mg**

The workpiece materials were a sand cast 319 Al and a die cast AM60 Mg both tested in rectangular blocks of  $30 \times 15 \times 2.54\text{-cm}^3$  in the as-cast condition. 319 Al is a hypoeutectic aluminum alloy containing 6.5% Si, 3.5% Cu, 0.1% Mg, 0.01% Mn, and 0.01% Ni. The matrix Vickers microhardness of the 319 Al tested at 10 g was  $69.00 \pm 7.50$  (HV<sub>10</sub>). The composition of the AM60 Mg was (in wt. %) as follows: 6.0% Al, 0.5% Si, 0.2% Zn, 0.3% Cu, 0.6% Mn, 0.01% Ni, and the balance Mg. The matrix hardness of the AM60 Mg alloy was HV<sub>10</sub>  $57.19 \pm 6.10$ .

### **7.2.2. Cutting Tools**

The cutting tools used for the drilling were  $6.35 \pm 0.01$  mm-diameter high-speed steel (HSS) twist drills with the following composition (in wt.%): 0.95% C, 6.00% W, 5.00% Mo, 4.20% Cr, 2.00% V, and the balance Fe. The drill consists of two flutes with high helix angle of  $37^\circ$  and point angle of  $118^\circ$ . The average hardness of the high-speed steel twist drills used was 64 HRC. Before the tests, the drills were cleaned ultrasonically in acetone.

### **7.2.3. Drilling Test**

All the drilling tests were performed in a CNC drill press with a maximum power of 2.237 kW and a maximum rotational speed of  $5 \times 10^3$  rpm (100 m/min). The drilling tests were performed at cutting speeds of 2500 rpm (50 m/min) using a feed rate of 0.25 mm/rev. Each blind hole was 19 mm deep. A total of 150 holes were drilled in lines with a horizontal center-to-center spacing of 10 mm between the holes and the rows. A non-contact magneto-static torque sensor was mounted on the chuck of the drilling machine between the drill tip and the drill motor

to measure the torque generated during drilling. The thrust force--acted along the Z direction of the drills--was also measured simultaneously with the torque by this sensor. A close up view of the experimental set-up, consisting of the CNC drilling machine, torque and thrust force sensor, drilled block, MQL nozzle and infrared thermometer are shown in **Fig.3.2**.

#### **7.2.4. MQL Supply**

Distilled water and a fatty acid based MQL (FA- MQL) were supplied using an external MQL system (LubriLean Smart, Vogel, Germany). MQL agents were directed to the tip of the drill with a flow rate of 30 ml/h for 319 Al and 10 ml/h for AM60. The quantity of MQL flow rate was chosen based on previous experiments which showed that there is no difference in average torque responses when 10, 30 and 40 ml/h MQL were used. A commercial water soluble coolant (Hangsterfers 500S, USA) in a flow rate of 30,000 ml/h was used as the flooded coolant. Tests were also done without the use of any metal removal fluid (i.e. under the dry drilling condition).

#### **7.2.5. Measurements of Torque, Thrust Force and Temperatures**

The torque required to drill each hole was measured. Each drilling cycle had a duration of approximately 5 seconds between the initial contact and the complete retraction of the drill bit. The average torque (in N-m) and average thrust force (in N) were calculated from the difference in torque and thrust force between the onset of chip clogging and the drill's retraction, as indicated in **Fig. 7.1**. **Fig. 7.1 (a)** illustrates a typical uniform torque curve where there is no significant difference in torque between entrance and exit. In certain holes, at the hole's innermost position the chips did not evacuate through the drill flute, causing the formation of a

“torque spike” at the end of the drilled hole as depicted in **Fig. 7.1 (b)** for 319 Al and **Fig. 7.1 (c)** for AM60 Mg. The details of torque and thrust force measurements can be found in [Bhowmick and Alpas, 2008]. The temperature increase of 319 Al cast block during drilling of first 25 holes was measured by a non- contact infrared thermometer (OS 553, Omega, Canada) from the side of the workpiece materials 3 mm away from the hole being drilled. The cumulative mass of the adhered aluminum and magnesium was calculated by the difference of the mass of drill before and after the drilling operation, using a balance with sensitivity of  $\pm 10^{-4}$  g.

## 7.3. Results

### 7.3.1. Analysis of Torque Responses

#### 7.3.1.1 Drilling of 319 Al

It was previously reported that [Bhowmick and Alpas, 2008] during drilling in 319 Al the drill failed as a result of extensive aluminum adhesion soon after the drilling process started (<50 holes). The average torque increased from 2.01 N-m in the 1<sup>st</sup> hole to 4.11 N-m in the 49<sup>th</sup> hole by an increase of 105% (**Fig. 7.2a**). The mass of aluminum that had adhered to the drill surfaces (i.e. cutting edge and drill flutes) after the drilling of the 49<sup>th</sup> hole was  $342 \times 10^{-3}$  g (**Fig. 7.3**). 65% of holes drilled exhibited torque spikes indicative of adhesion. In the case of H<sub>2</sub>O-MQL drilling, 150 holes were drilled without significant adhesion. At the end of the test, the mass of adhered aluminum was only  $4.8 \times 10^{-3}$  g (**Fig. 7.3**). A smaller number of torque spikes were also observed. Namely, a total of 27 spikes were found--indicating that only 18% of 150 holes exhibited spikes. A gradual increase occurred in the average torque generated during H<sub>2</sub>O-MQL drilling up to the 130- 135<sup>th</sup> hole, where an increase of 15% was noted from the first hole 1.67 N-m to 1.92 N-m (**Fig. 7.2a**).

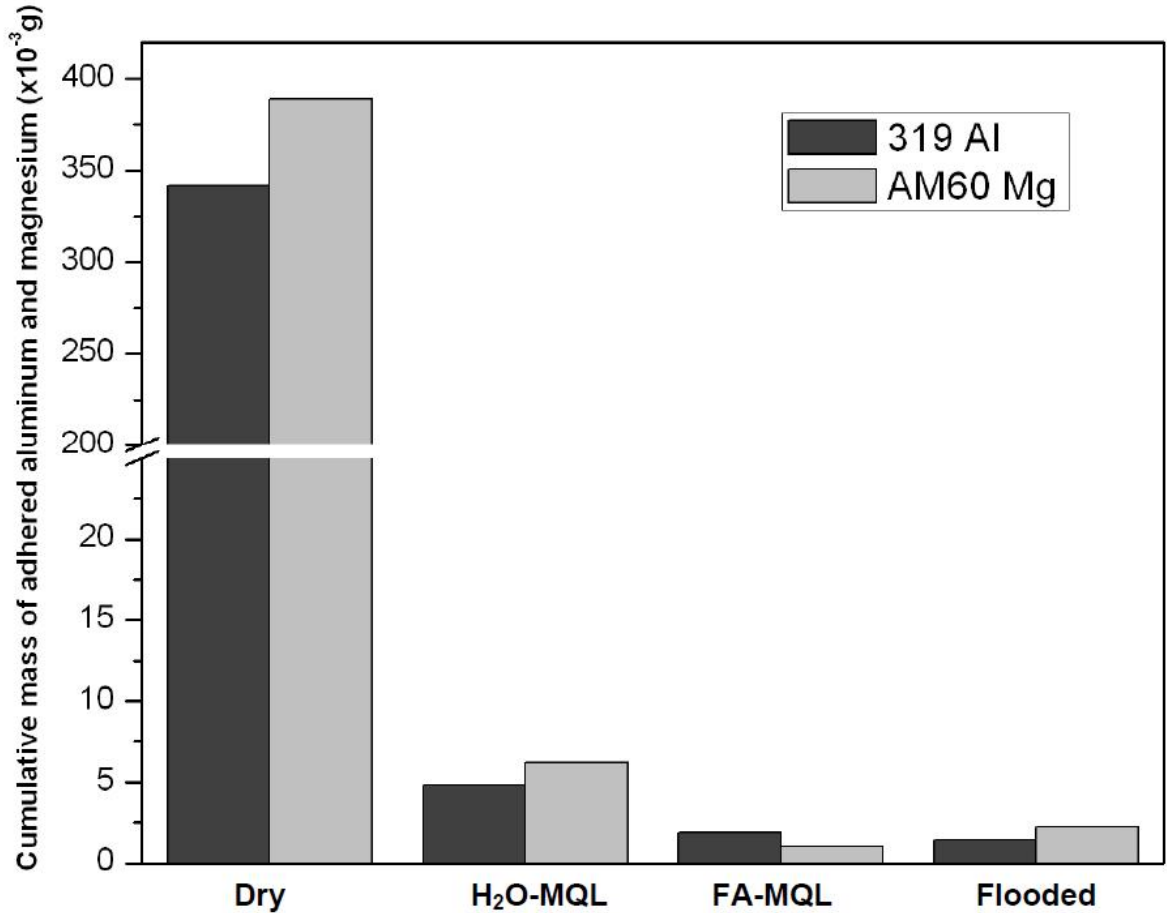
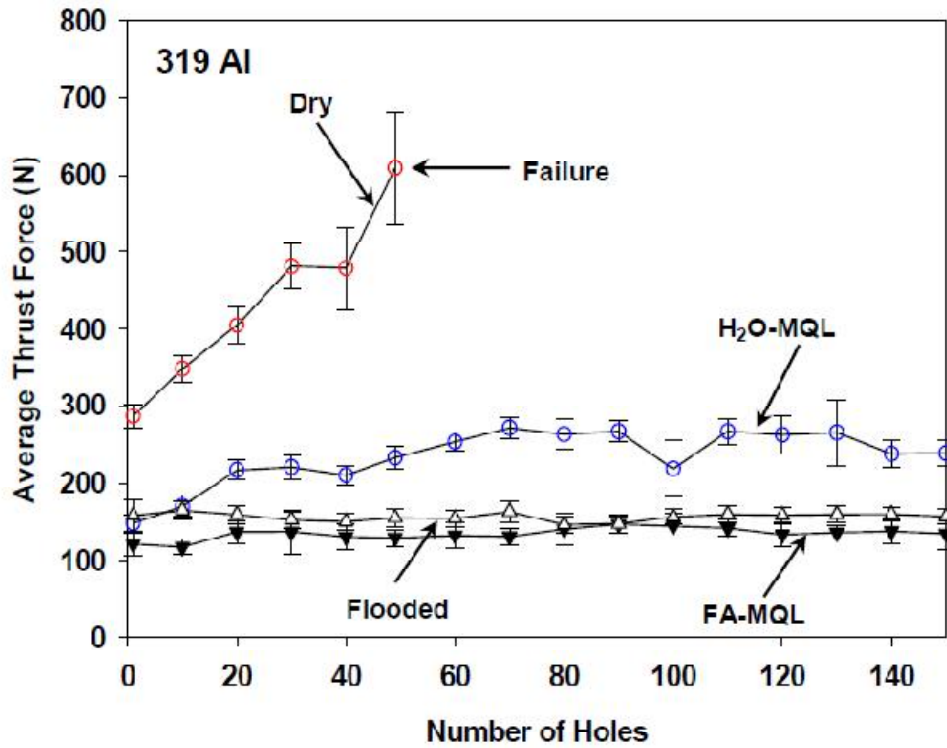
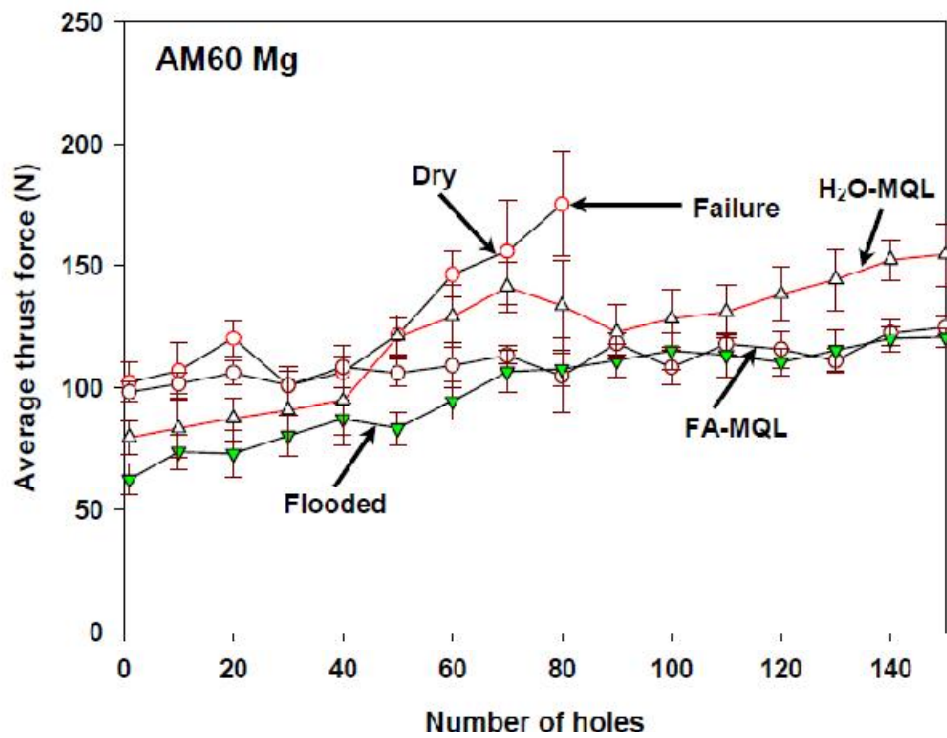


**Figure 7. 3** The cumulative mass of adhered aluminum and magnesium in dry and H<sub>2</sub>O-MQL, FA-MQL and flooded conditions.

During drilling with FA-MQL (**Fig. 7.2a**), an increase from 1.62 (1<sup>st</sup> hole) to 1.97 N-m (150<sup>th</sup> hole) was noted --a corresponding increase of 20%. The mass of adhered aluminum at the 150<sup>th</sup> hole was only  $1.9 \times 10^{-3}$  g (**Fig. 7.3**). The torque response using flooded cooling drilling was similar to FA-MQL drilling (**Fig. 7.2a**). The average torque increased from 1.69 N-m (1<sup>st</sup> hole) to 2.01 N-m (59<sup>th</sup> hole) by 19% and then decreased from 2.01 N-m (59<sup>th</sup> hole) to 1.71 N-m (150<sup>th</sup> hole). No torque spikes were observed among the 150 holes drilled. The mass of adhered aluminum measured after 150<sup>th</sup> hole was  $1.4 \times 10^{-3}$  g (**Fig. 7.3**).



(a)



(b)

**Figure 7. 4** The average thrust force responses of the first 49 holes for dry and first 150 holes for H<sub>2</sub>O-MQL, FA-MQL and flooded conditions for (a) 319 Al; (b) AM60 Mg.

### 7.3.1.2 Drilling of AM60 Mg

During dry drilling of AM60 Mg, the drill was stuck to the block while drilling the 78<sup>th</sup> hole (Figure 3b). The average torque, on the other hand, was also high and increased from 2.28 N-m (1<sup>st</sup> hole) to 9.32 N-m (78<sup>th</sup> hole), corresponding to an increase of 309%. The mass of magnesium after the drilling of 78<sup>th</sup> hole was  $389 \times 10^{-3}$  g (**Fig. 7.3**). A total of 58 holes, so that 73% of the total number of holes exhibited torque spikes.

During drilling with H<sub>2</sub>O-MQL, the average torque increased from 1.42 N-m in the 1<sup>st</sup> hole to 2.43 in the 150<sup>th</sup> hole (**Fig. 7.2b**), which is almost 4-folds lower compared to dry drilling. 37% of total holes exhibited torque spikes. The mass of adhered magnesium was found  $6.2 \times 10^{-3}$  g (**Fig. 7.3**).

During drilling using FA-MQL, a uniform torque response was observed through the entire range. The mass of adhered magnesium was very low at  $0.98 \times 10^{-3}$  g (**Fig. 7.3**). Only 5% of the 150 holes drilled exhibited torque spikes. The maximum torque never exceeded 2.00 N-m. From the average torque variation curves shown in **Fig. 7.2 (b)**, an increase from 2.27 (1<sup>st</sup> hole) to 2.55 N-m (150<sup>th</sup> hole) can be observed, i.e., as an increase of 12%, confirming a steady-state behaviour.

During drilling under flooded conditions, the average torque increased from 2.08 N-m (1<sup>st</sup> hole) to 2.75 N-m (150<sup>th</sup> hole) by 32%, as shown in **Fig. 7.2 (b)** and about 40% of total holes exhibited torque spikes.

These results indicate that MQL drilling of light weight alloys is as effective as the conventional flooded drilling. In fact the use of FA-MQL proved to be more advantageous than the flooded drilling in certain ways including as will be discussed in **Section 4**.



## 7.3.2. Analysis of Thrust Force Responses

### 7.3.2.1. Drilling of 319 Al

According to **Fig. 7.4 (a)** an increase in the average thrust force from 300 N at the 1<sup>st</sup> hole to 619 N at the 49<sup>th</sup> hole (drill failure) was recorded, corresponding to an increase of 106%. In general, thrust forces followed the same trends as the torque responses. A total of 21 holes (i.e., 43% of the 49 holes) exhibited thrust force spikes during drilling in dry condition. While drilling using H<sub>2</sub>O-MQL, the maximum thrust force recorded for 319 Al did not exceed 273 N. Only 12 holes exhibited thrust force spikes, i.e., 8% of the 150 holes, which was a drastic decrease compared to dry drilling for which 43% of 49 holes showed spikes. The average thrust force increased by 75% between the 1<sup>st</sup> hole (148 N) and the 150<sup>th</sup> hole (259 N) as shown in **Fig. 7.4 (a)**.

The thrust force variation from the first hole to the last was uniform during drilling using FA-MQL. Similar to the torque responses, no thrust force spike was observed. The average thrust force increased by 12% between the 1<sup>st</sup> hole (121 N) and the 150<sup>th</sup> hole (135 N) [**Fig. 7.4 (a)**].

While drilling in flooded condition, a slight increasing in the average thrust force was observed between the 1<sup>st</sup> hole and the 49<sup>th</sup> hole to 164 N, and then decreased slightly [**Fig. 7.4 (a)**]. Thus, a slightly lower average thrust force generation during drilling under flooded condition compared to FA- MQL occurred.

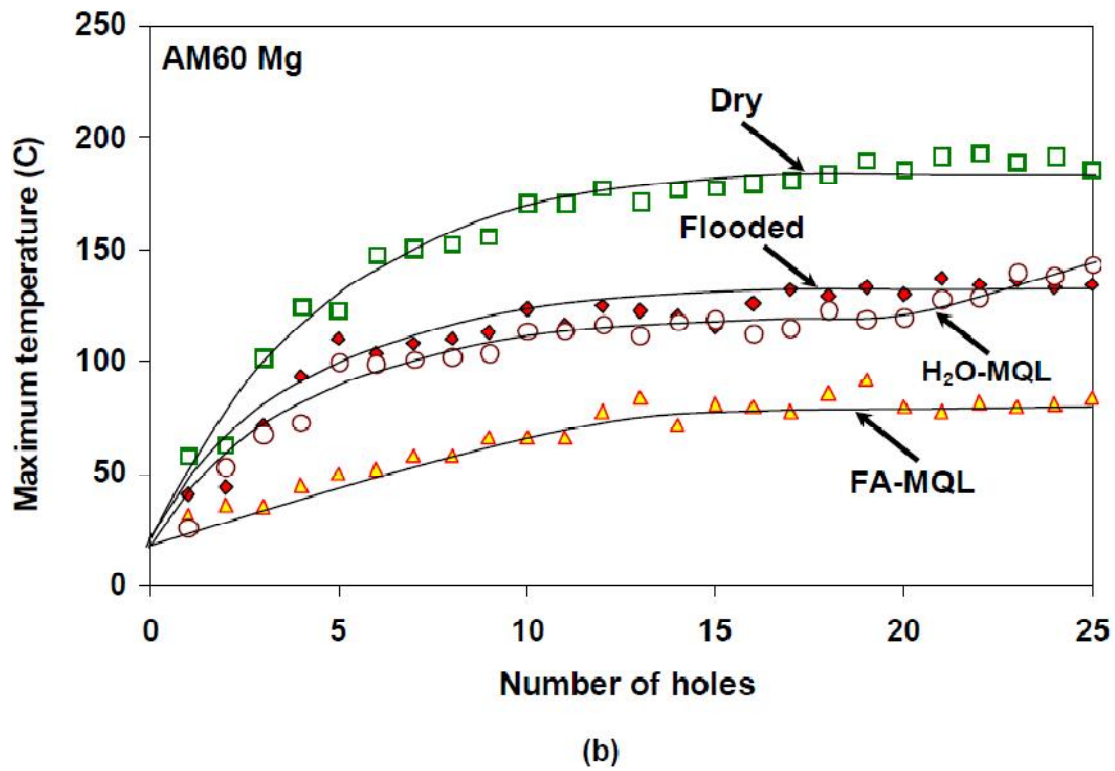
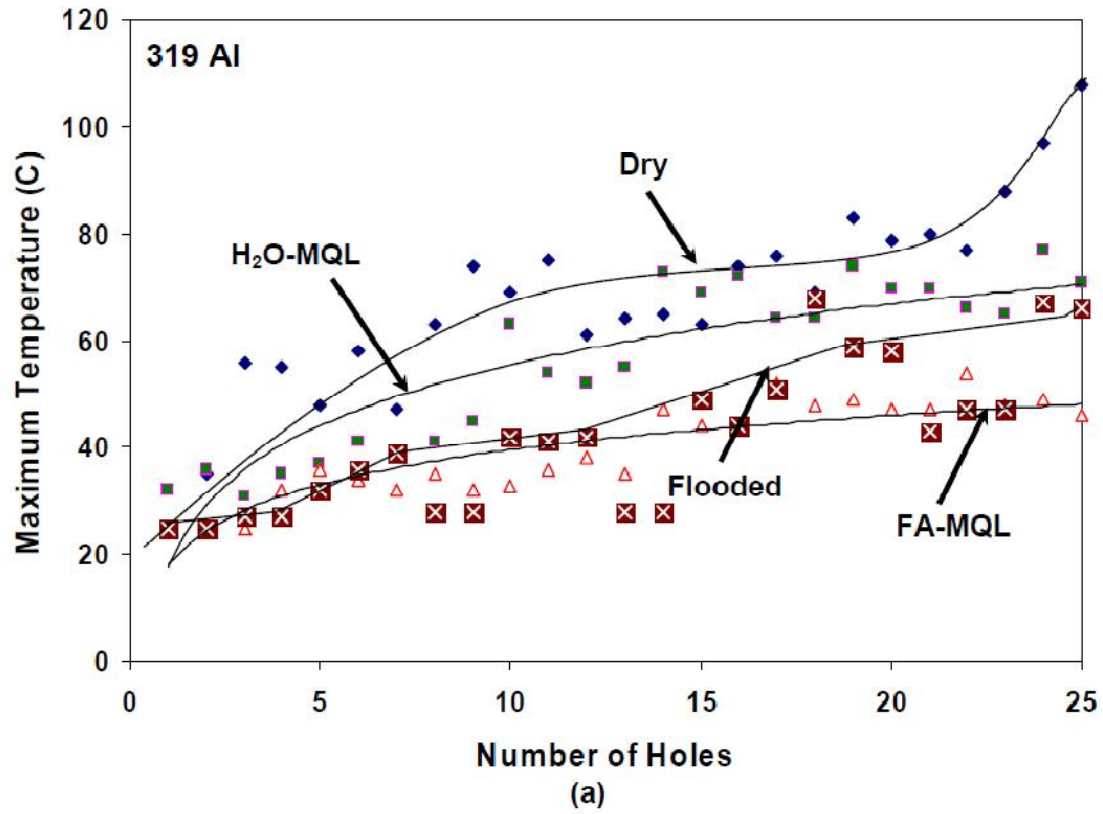


**Figure 7. 5** Maximum temperature variations for the first 25 holes during drilling in dry, FA-MQL, H<sub>2</sub>O-MQL and flooded conditions (a) 319 Al; (b) AM60 Mg.

### 7.3.2.2. Drilling of AM60 Mg

During drilling in dry condition, the average thrust force increased from 102 N for the 1<sup>st</sup> hole to 165 N at the 78<sup>th</sup> hole, corresponding to a total increase of 62% (**Fig. 7.4b**). 34% of the total hole exhibited thrust force spikes. During drilling in H<sub>2</sub>O-MQL, the thrust force increased by 93% between the 1<sup>st</sup> hole (80 N) and the 150<sup>th</sup> hole (154 N) (**Fig. 7.4b**). Using FA-MQL, the average thrust force increased only 14% between the 1<sup>st</sup> hole (98 N) and the 150<sup>th</sup> hole (112 N) (**Fig. 7.4b**). Compared to the FA-MQL, a steeper increase in average thrust forces was observed during drilling in flooded conditions (**Fig. 7.4b**). The average thrust force values for flooded conditions were low initially, i.e., 63 N in the 1<sup>st</sup> hole, but increased faster (92%) at the end of the drilling process. This analysis agrees with the average thrust force responses of H<sub>2</sub>O-MQL drilling, which increased at the same rate (93%).

### 7.3.3. Temperature Increase

**Fig. 7.5 (a)** shows the results of the maximum temperature variations with the number of holes in 319 Al for each drilling condition. The temperature reached 108 °C at the 25<sup>th</sup> hole during drilling in dry condition. However, in H<sub>2</sub>O-MQL, the temperature did not exceed 77 °C. During drilling using flooded coolant system, the maximum temperature was 64 °C (at the 18<sup>th</sup> hole). Overall flooded and FA-MQL conditions generated similar low temperature profile, with the apparently steady increase in temperature to 46 °C.

**Fig. 7.5 (b)** shows the results pertaining to the highest temperature rise during drilling in AM60. The temperature during dry drilling increased rapidly above 150 °C after the first 10 holes were drilled, although the rate of temperature increase decreased after that and reached 193

°C at the 25<sup>th</sup> hole. In H<sub>2</sub>O-MQL, the temperature profile was similar to dry drilling. The maximum temperature recorded was 134 °C at the end of the test. During the course of FA-MQL drilling an initial rapid temperature increase to 50 °C was observed, but the maximum temperature did not exceed 86 °C. During drilling in flooded conditions, the maximum temperature was higher compared to the measurements taken in FA-MQL.

#### 7.3.4. SEM Observation of Drill Flutes

The tested drills were analyzed using a scanning electron microscope (JEOL JSM- 5800LV SEM) to investigate aluminum chips that had adhered to the flute faces. **Fig. 7. 6 (a-d)** shows SEM micrographs of the drill flute morphologies during drilling in 319 Al. Drill flutes display extensive transfer of aluminum when using a HSS drill in dry conditions (**Fig. 7.6a**). The transfer of aluminum was also observed during drilling in H<sub>2</sub>O-MQL conditions (**Fig. 7.6 b**), but the amount of adhered aluminum was less. Even smaller amounts of aluminum transfer was observed in the drill flutes during drilling in FA- MQL condition as well as drilling done in flooded coolant system (**Fig. 7.6 [c-d]**). Similar observations were also noted for the AM60 Mg. Extensive magnesium adhesion onto the drill flutes under dry drilling conditions can be seen. The drill flute was entirely covered by the magnesium during drilling in dry conditions (**Fig. 7.6e**). The transfer of magnesium was also observed during drilling in FA-MQL, H<sub>2</sub>O-MQL, and flooded conditions (**Fig. 7.6 [f -h]**), but in much smaller quantities. Lowest amount of magnesium adhesion seemed to have occurred during FA- MQL drilling. These results imply that FA-MQL is effective to reduce the adhesion of aluminum and magnesium to the drill flutes.

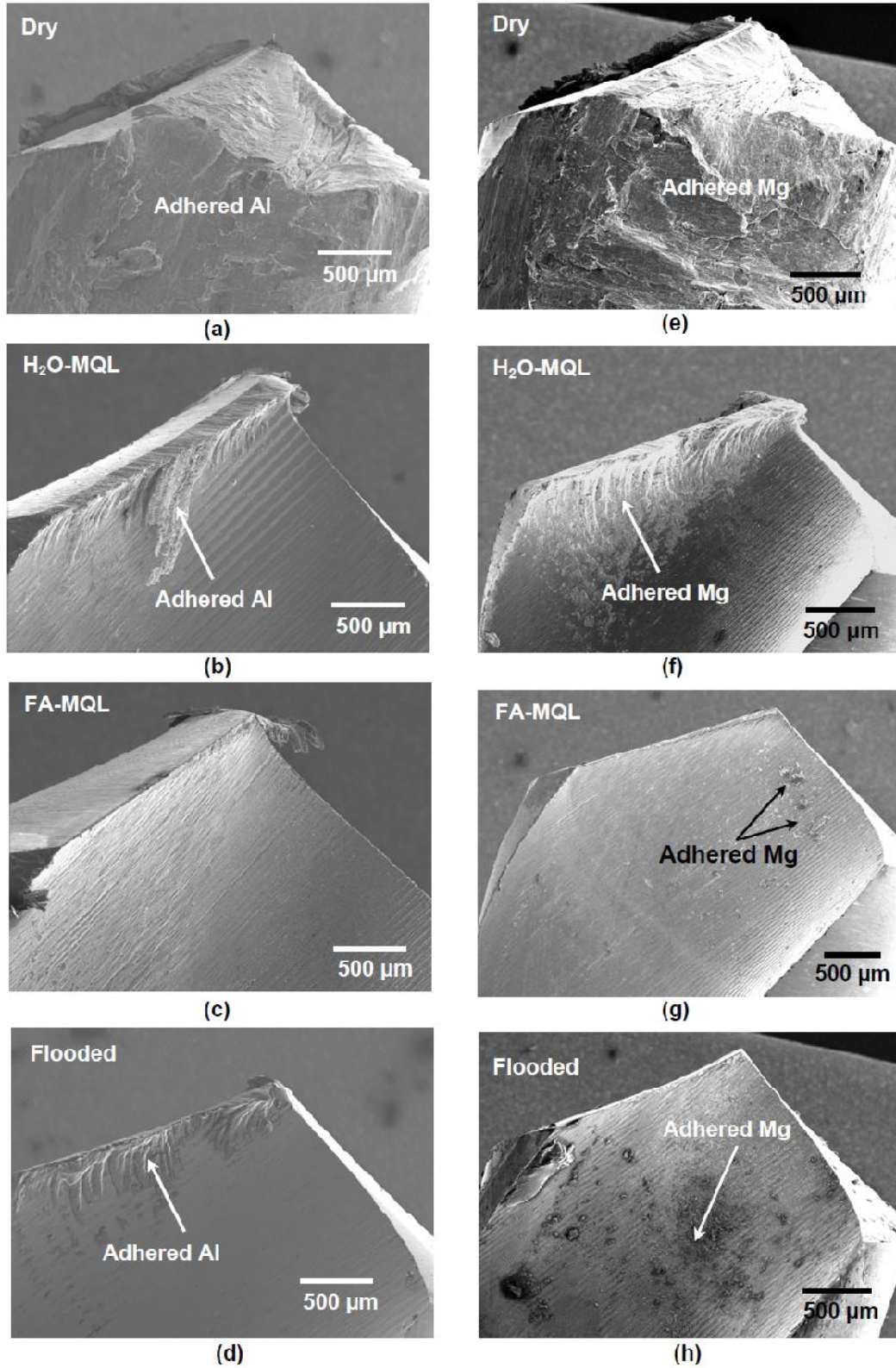


**Figure 7. 6** SEM secondary electron images showing aluminum and magnesium adhesion to drill flutes: (a, b, c, d) HSS drill in dry, H<sub>2</sub>O-MQL, FA-MQL and flooded conditions for 319 Al; (e, f, g, h) HSS drill in dry, H<sub>2</sub>O-MQL, FA-MQL and flooded conditions for AM60 Mg.

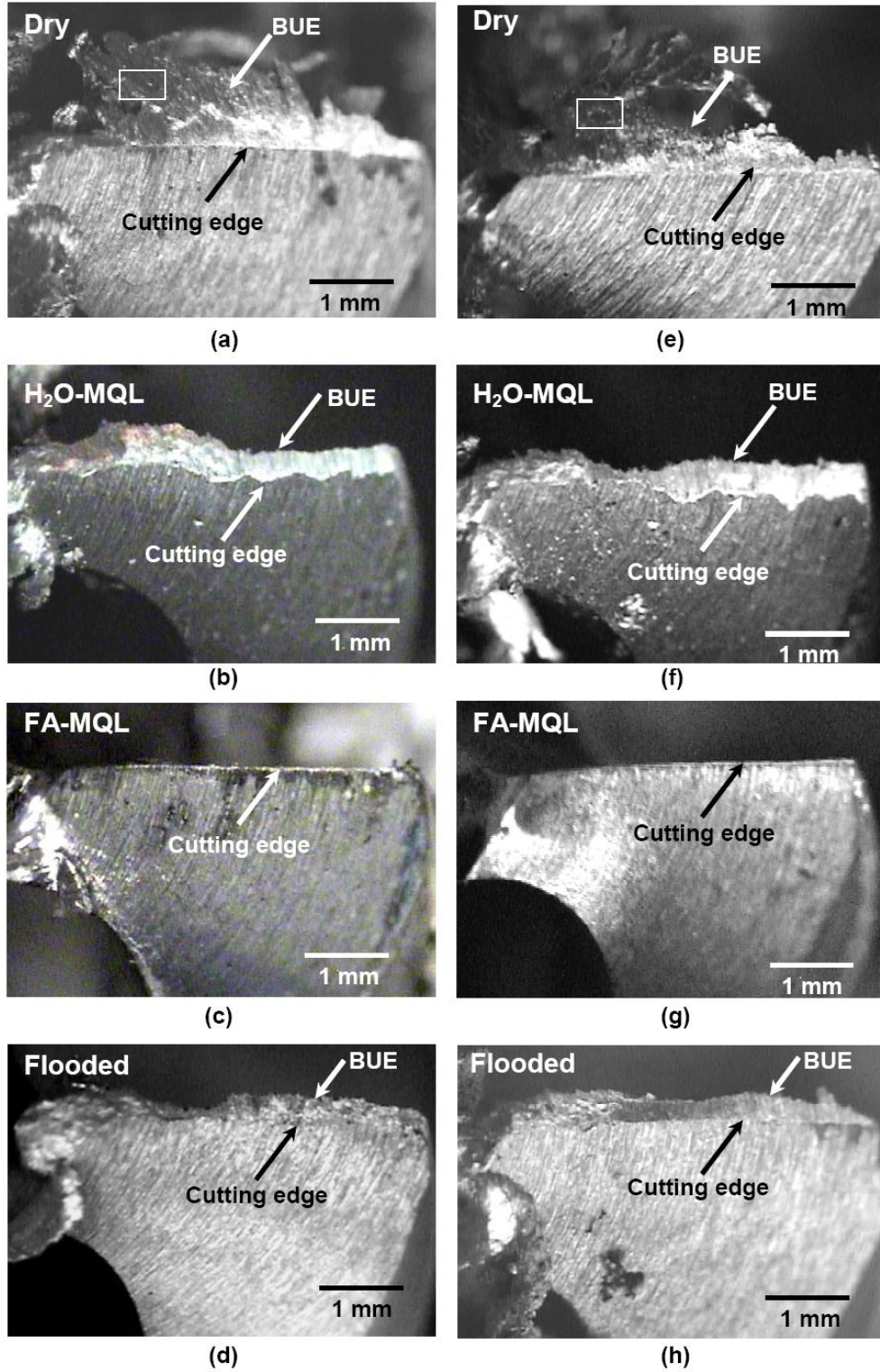


**Figure 7. 7** Optical micrographs of cutting edge after drilling of 319 Al in (a) dry; (b) H<sub>2</sub>O-MQL; (c) FA-MQL; (d) flooded conditions. Optical micrographs of cutting edge after drilling of AM60 Mg in (e) dry; (f) H<sub>2</sub>O-MQL; (g) FA-MQL; (h) flooded conditions.

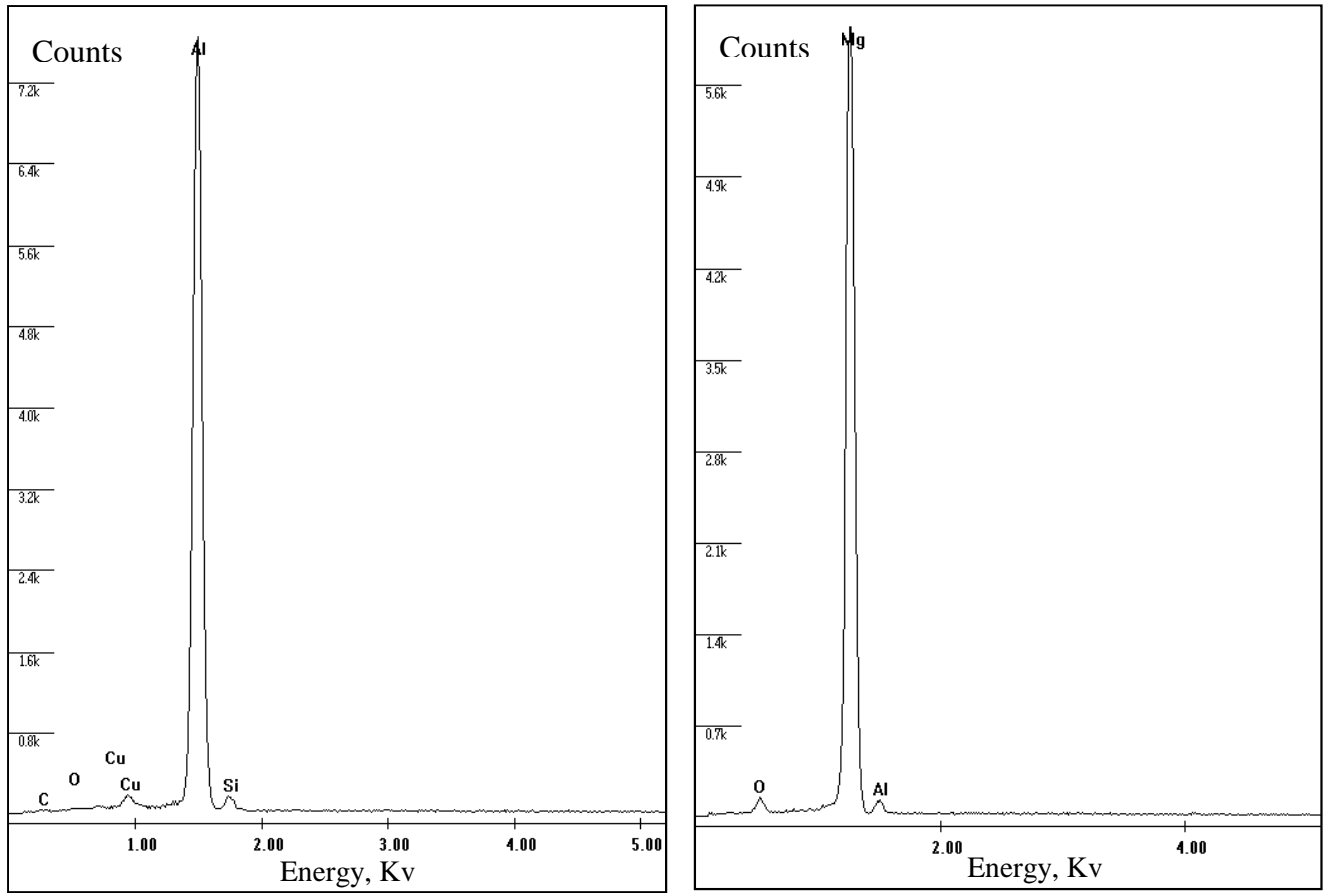


**Figure 7. 8** The EDS spectra of inset in plate Figure 7.7 (a) and 7.7 (b) showing (a) the BUE was composed of Al and other alloying elements during drilling of 319 Al; (b) the BUE was composed of Mg, O and Al in drilling of AM60.

### 7.3.5. Analysis of BUE Formation

**Figs. 7.7 (a-d)** show the cutting edge of the drill after 49<sup>th</sup> and 150<sup>th</sup> holes in dry, H<sub>2</sub>O-MQL, FA-MQL and flooded conditions using low magnification optical images after drilling 319 Al. Adhered 319 Al pieces can be seen on the drill tips in all cases. A relatively thick BUE is formed along the cutting edge of the HSS drill in dry condition (**Fig. 7.7 (a)**), and the drills in H<sub>2</sub>O-MQL and flooded condition also exhibited a BUE (**Figs 7. 7 (b, e)**) --but not as thick as those found in dry condition. **Fig. 7.7 (c)** shows the drill in FA-MQL with fresh cutting edge revealing no significant aluminum smearing when compared to the drills in other conditions. The EDS analysis confirmed that the BUE was composed of Al and O (**Fig. 7.8 a**).

**Figs 7.7 (e-h)** are the optical images of the drill cutting edge in dry (after 78 holes), H<sub>2</sub>O-MQL (after 150 holes), FA-MQL (after 150 holes) and flooded conditions (after 150 holes) after drilling of AM60 Mg, respectively. Similarly to 319 Al, a thick BUE was observed in dry condition compared to other conditions. The EDS analysis confirmed that the BUE was composed of Mg and O (**Fig. 7.8 b**). FA-MQL appeared to have fresh cutting edge after drilling 150 holes (**Fig. 7.7 (c)**).

## 7.4. Discussion

During dry drilling in 319 Al, the drill failed due to adhesion of aluminum while drilling the 49<sup>th</sup> hole and could not be retrieved. However, in H<sub>2</sub>O-MQL no significant aluminum adhesion was noted even after drilling the 150<sup>th</sup> hole. The torque data obtained during H<sub>2</sub>O-MQL drilling



suggested several improvements over dry drilling, characterized by a reduction in the maximum and the average torque and thrust force values. During drilling in FA-MQL, almost constant torque and thrust force values were recorded through the entire range of drilling cycle (**Fig. 7.2 [a, b]**). During drilling using flooded coolant, the average torque increased from 1<sup>st</sup> hole to 59<sup>th</sup> hole and then started to decrease implying that the flooded coolant diminished the adhesion of aluminum. Thus, FA- MQL drilling is equally effective as the flooded coolant. The average values of torque and thrust force using FA-MQL are comparable to flooded coolant system, indicating the feasibility of MQL in drilling Al-Si alloys in this way.

Similar to 319 Al, the drill became failed due to the extensive adhesion of magnesium to the drills. H<sub>2</sub>O-MQL showed better performance to reduce the average torque from 309% to 71% when compared to dry drilling. However, H<sub>2</sub>O-MQL did not show any adequate performance to reduce the average thrust force compared to dry drilling. Accordingly, H<sub>2</sub>O-MQL is more effective to reduce the adhesion of magnesium to the drill flutes than the adhesion of magnesium to the cutting edge. Similar to the drilling in 319 Al, FA-MQL showed a stable average torque and thrust force responses through the drilling experiments. During drilling in AM60 Mg, conventional flooded coolant did not show better effectiveness in either average torque or average thrust force compared to FA-MQL.

It was noted that the use of FA-MQL led to several improvements, compared to H<sub>2</sub>O-MQL and flooded drilling for both 319 Al and AM60 Mg. This improved drilling performance using FA-MQL can be attributed to the formation of phosphorous (P) and sulphur (S) containing layers on the tool surface. The electron diffraction spectroscopy (EDS) analyses performed on the drills examined after the tests provided evidence of the existence of elements like P and S on the drill surfaces used for drilling under FA-MQL conditions but not on the drills tested under other

conditions [Bhowmick et al. 2010]. Evidence of the presence of P and S on the surface of the drill used in FA-MQL drilling suggests that a lubricating layer enriched with these elements may have formed. A layer composed of P and S is usually indicative of the presence of extreme pressure additives, used to provide protection against high-pressure metal-to-metal contacts in tribological applications [Rahman et al., 2002; Trent and Wright, 2000]. It was suggested that these layers are formed by the physical adsorption of the additives within a temperature range that reached 120 °C. When the temperature generated during FA-MQL drilling reached about 86 °C, it is possible that the layers formed in this way. The salient point, however, is that the effectiveness of the FA-MQL drilling may be due to the formation of a protective layer consisting of extreme pressure additives, which significantly reduces the tendency to adhere, and tending towards a stable torque and thrust force responses.

## 7.5. Conclusion

- [1] The dry drilling of 319 Al and AM60 Mg can not be considered as a feasible process because the drills failed when drilling between 50-100 holes. In both cases the drill failure was the result of extensive adhesion of aluminum or magnesium.
- [2] Significant reductions in average torques and thrust forces were observed during drilling by H<sub>2</sub>O-MQL for 319 Al compared to dry drilling. The average torque of AM60 Mg while drilling using H<sub>2</sub>O-MQL was also reduced greatly but not the thrust force.
- [3] Drilling in the presence of FA- MQL required lower torques and thrust forces compared to H<sub>2</sub>O-MQL and flooded drilling of both 319 Al and AM60 Mg. Almost similar drilling performances were observed for both 319 Al and AM60 Mg when FA- MQL agent was used.
- [4] The highest temperature was generated during drilling under dry conditions for both alloys. FA- MQL reduced the temperature generation more effectively than the H<sub>2</sub>O-MQL and flooded conditions.
- [5] The smallest amount of aluminum adhesion to the drill flutes occurred in FA- MQL drilling for both alloys.
- [6] Overall, FA-MQL showed strong potential to be considered as the preferred drilling processes for drilling cast aluminum and magnesium alloys as similar performances to flooded drilling were observed for each case.

## List of References

- Weinert, K.; Inasaki, I.; Sutherland, J.W.; Wakabayashi, T.; "Dry machining and minimum quantity of lubrication"; CIRP Annals- Manufacturing Technology, 53 (2004) pp. 511-537.
- Bhowmick, S.; Alpas, A.T.; "The performance of hydrogenated and non-hydrogenated diamond-like carbon tool coatings during the dry drilling of 319 Al"; International Journal of Machine Tools and Manufacture, 48/7-8 (2008) pp. 802-814.
- Klocke, F.; Beck, T.; Eisenblatter, G.; Fritsch, R.; Lung, D.; Pohls, M.; "Application of minimal quantity of lubrication (MQL) in cutting and grinding"; In: Proceeding of the 12th International Colloquium Industrial and Automotive Lubrification, Technische Akademie, Esslingen, 11–13.
- Davim, J.P.; Sreejith, P.S.; Gomes, R.; Peixoto, C.; "Experimental studies on drilling of aluminum (AA1050) under dry, minimum quantity of lubricant, and flood-lubricated conditions"; Proc. IMechE Part B: J. Engineering Manufacture, 220/10 (2006) pp. 1605-1611.
- Bardetsky, A.; Attia, H.; Elbestawi, M.; "Evaluating of tool wear suppressive ability of lubricants used in minimum quantity of lubrication application in high speed machining of cast aluminum alloys"; Proceedings of ASME International Mechanical Engineering Congress and Exposition IMECE 80597 (2005) pp. 1-7.
- Kelly, J.F.; Cotterell, M.G.; "Minimal lubrication machining of aluminum alloys"; Journal of Materials Processing Technology, 120/1 (2002) pp. 327-334.
- Braga, D.U.; Diniz, A.E.; Miranda, G.W.A.; Coppini, N.L.; "Using a minimum quantity of lubricant (MQL) and a diamond coated tool in the drilling of aluminum–silicon alloys"; Journal of Materials Processing Technology, 122/1 (2002) pp. 127-138.
- Bhowmick, S.; Alpas, A.T.; "Minimum quantity lubrication drilling of aluminum–silicon alloys in water using diamond like carbon coated drills"; International Journal of Machine Tools & Manufacture, 48/12-13 (2008) pp. 1429-1443.
- Bhowmick, S.; Lukitsch, M.J.; Alpas, A.T.; "Dry and minimum quantity lubrication drilling of cast magnesium alloy (AM60)"; International Journal of Machine Tools & Manufacture, 50/5 (2010) pp. 444-457.
- Rahman, M.; Kumar, A.S.; Salam, M.U.; "Experimental evaluation on the effect of minimal quantities of lubricant in milling"; International Journal of Machine Tools & Manufacture, 42 (2002) pp. 539-547.
- Trent, E.; Wright, P.; "Metal cutting"; Butterworth–Heinemann Publications, London, 4th ed. p. 328.

## CHAPTER 8

### General Discussions

The objective of this work was to assess whether minimum quantity lubrication (MQL) machining, i.e. drilling and tapping of aluminum and magnesium alloys using very low quantities of cutting fluids typically less than 50 ml/h could demonstrate a comparable performance to conventional flooded conditions. Another objective was to understand whether the use of carbon based coatings would improve the machining performance of these alloys. A key performance limiting issue was adhesion of aluminum and magnesium to the cutting tools. An experimental drilling station with an MQL system was built to measure torque and thrust force responses. Uncoated and diamond- like carbon (DLC) coated HSS drills were tested against 319 Al and AZ91 alloys using 10-50 ml/h of distilled water (H<sub>2</sub>O-MQL) and a fatty acid based MQL agent (FA-MQL). DLC coatings were chosen because they showed low COF and low aluminum and magnesium adhesion --especially non-hydrogenated DLC's (NH-DLC) at high levels of relative humidity and in water --during tribological tests. The aluminum and magnesium alloys that were selected as model workpiece materials are the lightweight alloys favoured by the transportation industry.

The results indicated that H<sub>2</sub>O-MQL used in conjunction with NH-DLC coatings reduced the average torque and thrust force compared to dry cutting and achieved a performance comparable with conventional flooded drilling under the speed of 2500 rpm and feed rate of 0.25 mm/rev. The average torque decreased by 88% for 319 Al and 150% for AZ91 when compared to the drilling in dry conditions using uncoated HSS. At least 10<sup>3</sup> holes could be drilled using NH-DLC in H<sub>2</sub>O-MQL and uncoated HSS in FA-MQL in drilling of both 319 Al and AZ91. MQL drilling provided a stable drilling performance, which was evident from the uniform torque and force

patterns throughout the drilling cycles and also resulted in desirable machining characteristic, including a smooth hole surface and short chip segments. In this section the observed machining behaviour, namely the metallurgical and tribological factors responsible for adhesion, temperature increase and the role of MQL fluid were discussed.

### **8.1. Adhesion of Al to the tools and role of COF**

The experimental results presented in **Chapter 3** and **4** have clearly demonstrated an enhancement in the dry drilling and tapping performance of 319 aluminum alloys using DLC coated tools, in comparison to uncoated HSS tools. In addition to prolonging the tool life, reductions in average and maximum torques were evident. These results are in agreement with the tribological test results on DLC against 319 Al, which indicated the much smaller tendency of aluminum to adhere to the DLC surface, compared to uncoated steel as noted by Refs. [8.1-8.4]. Thus, a more thorough understanding of the effect of DLC coatings against 319 Al can be gained from the examination of the COF values obtained using the pin-on-disk test. As shown in Fig. 8.1 (a), the average COF for DLC coatings tested against 319 Al had a low value of  $0.20 \pm 0.12$  in ambient air, whereas the average COF of uncoated HSS was  $0.63 \pm 0.10$ . The frictional temperature increase due to sliding between two contacting solids pressed together by a normal force  $F$ , sliding at a relative velocity  $v$  depends on the COF  $\mu$  between the surfaces in contact [8.5]. The heat generated  $q$ , per unit of nominal contact area  $A_n$ , per second can be expressed as follows:

$$q = \frac{\mu F v}{A_n} \quad (1)$$

The temperature  $T_b$ , at the contacting (e.g., tool-chip) interface--as a result of injection of the frictional heating across  $A_n$ --is related to the heat flux  $J$  through the thermal conductivity of aluminum  $K$  as shown below:

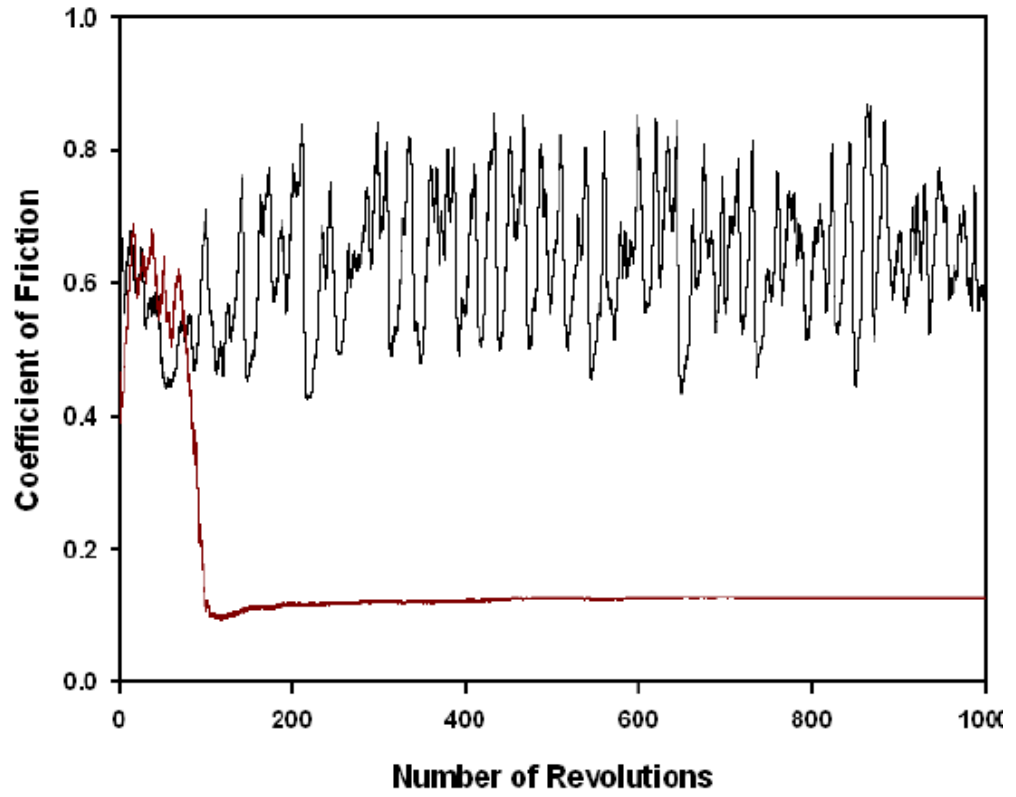
$$J = K \left( \frac{T_b - T_0}{L} \right) \quad (2)$$

where  $T_0$  is the ambient temperature and  $L$  is the equivalent linear heat diffusion distance as defined in Lim and Ashby [8.5]. From Equations (1) and (2), the COF  $\mu$  between the contacting surfaces is:

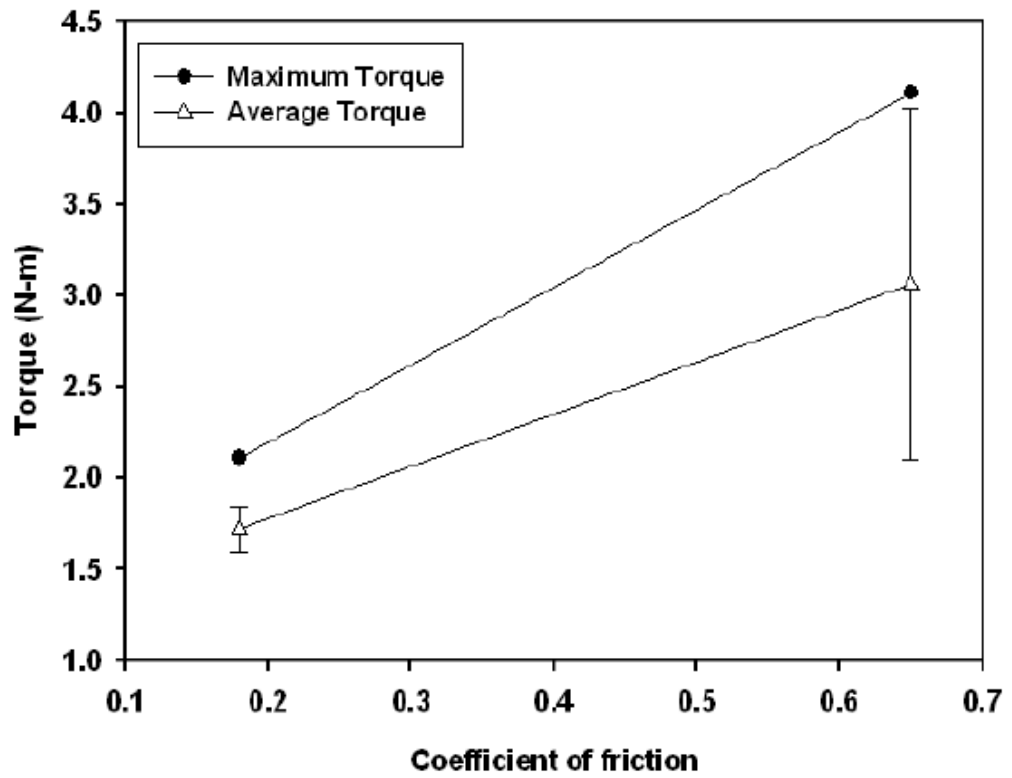
$$\mu = \frac{KA_n}{FvL} (T_b - T_0) \quad (3)$$

Using Equation 3, the COF can be correlated to the temperature generated during drilling and tapping. This is done in Fig. 8.1 (b, c), which shows a linear relationship between the sliding induced COF and the maximum drilling and tapping torque and temperature, as well as the average torque and temperature. A low COF between the tool and the workpiece materials restricts the contact surface temperature increase to low values, thus limiting aluminum adhesion to the tool in the case of dry drilling and tapping. The high COF between the 319Al and HSS surfaces in dry contact would lead to softening of aluminum (see Section 8.2) due to high temperature increase, promoting adhesion.

(a)



(b)





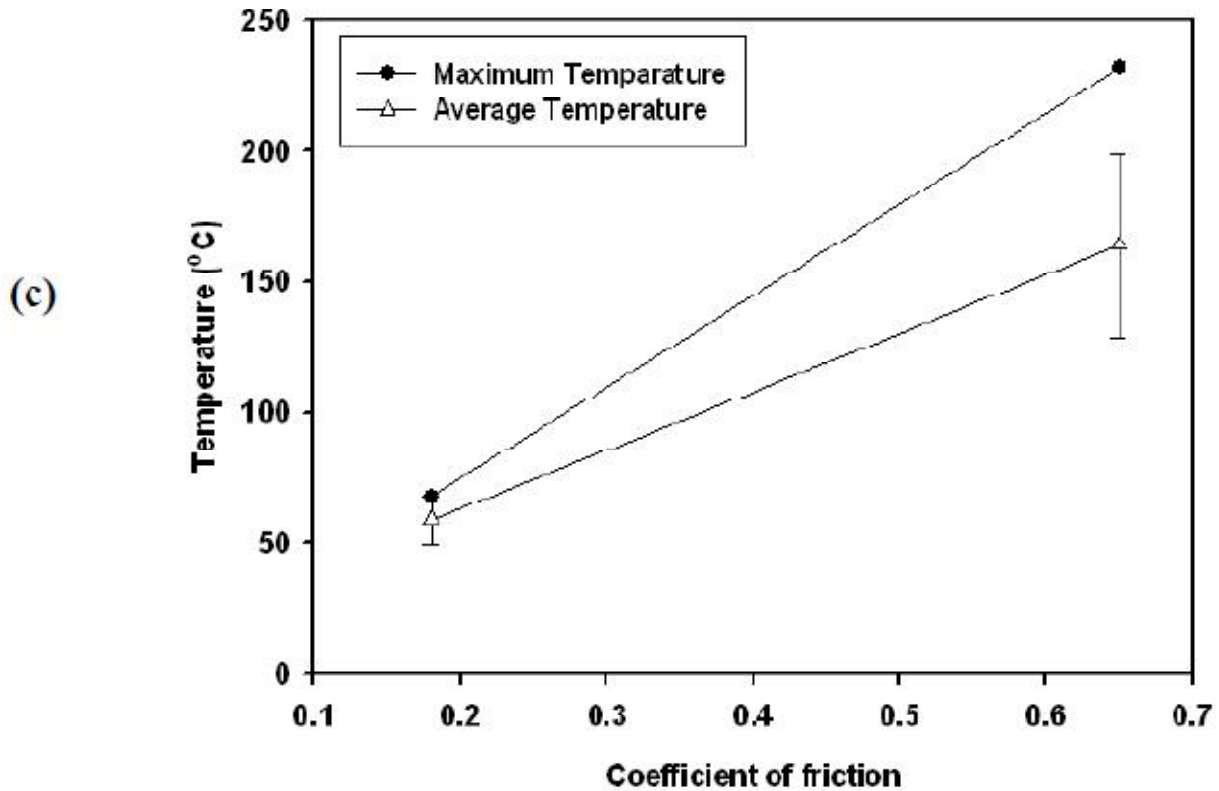


**Figure 8. 1** (a) COF vs. number of revolutions during pin-on-disk tests, where a 319 Al pin was sliding against DLC coated disk. (b) COF plotted against the maximum and average torque; (c) COF plotted against the maximum and average temperatures. The tests were done at the speed of 0.12 m/sec and at the load of 5 N.

## 8.2.The role of Subsurface Softening on Adhesion of Workpiece Materials to the Tools

It is well established that metal removal fluids facilitate removal of the chips and provide lubrication to the tool workpiece interface, thereby reducing the cutting temperature. Consequently, workpiece microstructures developed near the drilled holes during dry, H<sub>2</sub>O-MQL and flooded drilling are expected to be different. The high cutting temperatures generated during dry drilling of the 319 Al and AM60 Mg reduced the hardness of the material causing excessive adhesion of softer aluminum and magnesium to the drills, and

ensuring rapid drill failure. The effect that frictional contact-induced heating has on aluminum and magnesium softening during drilling can be determined from an examination of the hardness profiles of the material layers immediately beneath the holes. The generation of high cutting temperatures during dry drilling of the 319 Al and AM60 Mg was evident in **Chapter 7**. Another attempt has been taken to measure the drill-workpiece interface temperature. A K- type thermocouple was inserted at the 1.5 mm away from the bottom of the hole as shown in [Fig. 8.2](#). The drill workpiece interface temperature for both 319 Al and AM60 Mg is shown in [Fig. 8.2 \(b, c\)](#). The maximum temperature of 306 and 450 °C was observed for 319 Al and AM60 Mg alloy in dry condition, which is expected to reduce the hardness of the material and as the softer material would promote adhesion to the drills, rapid drill failure will occur. A more detailed understanding of the effect of drilling induced heating on the materials softening behaviour can be gained by examining the hardness profiles of the material located under the drilled holes. For this purposes, Vickers microhardness indentations were made ([Fig. 8.3](#)) starting from the edge of the drilled surface at intervals of 10 µm in a direction normal to this surface until a depth was reached at approximately 115 µm below the surface, where the hardness of the bulk material was attained. The microhardness gradients obtained in this way are shown in [Fig. 8.3 \(b, c\)](#), where it can be seen that after dry drilling the aluminum and magnesium hardness in the region within 5-90 µm below the hole surface was about  $49 \pm 2$  HV and  $32 \pm 2$  HV, i.e., 27% and 36% lower than the bulk hardness of 319 Al ( $67.0 \pm 8.0$  HV) and AM60 Mg ( $50.2 \pm 6.1$  HV). Clearly, temperatures generated during drilling of 319 Al using FA-MQL and flooded conditions were lower than those generated during dry drilling and did not exceed 122 °C and 111 °C ([Fig. 8.3c](#)) respectively. Similarly, the maximum drill workpiece interface

temperature for AM60 Mg was as high as 440 °C, while the temperature did not exceed 147 and 142 °C for FA-MQL and flooded conditions. The corresponding microhardness profiles obtained after FA-MQL and flooded drilling were characterized by an increase towards the hole surface; for FA-MQL drilling revealed a 5% and 26% increase for 319 Al and AM60 Mg and for flooded drilling a 10% and 34% increase compared to bulk hardness were noted. Thus, in these cases the temperature generation was not sufficient to cause softening, on the contrary drilling induced hardening of the material layers adjacent to drilled holes. Softened aluminum and magnesium promoted adhesion to the tools resulted in the formation of a built-up edge (BUE) and consequently high torques and thrust forces were generated (Chapter 5 and 6).

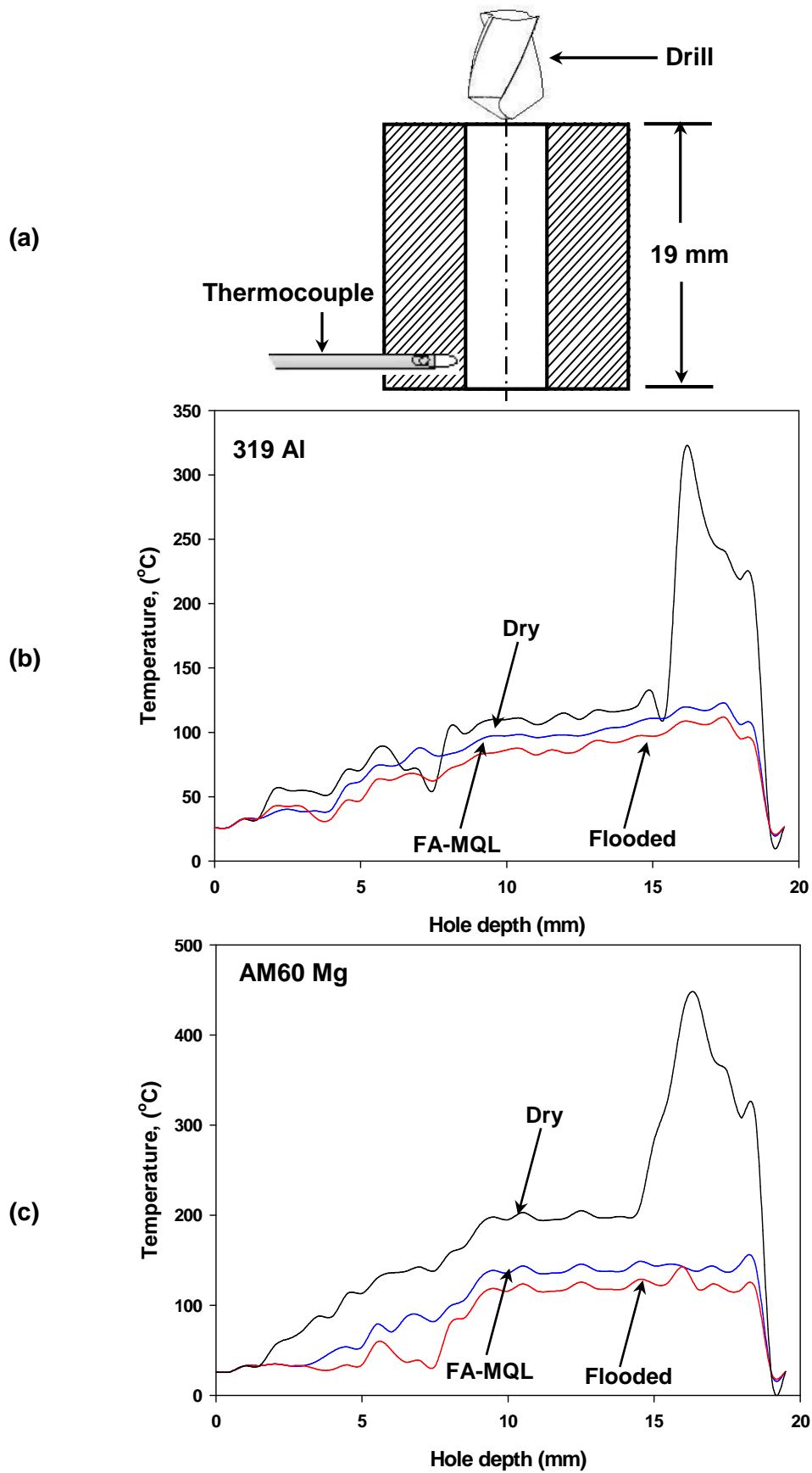
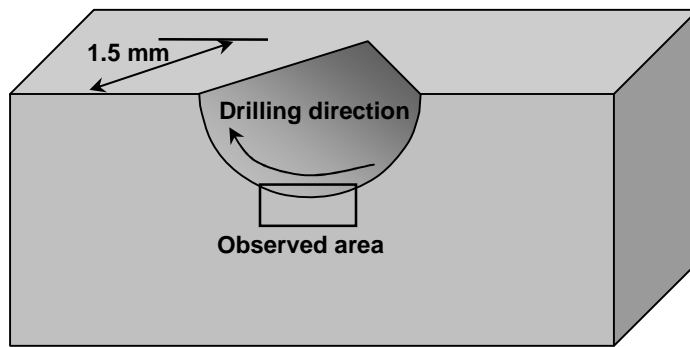
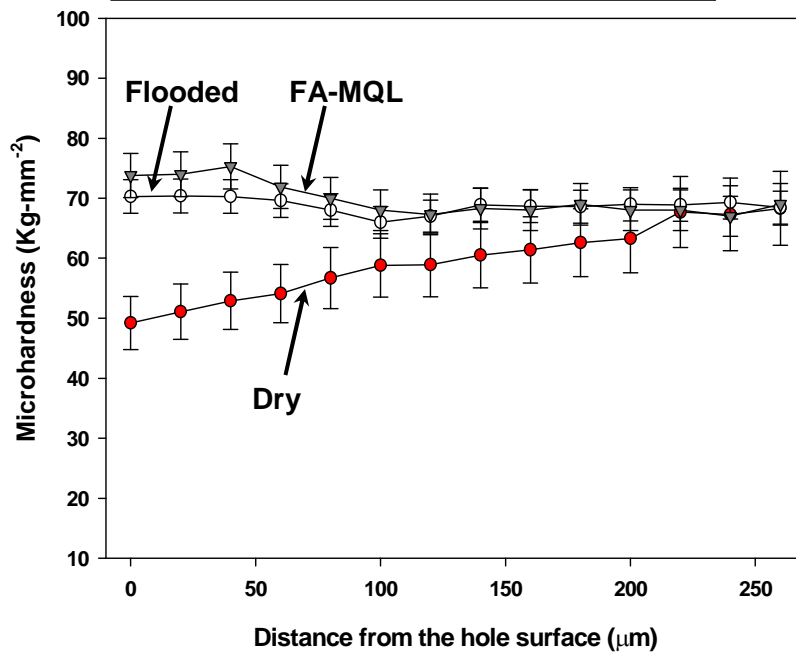


**Figure 8. 2** (a) Schematic diagram of the hole with the inserted thermocouple. Temperature responses in dry, H<sub>2</sub>O-MQL and flooded conditions for (b) 319 Al and (c) AM60 Mg.

(a)



(b)



(c)

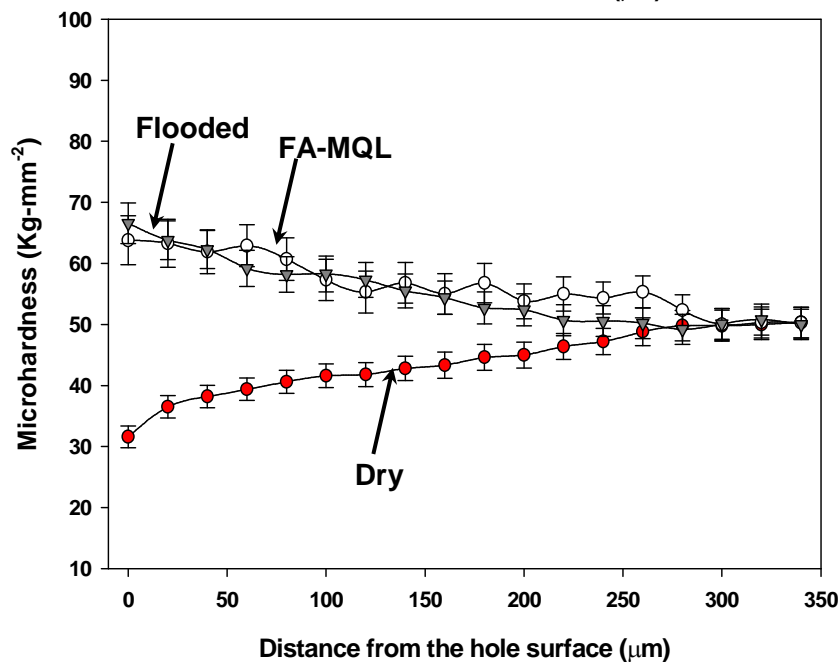
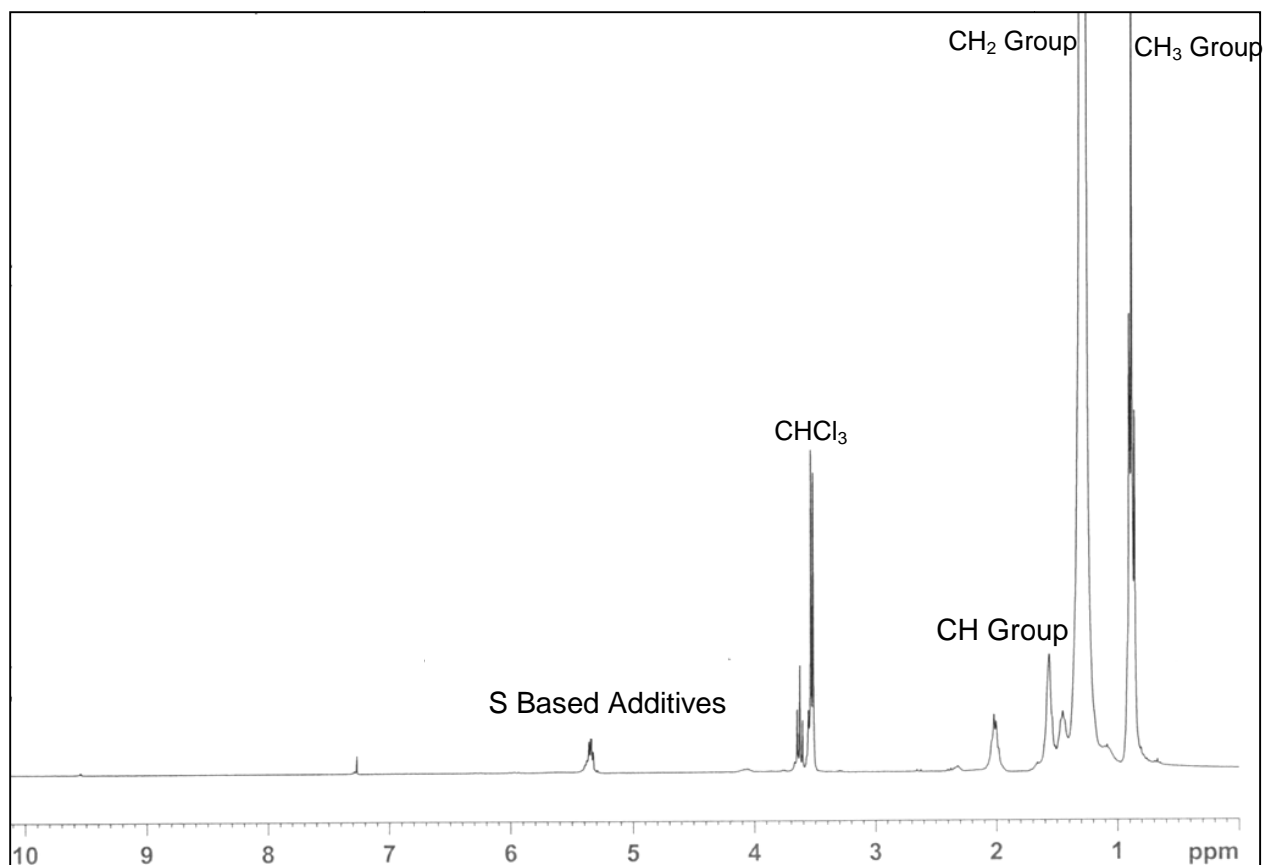


**Figure 8. 3** (a) Schematic diagram of a quarter section of a drilled hole showing the plane (mid-section of the hole parallel to the workpiece surface) where microhardness indentations were made. Average hole sub-surface hardness variations with increasing the depth from the hole surface for dry, FA-MQL and flooded conditions (b) 319 Al and (c) AM60 Mg.

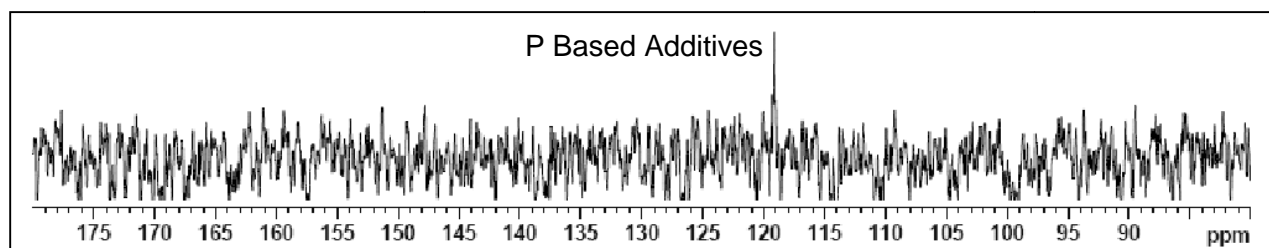
### **8.3. Role of MQL Fluid in Reducing Al and Mg Adhesion to the Tools**

It was noted in **Chapter 4** and **5** that the use of FA-MQL agent led to several key improvements compared to H<sub>2</sub>O-MQL and flooded drilling and tapping of AM60 and 319 Al. Enhanced drilling and tapping performances using FA-MQL can be attributed to the presence of extreme pressure additives in the MQL agent containing S and P. The presence of these elements in the MQL agent was confirmed by NMR tests (**Fig. 8.4**), as well as electron diffraction spectroscopy (EDS) analyses (**Chapter 4**). It has been noted that the formation of protective layers by adsorption occurs at temperatures up to 120 °C. Results of DSC analyses performed to evaluate the thermal stability of MQL and conventional (flooded) tap oil are represented in **Fig. 8.5**. The two exothermic peaks starting at 140 °C for conventional tap oil (mineral oil-MO) in **Fig. 8.5 (a)** arise as a result of the thermal decomposition of hydrocarbon molecules in the tap oil [6]. For FA-MQL, the first exothermic peak was observed at 206 °C (**Fig. 8.5b**), indicating the high thermal stability of FA-MQL. As reported in **Chapter 6**, the temperature generated during FA-MQL tapping was about 55 °C. Similarly, the temperature did not exceed 48 °C during flooded tapping, suggesting that the decomposition of tap oil during flooded tapping is unlikely. During MO-MQL tapping, however, the temperature exceeded 120 °C (**Chapter 4**) and reached a temperature nearly equal to the decomposition temperature of MO tap oil. This led to an interpretation of the effectiveness of FA-MQL in maintaining stable and low torque values and providing an equal performance compared to flooded tapping conditions--based of the stability of the FA-MQL agent during the tapping operation. The build up of a protective layer of those additives prevents direct contact between the interacting surfaces of the workpiece material and the tool surface, which minimizes aluminum and magnesium adhesion. The protective layers can

be formed either by the physical adsorption of the additives, or by the chemical reaction between the metal surface and the additives.



(a)



(b)

**Figure 8. 4** NMR analysis of MQL showing (a) the presence of S-based additives and (b) the presence of P-based additives. A proton NMR (<sup>1</sup>H) in CHCl<sub>3</sub> environment was chosen to identify the additives in MQL agent.

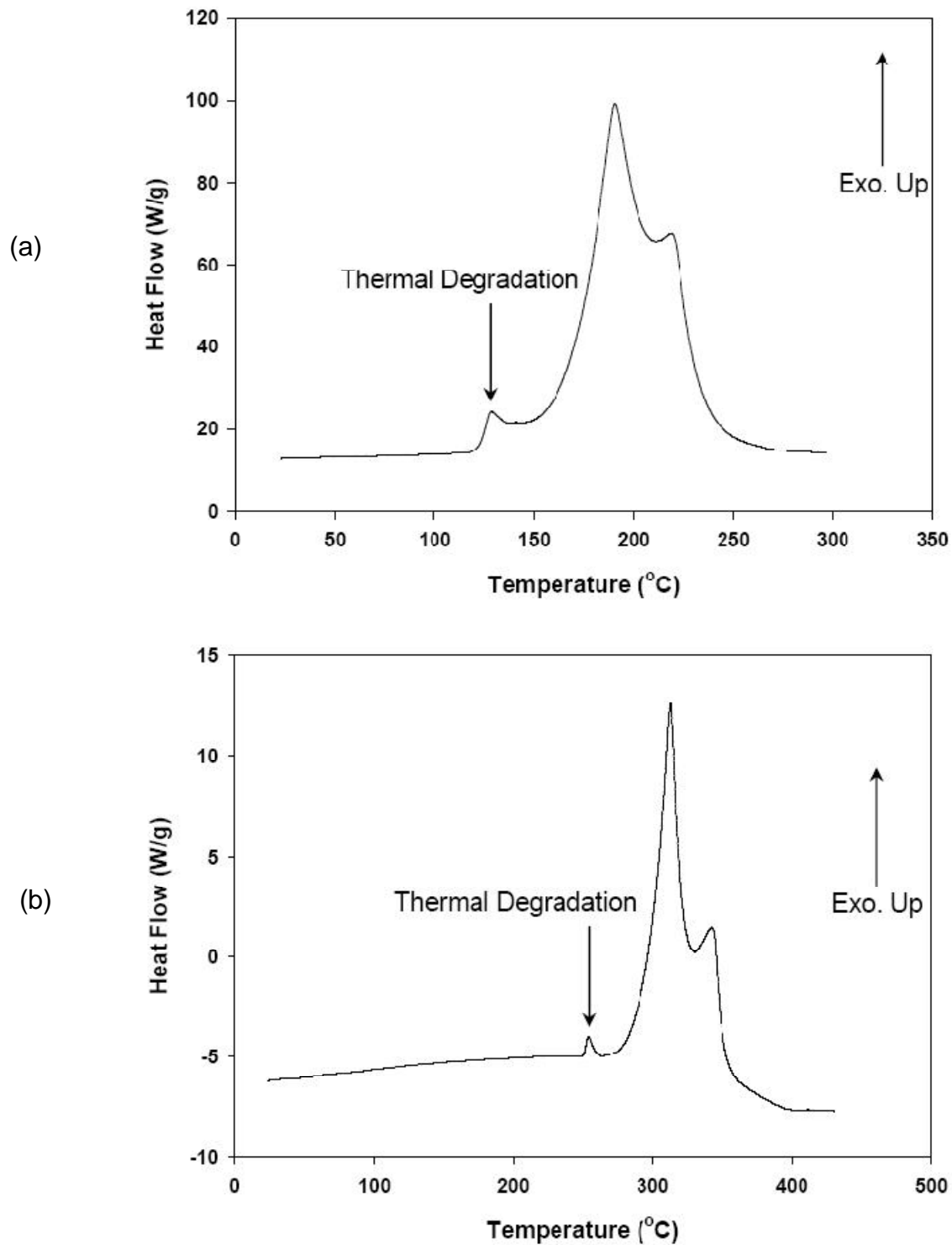


**Figure 8. 5** DSC spectra for (a) conventional flooded tap oil and (b) MQL. Thermal analysis was performed using a DSC-TGA Q600 manufactured by TA Instrument at a heating rate of 10 °C/min. Argon gas was used to prevent oxidation of the samples. After heating, nitrogen-cooling was used for all runs. Exothermic peak reveals the thermal degradation of lubricants.



## **8.4 Comparison of Dry Drilling Behaviour of Aluminum and Magnesium using DLC**

### **Coated Drills**

It is noted that there is a clear contrast to the longer tool life and low torques observed when the same NH-DLC coated drills were used in the dry drilling of cast aluminum alloy 319 Al, for which tool life was prolonged by at least a factor of 3 compared to the uncoated HSS drills [8.7]. The reasons for this difference are the drilling induced temperature, which never exceeded 68 °C during drilling of 319 Al using NH-DLC coated drills in dry condition and hence showed lower resultant torques in the range of 1.89-2.63 N-m. According to pin-on-disk tests, it can be seen that a more stable COF responses were observed when a 319 Al pin sliding against NH-DLC coated disk (Fig. 8.6). It should be noted that the running-in period (COF=0.18) of 319 Al/NH-DLC pair is almost half of the running-in (COF=0.41) period of AZ91/NH-DLC pair, indicating high energy consumption and plastic deformation of AZ91 compared to 319 Al. As the drilling temperature never exceeded the NH-DLC coatings deterioration temperature, the coatings were intact in drilling of 319 Al, however, a significant flank wear was evident in drilling of AZ91 because of high temperature generation (Chapter 6, Section 3.2).

A more thorough understanding of the effect of NH-DLC coatings against AZ91 and 319 Al can be gained from the examination of the COF values obtained using the pin-on-disk test. The frictional temperature increase due to sliding between two contacting solids pressed together by a normal force  $F$ , sliding at a relative velocity  $v$  depends on the COF  $\mu$  between the surfaces in contact [8.5]. The heat generated  $q$ , per unit of nominal contact area  $A_n$ , per second can be expressed as follows:

$$q = \frac{\mu F v}{A_n} \quad (1)$$

The temperature  $T_b$ , at the contacting (e.g., tool-chip) interface--as a result of injection of the frictional heating across  $A_n$ --is related to the heat flux  $J$  through the thermal conductivity of aluminum  $K$  as shown below:

$$J = K \left( \frac{T_b - T_0}{L} \right) \quad (2)$$

where  $T_0$  is the ambient temperature and  $L$  is the equivalent linear heat diffusion distance as defined in Lim and Ashby [8.5]. From Equations (1) and (2), the COF  $\mu$  between the contacting surfaces is:

$$(T_b - T_0) = \frac{\mu T v}{K A_n} \quad (3)$$

Considering  $v l = T$  and using equation 3, the tool-chip interface temperature is directly proportional to the COF ( $\mu$ ) and torque ( $T$ ) generated during drilling. A low COF between the tool and the workpiece materials restricts the contact surface temperature (47 °C) increase and drilling torque (6.17 N-m) as well to low values compared to AZ91 (109 °C), thus limiting aluminum adhesion to the tool in the case of dry drilling using NH-DLC. This is why, the dry drilling of 319 Al using NH-DLC is plausible compared to dry drilling of AZ91 using NH-DLC.

The high wear resistance of NH-DLC in H<sub>2</sub>O-MQL compared to NH-DLC in dry conditions ensured that the coating remained intact on the tool and, consequently, the beneficial —machining properties such as low drilling torque and long tool life were observed. Thus preventing the temperature rise during drilling is critical to reduce tool wear and the contact temperature generated during tool-workpiece interaction should be related to the frictional properties of the coatings in machining environment, namely air and water. In order to better understand the tribological behaviour of NH-DLC coatings under water and air environments, tribological tests were conducted using a pin-on-disk configuration as described in Chapter 6

(Section 2.5). During dry sliding (ambient air with 45% RH), an average COF value of  $0.24 \pm 0.06$  was measured. The average COF decreased to  $0.11 \pm 0.01$  when the sliding tests were conducted using a distilled water spray of 30 ml/hr (Fig. 8.6). The uncoated M2 tool steel tested under fully lubricated conditions, as a reference; using the same mineral oil used for the flooded drilling tests resulted in a COF of  $0.08 \pm 0.01$ . The low COF obtained when the water spray was used on NH-DLC coatings may be attributed to the passivation of carbon bonds by -OH and -H that become dissociated from H<sub>2</sub>O. Theoretical and experimental studies have shown that water effectively passivates the free (or dangling) carbon bonds on the NH-DLC's surface as more H and -OH are provided to these free carbon atoms [8.8]. Qi et al. [8.9] used first principles calculations to show how H<sub>2</sub>O would dissociate at the diamond and DLC surfaces into -OH and H and how where chemical bonding between these surfaces and -OH is then established. The H atom serves as a bridge between the two carbon atoms. A counterface atom such as aluminum that would transfer to a clean NH-DLC surface will not transfer readily to H or -OH passivated surfaces because these surfaces have a much smaller work of separation compared to a non-passivated carbon interface. Consequently, it is conceivable that the passivation of NH-DLC surfaces in the presence of H<sub>2</sub>O-MQL would prevent adhesion between the magnesium and the drill bit coated with NH-DLC, resulting in a performance comparable to flooded drilling with HSS (Chapter 7). Therefore, NH-DLC-coated drills used under H<sub>2</sub>O-MQL drilling conditions may be an environmentally sustainable alternative to the flooded drilling of Al-Si (319Al) and AZ91 alloys.

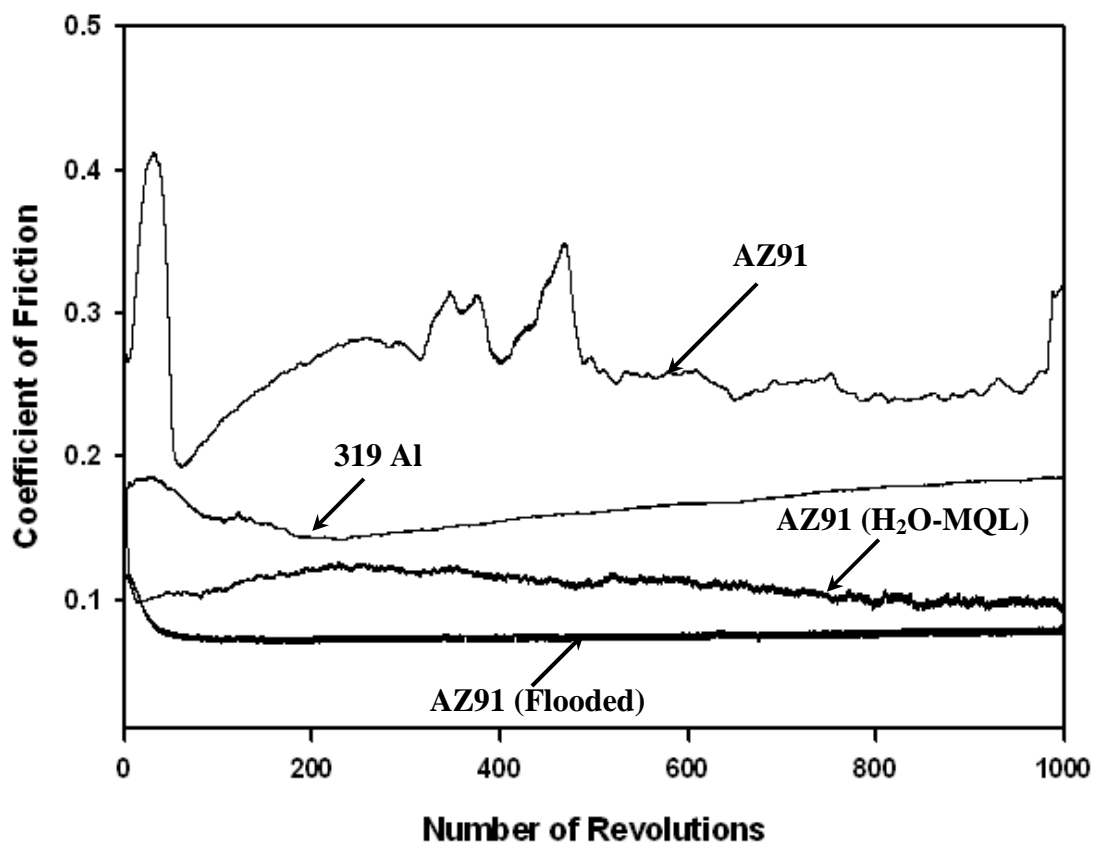


**Figure 8. 6** COF curves with number of revolutions during the sliding of AZ91 and 319 Al pin against NH-DLC-coated disks in dry and H<sub>2</sub>O-MQL conditions and uncoated HSS in flooded conditions. The applied load and sliding speed were 5 N and 0.12 m/sec.

### 8.5. Consideration of parameters to optimize the MQL machining

This section describes the overall MQL machining processes for aluminum and magnesium alloys. This section also relates the laboratory test conditions to the industrial machining processes.

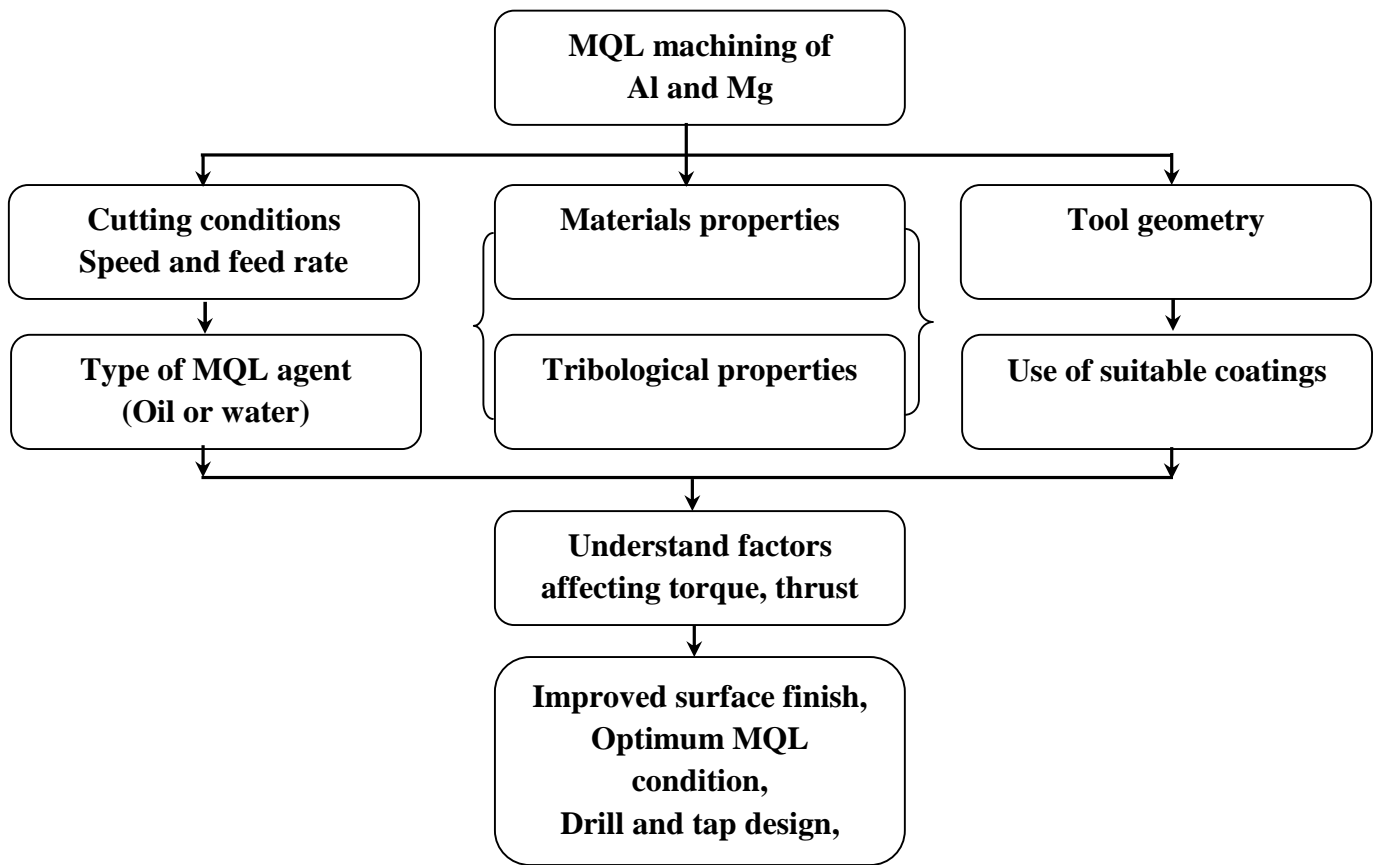


**Figure 8. 7** The flow chart for the MQL machining processes of aluminum and magnesium.

As machining at high speeds and feed rates increases industrial productivity, the highest speeds and feed rates should be selected for the production cycles. However, drilling and tapping of aluminum and magnesium at high speeds results in high temperature and stress development at the chip–tool and workpiece–tool interfaces leading to a faster adhesion of workpiece materials, tool wear and distortion of workpiece surface finish. The use of MQL can be an

effective way to reduce the rapid tool wear and transfer of workpiece materials to the tools because tribological experiments when studied together with the machining experiments showed that the use of MQL was effective in restricting temperature increase during machining, ensuring minimal adhesion to the tools that resulted in low torques. Therefore, the performance of MQL at high speeds and feed rates should be assessed.

As aluminum and magnesium alloys are the substitutes of the traditional role of steel and cast iron components used in the transportation industry due to their low density deep hole drilling of automotive powertrain components made of these alloys are of considerable importance. However, during machining of aluminum alloy (dry), the tool failure is commonly caused by the formation of an adhesive layer and built up edge, which also has negative on the quality of the machined surface. Thus, tribological behaviour of different coatings based on the carbon system needs to be understood using a series of tribological tests at room and elevated temperatures and different atmospheres. The relation between COF and mechanical properties of drilled holes will help to design a new tool for increasing productivity.

In laboratory tests, the external MQL system i.e. the oil and air are mixed externally, and piped through the spindle and tool to the cutting zone are used extensively [Chapter 2]. However, in industry the internal MQL system are effectively used, which consists two parallel tubes routed through the spindle to carry oil and air to an internal mixing device near the tool holder, where the oil and air mixture is created. Internal MQL system is effective in reduction of heat from the tool-chip interface than the external MQL system.

In industry, monitoring of torque and thrust force is very important to understand the dimensional accuracy and surface finish of the workpieces, adhesion of the workpiece materials

and wear of the cutting tools. The suggested non-contact measurement system is a unique approach for the industry that has very high sensitivity and superior to the existing methods of measuring forces through the workpiece in drilling and tapping under different machining conditions (dry, MQL and flooded).

## **References**

- [8.1] E. Konca, Y.-T. Cheng, A.M. Weiner, J.M. Dasch, A. Erdemir, A.T. Alpas, Transfer of 319 Al alloy to titanium diboride and titanium nitride based (TiAlN, TiCN, TiN) coatings: effects of sliding speed, temperature and environment, *Surface & Coatings Technology* 200 (2005) 2260–2270.
- [8.2] W. Ni, Y.-T. Cheng, A. M. Weiner, T. A. Perry, Tribological behaviour of diamond-like-carbon (DLC) coatings against aluminum alloys at elevated temperatures, *Surface & Coatings Technology* 201 (2006) 3229–3234.
- [8.3] S. C. Tung, Automotive tribology overview of current advances and challenges for the future, *Tribology International* 37 (2004) 517-536.
- [8.4] E. Konca, Y.-T. Cheng, A.T. Alpas, Sliding wear of non- hydrogenated diamond- like carbon coatings against magnesium, *Surface & Coatings Technology* 201 (2006) 4352–4356.
- [8.5] S.C. Lim, M.F. Ashby, Wear mechanism maps, *Acta Metallurgica* 35 (1987) 1-24.
- [8.6] U.S. Choi, B.G. Ahn, O.K. Kwon, Y.J. Chun, Tribological behaviour of some antiwear additives in vegetable oils, *Tribology International* 30 (1997) 677-683.
- [8.7] S. Bhowmick, A.T. Alpas, The performance of hydrogenated and non-hydrogenated diamond-like carbon tool coatings during the dry drilling of 319 Al, *International Journal of Machine Tools & Manufacture* 48 (2008) 802–814.
- [8.8] J. Andersson, R.A. Erck, A. Erdemir, Friction of diamond-like carbon films in different atmospheres. *Wear* 254 (2003) 1070- 1075.
- [8.9] Y. Qi, E. Konca, A.T. Alpas, Atmospheric effects on the adhesion and friction between non-hydrogenated diamond-like carbon (DLC) coating and aluminum – A first principles investigation. *Surface Science* 600 (2006) 2955–2965.

## CHAPTER 9

Conventional cutting fluids used for machining processes are considered a problem for industries because these substances can cause serious damage to workers' health and nature, and are expensive to acquire and maintain, following environmental norms. Economic pressure on industries due to waste disposal is increasing progressively. Today, costs of cutting fluids can reach 20% of production costs. Machining with the minimum quantity lubrication (MQL) technique can be triggered special interest from researchers who work in the area of material removal as an alternative to traditional fluids.

The key conclusions arising from this dissertation are as follows:

- [9.1] The uncoated HSS drills failed after drilling only 49 holes in drilling of 319 Al as a result of extensive aluminum adhesion to the cutting edge and drill flutes. Dry drilling and tapping performed by the H-DLC coated drill produced consistently lower average torque and thrust force when compared to HSS drills and taps. Other indicators such as the mass of adhered aluminum and the number of torque spikes were less significant during drilling and tapping by the H-DLC drills.
- [9.2] Drilling by using 30 ml/h water spray (H<sub>2</sub>O-MQL) in conjunction with NH-DLC or fatty acid based minimum quantity lubricant (MQL) required lower torques and thrust forces compared to dry drilling of 319 Al and AZ91. The average torque and thrust force responses obtained using NH-DLC and H<sub>2</sub>O-MQL was comparable to those measured for conventional flooded cooling.



[9.3] A built-up edge (BUE) was observed on the cutting edge of both uncoated and coated drills in drilling of both aluminum and magnesium. At failure condition, the uncoated HSS drill flutes were entirely covered by the adhered aluminum and magnesium while the BUE was not as thick, nor were the drill flutes totally covered by aluminum and magnesium on the NH-DLC coated drills in water MQL condition (H<sub>2</sub>O-MQL). In addition, the NH-DLC coated drill in H<sub>2</sub>O-MQL diminished aluminum and magnesium smearing on the flank faces in dry drilling of 319 Al and AZ91.

[9.4] The maximum temperature generated in the workpiece during MQL drilling was lower than that observed in dry drilling, and comparable to flooded conditions. The mechanical properties of the material adjacent to drilled holes, as evaluated through plastic strain and hardness measurements, revealed a notable softening in the case of dry drilling, with magnesium alloys exhibiting a recrystallized grain zone, but not for MQL drilling. Softened aluminum and magnesium promoted adhesion to the tools resulted in the formation of a built-up edge (BUE) and consequently high torques and thrust forces were generated. NH-DLC coatings' low COF in H<sub>2</sub>O-MQL against 319 Al and AZ91 compared to uncoated HSS limited the temperature increase during NH-DLC in H<sub>2</sub>O-MQL drilling and hence both torques and thrust forces were effectively reduced.

[9.5] Scanning electron microscopy observations confirmed that the smallest aluminum and magnesium adhesion to the drill flutes occurred in MQL drilling and tapping.

Finally, the following practical recommendations could be made regarding the MQL machining of aluminum and magnesium alloys: (i) both alloys could be drilled using NH-DLC coated tools

under the H<sub>2</sub>O-MQL condition; (ii) FA-MQL with uncoated HSS is a viable alternative to the conventional flooded drilling and tapping and (iii) the use of NH-DLC coated tools and H<sub>2</sub>O-MQL is the most economical process among the tools and conditions considered.

## **SUGGESTIONS FOR FUTURE WORK**

[1] Transmission electron microscopy (TEM) study can be considered for dislocation microstructures of the machined chips and material ahead of the tool tip. The dislocation structures can be investigated systematically by taking samples from each deformation zone in the machined chips.

[2] Detailed examination of the DLC coated drill at failure condition using cross sectional FIB technique. The aim will be to recognize the failure mechanism of DLC coatings during machining of aluminum and magnesium alloys.

[3] Finite element analysis of drilling torque and thrust force in machining of aluminum and magnesium can be considered to understand the drill wear and materials adhesion to the tools. In the drilling simulations, due to the complexity of drill geometry, the drill cutting and chisel edges are frequently characterized as a series of oblique cutting to simplify the problem. This process has limited accuracy because of the interaction between adjacent segments. However, a 3-D updated-Lagrangian finite element modeling treating the whole drill cutting and chisel edges can be applied to simulate drilling torque and thrust force in the drilling of Al and Mg.

## APPENDIX

### APPENDIX A: COPYRIGHT RELEASES FROM PUBLICATIONS

#### Chapter 3

License Number	2611090427880
License date	Feb 16, 2011
Licensed content publisher	Elsevier
Licensed content publication	International Journal of Machine Tools and Manufacture
Licensed content title	Minimum quantity lubrication drilling of aluminium–silicon alloys in water using diamond-like carbon coated drills
Licensed content author	Sukanta Bhowmick, Ahmet T. Alpas
Licensed content date	October 2008
Licensed content volume number	48
Licensed content issue number	12-13
Number of pages	15
Type of Use	reuse in a thesis/dissertation
Portion	full article
Format	both print and electronic
Are you the author of this Elsevier article?	Yes
Will you be translating?	No
Order reference number	
Title of your thesis/dissertation	Minimum Quantity Lubrication Machining of Lightweight Materials
Expected completion date	Apr 2011
Estimated size (number of pages)	200
Elsevier VAT number	GB 494 6272 12
Permissions price	0.00 USD
VAT/Local Sales Tax	0.0 USD / 0.0 GBP
Total	0.00 USD

## **Chapter 4**

License Number	2611090649377
License date	Feb 16, 2011
Licensed content publisher	Elsevier
Licensed content publication	Journal of Materials Processing Technology
Licensed content title	Tapping of Al–Si alloys with diamond-like carbon coated tools and minimum quantity lubrication
Licensed content author	S. Bhowmick, M.J. Lukitsch, A.T. Alpas
Licensed content date	19 November 2010
Licensed content volume number	210
Licensed content issue number	15
Number of pages	12
Type of Use	reuse in a thesis/dissertation
Portion	full article
Format	both print and electronic
Are you the author of this Elsevier article?	Yes
Will you be translating?	No
Order reference number	
Title of your thesis/dissertation	Minimum Quantity Lubrication Machining of Lightweight Materials
Expected completion date	Apr 2011
Estimated size (number of pages)	200
Elsevier VAT number	GB 494 6272 12
Permissions price	0.00 USD
VAT/Local Sales Tax	0.0 USD / 0.0 GBP
Total	0.00 USD

## **Chapter 5**

License Number	2611090827328
License date	Feb 16, 2011
Licensed content publisher	Elsevier
Licensed content publication	International Journal of Machine Tools and Manufacture
Licensed content title	Dry and minimum quantity lubrication drilling of cast magnesium alloy (AM60)
Licensed content author	Sukanta Bhowmick, Michael J. Lukitsch, Ahmet T. Alpas
Licensed content date	May 2010
Licensed content volume number	50
Licensed content issue number	5
Number of pages	14
Type of Use	reuse in a thesis/dissertation
Portion	full article
Format	both print and electronic
Are you the author of this Elsevier article?	Yes
Will you be translating?	No
Order reference number	
Title of your thesis/dissertation	Minimum Quantity Lubrication Machining of Lightweight Materials
Expected completion date	Apr 2011
Estimated size (number of pages)	200
Elsevier VAT number	GB 494 6272 12
Permissions price	0.00 USD
VAT/Local Sales Tax	0.0 USD / 0.0 GBP
Total	0.00 USD

## VITA AUCTORIS

**NAME:** Sukanta Bhowmick

**COUNTRY OF BIRTH:** Bangladesh

**EDUCATION:** University of Windsor, Windsor, ON

Dept. of Mechanical, Automotive and Materials Eng.

**2007-2011 , Ph.D.**

University of Windsor, Windsor, ON

Dept. of Mechanical, Automotive and Materials Eng.

**2005-2007, MAsC.**

Bangladesh University of Engineering and Technology, Dhaka,  
Bangladesh

Dept. of Materials and Metallurgical Eng.

**1996-2001, B.Sc.**

### REFEREED JOURNAL PAPERS:

1. S. Bhowmick, A.T. Alpas, The role of diamond-like carbon coated drills on minimum quantity lubrication drilling of magnesium alloys, Submitted to the Surface and Coatings Technology, May 2011.
2. S. Bhowmick, M.J. Lukitsch, A.T. Alpas, Tapping of Al-Si alloys with diamond- like carbon coated tools and minimum quantity lubrication, Journal of Materials Processing Technology 210 (2010) 2142-2153.
3. S. Bhowmick, M.J. Lukitsch, A.T. Alpas, Dry and minimum quantity lubrication drilling of cast magnesium alloy (AM60), International Journal of Machine Tools and Manufacture 50 (2010) 444-457.

4. S. Bhowmick, A.T. Alpas, Minimum quantity lubrication drilling of aluminum– silicon alloys in water using diamond like carbon coated drills, *International Journal of Machine Tools and Manufacture* 48 (2008) 1429-1443.
5. S. Bhowmick, A.T. Alpas, The performance of hydrogenated and non- hydrogenated diamond-like carbon tool coatings during the dry drilling of 319 Al, *International Journal of Machine Tools and Manufacture* 48 (2008) 802–814.

#### **REFEREED CONFERENCE PAPERS:**

1. S. Bhowmick, A.T. Alpas, Minimum quantity lubrication machining of lightweight aluminum and magnesium alloys used in automotive components, *CIRP 2<sup>nd</sup> International Conference on Process Machine Interactions*, 10-11 June, 2010, Vancouver, Canada.
2. S. Bhowmick. A. T. Alpas, Sustainable machining processes for aluminum castings: dry and near-dry drilling, *Proceedings of the 13<sup>th</sup> International Conference on Machine design and production, UMTIK*, September 3-5, 2008, Istanbul, Turkey.

#### **CONFERENCE PRESENTATIONS:**

1. S. Bhowmick, A.T. Alpas, Minimum quantity lubrication (MQL) drilling of aluminum and magnesium alloys using diamond-like carbon coated drills, *CIRP 2<sup>nd</sup> International Conference on Process Machine Interactions*, 10-11 June, 2010, Vancouver, Canada.
2. S. Bhowmick, A.T. Alpas, Minimum quantity lubrication machining (drilling and tapping) of aluminum and magnesium alloys using diamond-like carbon coated drills, the *APMA-AUTO21 Conference and Exhibition* (June 7-10, 2010), Windsor, ON, Canada.
3. S. Bhowmick, A.T. Alpas, Minimum quantity lubrication (MQL) drilling of aluminum and magnesium alloys, the *APMA-AUTO21 Conference and Exhibition* (May 26-28, 2009), Hamilton, ON, Canada.

4. S. Bhowmick, A. T. Alpas, Performance of hydrogenated and non-hydrogenated diamond like carbon tool coatings during dry drilling of 319 Al, Canadian Materials Science Conference (June 20-22, 2007), Hamilton, ON, Canada.
5. S. Bhowmick, X. Meng-Burany, E. Konca, S.S. Akarca, A.T. Alpas, Coatings for dry machining of aluminum alloys, Discovery 2007 (Poster), Toronto, ON, Canada.

#### **TECHNICAL REPORTS:**

1. S. Bhowmick, A.T. Alpas, Drilling of AM60 magnesium alloy using minimum quantity lubrication: a comparative study with dry and flooded conditions, GM Collaborative Report, April, 2009, 60 p.
2. S. Bhowmick, A.T. Alpas, Minimum quantity lubrication drilling of aluminum– silicon alloys in water using diamond like carbon coated drills, General Motors of Canada, February, 2008, 52 p.
3. S. Bhowmick, A.T. Alpas, The performance of hydrogenated and non-hydrogenated diamond like carbon tool coatings during the dry drilling of 319 Al, General Motors of Canada, August, 2007, 40 p.